Investigating the role of nuclear receptor NR4A1 in human cardiac fibroblasts and atrial fibrillation

Chi Him Kendrick Yiu

Wolfson College

Division of Cardiovascular Medicine

Radcliffe Department of Medicine

University of Oxford

Thesis presented for the degree of Doctor of Philosophy in Medical Sciences

Hilary 2026

Declarations

I declare that the following work and data presented in the thesis are my own, with the exception of the following multi-omics profiling outsourced to external service providers:

- RNA sequencing (Chapter 4): outsourced to Azenta Life Sciences, UK
    - Section 4.2.2 – Library preparation and sequencing performed by Azenta
    - Section 4.2.3 – Raw data processing performed by Azenta
- Interactome proteomics (Chapter 6): outsourced to Biogenity, Denmark
    - Section 6.2.2 – Sample preparation and analysis for mass spectrometry performed by Biogenity
    - Section 6.2.3 – Raw data processing and analysis performed by Biogenity
    - Section and Figure 6.3.2 – Differential analysis performed by Biogenity. Interpretation and generation of the associated plots remain my own work.

I declare that generative AI tools ChatGPT-5 (OpenAI) and Gemini (Google) were used for background research and general subject understanding.

Acknowledgements

The completion of my DPhil and this thesis would not have been possible without the people mentioned below, as well as everyone who supported me throughout this journey. I am deeply grateful to the NIHR Oxford BRC for funding my research and for the opportunity to work within such a collaborative local research community

I would like to first express my sincere gratitude to my supervisors. To Prof Svetlana Reilly, I am truly grateful to have worked under your supervision over the last four years. Thank you for offering me so many opportunities to learn, for encouraging me to step out of my comfort zone, and for guiding me toward becoming a better researcher. I also appreciate your support as a mentor, helping me navigate my career progression with consistent encouragement both inside and outside of the academic environment. To Dr Paul Robinson, I am deeply honoured to have been supervised by you. Thank you for supporting me in every aspect of this project, whether tackling technical hurdles or navigating general challenges. I truly enjoyed our conversations, and it has always been a pleasure to learn from someone so passionate and knowledgeable. To Prof Robin Choudhury, I sincerely appreciate your invaluable insights. Your expertise brought a fresh perspective and clinical relevance that constantly stimulated my thinking, and I am thankful for your guidance throughout this journey.

I would also like to extend my gratitude to all the colleagues who I worked with during my DPhil, with a very special thanks to Lucia and Aaron. I honestly would not have survived the "hectic" moments of this degree without your mental support. Thank you for standing by me during the tough times and for bringing so much joy to the lab. I learned more from you both than I ever imagined I would before coming to Oxford. Thank you also to Sam and Lorena for

your support, and to the rest of the Reilly group and CVMed. It has been a pleasure to work with you all.

To my friend Jacky, you have been an amazing companion. I am glad to see how far we have both come since our Master's. Thank you for pulling me through the "down" periods of my DPhil. Enjoying life in Oxford outside the lab with you and others has been an amazing experience. I also want to thank my friends on the volleyball team, the friendships that we built over the last four years are truly precious and provided the mental escape I needed during difficult moments at work. To my friends outside of academia, and my former supervisors and colleagues from my undergraduate and Master's degrees, the experiences I shared with you shaped who I am today as both a researcher and a person.

Last but not least, I am deeply thankful to my family, without whom I would not have made it so far. To my parents, thank you for your indefinite support in all aspects of my life, including my decision to move abroad and develop my career in the UK. I am still at an early stage of my journey, but I hope I have made you proud. Your encouragement is my greatest energy sources as always. To my sister Cherry, you have been my biggest supporter from the very beginning, I have lost count of how many times I have laughed sharing silly moments with you. Even though we are physically miles apart, you are the best companion in every part of my life.

Publications

Leblanc, F. J. A.*, **Yiu, C. H. K.***, Moreira, L. M., Johnston, A. M., Mehta, N., Kourliouros, A., Sayeed, R., Nattel, S., Reilly, S., Lettre, G. (2025). Single-nucleus multi-omics implicates androgen receptor signaling in cardiomyocytes and NR4A1 regulation in fibroblasts during atrial fibrillation. Nature Cardiovascular Research. 4(4):433-444. *Contributed equally.

Zhao, S., Johnston, A. M., **Yiu, C. H. K.**, Moreira, L. M., Reilly, S., Wehrens, X. H. T. (2024). Aging-associated mechanisms of atrial fibrillation progression and their therapeutic potential. Journal of Cardiovascular Aging. 4(4):22.

Zhao, S., Hulsurkar, M. M., Lahiri, S. K., Aguilar-Sanchez, Y., Munivez, E., Müller, F. U., Jain, A., Malovannaya, A., **Yiu, C. H. K.**, Reilly, S., Wehrens, X. H. T. (2024). Atrial proteomic profiling reveals a switch towards profibrotic gene expression program in CREM-IbΔC-X mice with persistent atrial fibrillation. Journal of Molecular and Cellular Cardiology. 190:1-12.

Johnston, A. M.*, **Yiu, C. H. K.***, Reilly, S. (2024). Decoding Long Noncoding RNAs in Myocardial Infarction: A Step Closer to a "Magic Bullet"?. Canadian Journal of Cardiology. 40(4):726-729. *Contributed equally.

Conference Communications

Yiu, C. H. K., Moreira, L. M., Johnston, A. M., Sayeed, R., Krasopoulos, G., Srivastava, V., Kourliouros, A., Robinson, P., Choudhury, R., Reilly, R. Investigating the role of an orphan nuclear receptor NR4A1 in atrial fibrillation. Awarded the World Congress Early Career Investigator Travel Award. Selected for oral presentation at: ISHR2025 Nara; 11-14 May 2025, Nara, Japan.

Yiu, C. H. K., Moreira, L. M., Johnston, A. M., Sayeed, R., Krasopoulos, G., Srivastava, V., Kourliouros, A., Robinson, P., Choudhury, R., Reilly, R. Investigating the role of an orphan nuclear receptor NR4A1 in atrial fibrillation. Selected for oral presentation at: ESC Congress 2024; 30 August – 2 September 2024, London, UK.

Yiu, C. H. K., Moreira, L. M., Johnston, A. M., Sayeed, R., Krasopoulos, G., Srivastava, V., Robinson, P., Choudhury, R., Reilly, R. Investigating the role of nuclear receptor NR4A1 in atrial fibrillation. Poster presentation at: RDM Day 2024; 18 April 2024, Oxford, UK.

Contents

Abstract

Atrial fibrillation (AF) is the most common sustained cardiac arrhythmia, posing clinical and therapeutic challenges. AF is characterised by electrical and structural remodelling in the atria. The latter involves atrial fibrosis that promotes AF maintenance and progression while hampering treatment. Atrial cardiac fibroblasts (ACFs) are central drivers of structural remodelling, existing in a heterogenous state. We recently identified three transcriptional ACF subpopulations in the human left atrial appendage, one highly enriched for nuclear receptor subfamily 4 group A member 1 (NR4A1). Although NR4A1 regulates fibrosis across multiple organs, its role in human ACF fibrotic responses and relevance to persistent AF remain unclear, forming the rationale of my thesis.

NR4A1 knockdown in human ACFs reduced fibrotic marker expression and suppressed proliferation, while pharmacological activation increased fibrotic marker protein levels. Bulk RNA-sequencing of NR4A1-deficient ACFs revealed downregulation of gene signatures for ECM remodelling and immunomodulation, and upregulation of those linked to metabolic and stress-responsive signalling. Interleukin-6 (IL-6), a top-ranked hub among NR4A1 knockdown differentially expressed genes, promoted collagen secretion in human ACFs. Prostaglandin A2 (PGA2), an endogenous NR4A1 ligand, upregulated pro-inflammatory cytokines (IL-6 and interleukin-1β) – an effect abolished by NR4A1 knockdown. ACFs from persistent AF patients exhibited higher total NR4A1 protein levels and increased cytoplasmic accumulation compared with sinus rhythm controls. IL-6 and PGA2 levels were also elevated in ACF secretomes from AF patients. Proteomics revealed distinct NR4A1 interactome profiles between sinus rhythm and persistent AF ACFs. Nucleoporin 214 was identified as an AF-specific NR4A1 interactor, potentially driving increased nucleocytoplasmic translocation of NR4A1 in AF ACFs.

Collectively, my findings identify NR4A1 has a pro-fibrotic role in human ACFs, acting through ECM remodelling and pro-inflammatory pathways, with elevated protein abundance and cytoplasmic enrichment in persistent AF. Targeting NR4A1 and its associated signalling pathways may represent a novel fibroblast-targeted therapeutic strategy for persistent AF.

Abbreviations

αSMA	α-Smooth Muscle Actin
ABC	Atrial Fibrillation Better Care
ACF	Atrial Cardiac Fibroblast
AF	Atrial Fibrillation
AF-1	Activation Function 1
ANOVA	Analysis of Variance
ATP	Adenosine Triphosphate
BCA	Bicinchoninic Acid
BP	Biological Process
BSA	Bovine Serum Albumin
CABG	Coronary Artery Bypass Grafting
CALR	Calreticulin
CC	Cellular Component
cDNA	Complementary Deoxyribonucleic Acid
ChIP-seq	Chromatin Immunoprecipitation-Sequencing
CIP	Calf Intestinal Alkaline Phosphatase
CMap	Connectivity Map
Co-IP	Co-Immunoprecipitation
Csn-B	Cytosporone-B
CTGF	Connective Tissue Growth Factor
DBD	DNA-Binding Domain
DEG	Differentially Expressed Gene
DIM	1,1-bis(3'-indolyl)-1-(3,5-disubstitutedphenyl)methane
DMSO	Dimethyl Sulfoxide

ECL	Enhanced Chemiluminescence
ECM	Extracellular Matrix
ECV	Extracellular Volume Fraction
EDTA	Ethylenediaminetetraacetic Acid
EndMT	Endothelial-to-Mesenchymal Transition
ELISA	Enzyme-Linked Immunosorbent Assay
EMT	Epithelial-to-Mesenchymal Transition
FBS	Foetal Bovine Serum
FDR	False Discovery Rate
FHL2	Four and a Half LIM Domains Protein-2
gDNA	Genomic Deoxyribonucleic Acid
GLP-1R	Glucagon-Like Peptide-1 Receptor
GO	Gene Ontology
GTP	Guanosine Triphosphate
HIF-1	Hypoxia-Inducible Factor-1
HRP	Horseradish Peroxidase
IBS	Integrated Backscatter
IgG	Immunoglobulin G
IL-1β	Interleukin-1β
IL-6	Interleukin-6
IL-18	Interleukin-18
IMPase	Inositol Monophosphatase
ITGB1	Integrin β1
JNK	c-Jun N-terminal Kinase
KEGG	Kyoto Encyclopedia of Genes and Genomes
KPNA2	Importin α-1

KPNB1	Importin β-1
LBD	Ligand-Binding Domain
LCS	Low Ca^{2+} Solution
LGE	Late Gadolinium Enhancement
lncRNA	long non-coding Ribonucleic Acid
Log2FC	Log2 Fold Change
LPS	Lipopolysaccharide
MAPK	Mitogen-Activated Protein Kinase
miRNA	micro Ribonucleic Acid
MCC	Maximal Clique Centrality
MCP	Monocyte Chemoattractant Protein
MF	Molecular Function
MMP	Matrix Metalloproteinase
MRI	Magnetic Resonance Imaging
NES	Nuclear Export Signal
NF-κB	Nuclear Factor-κB
NGFI-B	Nerve Growth Factor-Induced Gene B
NLRP3	NOD-, LRR- and Pyrin Domain-Containing Protein 3
NLS	Nuclear Localisation Signal
NPC	Nuclear Pore Complex
NR4A1	Nuclear Receptor Subfamily 4 Group A Member 1
NUP214	Nucleoporin 214
PBS	Phosphate Buffered Saline
PCA	Principal Component Analysis
PGA2	Prostaglandin A2
PGE2	Prostaglandin E2

PI3K	Phosphoinositide 3-Kinase
PPI	Protein-Protein Interaction
PTM	Post-Translational Modification
qPCR	Quantitative Polymerase Chain Reaction
RNA-seq	RNA-sequencing
RT	Reverse Transcription
RXR	Retinoid X Receptor
scRNA-seq	Single-Cell RNA-sequencing
Ser351	Serine 351
siRNA	small interfering RNA
snRNA-seq	Single-Nucleus RNA-sequencing
Sp1	Specificity Protein 1
STAT3	Signal Transducer and Activator of Transcription 3
SUMO	Small Ubiquitin-like Modifier
TAC	Transverse Aortic Constriction
TCF21	Transcription Factor 21
TFA	Trifluoroacetic Acid
TGF-β	Transforming Growth Factor-β
TIMP	Tissue Inhibitors of Metalloproteinase
TKT	Transketolase
TNF-α	Tumour Necrosis Factor-α
UUO	Unilateral Ureteral Obstruction
VEGF	Vascular Endothelial Growth Factor
XPO1	Exportin 1

List of Figures

List of Tables

CHAPTER 1: INTRODUCTION

1.1 Atrial Fibrillation

1.1.1 Epidemiology and clinical significance of atrial fibrillation (AF)

Atrial fibrillation (AF) is the most common sustained cardiac arrhythmia globally, representing a notable public health challenge with profound clinical implications, including increased risk of stroke, heart failure, and mortality[1]. The evolution of our understanding of AF has progressed substantially over recent decades, transitioning from viewing it merely as a rhythm disturbance to recognising it as a complex disease involving multifactorial pathophysiological mechanisms. The Global Burden of Disease 2010 Study documented progressive increases in overall AF burden, incidence, prevalence, and AF-associated mortality between 1990 and 2010, with important public health implications necessitating better prevention and therapeutic strategies[1]. The prevalence of AF in the general population continues to rise, with an estimated prevalence of more than 60 million patients worldwide currently. Projections indicate this burden will increase significantly in the coming decades, with an estimated 17.9 million individuals affected in Europe in 2060[2].

Advancing age, male sex, and Caucasian race are established risk factors for AF development[3], while female sex is correlated with higher AF-related mortality worldwide likely attributed to enhanced thromboembolic risk[4]. The epidemiology of AF is also influenced by significant genetic components, with more than 100 genetic loci identified as contributing to AF susceptibility[5]. Hypertension remains the most important modifiable risk factor for AF development, which may be considered a cardiac manifestation of hypertensive target organ damage[6]. AF frequently coexists with numerous cardiovascular and non-cardiovascular conditions, including heart failure, diabetes mellitus, obesity, sleep apnoea, and chronic kidney disease, with each comorbidity amplifying both the prevalence and complications of AF[7]. The

bidirectional relationship between AF and these conditions creates a vicious cycle, where each condition perpetuates the other through shared pathophysiological mechanisms.

1.1.2 Clinical classification of AF

Current clinical classification of AF is primarily based on arrhythmia patterns and temporal characteristics[8] (Figure 1.1.2). Paroxysmal AF is defined as episodes that terminate spontaneously or with intervention within 7 days. Persistent AF refers to continuous AF lasting longer than 7 days (or requiring intervention for termination), and long-standing persistent AF is longer than 12 months. Permanent AF describes instances where sinus rhythm is no longer attempted or achievable. This traditional classification has been applied in clinical settings for decades. However, recognition of substantial clinical heterogeneity among AF patients has promoted development of more nuanced classification systems.

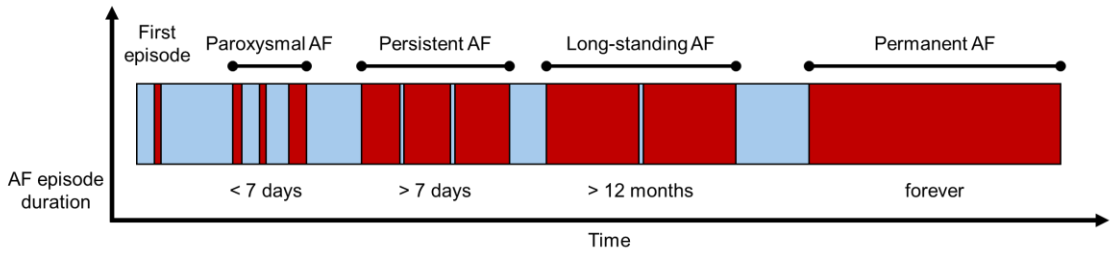

Figure 1.1.2 Clinical classification and progression of AF. AF progresses into different types according to the duration of episodes.

Contemporary approaches of AF classification increasingly incorporate clinical phenotyping and quantitative assessment of arrhythmia burden[9]. Cluster analysis of AF patients has identified clinical phenotypes characterised by varying profiles of cardiovascular risk factors and comorbidities, with these phenotypes showing significant associations with clinical

outcomes including stroke, thromboembolism, myocardial infarction, and mortality[10]. The emerging concept of AF burden, defined as a quantitative measure of arrhythmia presence and severity[11], provides additional prognostic and therapeutic information, with higher AF burden associated with worse outcomes and potentially serving as both an outcome predictor and therapeutic target[12].

Classification frameworks of AF also incorporate special populations that require distinct classification considerations. Valvular heart disease is closely associated with AF, with both pathologies perpetuating each other through volume and pressure overload mechanisms[13]. AF prevalence and treatment-related complications significantly increase in elderly patients (age ≥ 75 years)[14]. AF prevalence also increases markedly in patients with underlying structural heart disease such as hypertrophic cardiomyopathy (27%) or cardiac amyloidosis (40%)[15].

Together, these classification frameworks highlight the heterogeneous nature of AF and underscore the need for individualised approaches to its assessment and treatment.

1.1.3 Clinical management of AF

Modern AF management has evolved toward an integrated, holistic approach established in the "Atrial Fibrillation Better Care (ABC)" pathway, which emphasises three fundamental pillars: "A" for avoiding stroke through appropriate anticoagulation, "B" for better symptom control with patient-centred, symptom-directed rate or rhythm control decisions, and "C" for cardiovascular risk factor and comorbidity management[16]. Initial evidence indicates that comprehensive implementation of the ABC pathway approach, supported by mobile health technology and integrated care models, leads to greater reductions in symptoms, AF burden,

and improved outcomes compared to traditional non-ABC management[17]. The recognition that risk factor modification and upstream therapy are paramount components of contemporary AF management represents a paradigm shift from previous approaches focusing primarily on rate or rhythm control[18].

Catheter ablation is an invasive, yet safe and efficacious treatment for managing AF, with pulmonary vein isolation serving as the primary ablation approach[19]. Radiofrequency ablation and cryoablation are current standard strategies for pulmonary vein isolation, creating tiny scars in the heart to destroy abnormal electrical circuits[20]. For patients with heart failure (reduced left ventricular ejection fraction) and concurrent AF, catheter ablation shows promise for improving long-term prognosis compared to medical management alone[21]. In addition to ablation, electrical cardioversion applies a controlled electric shock on the heart to convert AF to normal sinus rhythm[22]. However, ablation is preferred over electrical cardioversion if the patient is at higher risk of AF recurrence after procedure.

The management strategy for AF employs either rate control (aimed at controlling ventricular rate while maintaining AF) or rhythm control (aimed at restoring and maintaining sinus rhythm). Common pharmacological agents for rate control include β-blockers, calcium channel blockers, and potentially amiodarone and digoxin[23]. Rhythm control agents include class Ic drugs (flecainide, propafenone) and class III drugs (amiodarone, dronedarone, dofetilide, sotalol)[24]. Clinical studies initially suggested no survival advantage of rhythm control over rate control, with potential advantages of rate control including lower risk of adverse effects from anti-arrhythmic drugs[25]. However, recent randomised evidence demonstrates that early rhythm control strategy is associated with a reduced risk of adverse cardiovascular outcomes compared to usual care in patients with early AF, reframing the role of early intervention[26].

Anticoagulation represents a critical component of AF management for stroke prevention, with evidence showing direct oral anticoagulants as the preferred choice compared to vitamin K antagonists[27]. Clinical evidence demonstrates that direct oral anticoagulant-treated patients have superior safety and effectiveness profiles compared to vitamin K antagonist users, indicated by lower risk of mortality, thrombotic events and minor bleeding[28]. For patients with contraindications to long-term oral anticoagulation, alternative interventions including left atrial appendage occlusion effectively reduce stroke and major bleeding risks across diverse patient populations[29].

Recent evidence increasingly supports comprehensive lifestyle modification and risk factor management as important components of AF prevention and management[18]. Multiple modifiable factors contribute to AF development and progression, including obesity, sleep apnoea, hyperlipidaemia, smoking, excessive alcohol consumption, physical inactivity, and genetic predisposition[30]. Structured risk factor modification programs demonstrate promising results, with comprehensive management leading to greater reduction in symptoms and AF burden, more successful ablations, and improved long-term outcomes[31].

1.1.4 Pathophysiology of AF: the "AF begets AF" mechanism

The seminal concept of "AF begets AF" emerged in the mid-1990s from experimental studies demonstrating that repetitive rapid pacing in animals induces progressively self-sustaining AF over time[32,33]. Tachycardia-induced changes develop progressively from seconds of AF during rapid pacing to sustained arrhythmia lasting 24 hours or more after 2-3 weeks of pacing (Figure 1.1.4), popularising the "AF begets AF" phenomenon and bringing this important mechanism to the forefront of arrhythmia research. These foundational experiments established that maintenance of AF results in a propensity for sustained fibrillation, creating a vicious cycle

through which the arrhythmia itself perpetuates its own persistence and progression from paroxysmal to persistent forms.

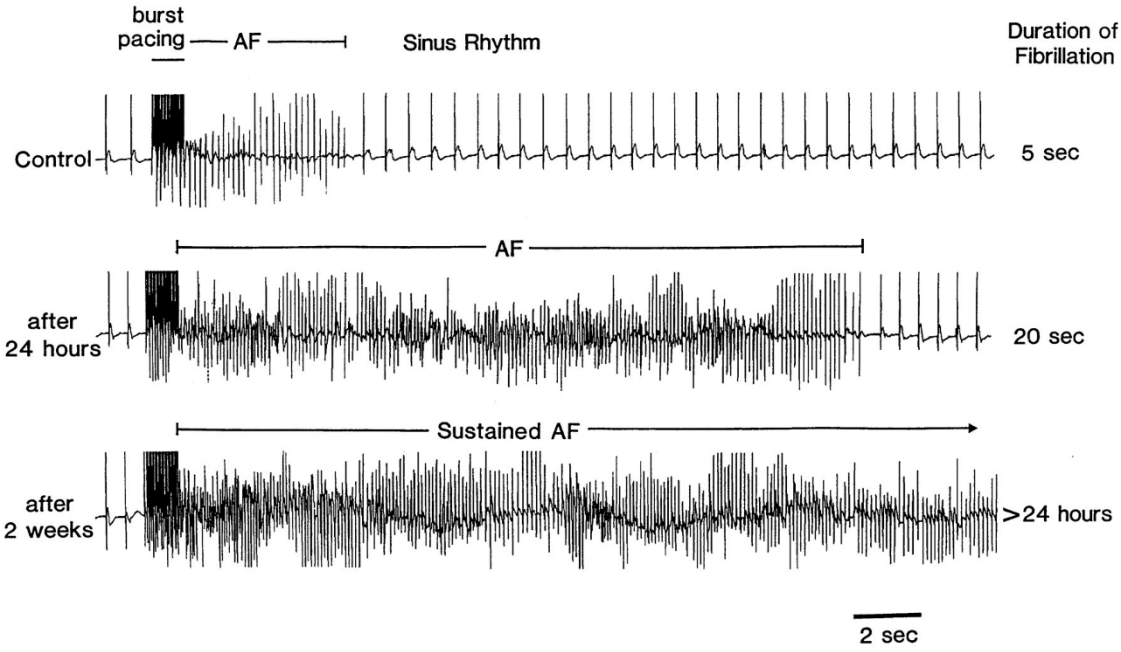

Figure 1.1.4 Electrogram recordings from goat showing the "AF begets AF" concept. AF induction was performed using a 1-second stimuli burst (50 Hz, 4 times threshold). AF episodes were prolonged after 24 hours of pacing, and sustained AF was observed after 2 weeks of induction without self-termination. Adapted from the study conducted by Wijffels et al., 1995[32].

Electrical remodelling in AF is characterised by shortening of the atrial effective refractory period and heterogeneous conduction properties that facilitate AF perpetuation[33]. Studies have delineated the ionic currents that underlie electrical remodelling in AF, revealing that key changes occur in multiple ion channel populations including downregulation of L-type calcium current, reduction of transient outward potassium current, elevated inward-rectifier potassium currents, and constitutive activation of acetylcholine-activated potassium current[34]. The upregulation of inward rectifier potassium current occurs uniformly during AF, while alterations in sodium channel properties and lateralisation of connexin distribution (connexins

40 and 43) contribute to abnormal conduction patterns[35]. These ion channel remodelling changes are partially reversible early in the disease process but become difficult to reverse in chronic AF, explaining why spontaneous cardioversion to sinus rhythm is more likely early in the course of AF and decreases with arrhythmia duration[36].

Multiple mechanisms contribute to electrical remodelling during AF, operating across different time scales. Short-term mechanisms drive increased intracellular calcium overload, activation of proteases and kinases, and downregulation of L-type calcium channel expression[34,37]. Electrical remodelling involves the changes in ion channel expression and redistribution of connexins[38], while long-term structural changes involve fibrosis and atrial dilatation[39].

The concept of shortened re-entry wavelength represents a fundamental mechanism by which electrical remodelling perpetuates AF[40]. The wavelength of re-entrant activity is determined by conduction velocity and refractory period. The shortening of refractory period and slowed conduction both reduce wavelength, allowing multiple smaller re-entry circuits to coexist simultaneously in atrial tissue and sustaining the arrhythmia[3]. Computer modelling studies demonstrate that both electrical and structural remodelling contribute synergistically to AF perpetuation[40]. These changes create a pro-arrhythmic substrate characterised by heterogeneous refractoriness, altered conduction velocity, and discontinuous conduction patterns that favour initiation and maintenance of multiple re-entry circuits.

Structural remodelling represents a critical component of the “AF begets AF” mechanism, involving progressive atrial dilation, loss of myocytes, and fibrosis[41]. Tachycardia-induced structural changes occur on different time scales than electrical remodelling, developing over weeks to months of AF, and likely represent adaptation to rapid firing but may also contribute to arrhythmia perpetuation[41]. Atrial fibrosis, which develops during AF primarily through

fibroblast activation, extracellular matrix (ECM) deposition, and myofibroblast proliferation, creates heterogeneous conduction abnormalities and disrupts tissue integrity, thereby creating and sustaining anatomically anchored re-entry circuits[42].

1.2 Cardiac Fibrosis in AF

Cardiac fibrosis, characterised by the pathological accumulation of collagen and other ECM components, creates a structural substrate that perpetuates arrhythmia through altered electrical conduction and mechanical remodelling. The extent of atrial fibrosis increases when AF progresses from paroxysmal to persistent AF[43] (Figure 1.2). Understanding the molecular mechanisms underlying both atrial and ventricular fibrosis in the context of AF is essential for developing effective anti-fibrotic strategies beyond conventional rhythm and rate control.

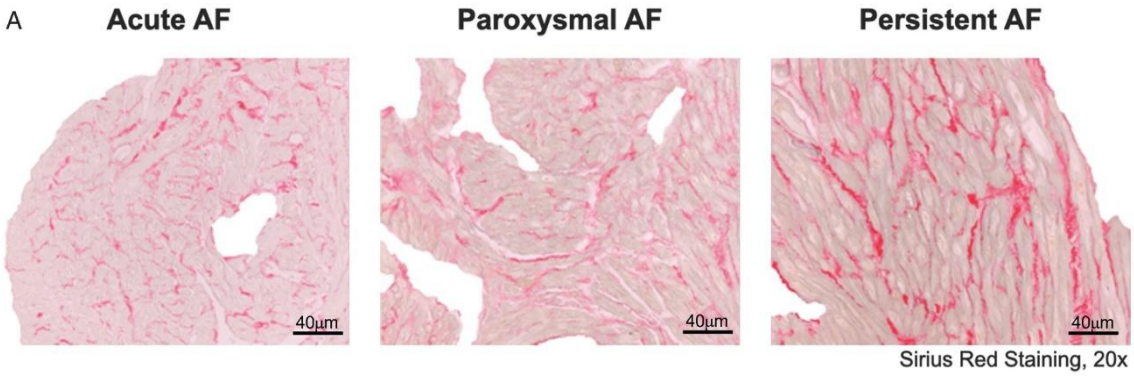

Figure 1.2 Atrial fibrosis increases with the progression of AF phenotypes. Fibrosis is identified by Sirius Red staining (collagen). Representative images show a progressive increase in atrial fibrosis from acute to paroxysmal to persistent AF. Adapted from the study conducted by Maesen et al., 2022[43].

1.2.1 Atrial fibrosis in AF

Atrial fibrosis arises from a wide range of signalling mechanisms and is recognised as a clinical hallmark of atrial remodelling, playing a pivotal role in AF perpetuation[44,45]. Fibrotic remodelling disrupts normal myocyte-to-myocyte electrical coupling through increased collagen deposition and disorganised ECM architecture, creating regions of slow and inhomogeneous conduction that favour re-entry circuit formation[42]. Three-dimensional

mapping studies using cardiac magnetic resonance imaging (MRI) have demonstrated that fibrotic regions exhibit reduced conduction velocity and direction heterogeneity, establishing a substrate for stable and long-lasting re-entry[46]. The association between fibrosis burden and electrophysiological properties is particularly striking in persistent AF, where extensive fibrosis impairs both electrical conduction and mechanical function. Left atrial fibrosis has been extensively characterised using late gadolinium enhancement (LGE) cardiac MRI, with severity classified according to the Utah scale ranging from stage I (minimal fibrosis) to stage IV (extensive fibrosis)[47]. Clinical studies have demonstrated that higher degrees of atrial fibrosis are independently associated with reduced atrial strain parameters measured by speckle-tracking echocardiography[48]. These mechanical abnormalities reflect the impaired ability of fibrotic atrial tissue to generate electrical conduction and sufficient force for effective atrial contraction and electrical conduction, thereby promoting AF perpetuation.

Circulating biomarkers of AF have also been identified. Circulating galectin-3 levels correlate with atrial fibrosis burden and predict AF recurrence after catheter ablation, making it a valuable prognostic biomarker[49,50]. N-terminal pro-B-type natriuretic peptide and C-telopeptide of type I collagen are circulating biomarkers of collagen turnover that correlate with atrial fibrosis severity[51,52]. Notably, serum microRNA (miRNA)-15a-5p has been identified as a biomarker predictive of AF recurrence post-ablation, with elevated levels correlating with the extent of myocardial fibrosis[53]. Therefore, the integration of multiple biomarkers with advanced imaging enables comprehensive phenotype of atrial fibrosis and remodelling in AF.

Atrial fibrosis in AF is also contributed by different non-cardiac factors, such as smoking, obesity, obstructive sleep apnoea[45,54,55]. However, they are beyond the scope of my current work.

1.2.2 Ventricular fibrosis in AF

While atrial fibrosis has been extensively studied, left ventricular fibrosis has emerged as an independent predictor of AF and AF recurrence after catheter ablation[56]. Left ventricular extracellular volume fraction (ECV), measured using T_1 mapping before and after contrast administration in cardiac MRI, represents a non-invasive marker of diffuse myocardial fibrosis and independently predicts new-onset AF in patients with acute myocardial infarction[57]. Imaging studies show a greater extent of left ventricular fibrosis in patients with persistent AF compared with paroxysmal AF and sinus rhythm controls[58,59].

The mechanistic basis of left ventricular fibrosis-mediated AF susceptibility involves complex interactions between ventricular structural remodelling and atrial electrophysiology. AF-mediated tachycardia can induce ventricular remodelling and dysfunction, while the resulting ventricular dysfunction and increased ventricular filling pressures contribute to atrial stretch and electrophysiological remodelling[60]. In patients with arrhythmia-induced cardiomyopathy, left ventricular LGE (indication of left ventricular fibrosis) correlated positively with the time to recovery from systolic dysfunction after rhythm restoration, suggesting that ventricular fibrosis impedes functional recovery[61].

Ventricular fibrosis represents an emerging area of interest in AF. However, the mechanistic focus of my work remains on atrial fibrosis.

1.2.3 Clinical implications of atrial and ventricular fibrosis in AF

The presence and extent of atrial fibrosis provide prognostic information essential for risk stratification and prediction of AF outcomes. Molecular biomarkers associated with the risk of

incident AF, including galectin-3[62,63] and procollagen type III N-terminal propeptide[64], have indirect implications for atrial fibrosis. Advanced imaging modalities have transformed the ability to characterise cardiac fibrosis and enable personalised AF management strategies. Quantitative assessment of atrial fibrosis using delayed enhancement MRI, T_1 mapping and integrated backscatter (IBS) demonstrates patients with increased risk for AF recurrence after ablation in multiple studies, with fibrosis burden serving as an independent predictor alongside clinical variables[45]. Patients with greater extent of atrial fibrosis (marked by corrected IBS $\geq$ 20 dB) have higher risk of progression from paroxysmal to persistent AF[65].

In contrast to atrial fibrosis, limited data exists on ventricular fibrosis in AF. Cardiac MRI with post-contrast-enhanced T_1 mapping allows the quantification of left ventricular fibrosis. Studies show that shorter duration of ventricular T_1 time and increased ECV predict AF recurrence after ablation and pulmonary vein isolation, respectively[66,67]. The specific relevance of ventricular fibrosis in AF prognosis remains to be further defined.

1.2.4 Molecular mechanisms

Fibrosis in AF is associated with a wide range of signalling mechanisms[45]. Many of the core pro-fibrotic signalling pathways shared between atrial and ventricular fibroblasts. Transforming growth factor-β (TGF-β) has emerged as the central pro-fibrotic cytokine orchestrating fibroblast activation and ECM remodelling in cardiac fibrosis[68]. TGF-β1 exerts its effects primarily through the canonical Smad-dependent pathway. TGF-β binds to its receptors and activates Smad2/3 proteins, which translocate to the nucleus to regulate the expression of pro-fibrotic genes including collagens, α-smooth muscle actin (αSMA), connective tissue growth factor (CTGF)[69]. The role of TGF-β1 is highly potentiated by thrombospondin-1, which converts latent TGF-β1 into its bioactive form[70]. Smad7, a negative feedback inhibitor of the

TGF-β/Smad pathway, exerts cell-specific anti-fibrotic effects particularly within fibroblasts[71]. Additionally, non-canonical pathways involving mitogen-activated protein kinases (MAPK) and phosphoinositide 3-kinase (PI3K)/Akt signalling have been implicated in TGF-β-mediated fibroblast activation[72], expanding the molecular complexity of this pro-fibrotic cascade.

Although TGF-β signalling represents a conserved pro-fibrotic pathway throughout the heart, fibroblasts in the atria display greater sensitivity to TGF-β1 and other growth factors (angiotensin II, platelet-derived growth factor) stimulation than ventricular fibroblasts[73,74], resulting in enhanced proliferation, myofibroblast differentiation and collagen synthesis. This heightened responsiveness may partially explain why atrial fibrosis develops readily in AF despite the absence of comparable ventricular remodelling.

ECM homeostasis is tightly regulated not only by synthesis, but also degradation of ECM proteins mediated by matrix metalloproteinases (MMPs)[75]. MMPs and their tissue inhibitors (TIMPs) are released by cardiac fibroblasts and cardiomyocytes. The elevated MMP-1 mRNA levels in atrial tissues and reduced TIMP-2 levels in blood are associated with higher risk of developing AF[76]. Moreover, ECM fragments following MMP cleavage are called matrikines, which promote ventricular fibroblast migration and fibrotic scar formation post-myocardial infarction[77].

In addition to these conserved pro-fibrotic mechanisms in cardiac fibroblasts, several signalling pathways appear to regulate fibrosis specifically within the atria. Our group previously identified paracrine signalling of atrial cardiomyocyte-produced calcitonin plays a protective role in atrial fibrosis in AF limiting fibroblast proliferation and ECM remodelling[78]. The atrial-

specific upregulation of miRNA-31 also contributes to electrical and structural abnormalities in the atria through the depletion of dystrophin and neuronal nitric oxide synthase[79]. Recent studies have identified novel regulators of cardiac fibroblast function, including the voltage-gated L-type calcium channel subunit CACNB2, which CACNB2 overexpression suppresses primary atrial fibroblast activation and reduces expression of fibrotic markers (αSMA, collagen 1 and collagen 3) and levels of inflammatory cytokines[80].

Inflammation plays an integral role in the atrial fibrotic cascade during AF pathogenesis, which operates with other risk factors including fibrosis, heart failure, diabetes, obesity, and hypertension[81]. The relationship between inflammation and AF is bidirectional and self-amplifying. Inflammatory signalling promotes the transition of resident fibroblasts into activated myofibroblasts through cytokine-mediated pathways in the atria, exacerbating atrial remodelling [82,83]. Fibrosis further disrupts atrial conduction and sustains AF, and hence, interfering and stopping this inflammation-AF feedback loop represents a key therapeutic opportunity in AF management.

The NOD-, LRR- and pyrin domain-containing protein 3 (NLRP3) inflammasome has emerged as the central effector in atrial remodelling, functioning not only in infiltrating immune cells but also in resident atrial cells like cardiomyocytes and fibroblasts[84]. Activation of the atrial NLRP3 inflammasome triggers downstream pathological processes such as interleukin-1β (IL-1β) and interleukin-18 (IL-18) maturation, oxidative stress accumulation, calcium dysregulation, and ECM remodelling[85]. These events collectively create pro-arrhythmic substrates that contribute to AF development, progression and recurrence[84]. Beyond IL-1β and IL-18, other pro-inflammatory cytokines released in the atria play integral roles in AF, including tumour necrosis factor-α (TNF-α), interleukin-6 (IL-6) and interleukin-11[86,87]. They promote

fibroblast proliferation and ECM accumulation through activation of nuclear factor-κB (NF-κB) and signal transducer and activator of transcription 3 (STAT3) signalling pathways[88], generating an AF-promoting atrial substrate.

Increased monocyte and macrophage infiltration sustain the low-grade inflammation in AF[89]. Macrophage polarisation plays a critical role in AF-associated fibrosis. M1-polarised macrophages release pro-inflammatory mediators to promote electrical instability, while M2-polarised macrophages trigger fibroblast activation through paracrine secretion of pro-fibrotic mediators in the atria[90].

1.2.5 Therapeutic approaches to reduce cardiac fibrosis in AF

Currently available pharmacological agents have demonstrated anti-fibrotic mechanisms in the context of AF. Sodium-glucose cotransporter-2 inhibitors have emerged as promising agents with pleiotropic effects on AF-related fibrosis and structural remodelling. Notably, dapagliflozin attenuates cardiac dysfunction and reduces myocardial fibrosis and inflammation in AF rats through inhibiting the High Mobility Group Box 1/Receptor for Advanced Glycation End products pathway[91]. Previous preclinical studies reported that pirfenidone, an anti-fibrotic drug, significantly reduces left atrial remodelling, fibrosis and AF duration in a heart failing-canine model[92]. Semaglutide, a glucagon-like peptide-1 receptor (GLP-1R) agonist, significantly lowers the risk of AF occurrence in patients with high cardiovascular risk, mainly attributed to diabetes and obesity[93]. Liraglutide, another GLP-1R agonist, reduces AF susceptibility and atrial fibrosis in a type 2 diabetic mouse model[94].

Emerging experimental strategies target specific signalling pathways within the fibrotic cascade. Restoration of the calcitonin signalling in the atria may reduce the arrhythmogenic substrates in persistent AF[78]. Omentin-1 overexpression reduces AF susceptibility and atrial fibrosis in angiotensin II-treated mice through targeting the Src/PI3K/Akt signalling pathway in atrial fibroblasts[95]. Similarly, paeoniflorin, a natural compound derived from *Paeonia lactiflora*, attenuates angiotensin II-induced AF and atrial fibrosis by suppressing the PI3K/Akt pathway[96]. The angiotensin II-induced AF inducibility and atrial fibrosis are also attenuated by JQ1, a bromodomain and extra-terminal domain inhibitor, through downregulating the expression of pro-fibrotic genes (*Col1a1*, *Col3a1*, *Mmp2*, *Tgfb2*) and restoring the expression of *Sirt1*[97].

In clinic, catheter ablation remains the cornerstone rhythm control intervention for AF. Recent clinical trials demonstrate that early rhythm control reduces the incidence of major adverse cardio-cerebrovascular events and long-term AF burden compared to rate control[98]. In patients with AF-mediated cardiomyopathy, catheter ablation enables the reversal of ventricular dysfunction and diffuse fibrosis[99], emphasising the importance of timely rhythm restoration before fibrosis becomes irreversible. Novel technologies, such as low-intensity pulsed ultrasound treatment, attenuate atrial fibrosis, electrical remodelling and AF susceptibility in post-myocardial infarction rat models through the modulation of Adam19/TGF-β/Smad2/3 signalling[100], suggesting non-invasive approaches may complement ablation therapy.

1.3 Cardiac Fibroblasts

Cardiac fibroblasts are the most abundant non-myocyte cell population in the human heart (24.3% in atria and 15.5% in ventricles)[101], which play essential roles in maintaining normal cardiac structure and function[102]. Fibroblasts can detect and respond to different signals in the cellular environment, such as chemical, mechanical and electrical cues. Under physiological conditions, cardiac fibroblasts are primarily responsible for producing and maintaining ECM components, which provides structural integrity to facilitate interaction with cardiomyocytes for coordinated electrical and mechanical coupling in the heart[102]. The cardiac ECM is mainly comprised of collagen 1 and collagen 3, forming an organised scaffold that enables contractile forces to propagate throughout the myocardium and intercellular connection[103]. Beyond their structural roles, cardiac fibroblasts engage in complex cell-cell signalling with other cardiac cell types. They secrete chemical signals including growth factors, cytokines and other paracrine factors that modulate cardiac electrophysiological features[104]. Cardiac fibroblasts also contribute to vascular remodelling by secreting pro- and anti-angiogenic factors to support angiogenesis[102].

When the heart encounters injury or chronic stress, cardiac fibroblasts undergo pathological remodelling. The transformation of quiescent fibroblasts into activated myofibroblasts represents a critical transition in pathological fibrosis[102]. Myofibroblasts are characterised by increased contractility and enhanced ECM production. Persistent myofibroblast activation results in excessive collagen deposition, increased myocardial stiffness, diastolic dysfunction and ultimately, impaired contractility[105].

1.3.1 Embryonic origins and lineages of cardiac fibroblasts

Cardiac fibroblasts arise from multiple embryonic sources, with increasing evidence demonstrating that cardiac fibroblast population is developmentally heterogenous. Early studies have identified two main embryonic origins for cardiac fibroblasts[106]. The predominant population originates from the epicardium through epithelial-to-mesenchymal transition (EMT), where epicardial-derived cells migrate into the myocardium and differentiate into fibroblasts. The transcription factor 21 (TCF21) is a crucial regulator of this cell lineage in the developing heart. A second important source of cardiac fibroblasts derived from the endocardium through endothelial-to-mesenchymal transition (EndMT), and they express markers including vascular endothelial-cadherin and Nuclear Factor of Activated T-Cells 1[107]. Studies employing lineage tracing demonstrated that fibroblast activation and proliferation in response to myocardial injury is not restricted to specific developmentally defined populations, suggesting that developmental origin alone does not determine fibroblast response to pathological stimuli[108].

1.3.2 Interaction between cardiac fibroblasts and cardiomyocytes

The interaction between cardiac fibroblasts and cardiomyocytes is fundamental to both cardiac development and diseases, including AF progression. Communication between these two cardiac cell types occurs through direct contact via gap junctions (connexins), membrane nanotubes, ECM and paracrine signalling[104]. *In vitro* co-culture studies demonstrate that cardiac fibroblasts directly influence cardiomyocyte function by altering cardiomyocyte viability, size and Ca^{2+} transients[109]. Conversely, cardiomyocytes release paracrine factors to increase fibroblast proliferation including TGF-β1, CTGF, vascular endothelial growth factor (VEGF), adenosine triphosphate (ATP) signal from pannexin 1, and non-coding RNAs within extracellular vesicles[110–113]. Mechanical coupling through the ECM enables transmission of

mechanical forces between fibroblasts and cardiomyocytes and influences cardiomyocyte electrophysiological properties[114]. In the physiological heart, cardiomyocytes and fibroblasts maintain structural homeostasis through bidirectional paracrine signalling, mediated through growth factors and miRNAs, to prevent excessive collagen buildup[115]. In the pathological setting, cardiomyocyte death and dysfunction trigger fibroblast activation through damage-associated molecular patterns, inflammatory mediators and pro-fibrotic signals[116]. Prolonged fibroblast activation subsequently leads to excessive ECM deposition, impaired cardiomyocyte function and disruption of electrical conduction[117].

Although much of the current understanding of fibroblast-cardiomyocyte interactions originates from ventricular studies, accumulating evidence suggests that these interactions are particularly important in the atria, where they contribute directly to AF initiation and maintenance. Atrial cardiomyocytes can undergo profound electrical remodelling in AF through atrial-selective mechanisms[118]. Atrial fibroblasts possess distinct phenotypic and functional characteristics compared with ventricular fibroblasts[73,74]. They undergo marked phenotypic remodelling during AF, including enhanced myofibroblast differentiation, altered ion channel expression and changes in connexin-mediated intercellular communication. Compared with atrial fibroblasts isolated from patients in sinus rhythm, cells from AF patients express greater numbers of functional Nav1.5 channels and larger sodium currents, together with a lower open probability of the big conductance calcium-activated potassium channels[119,120]. These changes suggest that atrial fibroblasts are active participants in electrical remodelling rather than passive producers of ECM.

Bidirectional communication between atrial cardiomyocytes and fibroblasts contributes to the establishment of a self-perpetuating arrhythmogenic substrate, occurring through direct

electrical and mechanical coupling, and paracrine signalling. Rapid atrial activation and cellular stress stimulate atrial cardiomyocyte release of pro-fibrotic mediators, including TGF-β1, angiotensin II and miRNA-21[45,121], which stimulate atrial fibroblast activation and collagen synthesis. Activated atrial fibroblasts and myofibroblasts subsequently alter atrial electrophysiology through excessive ECM deposition and altered gap junction signalling and potentially through electrotonic coupling with neighbouring cardiomyocytes, resulting in conduction slowing, increased conduction heterogeneity and facilitation of re-entry circuits. Inflammatory pathways, including NLRP3 inflammasome signalling and downstream IL-1β/IL-18 production[84,85], further amplify these fibroblast-cardiomyocyte interactions within the atrial myocardium. Together, these reciprocal interactions establish a self-perpetuating cycle in which AF promotes atrial fibrosis and remodelling, while the resulting fibrotic substrate further stabilises and sustains AF, underpinning the concept that "AF begets AF"[32].

1.3.3 Anatomical and regional differences of cardiac fibroblasts

Cardiac fibroblasts exhibit substantial regional heterogeneity, with atrial and ventricular populations displaying distinct molecular signatures and functional properties[73,74]. *In vitro* studies demonstrate that atrial fibroblasts exhibit enhanced reactivity compared to ventricular fibroblasts, with higher basal proliferation rate and greater response to different proliferative stimuli[73,74]. These differences in fibroblast behaviour correspond to distinct chamber functions, as the atria primarily generate electrical impulses and coordinate filling, whereas ventricles perform the main pumping function[122]. Transcriptional profiling reveals that atrial and ventricular fibroblasts exist as functionally distinct cell subsets with divergent gene expression profiles[74]. Chamber-specific fibroblast subpopulations show differential expression of genes involved in ECM formation, cell signalling, metabolism, immunity and coagulation and other functional classes. These regional differences may explain why AF and atrial fibrosis are

particular common complications in certain disease states, whereas ventricular fibrosis develops under different pathological conditions. Beyond atrial-ventricular differences, cardiac fibroblasts display complex spatial heterogeneity within distinct cardiac regions and layers. A proteome mapping study of the bovine heart reveals that distinct proteomic signatures and abundance of fibroblasts exist in different anatomical regions[123].

1.3.4 Subpopulations of cardiac fibroblasts

Cardiac fibroblasts are now recognised as a highly heterogeneous cell population consisting of multiple distinct subpopulations with specialised molecular and functional properties[107]. Recent advances in single-cell RNA-sequencing (scRNA-seq) or single-nucleus RNA-sequencing (snRNA-seq) and lineage tracing have classified several major cardiac fibroblast subpopulations (Figure 1.3.4).

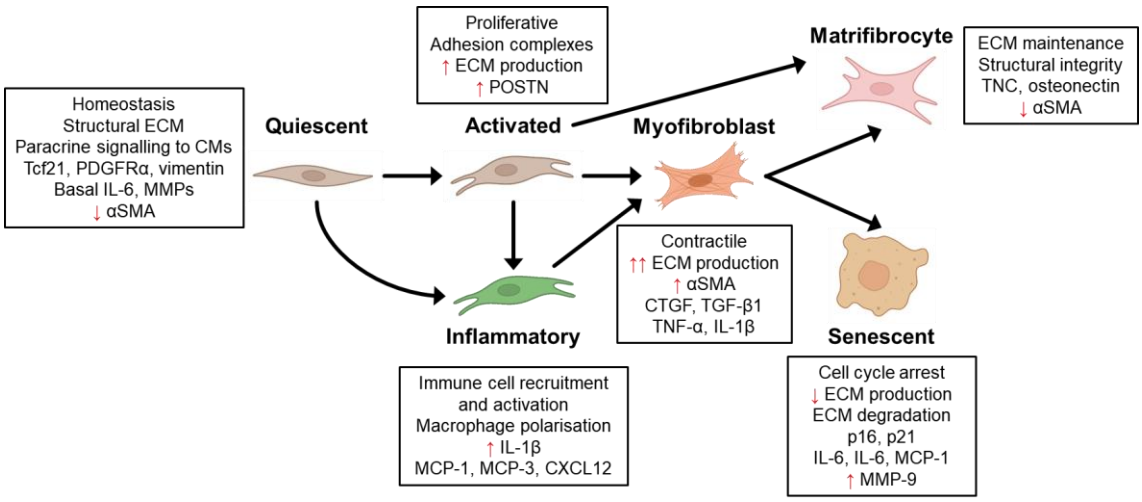

Figure 1.3.4 Schematic illustration of cardiac fibroblast heterogeneity. Fibroblast differentiation into different subpopulations, characterised by specific cellular functions and expression markers. Created with BioRender.

Residential/quiescent cardiac fibroblasts represent the predominant fibroblast subpopulation under homeostatic conditions[124]. These cells maintain the basal ECM turnover and support cardiomyocyte function through paracrine signalling. Resident fibroblasts are spindle-shaped, enriched in the expression of canonical marker such as TCF21, platelet-derived growth factor receptor α and vimentin, and minimal expression of αSMA[125]. They release controlled and balanced levels of cytokines (IL-6) and MMPs to support ECM homeostasis.

Myofibroblasts represent the primary pathogenic fibroblast subset in cardiovascular diseases and are characterised by high expression of αSMA, enhanced contractility, and robust ECM proteins production and crosslinking[107]. Myofibroblasts arise from the differentiation of quiescent fibroblasts in response to pro-fibrotic stimuli (such as TGF-β), mechanical stress, and inflammatory mediators. These cells also secrete substantial levels of pro-fibrotic factors (TGF-β1, CTGF) and pro-inflammatory cytokines (IL-1β, TNF-α). This favours a positive feedback loop to sustain the fibrotic and inflammatory remodelling. Notably, lineage tracing studies using periostin as a myofibroblast marker demonstrated that cardiac myofibroblasts are exclusively derived from the tissue-resident TCF21+ fibroblasts, excluding contributions from endothelial, smooth muscle cells or immune/myeloid cells[126].

Inflammatory fibroblasts represent a distinct subpopulation of cardiac fibroblasts with marked upregulation of inflammatory genes and immune-related functions[107]. They express elevated levels of inflammatory cytokines (IL-1β, monocyte chemoattractant protein (MCP)-1, MCP-3), chemokines (CXC motif chemokine 12) and other immune mediators. Inflammatory fibroblasts promote immune cell recruitment and activation through macrophage polarisation and T-cell activation. Recent studies have identified endogenous cardiac fibroblasts acquire immune cell-like features under inflammatory conditions in pulmonary arterial hypertension,

expressing CD4 (helper T-cell marker) and myofibroblast markers (αSMA, vimentin)[127]. These immune-competent cardiac fibroblasts are induced by IL-1β signalling. Therefore, the acquisition of immune functions by cardiac fibroblasts indicates novel mechanisms of driving fibroblast heterogeneity in pathological contexts.

Senescent fibroblasts represent an alternative fibroblast state, characterised by cell cycle arrest and expression of senescence markers such as p16 and p21[107]. These cells are characterised by the acquisition of a senescence-associated secretory phenotype that includes pro-inflammatory cytokines and other paracrine factors including IL-6, interleukin-8 and MCP-1. Senescent fibroblasts exhibit reduced ECM production capability, but they express high levels of MMP-9. Upon persistent damage, this pro-inflammatory phenotype promotes the fibrotic scar formation, which facilitates the clearance of senescent cells and tissue regeneration[128].

Matrifibrocytes represent a more recently identified fibroblast subtype with specialised roles in late-stage ECM remodelling in fibrosis. These cells are characterised by abundance of specific ECM proteins including osteonectin and tenascin C[129]. Matrifibrocytes appear particularly in regions of active tissue remodelling where the ECM scaffold is stabilised through cell-matrix interactions and crosslinking of collagen, favouring a prolonged structural integrity of the fibrotic scar[130].

1.3.5 Cardiac fibroblast heterogeneity in AF

A recent scRNA-seq analysis has revealed remarkable heterogeneity within the fibroblast populations of persistently fibrillating pig hearts[131]. Fibroblast populations in AF driver regions (specific areas that drive chronic AF maintenance) display distinct transcriptional phenotypes

compared with non-driver regions. Driver regions are enriched in pentraxin 3-positive fibroblasts with specific gene signatures favouring pro-fibrotic and pro-inflammatory pathways compared to remote regions.

In humans, our previous work identified using scRNA-seq identified three transcriptional clusters of atrial cardiac fibroblast (ACF) freshly isolated from the human right atrial appendage[78]. In our snRNA-seq study more recently, we found three distinct ACF subpopulations in the left atrial appendages[132] (Figure 1.3.5a), relevant to the focus of my work. Two subpopulations correspond to quiescent fibroblasts (aFB1) and activated fibroblasts (aFB2). However, the functional phenotype of the third subtype (aFB3) has not been well characterised. Cells in this fibroblast subpopulation express gene signatures associated with inflammatory signalling pathways, and they are highly enriched in markers including *NR4A1*, *NAMPT*, *THBS1* and *CCL2* (Figure 1.3.5b). Interestingly, *NR4A1* is one of the most specific markers of aFB3, which has been significantly implied in multiple fibrotic diseases[133]. *NR4A1* is expressed in all three subtypes; however, it is identified as a specific marker only for aFB3, meeting the subclustering criteria of an area under curve > 0.5 and a false discovery rate (FDR) < 0.05. Given that the proportion of the aFB3 subtype is not significantly different between persistent AF and sinus rhythm (Figure 1.3.5c), it suggests that there are underlying alterations within these cells that modulate the function in AF. Understanding the role of *NR4A1* in human ACFs may yield novel mechanistic insights into cardiac fibroblast biology in persistent AF.

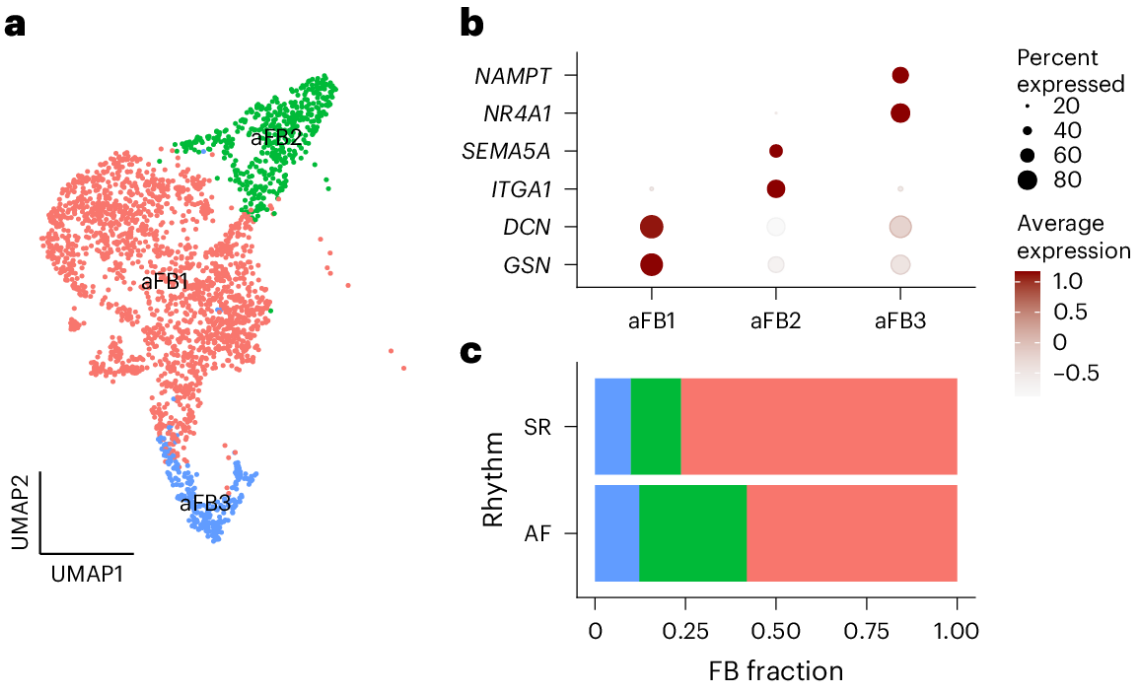

Figure 1.3.5 Fibroblast subtypes in the human left atrial appendage. (**a**) Three ACF subpopulations were identified in human left atrial appendage: aFB1, aFB2 and aFB3. (**b**) *NR4A1* expression was highly enriched in the aFB3 subpopulation. (**c**) Proportion of the three ACF subpopulations were not significantly different between sinus rhythm (SR) and persistent AF (aFB1: $P = 0.057$, aFB2: $P = 0.4$, aFB3: $P = 0.4$). Adapted from the study conducted by Leblanc and Yiu et al., 2025[132].

1.4 Nuclear Receptor Subfamily 4 Group A Member 1 (NR4A1)

Nuclear receptor subfamily 4 group A member 1 (NR4A1), commonly known as Nur77, nerve growth factor-induced gene B (NGFI-B), or testicular receptor 3, is a member of the NR4A subfamily within the nuclear receptor superfamily[134]. NR4A1 functions as an immediate-early gene transcription factor that is rapidly and transiently induced in response to diverse cellular stressors, including inflammatory mediators, growth factors, and environmental stimuli[135]. Unlike classical nuclear receptors, NR4A1 is an orphan nuclear receptor, meaning no endogenous ligands have been identified, though numerous exogenous compounds have been characterised as NR4A1 ligands[135]. This unique characteristic distinguishes NR4A1 from ligand-dependent nuclear receptors and provides insight into its ligand-independent regulatory mechanisms.

Similar to other nuclear receptors, NR4A1 possess the characteristic modular structure of the nuclear receptor family, comprising distinct functional domains[135]. The protein contains an N-terminal activation function 1 (AF-1) domain, a DNA-binding domain (DBD) with zinc fingers that mediate interaction with specific DNA sequences, and a C-terminal ligand-binding domain (LBD)[134] (Figure 1.4a). The N-terminus of NR4A1 exhibits intrinsic disorder, which contributes to its flexibility and ability to interact with diverse regulatory proteins. Notably, the LBD of NR4A1, while present, lacks a classical ligand-binding cavity and instead contains a surface pocket that can accommodate various small molecules[136]. The DBD of NR4A1 recognises and binds as a monomer to specific DNA sequences called NBRE (NR4A binding element, AAAGGTCA), binds as a homodimer or heterodimer with other NR4A family members (NR4A2 or NR4A3) to NurRE (Nur response element, TGATATTTnnnnnnAAATGATCA), or binds as a heterodimer with the retinoid X receptor

(RXR) to direct repeat 5 (DR5, AGGTCA n(5) AGGTCA) within promoter regions of target genes (Figure 1.4b), allowing it to directly regulate gene expression[137].

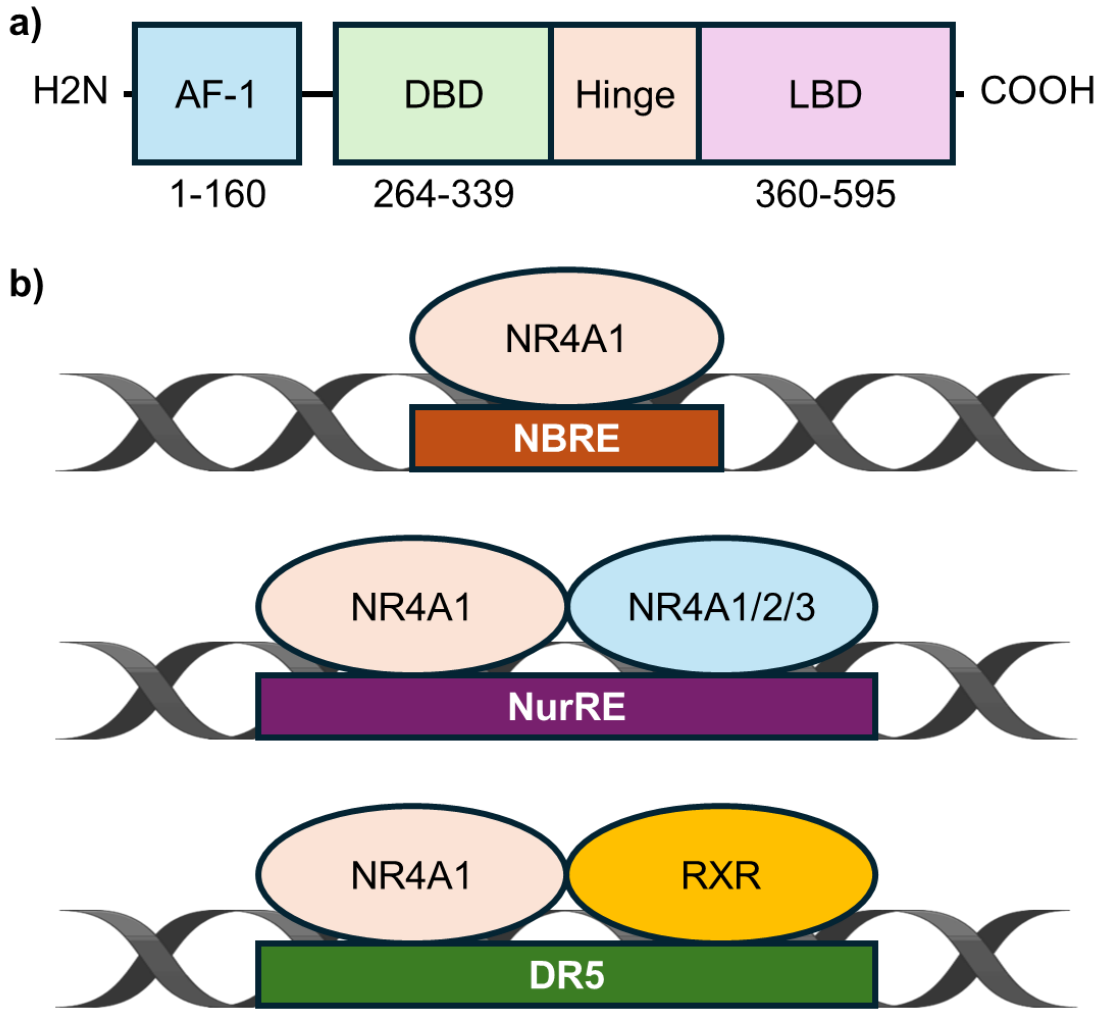

Figure 1.4 NR4A1 structure and binding modes. (**a**) Regions and domains of the human NR4A1 protein, including activation function-1 domain (AF-1), DNA binding domain (DBD), hinge region, and ligand binding domain (LBD). (**b**) NR4A1 DBD binds to different elements within promoter of target genes. It binds as a monomer to NR4A binding element (NBRE), as a homodimer or heterodimer to Nur response element (NurRE), or as a heterodimer with retinoid X receptor (RXR) to direct repeat 5 (DR5). Created with Servier Medical Art images.

The tissue and cellular expression of NR4A1 varies considerably, with documented expression in immune cells, neurons, fibroblasts and endothelial cells. The regulatory control of NR4A1 involves multiple levels of regulation, including transcriptional activation by various stressors and cytokines, post-transcriptional and post-translational mechanisms that modulate its activity and subcellular localisation[134]. Understanding the multifunctional nature of NR4A1 requires appreciation of its complex domain architecture and the dynamic regulatory mechanisms that control its expression and function across different cellular contexts and tissue types.

1.4.1 Ligand-based modulation and direct binding of NR4A1

Although NR4A1 is classified as an orphan nuclear receptor without an identified endogenous ligand, accumulating evidence suggests that prostaglandin A2 (PGA2) may function as an endogenous ligand for NR4A1, though this remains incompletely characterised in human ACFs[135]. Among the most extensively studied NR4A1 ligands are the cytosporone-B (Csn-B) and structurally related compounds, which were among the first identified small-molecule modulators of NR4A1[138]. These exogenous compounds demonstrate varying affinities and functional outcomes depending on their chemical structure and the cellular context in which they operate. Additionally, bis-indole derived compounds, including 1,1-bis(3'-indolyl)-1-(3,5-disubstitutedphenyl)methane (DIM) analogues have been identified as potent NR4A1 ligands that act as inverse agonists and effectively suppress NR4A1-dependent transcriptional activity[138]. These compounds bind to distinct regions of the NR4A1 LBD, potentially contributing to their selective modulation profiles.

Natural product-derived compounds represent another important category of NR4A1 modulators[138]. Hydroxyflavones, including the well-characterised quercetin and kaempferol, bind the NR4A1 LBD with micromolar affinities and act as antagonists that inhibit NR4A1-

dependent transcription. The binding affinity of these flavonoid compounds is highly dependent on the number and position of hydroxyl groups on the flavone backbone, suggesting that these compounds function as selective NR4A1 modulators[139]. Resveratrol, a polyphenolic phytochemical found in various dietary sources, binds to NR4A1 with a K_D value of 2.4 μM and functions as an NR4A1 antagonist, inhibiting both NR4A1-dependent transactivation and pro-oncogenic functions in cancer cells[140]. These natural compounds offer potential therapeutic opportunities for targeting NR4A1 in disease contexts where receptor antagonism is beneficial.

Computational studies have revealed that NR4A1 possesses multiple ligand-binding sites beyond the classical orthosteric pocket[136]. Molecular dynamics simulations identified a previously undetected binding pocket located remotely from the usual nuclear receptor ligand-binding site, with bis-indole ligands stabilising at this alternate site[136]. This discovery of alternate site modulators expands the therapeutic targeting potential of NR4A1 and suggests that different ligands may exploit distinct mechanisms to modulate NR4A1 function depending on their binding location and interactions with specific amino acid residues.

1.4.2 NR4A1 post-translational modifications (PTMs) and subcellular localisation

Post-translational modifications (PTMs) play a central role in regulating NR4A1 activity, stability, and subcellular localisation[134] (Figure 1.4.2). Phosphorylation represents a critical mechanism for modulating NR4A1 activity. The NR4A1 protein can be phosphorylated by different kinases at different amino acid residues, including Akt at serine 351 (Ser351), c-Jun N-terminal kinase (JNK) at serine 95, MAPK1 at serine 431, which induce its nucleocytoplasmic translocation[141,142]. MAPK1 also induces NR4A1 mitochondrial translocation, where it can exert non-genomic functions in melanoma cells[143].

Ubiquitin-proteasomal degradation constitutes a major mechanism for controlling NR4A1 protein levels and activity. Bruceine A, a natural compound, binds to the LBD of NR4A1 and sterically blocks K48-linked polyubiquitination at lysine 558, and thus, stabilising NR4A1 protein levels and amplifying its transcriptional activity[144]. SUMOylation, the covalent attachment of small ubiquitin-like modifier (SUMO) proteins, represents another critical modification regulating NR4A1 function. Studies reveal SUMOylation of NR4A1 happen at different sites including lysine 101 and lysine 577. SUMOylation regulates NR4A1 half-life, transcriptional activity and translocation[145,146].

NR4A1 possesses both nuclear localisation signals (NLS) and nuclear export signals (NES), enabling dynamic subcellular translocation in response to cellular conditions[134]. Through phosphorylation or SUMOylation at specific sites, NR4A1 alters its subcellular localisation between the nucleus, cytoplasm, mitochondria, and endoplasmic reticulum, with each compartment-specific localisation associated with distinct functional outcomes[147].

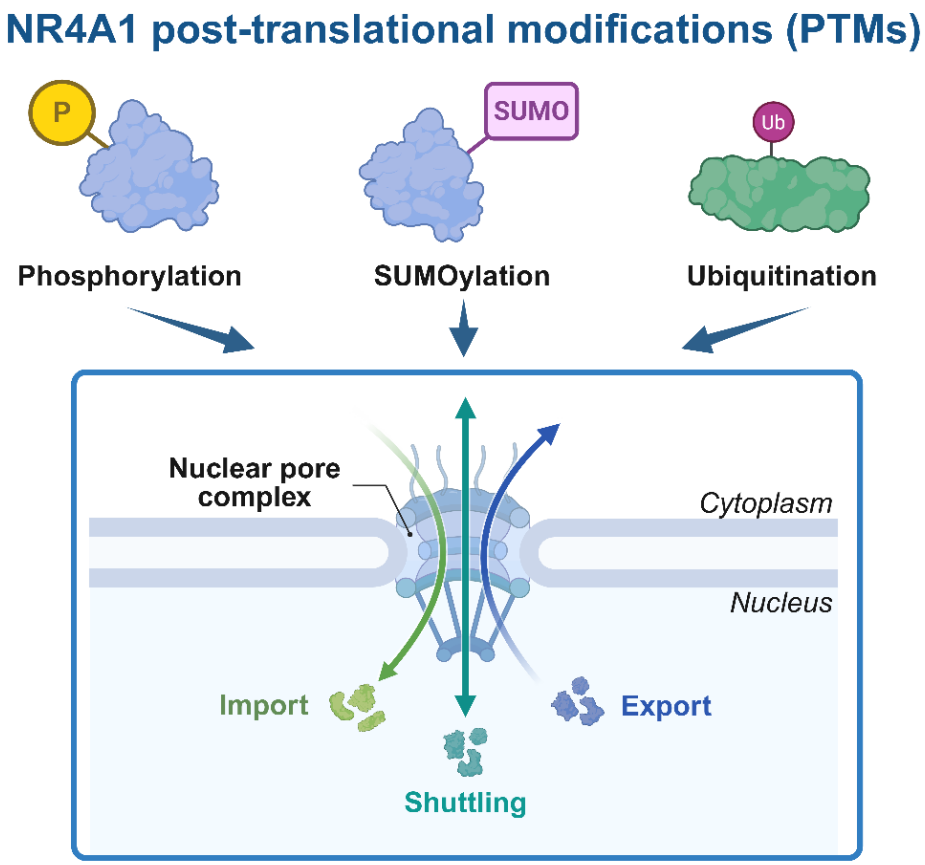

Figure 1.4.2 Schematic illustration of NR4A1 PTMs. Phosphorylation, SUMOylation, and ubiquitination at multiple sites on the NR4A1 protein. Upon these modifications, NR4A1 may undergo subcellular translocation through the nuclear pore complex. Created with BioRender.

1.4.3 Coregulator-mediated modulation of NR4A1

NR4A1 activity is substantially modulated through interactions with coregulatory proteins that either enhance or suppress its transcriptional function[134]. The protein Four and a half LIM domains protein-2 (FHL2) was identified as a novel corepressor of NR4A1 through yeast two-hybrid screen and biochemical analyses[137]. FHL2 binds to multiple domains of NR4A1 in a dose-dependent manner and represses NR4A1 transcriptional activity by inhibiting NR4A1 association with genomic DNA[137]. Short hairpin RNA-mediated knockdown of FHL2 results

in increased NR4A1 transcriptional activity, demonstrating the pivotal role of FHL2 in negative feedback regulation of NR4A1[137]. Glycerol kinase, identified as a nuclear corepressor of NR4A1, interacts with the C-terminal LBD in a manner independent of its enzymatic activity, thereby suppressing NR4A1-dependent gene expression and regulating liver glucose homeostasis[148].

The specificity protein 1 (Sp1) family of transcription factors plays a complex role in NR4A1-mediated gene regulation[149]. Many NR4A1-responsive genes contain GC-rich cis-elements that bind Sp1, Sp3, or Sp4, with NR4A1 directly interacting with these Sp factors to form regulatory complexes that control target gene expression[149]. This NR4A1/Sp protein cooperation extends the regulatory repertoire of NR4A1 beyond its binding to NBRE, NurRE or DR5 sites and allows for cell type-specific and context-dependent regulation of gene expression, including the canonical TGF-β/Smad signalling[150].

1.4.4 Transcriptional functions of NR4A1

In the nucleus, NR4A1 plays a crucial role in regulating gene expression through direct binding to genomic DNA at NBRE, NurRE or DR5 sites and through indirect effects on other transcription factors[134]. The orphan nuclear receptor acts as a transcriptional activator of immediate-early genes that mediate rapid cellular responses to stress signals[135]. NR4A1 target genes include diverse genes involved in cell cycle regulation, apoptosis, inflammation, metabolism, and cell survival.

The role of NR4A1 in cancer demonstrates remarkable context-dependency, functioning as both an oncogenic driver and a tumour suppressor depending on cancer type[135]. In many solid

tumours including lung cancer, pancreatic cancer, melanoma and breast cancer, NR4A1 exhibits pro-oncogenic activity by promoting cell proliferation, survival, and metastasis through multiple signalling pathways, including p300/Sp1-mediated transcription, mechanistic target of rapamycin signalling, TGF-β signalling, and VEGF-A regulation[151]. In breast cancer, NR4A1 directly interacts with the transcription factor c-Fos and competitively inhibits c-Fos binding to the peroxiredoxin 6 promoter[152]. In contrast, NR4A1 exhibits tumour suppressor activity in triple-negative breast cancer, with ectopic expression of NR4A1 reducing cell proliferation and invasion through a downregulated JNK1-AP-1-cyclin D1 signalling pathway[153].

NR4A1 plays an essential role in metabolic diseases, acting as a key transcriptional regulator of genes involved in carbohydrate and lipid metabolism in hepatic gluconeogenesis and influencing energy homeostasis and insulin secretion in adipose tissue and pancreatic β-cells[154]. The immunological functions of NR4A1 are equally diverse, with the receptor modulating the balance between inflammatory and immunosuppressive functions across multiple immune cell types[155].

1.4.5 Non-transcriptional and non-genomic functions of NR4A1

Beyond its well-characterised nuclear transcriptional functions, NR4A1 exerts profound effects through non-genomic mechanisms (Figure 1.4.5). It localises to the mitochondria and endoplasmic reticulum to regulate autophagic cell death and apoptosis through the interaction with proteins including Nix, B cell/chronic lymphocytic leukaemia lymphoma 2, and translocon-associated protein subunit γ[134]. NR4A1 also regulates mitochondrial bioenergetics in cardiac hypertrophy and myocardial ischaemia-reperfusion injury models through the control of mitochondrial fission and mitophagy[156,157].

NR4A1 localisation in the cytoplasm regulates inflammatory responses through the binding with cytoplasmic lipopolysaccharide (LPS), resulting in the activation of non-canonical NLRP3 inflammasome[158]. Cytoplasmic NR4A1 also interacts with hypoxia-inducible factor-1α (HIF-1α) and β-catenin and regulates proteasomal degradation of these targets[147]. In addition to protein stability, recent studies show that cytoplasmic NR4A1 functions as an RNA-binding protein to regulate mRNA stability, specifically the destabilisation of *Tnf* mRNA in microglia, to modulate ischaemic stroke outcomes[159].

NR4A1 represents a unique and highly multifunctional nuclear receptor whose complexity extends far beyond classical ligand-dependent transcriptional regulation. Given NR4A1's emerging role in regulating fibrotic responses through different mechanisms, targeted NR4A1 modulation represents a promising therapeutic strategy for fibrotic diseases, warranting detailed investigation of NR4A1's specific contributions to cardiac fibrosis in AF.

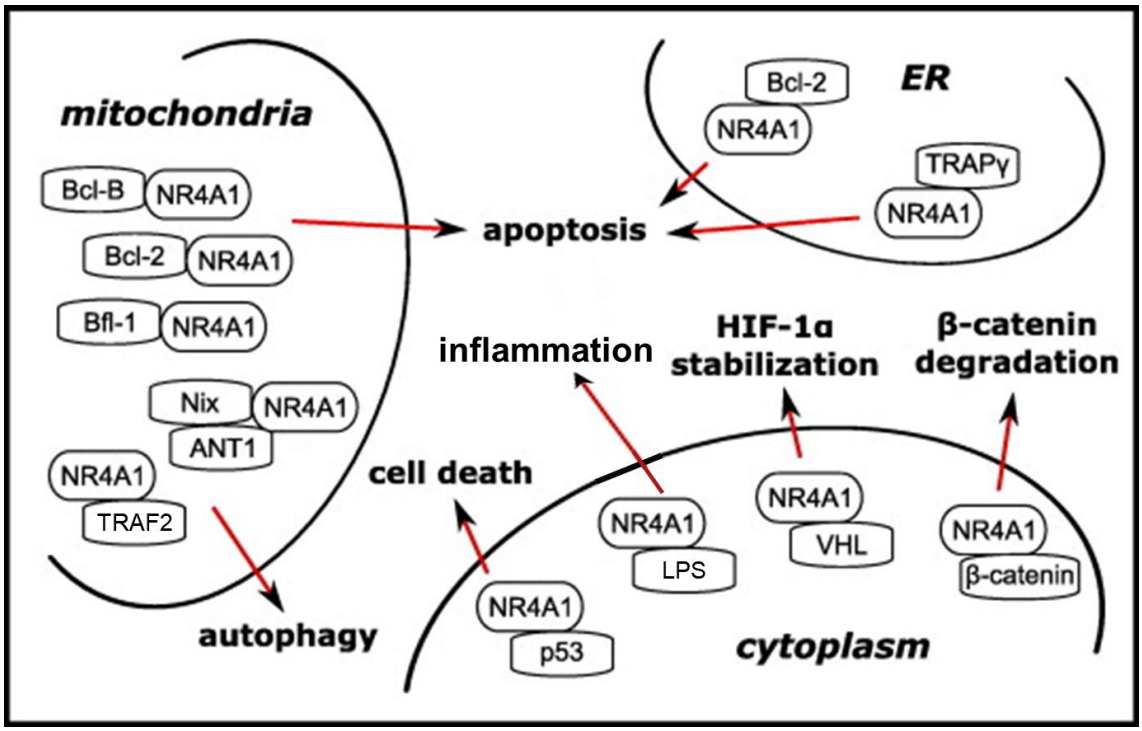

Figure 1.4.5 Schematic summary of non-transcriptional functions of NR4A1. NR4A1 interacts with non-nuclear protein-binding partners across different subcellular compartments to promote different biological functions. Adapted and modified from the study conducted by Pawlak, Strzadala and Kalas, 2015[147].

1.5 Regulation of Fibrosis by NR4A1

1.5.1 The role of NR4A1 in cardiac fibrosis

NR4A1 exerts both pro- and anti-fibrotic functions in preclinical studies. NR4A1 plays a pro-fibrotic role in cardiac fibrosis by regulating TGF-β signalling[160,161]. It promotes differentiation of cardiac fibroblasts into myofibroblasts, enhances collagen production, and accelerates cell proliferation and migration. Deletion of NR4A1 prevented angiotensin II-induced cardiac fibrosis and maintained normal cardiac function in mice[160]. In this model a macrophage-fibroblast crosstalk has been implied, where NR4A1 deletion prevents the angiotensin II-induced pro-inflammatory phenotype in macrophages and drives a shift towards anti-inflammatory phenotype. Moreover, a study demonstrates that isoprenaline-induced mouse model of myocardial fibrosis is dampened by bellidifolin through blocking TGF-β1 signalling and inhibiting NR4A1 cytoplasmic localisation[162]. In contrast to fibroblasts, NR4A1 also exhibits an anti-fibrotic function in cardiomyocytes by inhibiting paracrine TGF-β-mediated fibroblast differentiation[161].

In addition to TGF-β signalling, recent studies have implicated NR4A1 in cardiac fibrosis through distinct signalling pathways. One of the well-characterised pathways involves polypyrimidine tract binding protein 1, which acts as a pro-fibrotic mediator in cardiac fibrosis by destabilising NR4A1 mRNA and suppressing expression of fatty acid-binding protein[163]. The destabilisation of NR4A1 mRNA increases the proliferative capacity and collagen production in cardiac fibroblasts, suggesting the maintenance of sufficient NR4A1 expression is protective against cardiac fibrosis. Another mechanism involves the Creb5/NR4A1 axis in a mouse transverse aortic constriction (TAC) heart failure model, in which semaglutide ameliorates cardiac fibrosis through downregulating cAMP Responsive Element Binding Protein 5/NR4A1 expression and activation[164]. Additionally, in the same model, semaglutide

suppresses TAC-induced upregulation of NR4A1 expression and mitochondrial translocation, maintaining the metabolic homeostasis and it ameliorates the pathological remodelling in the heart. In a post-myocardial infarction model, kallistatin suppresses cardiac fibrosis through NR4A1 activation, followed by downregulation of enolase expression[165]. NR4A1 also targets EndMT in a myocardial infarction mouse model[166]. In this context, NR4A1 reduces cardiac fibrosis through inhibiting NF-κB-induced EndMT.

1.5.2 The role of NR4A1 in non-cardiac fibrotic diseases

NR4A1 has emerged as a complex and context-dependent regulator of fibrosis whose function varies substantially across organ systems and cellular context.

Renal fibrosis – Studies suggest that NR4A1 has opposing roles in regulating renal fibrosis. In age-associated renal tubulointerstitial fibrosis, NR4A1 exhibits anti-fibrotic effects by inhibiting TGF-β/Smads signalling in age-associated renal tubulointerstitial fibrosis[167] and unilateral ureteral obstruction (UUO)-induced renal fibrosis[168]. However, NR4A1 promotes renal through the PI3K/AKT pathway fibrosis in high glucose-activated HK-2 cells (human proximal tubular cell line)[169], and through p38 MAPK kinase phosphorylation in UUO mouse model[170]. Thus, the role of NR4A1 in renal fibrosis appears to be dependent on disease aetiology.

Dermal fibrosis – NR4A1 consistently demonstrates anti-fibrotic and protective properties in dermal fibrosis. Findings suggest that NR4A1 acts as an endogenous inhibitor to downregulate TGF-β signalling in patients with systemic sclerosis, a disease characterised by severe cutaneous fibrosis[150]. NR4A1 agonist promotes the conversion of inflammatory Ly6C^{high}

monocytes to non-inflammatory Ly6C^{low} monocytes through the NR4A1/interferon stimulated gene 12 axis, resulting in reduced dermal fibrosis[171]. Transcriptional analysis further reveals *NR4A1* expression is significantly downregulated in conventional dendritic cells from patients with systemic sclerosis[172].

Intestinal and hepatic fibrosis – Similar to dermal fibrosis, NR4A1 functions as a negative regulator of fibrosis in intestinal and hepatic fibrosis. In a Crohn's-like ileitis mouse model, NR4A1 inhibits intestinal fibrosis that is marked by reduced overall ECM deposition[173]. NR4A1 agonist treatment reduces TGF-β-induced collagen production and cell proliferation in human intestinal myofibroblasts[173]. Furthermore, hepatic fibrosis is marked by activation and EMT of hepatic stellate cells (HSCs)[174], in which these pathological events are inhibited by NR4A1 activation through the TGF-β-Smad2/3/4- Zinc finger E-box-binding homeobox signalling[175]. The regulatory effect on TGF-β signalling by NR4A1 in hepatic fibrosis has also been demonstrated in another study with an established mouse model of glucagon-like peptide-2-treated sclerosing cholangitis[176].

In addition to the mechanisms described above, the NR4A1 regulation on fibrosis is also described in lung diseases, vocal fold injury and ovarian endometriosis[177–179]. However, they are beyond the scope of my current work. The regulatory role of NR4A1 in fibrosis is summarised in Figure 1.5.

Together, the diverse and organ-specific roles of NR4A1 in fibrotic disease underscore its importance as a regulatory mediator. However, its specific role in atrial fibrosis and AF remains incompletely understood, providing the rationale for its focused investigation in my work.

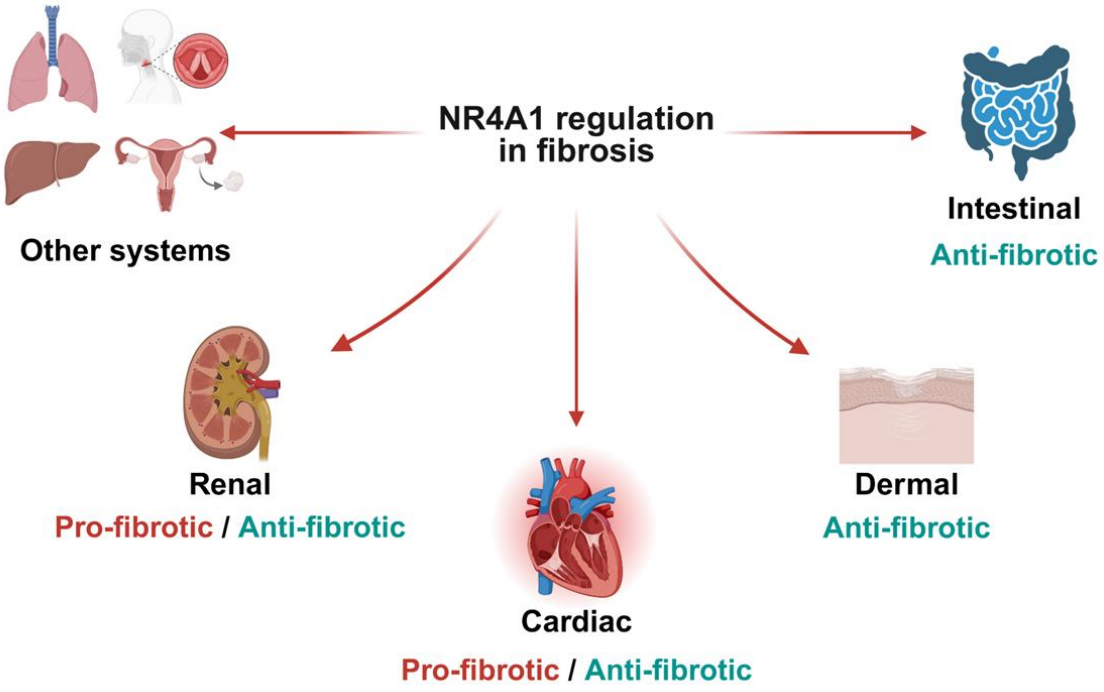

Organ/system	Role in fibrosis	Signalling pathways/mechanisms
Cardiac	Pro- / Anti-	• TGF-β • Ang II-induced inflammation • PTBP1/NR4A1/FABP5 • Creb5/NR4A1 • KS/NR4A1/ENO1 • NF-κB-induced EndMT
Renal	Pro- / Anti-	• TGF-β/Smads • PI3K/AKT • p38 MAPK phosphorylation
Dermal	Anti-	• TGF-β • $Ly6C^{high}$ to $Ly6C^{low}$ monocyte
Intestinal	Anti-	• TGF-β
Hepatic	Anti-	• TGF-β-Smad/2/3/4-ZEB

Figure 1.5 Schematic summary of the regulatory role of NR4A1 in fibrotic diseases. Signalling pathways and mechanisms associated with NR4A1 in different fibrotic diseases are listed, with a specific focus on cardiac fibrosis (highlighted in red) in my current work. Created with BioRender.

1.6 Hypothesis and Aims of the Project

Existing pharmacological therapies for AF have limited efficacy and are associated with complications and high recurrence rates. The remodelled atria in chronic stages of AF, including persistent AF, display progressive degree of fibrosis that hampers the successful AF treatment and clinical management. Given the emerging evidence showing the diversity and complexity of cardiac fibroblast roles and functions in the human heart, there is a clear unmet need for a better understanding of the molecular mechanisms of persistent AF to advance novel molecular-based therapeutic approaches.

While our previous findings identified a NR4A1-enriched fibroblast subpopulation in the human left atria, it remains uncertain whether NR4A1 may impact the functional responses of human ACFs and how the associated molecular changes may contribute to the persistent AF pathophysiology.

Overall hypothesis: Regulation of NR4A1 may impact on the function of human ACFs and determine the biological relevance of NR4A1 in persistent AF.

Project aims:

Aim 1: To investigate the effects of NR4A1 on fibrotic responses in human ACFs.

Aim 2: To explore the transcriptional changes regulated by NR4A1 in human ACFs.

Aim 3: To evaluate NR4A1 expression, subcellular localisation and protein interactions in ACFs from patients with persistent AF or controls in sinus rhythm.

CHAPTER 2: MATERIALS AND METHODOLOGY

2.1 Study Design and Tissue Collection

2.1.1 Patient cohort and recruitment

Ethical approval is in place and is granted under the approval by the South Central-Berkshire B Research Ethics Committee (UK, REF: 18/SC/0404). Patients aged between 18 and 85 years old were recruited if they were admitted for an elective cardiac surgery (valve repair/replacement or coronary artery bypass grafting, CABG) at the John Radcliffe Hospital, Oxford. All patients gave written informed consent before enrolment. The disease group in this study is persistent AF, defined as patients with AF episodes for longer than 7 days based on the European Society of Cardiology guidelines[180]. The AF group was compared to the control group, which is patients in sinus rhythm and without AF history. The diagnosis of AF and arrhythmic events were determined according to electronic patient records and electrocardiogram measurements. Demographic and clinical data of the patients enrolled to this study were extracted from the NHS electronic system by qualified clinicians and researchers delegated to this study. Data collection included age, sex, body mass index, medical history, and medications.

2.1.2 Collection of cardiac biopsies

Low Ca^{2+} solution (LCS) was prepared according to the components listed in Table 2.1.2 and diluted in distilled water. After filtering with sterile 33 mm membranes with 0.2 μm pore size (#15206869, Fisher Scientific, US), LCS was stored at 4°C for one month. Tissue biopsies from the left atrial appendage were provided by the surgeons in the operation theatre, collected in 50 mL conical-based centrifuge tubes with LCS and placed in an ice box. Biopsies were immediately transferred to the laboratory and processed for fibroblast isolation or transferred to 2 mL cryovials for storage at -80°C for long-term use.

Table 2.1.2 Preparation of low Ca^{2+} solution (LCS)

Chemical	Final concentration (mM)	Weight (g) for 1 L solution
NaCl	120	7.01
KCl	1.2	0.75
KH_2PO_4	10	0.16
$MgCl_2$	1.2	0.24
Glucose	10	1.8
HEPES	10	2.4
Taurine	20	2.5

2.2 Cell Isolation and Culture

2.2.1 Human ACF isolation

Human ACF isolation was performed in tissue culture hood according to previous protocol[78] (Figure 2.2.1). In brief, 0.1% bovine serum albumin (BSA) solution (#A7906-100G, Sigma-Aldrich, US) was prepared fresh for every isolation, diluted in LCS and filtered through sterile 33 mm membranes with 0.2 μm pore size. Left atrial appendage biopsies were placed on a petri dish to remove fat, staples or necrotic areas. Tissues were cut into small pieces (~ 2 mm^3) and washed with approximately 10 mL of LCS in a 50 mL conical-based centrifuge tube. The tube with minced tissues was placed on a water bath with shaking at 37°C for 10 min. LCS was discarded and tissues were digested twice at 37°C for 10 min with 10 mL of enzyme solution 1 (2 mg/mL collagenase type V [#C9263-1G] and 0.2 mg/mL protease type XIV [#P5417-1G] in 0.1% BSA; Sigma-Aldrich, US). The enzyme solution 1 was discarded and replaced with 10 mL of enzyme solution 2 (2 mg/mL collagenase type V in 0.1% BSA). After shaking the digested tissues at 37°C for 12 min, supernatant was discarded and incubated with 5-10 mL of diluted enzyme solution 2 (1:1 dilution with LCS) at 37°C for 9 min. Supernatant was collected and the tissue digestion with diluted enzyme solution 2 was repeated up to six times. After collection of all supernatants (containing fibroblasts), the solution was centrifuged at 700 rpm for 5 min to pellet cardiomyocytes. Supernatant was collected to a new tube and further centrifuged at 2000 rpm for 10 min. Finally, supernatant was discarded and the cell pellet was resuspended in 1 mL of FBM-3 Cardiac Fibroblast Growth Medium with 10% foetal bovine serum (FBS) and supplements (#CC-4526, Lonza, Switzerland). Cell suspension was transferred to a 6-well plate and incubated at 37°C and 5% CO_2 for overnight. Fresh growth media (2 mL) was replaced the next day, and cells were left in the incubator to grow.

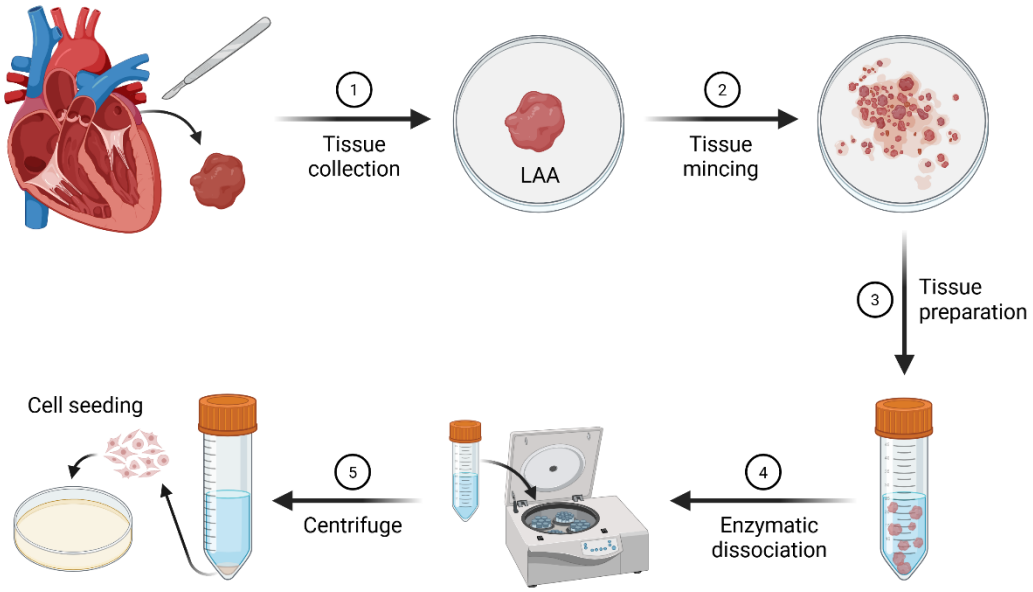

Figure 2.2.1 Schematic representation of human ACF isolation protocol. Left atrial appendage (LAA) biopsies were minced into small pieces, followed by enzymatic digestion. After centrifugation, fibroblast cell pellet was resuspended in fresh growth medium. Cells were seeded on cell culture plates to grow. Created with BioRender.

2.2.2 Cell culture

Primary human ACFs isolated from patient atrial biopsies and commercially available human ACFs (#CC-2903, Lonza, Switzerland) were cultured under identical conditions to ensure experimental consistency. Clinical and demographic characteristics of human ACFs from Lonza are summarised in Table 2.2.2. The source of human ACFs (patient donors or Lonza) for each experiment is indicated in the corresponding text and figure legends.

Human ACFs were cultured in a humidified incubator at 37°C and 5% CO_2 to provide physiological culture conditions and replenished with pre-warmed fresh growth medium every 2-3 days. Cells were routinely monitored under microscope to assess morphology, cell attachment and confluency. Once cells reached 80-90% confluency, they were passaged to prevent contact inhibition. ACFs were gently washed once with 1X Phosphate-buffered saline (PBS) to remove residual FBS proteins that could inhibit trypsin activity, followed by treating with 0.25% trypsin-ethylenediaminetetraacetic acid (EDTA) (1X) (#25200-056, Gibco, US) at 37°C for 5 min until cell detachment was observed under microscopic examination. To limit the culture-induced phenotypic drift and preserve the biological characteristics of primary fibroblasts, only early passage ACFs (P1-P5) were used for all experiments unless specified. Cell seeding densities and any modifications to the standard culture conditions are described within the specific experimental sections.

Table 2.2.2 Clinical and demographic characteristics of commercially available human ACFs from Lonza

Characteristics	Total (*N*=8)
Age, years (SD)	54.9 (12.1)
Sex, male (%)	4 (50)
Body mass index, kg/m^2 (SD)	32.9 (7.5)
Race (%) Caucasian Hispanic	 6 (75) 2 (25)
Diabetes mellitus (%)	1 (13)
Smoking (%)	5 (63)

2.3 Transfection and siRNA-Knockdown

For gene silencing of specific targets, small interfering RNA (siRNA)-mediated knockdown was performed in ACFs. ACFs were plated at 10,500 cells/cm^2 in 6-well plates. Prior to transfection, once cells reached 60-80% confluency, the culture medium was aspirated and replaced with FBM-3 antibiotic-free medium for 2 hours for serum starvation to minimise potential interference of antibiotics with transfection efficiency. ON-TARGETplus SMARTPool siRNA and ON-TARGETplus Non-targeting siRNA were prepared from a stock concentration of 20 μM and diluted to a final working concentration of 50 nM in RNase-free water for each transfection (listed in Table 2.3; all from Horizon Discovery, UK). Cells transfected with ON-TARGETplus Non-targeting siRNA served as the negative control for all knockdown experiments.

For transfection complex preparation, Lipofectamine RNAiMAX Transfection Reagent (#13778150, Invitrogen, US) and the siRNA were each diluted separately in Opti-MEM medium (#31985062, Gibco, US) according to the manufacturer's instruction. The diluted lipofectamine and siRNA solutions were then gently mixed and incubated at room temperature for 5 min. Following incubation, the lipofectamine-siRNA complexes were added to the cells, and the plates were incubated at 37°C for 24 or 48 hours. After transfection, knockdown efficiency was validated via measuring both gene and protein expression levels of the target.

Table 2.3 Details of siRNA for knockdown experiments

Target	**Catalogue #** **(Horizon Discovery, UK)**
Non-targeting	L-004734-00-0005
ON-TARGETplus SMARTPool Human ITGB1 siRNA	L-004506-00-0005
ON-TARGETplus SMARTPool Human NR4A1 siRNA	L-003426-00-0005
ON-TARGETplus SMARTPool Human NUP214 siRNA	L-011980-00-0005
ON-TARGETplus SMARTPool Human TKT siRNA	L-004734-00-0005

2.4 Reverse Transcription-quantitative Polymerase Chain Reaction

2.4.1 RNA isolation

ACFs were plated at 10,500 cells/cm^2 in 6-well plates for RNA extraction. Total RNA isolation was performed using the mirVana miRNA Isolation Kit (#AM1561, Invitrogen, US) according to the manufacturer's instruction. Cells were washed with 1X PBS and lysed in 300 µL of Lysis/Binding Buffer for each well of the 6-well plates. Lysed solutions were transferred to Eppendorf tubes and stored at -20°C or immediately proceeded with RNA extraction. 30 µL of miRNA Homogenate Additive was added to each cell lysate tube and vortexed. The solutions were kept on ice for 10 min, followed by mixing with 300 µL of Acid-Phenol:Chloroform in the fume hood. After pulse vortexing, centrifuge the tubes at 10,000 g at room temperature for 5 min for the layer separation. The upper (aqueous) phase was carefully removed by pipetting and transferred to a new Eppendorf tube. 375 µL of 100% ethanol was added to the tubes and mixed gently. The mixture was transferred to a Collection Tube with the Filter Cartridge from the kit. Samples were centrifuged at 10,000 g at room temperature for 15 seconds. Flow-through was discarded, and 700 µL of Wash Solution 1 was added to the Filter Cartridge. Tubes were centrifuged at 10,000 g at room temperature for 15 seconds, followed by two washes with 500 µL of Wash Solution 2/3. After aspirating final flow through, tubes were centrifuged at 10,000 g for 1 min to ensure the removal of residual fluid in the filter. Finally, the filter cartridge was transferred to a new collection tube. 30 µL of pre-heated (95°C) nuclease-free water was added to the filter and centrifuged at 10,000 g for 30 seconds to collect the RNA solution. RNA concentration was measured using the LVis Plate (BMG LABTECH, Germany), and the RNA purity was checked based on 260/280 and 260/230 ratios. Extracted RNA samples a were stored at -20°C.

2.4.2 Reverse transcription-quantitative polymerase chain reaction (RT-qPCR)

Complementary DNA (cDNA) was prepared by reverse transcription (RT) of using the QuantiTect Reverse Transcription Kit (#205311, Qiagen, Germany). Genomic DNA (gDNA) elimination was first performed by preparing the following reaction mix: 2 µL of 7X gDNA Wipeout Buffer and 12 µL of RNA template (100 ng diluted in RNase-free water). Samples were incubated at 42°C for 2 min and then kept on ice for 5 min. Subsequently, each RT reaction mix was prepared and composed of the following components: 14 µL of template RNA (from gDNA elimination step), 4 µL of 5X Quantiscript RT Buffer, 1 µL of Quantiscript Reverse Transcriptase and 1 µL RT Primer Mix. Tubes were placed on the Tetrad thermal cycler (Bio-Rad, US) and incubated at 42°C for 15 min, followed by the inactivation of Reverse Transcriptase at 95°C for 3 min. Once RT reactions were completed, tubes with cDNA templates were stored at -20°C.

Quantitative polymerase chain reaction (qPCR) was completed using 2X TaqMan Fast Advanced Master Mix (#4444557, Applied Biosystems, US) and 20X TaqMan Assays (listed in Table 2.4.2) for specific targets. The reaction mixes and cDNA templates (10 ng cDNA per reaction) were loaded to a 96-well fast plate in 10 µL per well in duplicates for each sample. PCR reaction was performed using the QuantStudio 7 Flex Real-Time PCR System (Applied Biosystems, US) with the following conditions: (1) Polymerase activation hold at 95°C for 20 seconds, followed by (2) 40 cycles of PCR reaction composed of denaturation at 95°C for 1 second per cycle and annealing/extension at 60°C for 20 seconds per cycle. Gene expression was quantified using the $2^{-\Delta Ct}$ method[181] and normalised to housekeeping genes (specified in the figures). ΔCt was calculated as the difference between the cycle threshold (Ct) value of the target gene and the housekeeping gene ($\Delta Ct = Ct_{target} - Ct_{housekeeping}$). Relative gene expression values were calculated as $2^{-\Delta Ct}$. The expression of the selected housekeeping genes was stable

across experimental conditions and was therefore suitable for normalisation of target gene expression.

Table 2.4.2 Details of TaqMan assay probes

Target transcript		TaqMan assay IDs
Housekeeping genes	Human *ACTB*	Hs01060665_g1 (VIC)
	Human *GAPDH*	Hs02786624_g1 (VIC)
	Human HPRT1	Hs02800695_m1 (VIC)
	Human *18S*	Hs99999901_s1 (VIC)
Target genes	Human *ACTA2*	Hs00426835_g1 (FAM)
	Human *COL1A1*	Hs00164004_m1 (FAM)
	Human *COL3A1*	Hs00943809_m1 (FAM)
	Human *FN1*	Hs01549976_m1 (FAM)
	Human *IL1B*	Hs01555410_m1 (FAM)
	Human *IL6*	Hs00174131_m1 (FAM)
	Human *ITGB1*	Hs01127536_m1 (FAM)
	Human *NR4A1*	Hs00374226_m1 (FAM)
	Human *NUP214*	Hs01090086_m1 (FAM)
	Human *POSTN*	Hs01566750_m1 (FAM)
	Human *TKT*	Hs01115545_m1 (FAM)

2.5 Western Blot

2.5.1 Protein extraction

Human ACFs were plated at 10,500 cells/cm^2 and cultured in 6-well plates for protein extraction. Protein lysis buffer was prepared by adding one cOmplete protease inhibitor cocktail tablet (#5892791001, Roche, Switzerland) and one PhosSTOP tablet (#4906837001, Roche, Switzerland) to 10 mL of CelLytic M reagent (#C2978-250ML, Sigma-Aldrich, US). The solution was vortexed thoroughly until the tablets were fully dissolved and stored at 4°C. To extract intracellular proteins, cells were washed with 1X PBS and lysed in 200 µL of lysis buffer using a cell scraper. Lysates were kept on ice for 15 min and then centrifuged at 10,000 g at 4°C for 15 min to remove insoluble debris. The cleared supernatant was collected, transferred to a new tube and stored at -20°C. Protein concentration was measured by the bicinchoninic acid (BCA) assay using the Pierce BCA Protein Assay Kit (#23227, Thermo Fisher Scientific, US) according to manufacturer's protocol. Standards were diluted in the lysis buffer, and reactions for the standards or samples were measured in technical duplicates in a clear 96-well plate. After incubating at 37°C for 30 min, the plate was cooled down at room temperature and absorbance was measured at 562 nm using a microplate reader (BMG LABTECH, Germany).

2.5.2 Gel electrophoresis and western blotting

Proteins were diluted in lysis buffer to obtain equal amounts of protein for all samples. Each sample was prepared as following: equal amounts (5 µg) of protein in 20 µL was mixed with 5 µL of 4X NuPAGE LDS Sample Buffer (#NP0007, Invitrogen, US) and 2 µL of 10X NuPAGE Sample Reducing Agent (#NP0009, Invitrogen, US), followed by heating at 95°C for 5 min. Amersham ECL Rainbow Full range Marker (#RPN800E, Cytiva, US) was used as the molecular weight marker. Protein marker (8 µL) or 20 µL of protein lysate was loaded to each

well and separated using the 4-12% NuPAGE Bis-Tris gels (#NP0335BOX) with 1X NuPAGE MOPS SDS Running Buffer (#NP0001) (all from Invitrogen, US) at constant 170 V for 1 h until dye front reached bottom of the gel. Proteins were then transferred by wet or dry approaches. Wet transfer was performed by assembling the sandwich stacked with gel, nitrocellulose 0.2 μm membrane, filter papers and sponges within the cassette. The cassette was then placed in the transfer tank filled with 1X NuPAGE Transfer Buffer (#NP00061, Invitrogen, US). Current was applied at 230 mA at 4°C for 1.5 h. Dry transfer was completed using the iBlot 2 Dry Blotting System and nitrocellulose transfer stacks (#IB23001) (all from Invitrogen, US). Transfer was conducted at 20A at 4°C for 7 min.

After transfer, membranes were stained with Ponceau S (#A40000279, Thermo Scientific, US) and rinsed with water for quick detection of protein bands and confirmation of the transfer efficiency. 1X PBS-T wash buffer (0.1%) was prepared adding 1 mL of Tween 20 to 1 L 1X PBS. Membranes were washed with 1X PBS-T, followed by blocking with 5% skimmed milk in 1X PBS-T at room temperature for 45 min. To perform immunodetection for specific proteins, membranes were incubated with primary antibodies (listed in Table 2.5.2) with gentle rocking at 4°C for overnight. Primary antibodies were diluted in 5% milk in 1X PBS-T. Subsequently, membranes were washed three times with 1X PBS-T with gentle rocking at room temperature for 15 min per wash. Horseradish peroxidase (HRP)-conjugated secondary antibodies (listed in Table 2.5.2) were added for incubation at room temperature for 1 h. Secondary antibodies were diluted in 5% milk in 1X PBS-T. Three 1X PBS-T washes were performed to remove unbound secondary antibodies. SuperSignal West Dura (#34076, Thermo Scientific, US) and West Femto (#34096, Thermo Scientific, US) Enhanced Chemiluminescence (ECL) substrates were added on top of the membrane, followed by the detection of chemiluminescence using the ChemiDoc Imaging System (Bio-Rad, US). Band intensities were quantified using the Image Lab Software (Bio-Rad, US). Target protein was

normalised to the corresponding housekeeping protein detected on the same membrane. The expression of the selected housekeeping protein was stable across experimental conditions and was therefore used as a loading control for normalisation.

Table 2.5.2 Details of antibodies for western blot

Antibodies		Manufacturer	Catalogue #	Host	Dilution
Primary	αSMA	Sigma-Aldrich, US	A5228	Mouse	1:1000
	β-tubulin	ABclonal, US	AC021	Mouse	1:5000
	Calpain 1	Proteintech, US	10538-1-AP	Rabbit	1:1000
	Collagen 1	Sigma-Aldrich, US	234167	Rabbit	1:2000
	Collagen 1α2	Proteintech, US	14695-1-AP	Rabbit	1:1000
	Collagen 3α1	Novus Biologicals, US	NBP2-15946	Rabbit	1:1000
	Fibronectin	Sigma-Aldrich, US	F3648	Rabbit	1:2000
	GAPDH	Sigma-Aldrich, US	G9295	Mouse	1:4000
	GAPDH	Sigma-Aldrich, US	ABS16	Rabbit	1:5000
	Histone H3	ABclonal, US	A17562	Rabbit	1:1000
	Integrin β1	Proteintech, US	12594-1-AP	Rabbit	1:5000
	Lamin A/C	Proteintech, US	10298-1-AP	Rabbit	1:5000
	N-cadherin	Proteintech, US	22018-1-AP	Rabbit	1:2000
	NR4A1	Invitrogen, US	MA5-32647	Rabbit	1:500
	NR4A1	Proteintech, US	25851-1-AP	Rabbit	1:500
	Nucleoporin 214	Invitrogen, US	PA5-114371	Rabbit	1:250
	Periostin	Cell Signaling Technology, US	91771S	Rabbit	1:1000
	Phospho-NR4A1 (Ser351)	Cell Signaling Technology, US	5095S	Rabbit	1:1000
	Transkelotase	Proteintech, US	11039-1-AP	Rabbit	1:2000

	Vimentin	Novus Biologicals, US	NBP1-97672	Mouse	1:250
Secondary	Anti-Rabbit IgG (H+L), HRP Conjugate	Promega, US	W4011		1:2000 (WB) 1:20000 (co-IP)
	Anti-Mouse IgG (H+L), HRP Conjugate	Promega, US	W4021		1:2000

2.6 Immunostaining

2.6.1 Sample preparation

Human ACFs were plated at 5,000 cells in each well of a sterilised microscope glass slide with removable 8-well chamber (#80841, ibidi, Germany) for immunostaining. Cells were allowed to adhere on the glass slide overnight before fixation. After cells were attached, they were fixed with ice cold (-20°C) methanol-acetone (1:1, v/v) solution for 5 min as previously described[78]. The wells were washed with 1X PBS twice (5 min each) and kept at 4°C for short-term storage for up to one week or immediately proceeded with immunostaining.

2.6.2 Immunocytochemistry

Fixed cells were blocked with serum-free blocking reagent (#X090930-2, Agilent, US) at room temperature for 1 hour, followed by incubation with primary antibodies (listed in Table 2.6.2, diluted in blocking buffer) at 4°C for overnight. After washing twice with 1X PBS (5 min each), cells were incubated with Alexa Fluor-488/-594-conjugated secondary antibodies (listed in Table 2.6.2, diluted in blocking buffer) at room temperature for 4 h and protected from light. The wells were rinsed with 1X PBS for twice (5 min each). Cells were counterstained with phalloidin for 20 min (protected from light) to visualise cell cytoskeleton by staining filamentous actin (F-actin). After removing the 8-well chamber from the glass slide, slides were mounted with SlowFade Gold Antifade Mountant with DAPI (#S36939, Invitrogen, US). A coverslip was placed on top of the slide and edges were sealed with nail polish. The slide was then incubated at room temperature for 30 min. Cells were imaged using the Leica DM 6000 CFS confocal microscope equipped with a 63x oil immersion objective. Images were acquired using identical laser power (30%) and acquisition settings for all samples within each

experiment to allow comparison of fluorescence signals. Images were taken from a minimum of three fields per well.

Quantification of the percentage of non-nuclear NR4A1 per cell was performed using the Fiji software. Individual cells were selected for analysis only if they were fully contained within the field of view and did not overlap with neighbouring cells. For each selected cell, the cell boundary was manually delineated using the F-actin (phalloidin) image, while the nuclear boundary was manually outlined using the corresponding DAPI image. The whole-cell and nuclear regions were saved as regions of interests (ROIs) and subsequently applied to the corresponding NR4A1 fluorescence image. The NR4A1 fluorescence image was converted to a binary image using the Otsu thresholding method to distinguish positive NR4A1 signal from background. The same thresholding method and analysis parameters were applied consistently to all images to ensure unbiased comparison between experimental groups. The previously generated whole-cell and nuclear ROIs were then overlaid onto the thresholded NR4A1 image. Fiji histogram function was used to determine the number of NR4A1-positive pixels within each ROI. The percentage of non-nuclear NR4A1 per cell was calculated using the following equation:

$$\%\ of\ non\ nuclear\ NR4A1\ per\ cell = \frac{whole\ cell\ NR4A1\ pixel\ count - nuclear\ NR4A1\ pixel\ count}{whole\ cell\ NR4A1\ pixel\ count}$$

Table 2.6.2 Details of antibodies for immunostaining

Antibodies		Manufacturer	Catalogue #	Host	Dilution
Primary	Filamin A	Sigma-Aldrich, US	MAB1678	Mouse	1:200
	NR4A1	Invitrogen, US	MA5-32647	Rabbit	1:100
Secondary	Anti-Rabbit IgG (H+L), Alexa Fluor 488	Invitrogen, US	A-21206	Donkey	1:500
	Anti-Mouse IgG (H+L), Alexa Fluor 594	Invitrogen, US	A-21201	Chicken	1:500

2.7 Statistical Analyses

Statistical analysis was performed using GraphPad Prism 10.1.2. Data distribution was determined by Shapiro-Wilk normality test. Outliers were identified using the robust regression and outlier removal method and excluded from subsequent analysis where appropriate.

For unpaired two-group comparisons, Student's t-test was used for normally distributed data, and Mann-Whitney test was used for non-normally distributed data. Paired statistical tests were applied when samples from the same biological donor were subjected to different treatments and treated as matched pairs. For paired normally distributed data, standard paired t-test was applied when analysing normally distributed absolute values between matched samples. When data were expressed as ratios between matched conditions, ratio paired t-test was performed to account for the multiplicative nature of the data. For paired non-normally distributed data, Wilcoxon test was used. Although data from paired experiments are presented in the figures as fold change values relative to the corresponding negative control condition for visualisation purposes, the reported *P*-values were calculated using the raw paired values from matched biological samples prior to transformation into fold changes.

For multiple comparisons within a single independent variable, paired or unpaired one-way analysis of variance (ANOVA) with post hoc test (as specified in the figure legends) was applied for normally distributed data. For non-parametric data, the Kruskal-Wallis test (unpaired data) or the Friedman test (paired data) was performed, followed by the post hoc multiple comparison test where applicable (as specified in the figure legends). For experiments involving two independent variables, two-way ANOVA with post hoc test (as specified in the figure legends) was used.

Associations between two continuous variables were assessed using the Spearman's rank correlation test. Unless otherwise stated, all experiments were performed using a minimum of three independent biological replicates ($N \geq 3$), where N denotes biological replicates and n represents independent technical replicates. Statistical significance was reached when two-tailed P-values were less than 0.05.

CHAPTER 3: EFFECTS OF NR4A1 ON FIBROTIC RESPONSES IN HUMAN ACFs

3.1 Introduction

AF is the most common sustained cardiac arrhythmia and is characterised by rapid, irregular electrical activity in the atria and leading to ineffective contraction[182,183]. A primary driver of AF persistence is atrial structural remodelling, a maladaptive process dominated by fibrosis – the excessive accumulation of ECM proteins. Cardiac fibroblasts are the principal effector cells in this process. Under physiological conditions, these cells maintain the structural integrity of the atrial myocardium. However, in response to pathological stress, they differentiate into a secretory and contractile myofibroblast phenotype. These activated fibroblasts drive the deposition of collagens (type 1 and 3) and other ECM components (like fibronectin, periostin). As a result, it disrupts electrical continuity and creating conduction barriers that favour re-entry circuits. Understanding the molecular mechanisms governing ACF activation is critical for developing targeted therapies to arrest the fibrotic substrates of AF.

Recent advances in multi-omics technologies, particularly single-cell and single-nucleus RNA sequencing (sc/snRNA-seq), have revolutionised our understanding of cardiac fibroblast biology by revealing significant cellular heterogeneity[101,184]. These high-resolution approaches have identified distinct fibroblast subpopulations associated with AF progression[185]. However, validating these transcriptomic findings and dissecting their functional roles remains a challenge due to the difficulty of accessing viable human atrial tissue for *in vitro* assays. While the scarcity of human atrial biopsies has compelled researchers to rely on animal models, these surrogates present significant translational limitations. Rodent cardiac models, for instance, often fail to fully recapitulate the electrophysiological and transcriptional responses of human atrial cells due to interspecies differences in ion channel expression and signalling pathways[186,187]. Therefore, establishing robust human ACF models derived directly from patient biopsies is essential to bridge the gap between omics discovery and clinical translation.

Transcriptomic analysis of human left atrial appendages has recently identified three distinct fibroblast subtypes[132]. While two of these correspond to well-characterised normal and activated phenotypes, the third subtype remains poorly defined and is distinguished by an inflammatory gene signature from pathway analysis. The nuclear receptor NR4A1 has emerged as the top differential marker for this unique fibroblast subpopulation. NR4A1 is a known regulator of fibrosis in various organs. Yet its specific role in cardiovascular disease remains controversial. In non-cardiac tissues, such as the liver and skin, NR4A1 has been reported to exert antifibrotic effects by inhibiting TGF-β signalling[150,173]. Conversely, in the context of cardiovascular disease – such as myocardial infarction and hypertrophy – NR4A1 function appears to be context-dependent[165,166,188]. To date, only one study has specifically linked NR4A1 to AF, suggesting it plays a role in atrial remodelling[189]. However, the mechanistic understanding of NR4A1 in cardiac fibroblasts is largely derived from studies on ventricular fibroblasts isolated from rodent models. Recent findings indicate that NR4A1 promotes a pro-fibrotic phenotype in mouse- and rat-derived ventricular fibroblasts in response to stimuli such as TGF-β1[160,161]. Given that AF-associated remodelling is primarily in the atria and that atrial and ventricular fibroblasts possess divergent embryological origins and signalling properties[74], these ventricular-derived rodent data may not reflect human atrial pathophysiology. Thus, there is a critical need to investigate the function of NR4A1 specifically within human-derived ACFS to determine its therapeutic potential in AF.

3.1.1 Hypothesis and aims

Hypothesis: NR4A1 may regulate fibrotic responses in human ACFs. The aims of this chapter are as follows:

1. Characterise the effects of NR4A1 deficiency on expression of fibrotic markers and cellular functions in human ACFs
2. Characterise the effects of NR4A1 pharmacological activation on fibrotic responses in human ACFs

3.2 Materials and Methods

The following methods described in this section were used specifically in this chapter.

3.2.1 Cell proliferation assay

Cell proliferation was quantified using the BrdU Cell Proliferation Assay (#QIA58, Sigma-Aldrich, US) as per manufacturer protocol. Briefly, after ACFs were transfected with negative control (NC-siRNA) or NR4A1-siRNA (as described in Section 2.3), cells were trypsinised, plated in 96-well plates in triplicates and cultured in FBM antibiotic-free medium with 10% FBS. At 70-80% confluency, cells were incubated with BrdU at 37°C for 24 hours. After BrdU was incorporated, cells were fixed with Fixative/Denaturing Solution and incubated with anti-BrdU antibody at room temperature for 1 hour. The wells were washed with 1X Wash Buffer for three times, followed by a 30 min incubation with Peroxidase Goat Anti-Moue IgG HRP Conjugate. After washing with 1X Wash Buffer and distilled water, cells were incubated with TMB Substrate Solution in the dark at room temperature for 15 min. Finally, a stop solution was added, and absorbance was measured at 450 nm with a microplate reader (BMG LABTECH, Germany).

3.2.2 Cell migration assay

Cell migration assay was performed using 35 mm µ-dish with a 2-well silicone insert with a defined cell-free gap (#81176, ibidi, Germany). After ACFs were transfected with negative control or NR4A1 siRNA and trypsinised, 5,000 cells were resuspended in 100 µL of 10% FBS-containing antibiotic-free medium and were seeded into each well. Migration dishes were incubated at 37°C for 24 hours, followed by removing the insert when cell confluency reached 95%. Medium (2 mL) was added to the dish, and images were taken at 0 hour, 8 hours, 12 hours

and 24 hours timepoints using a light microscope with 10x magnification. Changes in the cell-free area were analysed and quantified using the Fiji software with Wound healing size tool. Settings were adjusted as follows: “Variance window radius” = 5 “Threshold value” = 100, “Percentage of saturated pixels” = 0.400, “Set Scale global?” = Yes, “The scratch is diagonal??” = No.

3.2.3 TGF-β1 stimulation

TGF-β1 stimulation in human ACFs was performed as previously described[78]. TGF-β1 Recombinant Protein (#100-21, Gibco, US) at 10 ng/mL was diluted from stock concentration of 200 µg/mL in FBM-3 antibiotic-free medium with 0.5% FBS. TGF-β1 was added to the cells with or without NR4A1 siRNA-knockdown (as described in Section 2.3) and incubated at 37°C for 24 hours.

3.2.4 Pharmacological activation of NR4A1

Pharmacological activation of NR4A1 was achieved by treatment with Csn-B. Csn-B (#C2997, Sigma-Aldrich, US) was dissolved in dimethyl sulfoxide (DMSO) to a stock concentration of 20 mg/mL and further diluted in FBM-3 antibiotic-free medium with 0.5% FBS to reach a final concentration for treatment in human ACFs. Csn-B was added to the cells with or without 10 ng/mL TGF-β1 stimulation and incubated at 37°C for 24 hours. Cell viability was checked after treatment before proceeding with downstream experiments.

3.3 Results

3.3.1 NR4A1 siRNA knockdown reduces NR4A1 expression

I confirmed the expression of NR4A1 in human ACFs derived from patient donors (sinus rhythm and AF) on the gene (Figure 3.3.1a) and protein (Figure 3.3.1b) levels. To assess the biological function of NR4A1 in human ACFs, NR4A1 knockdown was performed by siRNA transfection. Successful knockdown of NR4A1 was confirmed by the reduction of *NR4A1* mRNA (Figure 3.3.1c) and NR4A1 protein levels (Figure 3.3.1d).

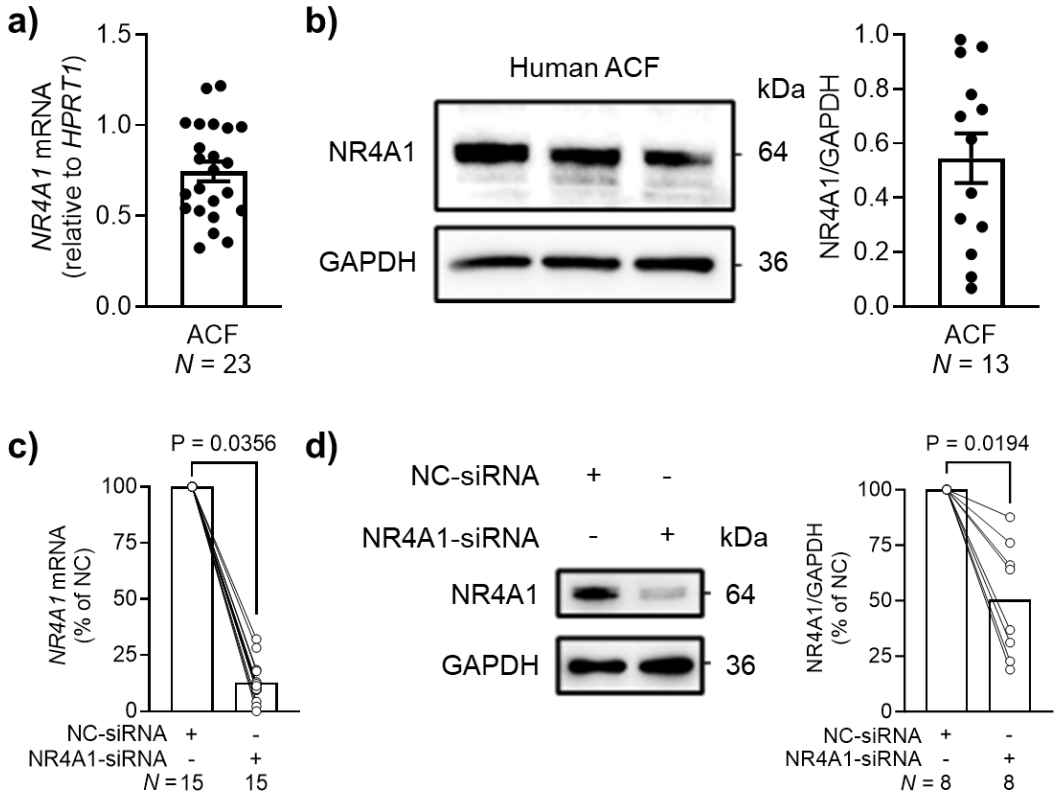

Figure 3.3.1 Confirmation of NR4A1 siRNA-mediated knockdown in human ACFs. (**a**) qPCR results showing *NR4A1* mRNA levels in human ACFs. (**b**) Representative blot and quantification showing NR4A1 protein levels in human ACFs. (**c-d**) Bar graphs and representative blot showing NR4A1 gene and protein expression in NR4A1 siRNA-mediated knockdown condition compared with negative control (NC-siRNA). Experiments performed

using donor-derived human ACFs (sinus rhythm and AF). Data are mean ± SEM (**a-b**) or mean with paired lines (**c-d**); each dot (**a-b**) or paired line (**c-d**) represents an independent biological replicate (*N*). Data are expressed as a percentage of the negative control group (NC-siRNA; **c-d**). *P*-values are determined from raw values and reported as two-sided using paired t-test (**c-d**).

3.3.2 NR4A1 deficiency downregulates gene expression of fibrotic markers

To assess fibrotic responses, I selected five gene markers: *ACTA2* (encoding αSMA), *POSTN* (encoding periostin), *FN1* (encoding fibronectin), *COL1A1* (encoding collagen 1α1) and *COL3A1* (encoding collagen 3α1). Only human ACFs derived from patient donors (sinus rhythm and AF) with successful NR4A1 knockdown were selected to assess the gene profiles. NR4A1 deficiency significantly downregulated the mRNA levels of *ACTA2*, *POSTN* ($P < 0.05$; Figure 3.3.2a-b), and a trend of reduction in *FN1* ($P = 0.0958$; Figure 3.3.2c). The effects of NR4A1 deficiency on *COL1A1* and *COL3A1* gene expression were not significant (Figure 3.3.2d-e).

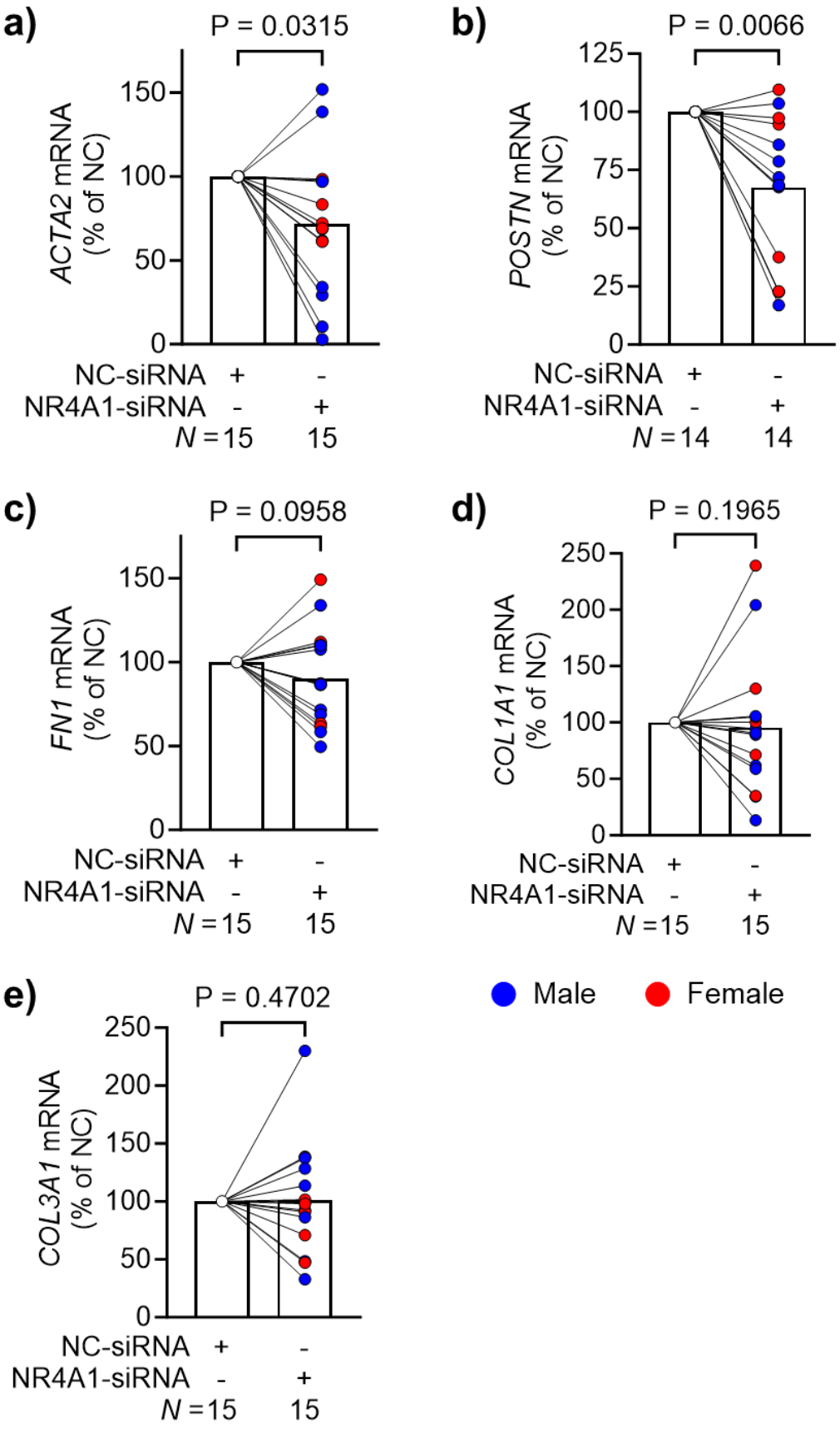
a)
P = 0.0315
ACTA2 mRNA (% of NC)
150
100
50
0
NC-siRNA + -
NR4A1-siRNA - +
N = 15 15
b)
P = 0.0066
POSTN mRNA (% of NC)
125
100
75
50
25
0
NC-siRNA + -
NR4A1-siRNA - +
N = 14 14
c)
P = 0.0958
FN1 mRNA (% of NC)
150
100
50
0
NC-siRNA + -
NR4A1-siRNA - +
N = 15 15
d)
P = 0.1965
COL1A1 mRNA (% of NC)
250
200
150
100
50
0
NC-siRNA + -
NR4A1-siRNA - +
N = 15 15
Male
Female
e)
P = 0.4702
COL3A1 mRNA (% of NC)
250
200
150
100
50
0
NC-siRNA + -
NR4A1-siRNA - +
N = 15 15

Figure 3.3.2 Effect of NR4A1 deficiency on gene expression of fibrotic markers in human ACFs. (**a**) Bar graph showing *ACTA2* mRNA expression in human ACFs with NR4A1 knockdown. (**b**) Bar graph showing *POSTN* mRNA levels in ACFs with NR4A1 knockdown. (**c**) Bar graph showing *FN1* mRNA levels in ACFs with NR4A1 knockdown. (**d**) Bar graph showing *COL1A1* mRNA levels in ACFs with NR4A1 knockdown. (**e**) Bar graph showing *COL3A1* mRNA levels in ACFs with NR4A1 knockdown. Experiments performed using donor-derived human ACFs (sinus rhythm and AF). Data are mean with paired lines; each paired line represents an independent biological replicate (*N*). Data are expressed as a percentage of the negative control group (NC-siRNA). *P*-values are determined from raw values and reported as two-sided using ratio paired t-test.

3.3.3 NR4A1 deficiency downregulates protein levels of fibrotic markers

To assess fibrotic responses, I selected five protein markers: αSMA, periostin, fibronectin, collagen 1 and collagen 3. Only human ACFs derived from patient donors (sinus rhythm and AF) with successful NR4A1 knockdown were selected to assess the protein profiles. NR4A1 deficiency downregulated the protein levels of αSMA, periostin and fibronectin ($P < 0.05$; Figure 3.3.3a-c). The effects of NR4A1 deficiency on mature collagen 1 and collagen 3α1 were not significant (Figure 3.3.3d-e).

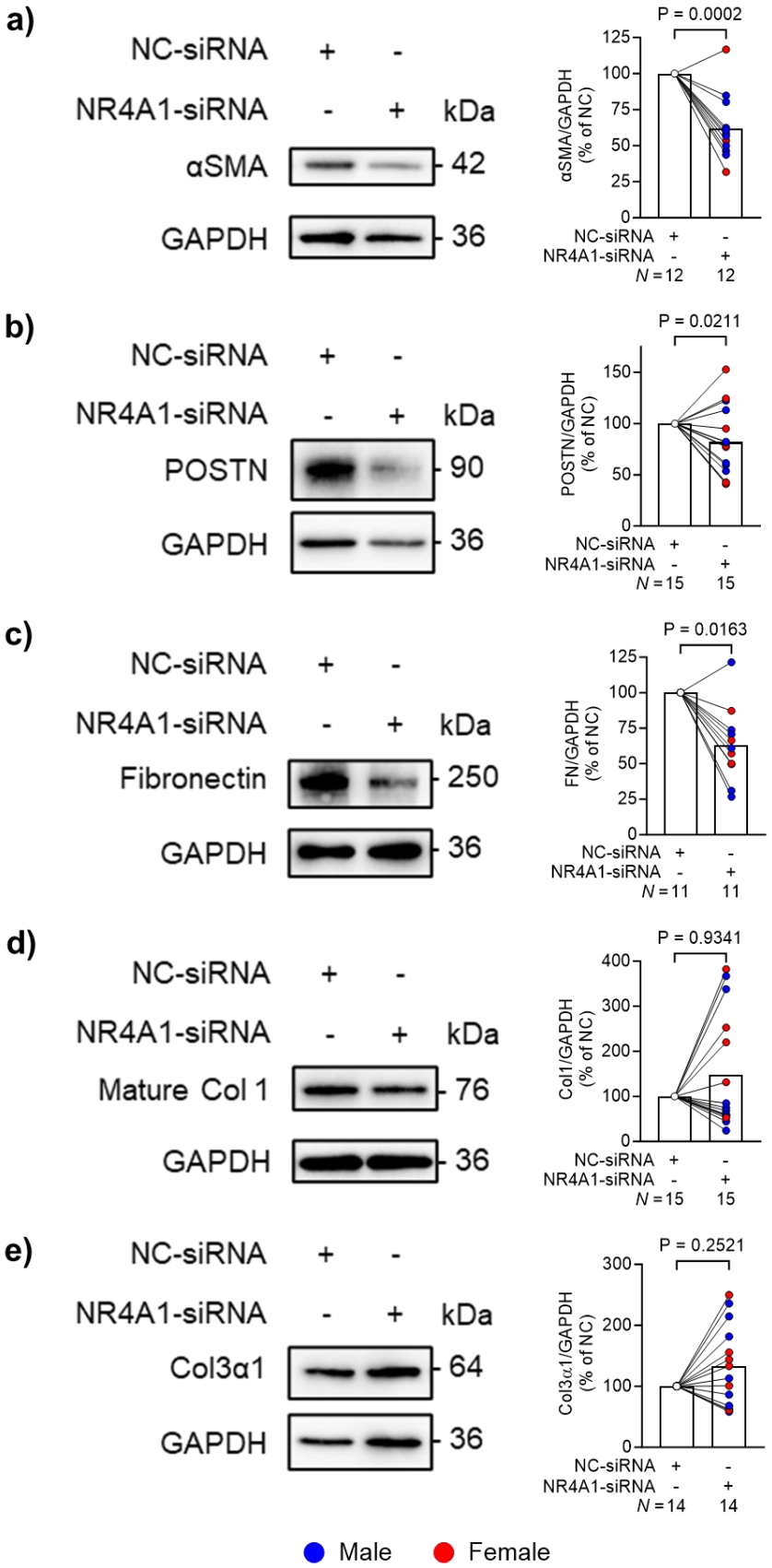
a)
NC-siRNA + -
NR4A1-siRNA - + kDa
αSMA 42
GAPDH 36
P = 0.0002
αSMA/GAPDH (% of NC)
125
100
75
50
25
0
NC-siRNA + -
NR4A1-siRNA - +
N = 12 12
b)
NC-siRNA + -
NR4A1-siRNA - + kDa
POSTN 90
GAPDH 36
P = 0.0211
POSTN/GAPDH (% of NC)
150
100
50
0
NC-siRNA + -
NR4A1-siRNA - +
N = 15 15
c)
NC-siRNA + -
NR4A1-siRNA - + kDa
Fibronectin 250
GAPDH 36
P = 0.0163
FN/GAPDH (% of NC)
125
100
75
50
25
0
NC-siRNA + -
NR4A1-siRNA - +
N = 11 11
d)
NC-siRNA + -
NR4A1-siRNA - + kDa
Mature Col 1 76
GAPDH 36
P = 0.9341
Col1/GAPDH (% of NC)
400
300
200
100
0
NC-siRNA + -
NR4A1-siRNA - +
N = 15 15
e)
NC-siRNA + -
NR4A1-siRNA - + kDa
Col3α1 64
GAPDH 36
P = 0.2521
Col3α1/GAPDH (% of NC)
300
200
100
0
NC-siRNA + -
NR4A1-siRNA - +
N = 14 14
Male
Female

Figure 3.3.3 Effect of NR4A1 deficiency on protein levels of fibrotic markers in human ACFs. (**a**) αSMA protein levels in human ACFs with NR4A1 knockdown. (**b**) Periostin protein levels in ACFs with NR4A1 knockdown. (**c**) Fibronectin protein levels in ACFs with NR4A1 knockdown. (**d**) Collagen 1 protein levels in ACFs with NR4A1 knockdown. (**e**) Collagen 3α1 protein levels in ACFs with NR4A1 knockdown. Experiments performed using donor-derived human ACFs (sinus rhythm and AF). Data are mean with paired lines; each paired line represents an independent biological replicate (*N*). Data are expressed as a percentage of the negative control group (NC-siRNA). *P*-values are determined from raw values and reported as two-sided using ratio paired t-test (**a**, **b**, **e**), paired t-test (**c**) and Wilcoxon test (**d**).

3.3.4 NR4A1 deficiency modulates functions of human ACFs

Cell proliferation and migration are important biological functions in fibrotic responses. Therefore, I next assessed these functional outcomes in the human ACFs derived from patient donors (sinus rhythm and AF) with NR4A1 knockdown. NR4A1 deficiency significantly suppressed proliferation of ACFs in 24 hours (P = 0.0041; Figure 3.3.4a). No difference was observed for migration in NR4A1-deficient cells compared with negative control at 4 hours timepoint (P = 0.4442; Figure 3.3.4b-c). A trend for increased migration was identified in NR4A1-deficient cells at 12 hours, indicated by a greater reduction of cell-free area, however, statistical significance was not reached (P = 0.0577; Figure 3.3.4b-c).

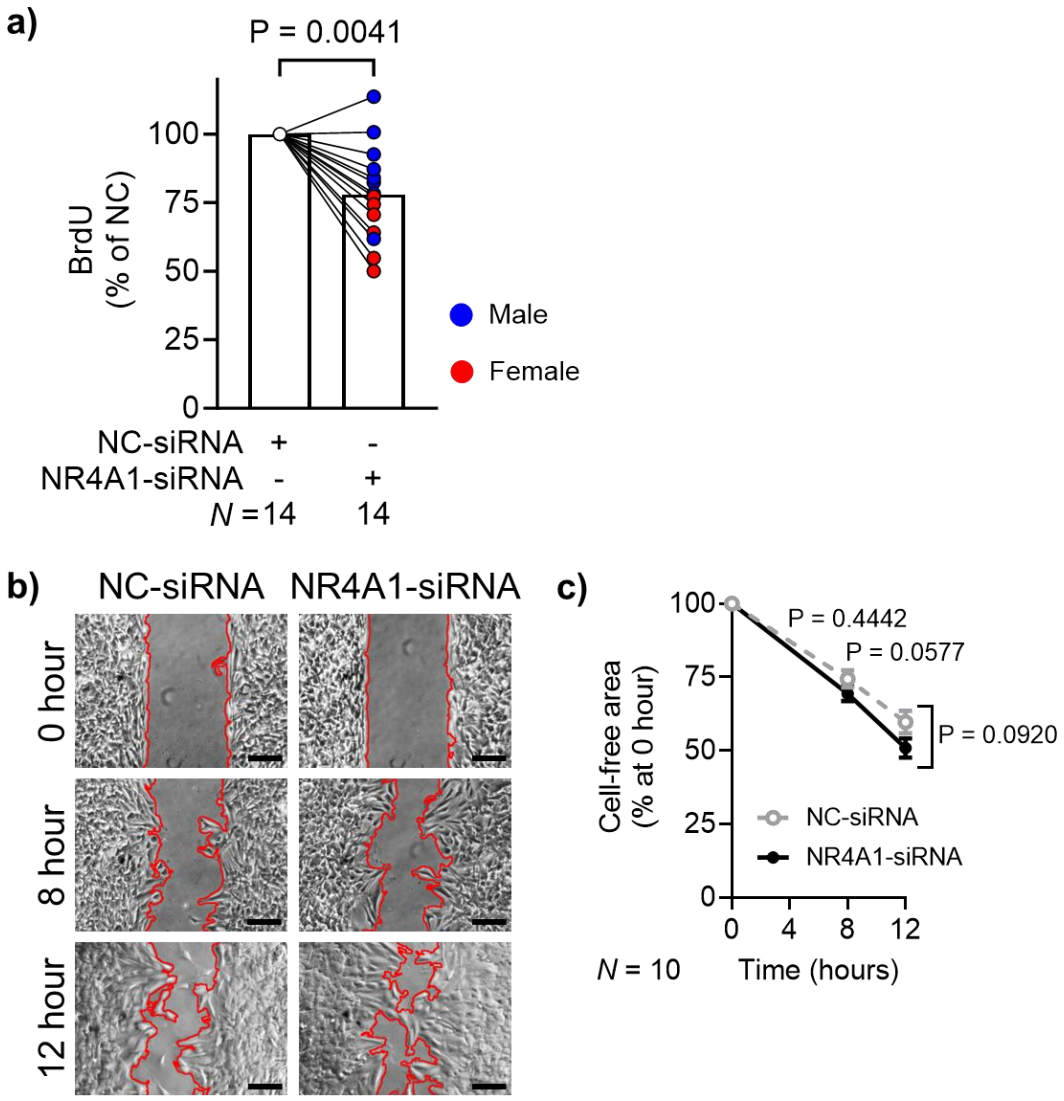

Figure 3.3.4 Effect of NR4A1 deficiency on cell proliferation and migration in human ACFs. (**a**) 24 hours proliferation (BrdU) of ACFs with NR4A1 knockdown. (**b**) Representative images showing migration of ACFs with NR4A1 knockdown at 0, 8 and 12 hours timepoints. Red traces indicating cell-free area. (**c**) Averaged traces showing the effects of NR4A1 knockdown on reducing cell-free area (migration) in ACFs at 0, 8, 12 hours timepoints. Scale bar, 200 µm. Experiments performed using donor-derived human ACFs (sinus rhythm and AF). Data are mean with paired lines (**a**) or mean ± SEM (**c**); each paired line represents an independent biological replicate (*N*). Data are expressed as a percentage of the negative control group (NC-siRNA; **a**) or the percentage of 0-hour timepoint (**c**). *P*-values are determined from

raw values (**a**) and reported as two-sided using paired t-test (**a**) and two-way ANOVA with Sidak correction (**c**).

3.3.5 NR4A1 deficiency suppresses pro-fibrotic effects of TGF-β1 stimulation

TGF-β1 treatment was tested as a pro-fibrotic stimulus in Lonza human ACFs. Pro-fibrotic effects of TGF-β1 were confirmed at 10 ng/mL, indicated by upregulated gene expression of some key fibrotic markers (Figure 3.3.5a). Subsequently, in TGF-β1-stimulated human ACFs derived from patient donors (sinus rhythm and AF), successful NR4A1 knockdown was validated (Figure 3.3.5b). When ACFs were treated by TGF-β1 alone, the *ACTA2*, *POSTN* and *COL1A1* mRNA levels were increased compared with vehicle control cells (Figure 3.3.5c-e). However, the TGF-β1-induced elevated levels of these fibrotic markers were attenuated in NR4A1-deficient cells (Figure 3.3.5c-e).

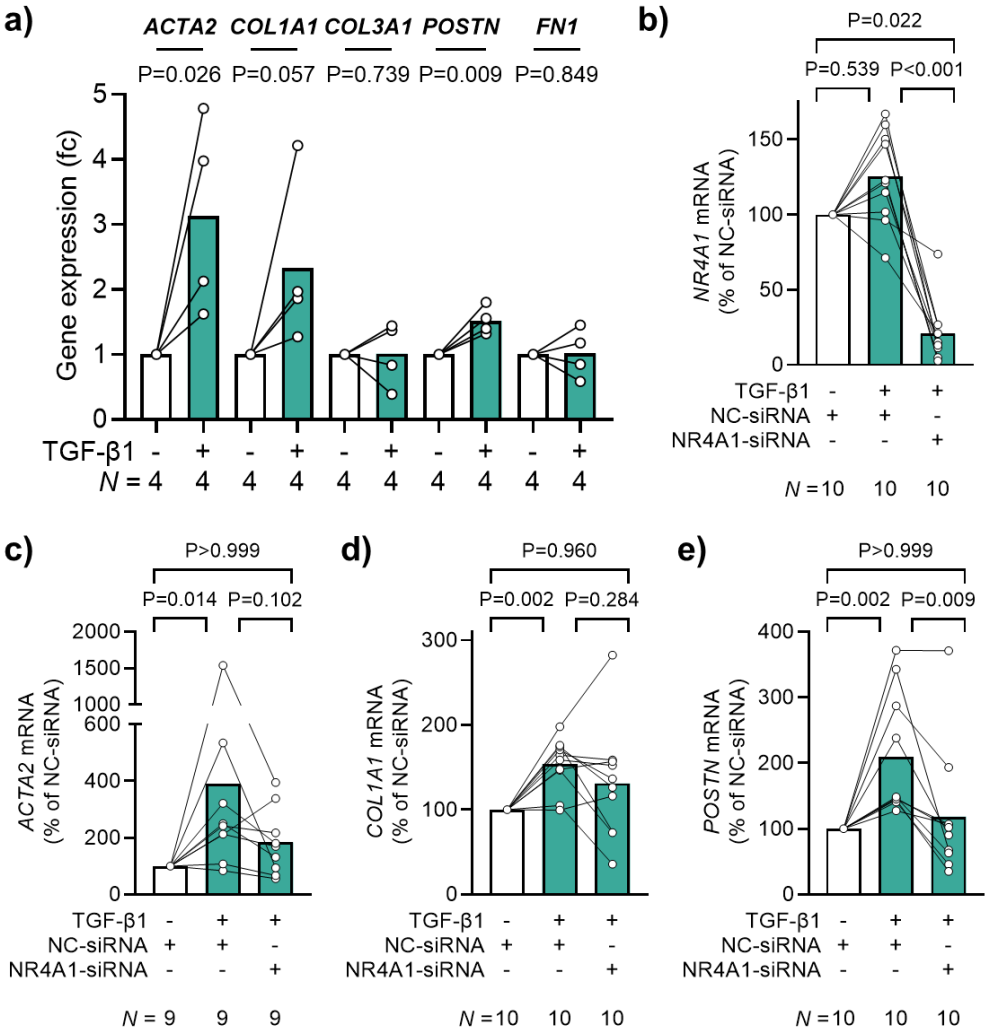

Figure 3.3.5 Effect of NR4A1 deficiency on gene expression of fibrotic markers following TGF-β1 stimulation in human ACFs. (**a**) mRNA levels of selected fibrotic markers with 10 ng/mL TGF-β1 stimulation in ACFs. (**b-e**) *NR4A1*, *ACTA2*, *COL1A1* and *POSTN* mRNA levels in TGF-β1-stimulated ACFs transfected with NR4A1-siRNA or NC-siRNA. Experiments performed using Lonza human ACFs (**a**) and donor-derived human ACFs (sinus rhythm and AF) (**b-e**). Data are mean with paired lines; each paired line represents an independent biological replicate (*N*). Data are expressed as a percentage of the negative control group (NC-siRNA without TGF-β1 stimulation). *P*-values are determined from raw values and reported as two-sided using ratio paired t-test (**a**), Friedman test with Dunn's correction (**b**, **c**, **e**) and repeated measures one-way ANOVA with Tukey correction (**d**).

3.3.6 Optimisation of Csn-B treatment

In addition to NR4A1 knockdown experiments, pharmacological activation of NR4A1 was performed using Lonza human ACFs to assess gain-of-function effects. Csn-B is a naturally occurring selective agonist for NR4A1 and commonly used in experimental settings[190]. Dose optimisation was carried out initially with a range of concentrations (0-20 μM). I observed that 20 μM Csn-B exerted cytotoxic effects in human ACFs (Figure 3.3.6a). Although cells remained viable at 10 μM Csn-B, changes in cell phenotype were marked by increased NR4A1 translocation to cytoplasmic compartment (Figure 3.3.6b). Therefore, 10 μM was not ideal for experiments in these cells and hence, 1 μM was determined to be the final concentration for Csn-B treatment.

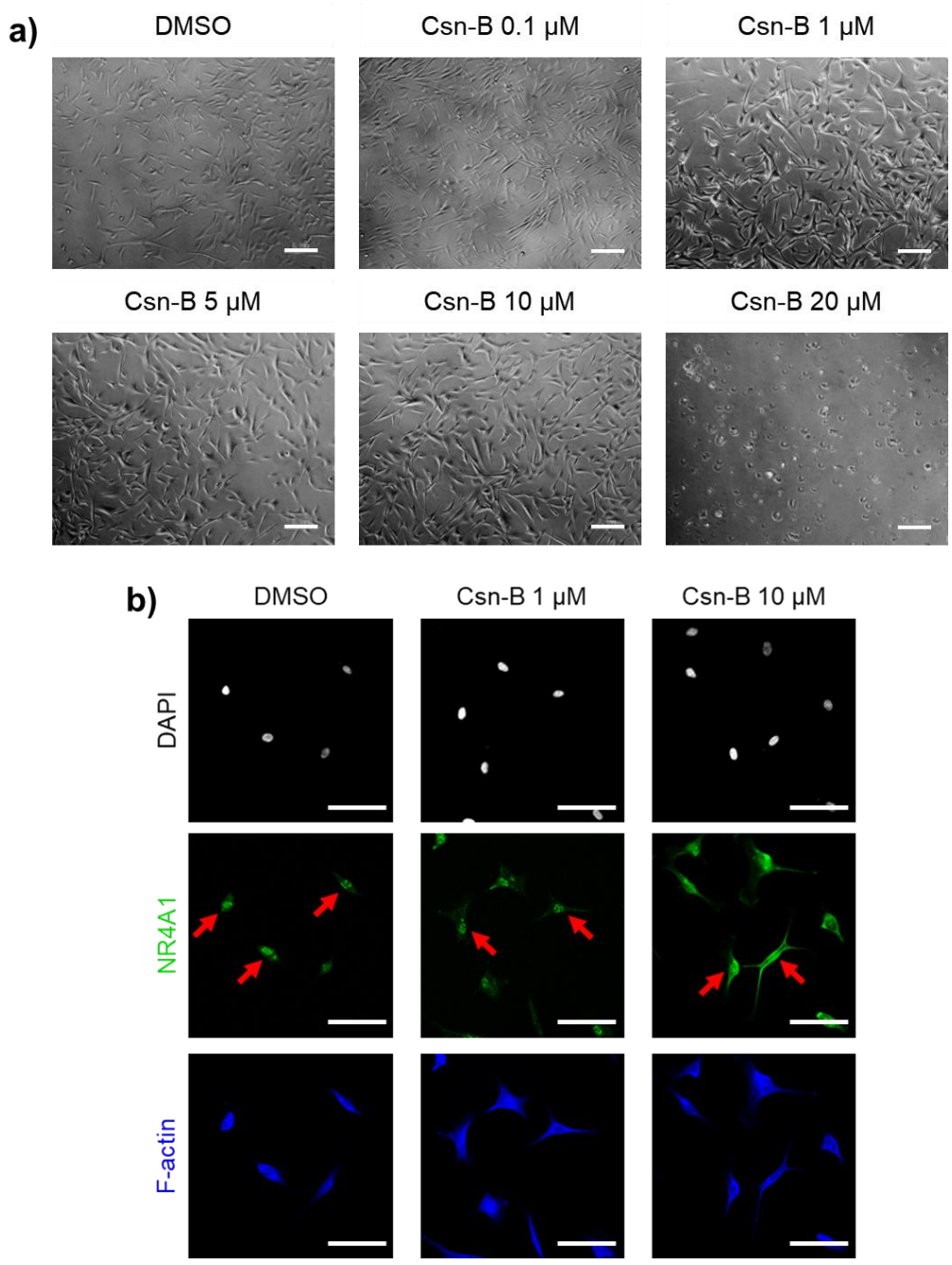

Figure 3.3.6 Concentration optimisation of Csn-B treatment in human ACFs. (**a**) Brightfield images visualising cell viability and cytotoxicity of ACFs with Csn-B treatment at 0, 0.1, 1, 5, 10 and 20 µM concentrations. Scale bar = 100 µm. (**b**) Fluorescence images visualising NR4A1 localisation in human ACFs with Csn-B treatment at 0, 1 and 10 µM concentrations. Red arrows indicating representative cells with nuclear or cytoplasmic expression of NR4A1. Scale bar = 75 µm. Experiments performed using Lonza human ACFs.

3.3.7 Activation of NR4A1 upregulates fibrotic responses in human ACFs

Csn-B treatment at 1 μM was established to induce NR4A1 activation in Lonza human ACFs, and subsequently, changes in the expression of fibrotic markers were evaluated. Gene expression of *ACTA2*, *COL1A1* and *POSTN* were not different between Csn-B treatment and vehicle-control group (Figure 3.3.7a). For proteins, αSMA expression was not altered by Csn-B ($P = 0.6918$; Figure 3.3.7b-c). However, protein levels of mature collagen 1α2 ($P = 0.0230$; Figure 3.3.7d) and periostin ($P = 0.0075$; Figure 3.3.7e) were significantly increased by Csn-B-induced NR4A1 activation.

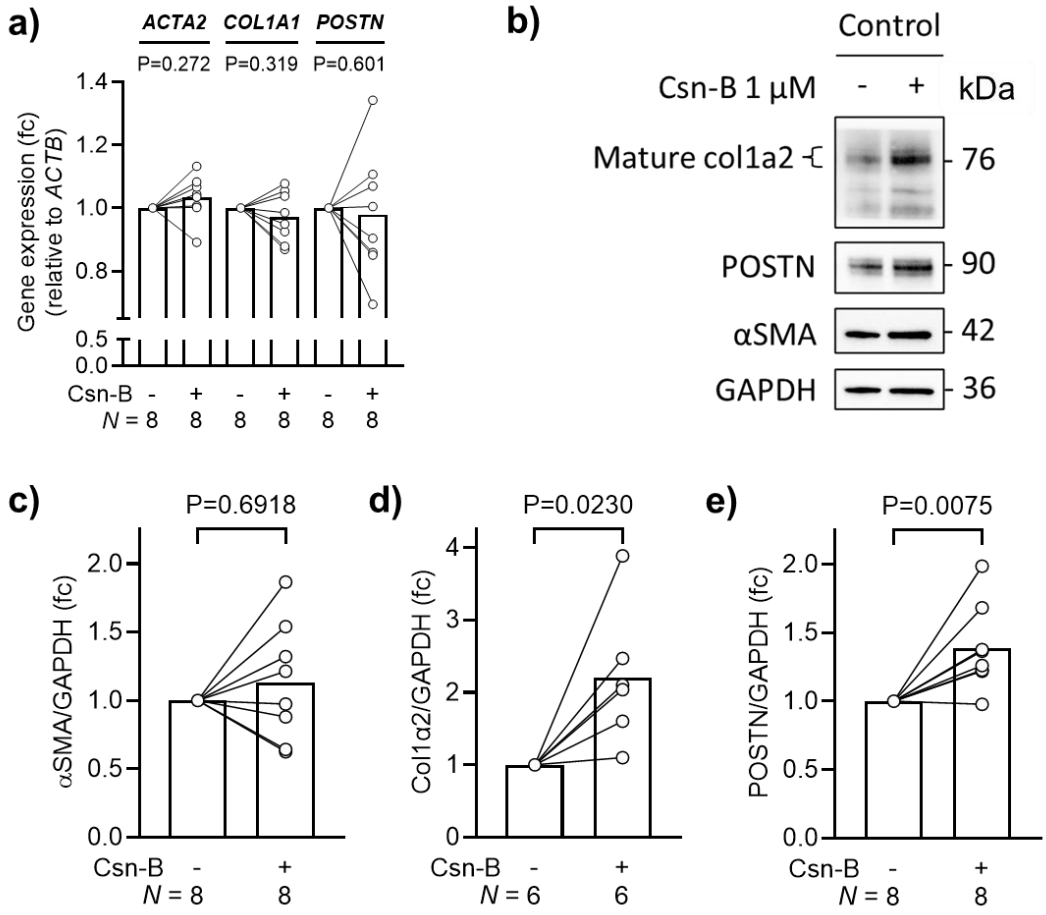

Figure 3.3.7 Effect of NR4A1 activation on human ACF fibrotic responses. (**a**) mRNA levels of selected fibrotic markers in Csn-B-treated human ACFs. (**b**) Representative blots showing protein bands of selected fibrotic markers in Csn-B treated human ACFs. (**c-e**)

Quantification of αSMA, mature collagen 1α2 and periostin protein levels in Csn-B-treated human ACFs. Experiments performed using Lonza human ACFs. Data are mean with paired lines; each paired line represents an independent biological replicate (*N*). Data are expressed as a percentage of the negative control group (vehicle). *P*-values are determined from raw values and reported as two-sided using ratio paired t-test (**a**, **c**) and paired t-test (**d**, **e**).

3.3.8 Activation of NR4A1 upregulates fibrotic responses in TGF-β1 stimulated human ACFs

To determine whether the NR4A1-mediated effects under basal conditions would remain in pro-fibrotic conditions, we performed the Csn-B treatment in TGF-β1-stimulated Lonza human ACFs. The transcriptional regulation of fibrotic markers by NR4A1 activation remained unchanged in TGF-β1-stimulated cells (Figure 3.3.8a). Levels of αSMA protein increased following NR4A1 activated TGF-β1-stimulated ACFs ($P = 0.0293$; Figure 3.3.8b-c). Consistent with the findings from ACFs in basal conditions, Csn-B also upregulated protein expression of mature collagen 1α2 ($P = 0.0312$; Figure 3.3.8d). In contrast, periostin levels remained unchanged ($P = 0.1132$; Figure 3.3.8e).

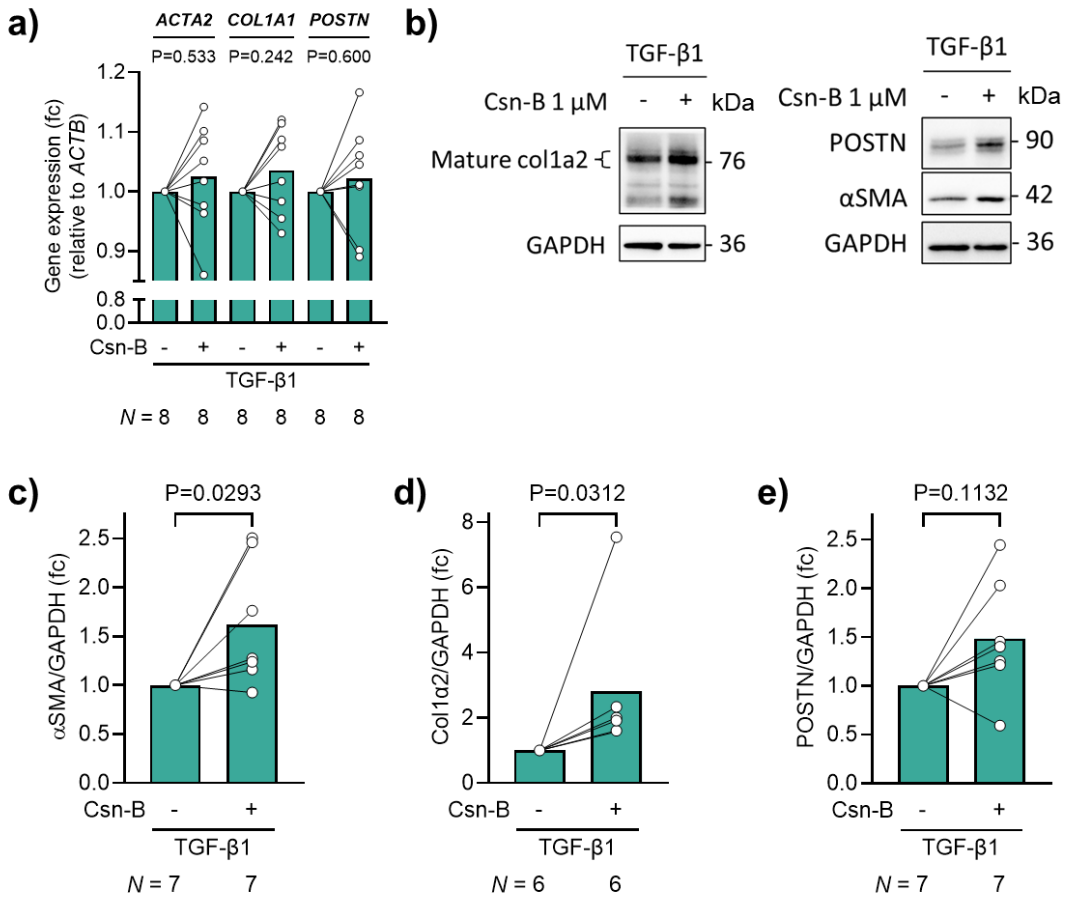

Figure 3.3.8 Effect of NR4A1 activation on TGF-β1-stimulated human ACF fibrotic responses. (**a**) mRNA levels of selected fibrotic markers in TGF-β1-stimulated human ACFs

with Csn-B treatment. (**b**) Representative blots showing protein bands of selected fibrotic markers in TGF-β1-stimulated human ACFs with Csn-B treatment. (**c-e**) Bar graph showing αSMA, collagen 1α2, and periostin protein levels in TGF-β1-stimulated human ACFs with Csn-B treatment. Experiments performed using Lonza human ACFs. Data are mean with paired lines; each paired line represents an independent biological replicate (*N*). Data are expressed as a percentage of the negative control group (vehicle). *P*-values are determined from raw values and reported as two-sided using ratio paired t-test (**a**, **c**, **e**) and Wilcoxon test (**d**).

3.4 Discussion

This chapter aimed to explore the role of a less-characterised fibroblast subtype (aFB3) identified in the human left atrium and evaluate the effects of NR4A1 on fibrotic responses in human ACFs. The aFB3 (*NR4A1*+) subcluster was less studied compared to the other fibroblasts representing the normal (aFB1) and activated (aFB2) phenotypes[132]. While transcriptional clustering of human fibroblasts from right atria has previously identified a proliferating subtype enriched with *NR4A1* expression[78], the functional role of this receptor in the human atrium remains distinct from the ventricle. Specifically, while a ventricular fibroblast subtype that expressed an aFB3-like transcriptome have been suggested to play a cardioprotective role in cardiomyopathy[191], it remains unclear if this interpretation translates to the distinct pathophysiology of AF and is consistent in human ACFs.

NR4A1, the top marker of the aFB3 subcluster, plays complex and often contradictory roles in cardiac fibrosis depending on the pathological context[165,166,188]. Emerging evidence highlights a dichotomy between ischaemic and non-ischaemic conditions. In ischaemic settings, such as post-myocardial infarction, NR4A1 exerts anti-fibrotic effects, limiting excessive scarring in the infarct[192]. Conversely, in non-ischaemic remodelling – which more closely resembles the pathophysiology of AF[165,166] - *in vivo* deletion of NR4A1 reduces cardiac fibrosis[188,193], implying a pro-fibrotic role. This aligns with findings in rodent models where NR4A1 mediates TGF-β signalling in cardiac fibroblasts[160,161]. Given that atrial remodelling in AF is primary driven by non-ischaemic substrates (e.g., tachycardia, stretch) rather than distinct infarcts or deficiency of blood supply[194,195], I hypothesised that NR4A1 exerts pro-fibrotic effects in human ACFs. To date, it was unknown whether the pro-fibrotic mechanisms observed in rodent models could be replicated in mature human cardiac fibroblasts.

In this chapter, I demonstrated that NR4A1 deficiency in human ACFs significantly suppresses the synthesis of crucial pro-fibrotic markers and attenuates cell proliferation. This confirms a pro-fibrotic role for NR4A1 in the atrial cells. Crucially, while previous studies have prioritised ventricular-derived cells, the left atrium is the primary compartment for remodelling in AF – due to a more prominent AF-associated left atrial dilatation. Therefore, establishing the pro-fibrotic function of NR4A1 specifically in human ACFs is clinically relevant.

Furthermore, NR4A1 knockdown inhibited fibrotic responses even in the absence of exogenous stimuli (baseline conditions). When challenged with TGF-β1, NR4A1-deficient cells displayed a blunted fibrotic response. This is consistent with previous literature suggesting that NR4A1 acts as a requisite regulator for TGF-β signalling[160,161]. However, the reduction of baseline fibrotic responses suggests that NR4A1 may also regulate fibrogenesis through TGF-β-independent pathways, potentially involving interactions with other signalling cascades such as p38 MAPK and PI3K/AKT pathways[170,196].

Cell proliferation was suppressed by NR4A1 knockdown in human ACFs, aligning with the observed anti-fibrotic effects on the fibrotic marker expression. However, the trend of increased cell migration is unexpected, as proliferation and migration typically act synergistically in cardiac fibroblast to promote fibrosis[197]. This contradiction could potentially be explained by the "go or grow" hypothesis, frequently observed in cancer cells[198], which postulates that cells can dynamically alter their functional behaviour based on microenvironment cues, the availability of energy (ATP) and cytoskeletal resources. In this context, NR4A1 deficiency may induce a phenotypic shift in ACFs, driving them into a state of cell cycle arrest (quiescence) while maintaining high motility through reallocation of metabolic energy and cytoskeletal

machinery. While this mechanistic link offers a compelling explanation for the observed results, it remains speculative and requires further exploration.

To demonstrate that NR4A1 gain of function yields opposite effects to its silencing, NR4A1 was pharmacologically activated using Csn-B. In contrast to the anti-fibrotic effects observed in NR4A1 loss of function experiments, Csn-B treatment resulted in a pro-fibrotic phenotype. It is worth noting that while high concentrations (10-20 μM) induced cytotoxicity – similar to effects reported in human dermal fibroblasts[150] – an optimal concentration at 1 μM successfully induced activation without compromising cell viability.

Interestingly, while Csn-B treatment upregulated fibrotic markers at the protein level, without changes at the gene expression level. This discrepancy warrants careful interpretation. Csn-B is a specific agonist for the C-terminal LBD of NR4A1[190]. However, as an orphan nuclear receptor, NR4A1 also relies heavily on its N-terminal AF-1 domain to interact with coactivators and corepressors to mediate transcription[199,200]. A likely explanation for the protein-mRNA discordance is the temporal dynamics of gene regulation. While speculatively, it is possible that transcriptional upregulation of fibrotic markers may have occurred rapidly and returned to baseline by the time of harvest[201], while the translated proteins remained stable as proteins have long half-lives[201,202]. Alternatively, NR4A1 activation may influence post-transcriptional mechanisms, such as enhancing the translation efficiency or inhibiting the proteasomal degradation of proteins[167,203]. By contrast, the siRNA approach degrades the *NR4A1* transcript entirely, dampening all downstream functions (transcriptional and post-transcriptional), leading to consistent reductions in both mRNA and protein.

In summary, this chapter provides evidence for a pro-fibrotic role of NR4A1 in human ACFs, demonstrated by changes in fibroblast activation, proliferation and ECM remodelling. These data challenge the cardioprotective view of NR4A1 seen in cardiac ischaemic models and position it as a potential therapeutic target for atrial fibrosis. The subsequent work delineates the precise downstream signalling partners of NR4A1 to determine if its effects are mediated solely through canonical TGF-β crosstalk or novel, atrial-specific pathways.

CHAPTER 4: IDENTIFICATION OF NR4A1-ASSOCIATED SIGNALLING TARGETS AND PATHWAYS IN ATRIAL FIBROTIC RESPONSES

4.1 Introduction

In the preceding chapter, I established a critical role for the NR4A1 in driving fibrotic responses within human ACFs. These findings crucially demonstrated that NR4A1 alone is sufficient to promote a pro-fibrotic phenotype under basal conditions, independent of exogenous stimulation. This challenges the prevailing view in the field, which has largely characterised NR4A1 solely as a modulator of TGF-β signalling in rodent ventricular fibroblasts. While previous studies have implicated NR4A1 in TGF-β-induced fibrosis[160,161], the observation from previous chapter that NR4A1 drives remodelling in the absence of pro-fibrotic stimuli suggests that it orchestrates a more complex, intrinsic regulatory network. Therefore, dissecting the specific molecular targets and biological pathways governed by NR4A1 in the human ACFs is essential to understand its translational significance.

To identify potential mechanisms underlying NR4A1-driven atrial fibrosis, it is pertinent to revisit the transcriptional landscape of the human left atrium. As mentioned in previous chapter, snRNA-seq analyses identified NR4A1 as the top differential marker for a specific fibroblast subpopulation, termed aFB3[132]. Gene set overrepresentation analysis of this subtype revealed a significant enrichment of TNF signalling via NF-κB, linking NR4A1 expression to inflammatory activation.

Inflammation is a well-established driver of AF, creating a substrate for re-entrant arrhythmia through structural remodelling[83]. Clinically, AF patients exhibit elevated circulating inflammatory markers, including C-reactive protein, IL-6 and TNF-α. However, this inflammatory burden is not merely systemic; it is also locally pronounced within the left atrium, where it plays a role in the progression to long-standing AF with increasing age in patients[204].

While infiltrating immune cells are known to release pro-inflammatory cytokines, cardiac fibroblasts themselves are potent sources of inflammatory mediators[205]. This autocrine and paracrine signalling create a vicious cycle of inflammation and fibrosis in the atrium.

The critical nature of this inflammatory-fibrotic axis is relevant to NR4A1 in cardiac fibroblasts and recently highlighted by Widiapradja et al.[160]. Their work demonstrated NR4A1 as a central regulator of the crosstalk between macrophages and cardiac fibroblasts during cardiac remodelling. Specifically, they found that NR4A1 drives macrophages towards a pro-inflammatory phenotype and these activated macrophages subsequently push cardiac fibroblasts into an activated, pro-fibrotic state. This establishes NR4A1 as a key facilitator of inflammation-driven fibrosis via intercellular communication. However, this model largely positions the fibroblasts as responders to external immune cues. Given that the aFB3 subtype exhibits high intrinsic inflammatory activity, and that cardiac fibroblasts are known to be capable of autocrine cytokine production, it remains questionable whether NR4A1 drive an intrinsic inflammatory program within human ACFs themselves, independent of macrophage input.

While elucidating these downstream inflammatory pathways is essential, it is equally critical to identify the upstream molecular triggers that activate NR4A1 to initiate this fibrotic cascade. Historically, NR4A1 has been classified as an orphan nuclear receptor, implying a lack of identified endogenous ligands[206,207]. While naturally occurring exogenous agonists of NR4A1 have been recognised – such as Csn-B and amoitone B – and have been used to probe its function[190,208], the endogenous trigger for NR4A1 activation has remained elusive. However, a study by Lakshmi et al. in 2019 provided the first evidence of a novel NR4A1 endogenous ligand: PGA2[209]. This study demonstrated that PGA2 binds covalently to the Cys566 residue

within the NR4A1 ligand-binding domain, regulating its transcriptional activity. PGA2 is a cyclopentenone prostaglandin and an endogenous metabolite derived from the dehydration of prostaglandin E2 (PGE2). PGA2 is biologically potent and known to regulate apoptosis, vasodilation, and endothelial permeability[210,211].

The potential role of the PGA2-NR4A1 axis in atrial fibrosis presents a fascinating paradox. In other contexts, such as pulmonary endothelial cells, PGA2 exerts anti-inflammatory effects by inhibiting LPS-induced inflammatory signalling through NF-κB pathway[210]. Similarly, PGE2 has been considered anti-inflammatory in adult mouse cardiac fibroblasts, acting via the reduced NF-κB activation[212]. These PGA2- or PGE2-induced anti-inflammatory effects are targeting the EP4 receptors. Also, the inhibition of NF-κB pathway by PGE2 involves a complicated mechanism with tight regulation of NF-κB subunits. However, the current findings suggest NR4A1 is pro-fibrotic and pro-inflammatory (via the aFB3 signature). This discrepancy implies that PGA2 signalling may be highly context dependent. While its interaction with surface receptors like EP4 may be protective, its binding to NR4A1 in human ACFs may trigger a distinct, maladaptive transcriptional program. Investigating this ligand-receptor interaction is therefore critical to "de-orphanise" the mechanism of NR4A1 in AF-associated fibrosis.

4.1.1 Hypothesis and aims

Hypothesis: NR4A1 may regulate transcriptional signatures and pathways that are associated with fibrosis in human ACFs. The aims of this chapter are as follows:

1. Profile the transcriptional landscape downstream of NR4A1 modulation in human ACFs

2. Map biological pathways to determine if NR4A1 regulation is functionally linked to inflammatory signalling or canonical fibrotic pathways
3. Shortlist and validate key downstream targets that mediate the pro-fibrotic activity of NR4A1 in human ACFs
4. Determine the relevance of PGA2 in the NR4A1-mediated response in human ACFs, thereby proposing a ligand-receptor-target axis in this cellular model

4.2 Materials and Methods

The following methods described in this section were used specifically in this chapter.

4.2.1 Preparation of bulk RNA-seq samples

ACFs from four biological donors (N = 4) were transfected with NR4A1-siRNA or non-targeting siRNA as described in Section 2.3. After transfection, cells were lysed and proceeded with RNA extraction as described in Section 2.4.1. For the final step, instead of 30 µL, RNA was collected in 20 µL of pre-heated (95°C) nuclease-free water and checked for RNA purity. Samples with concentration more than 40 ng/µL and good purity were stored at -20°C and subsequently sent to local service provider (Azenta Life Sciences) for bulk RNA-sequencing (RNA-seq).

4.2.2 Library preparation and sequencing

Library preparation and sequencing were performed by Azenta. After arriving the sequencing facility, RNA concentration was quantified again using the Qubit 4.0 Fluorometer (Invitrogen, US). RNA integrity was validated with RNA Kit on the Agilent 5300 Fragment Analyzer (Agilent Technologies, US). RNA sequencing libraries were prepared using the NEBNext Ultra II RNA Library Prep Kit for Illumina according to manufacturer's instructions (NEB, US). Initially, mRNAs were enriched using Oligo(dT) beads and fragmented at 94°C for 15 min. The first and second cDNA strands were then synthesised. cDNA fragments were end repaired and adenylated at 3'-ends, and universal adapters were ligated to cDNA fragments, followed by index addition and library enrichment by limited-cycle PCR. Sequencing libraries were validated using the NGS Kit on the Agilent 5300 Fragment Analyzer and quantified using the Qubit 4.0 Fluorometer.

The sequencing libraries were multiplexed and loaded on the flowcell on the Illumina NovaSeq instrument following manufacturer's instructions. Samples were sequenced using a 2x150 Pair-End configuration (v1.5). Image analysis and base calling were performed by the NovaSeq Control Software (v1.7) on the NovaSeq instrument. Finally, raw sequence data was generated from Illumina Novaseq as .bcl files, converting into fastq files and de-multiplexing using Illumina bcl2fastq program (v2.20). One mismatch was allowed for index sequence identification.

4.2.3 Data processing

Raw data processing was performed by Azenta. After checking the quality of raw data, the sequence reads were trimmed using Trimmomatic (v0.36) to exclude possible adapter sequences and nucleotides with poor quality. The trimmed reads were then mapped to the *Homo sapiens* reference genome (available on ENSEMBL) using the STAR aligner (v2.5.2b). This step detects splice junctions and incorporates them to facilitate the alignment of the entire read sequences and resulting in the generation of BAM files. Finally, unique gene hit counts were calculated using the featureCounts tool within the Subread package (v1.5.2). Counts were considered only for unique reads that fell within the exon regions.

4.2.4 Data analysis

Gene hit counts were extracted for downstream differential expression analysis using the R package DESeq2 (v1.42.1). Gene level normalised counts were obtained using the *counts()* function in DESeq2. Normalised counts are read counts adjusted for differences in sequencing depth between samples using the DESeq2 median-of-ratios normalisation method. It divides each raw count by its sample-specific size factor, allowing gene expression levels to be directly

compared across samples. Using DESeq2, gene expression was compared between the NR4A1-siRNA knockdown group and negative control-siRNA group, and the donor effect (paired samples) was also included in the model. Genes with low counts (< 10) were filtered and excluded for analysis. Wald test was used to generate log2 fold changes (log2FC) and *P*-values. Genes with adjusted *P*-values < 0.05 and log2FC > 0.25 or < -0.25 were labelled as differentially expressed genes (DEGs). The principal component analysis (PCA) was performed using the *plotPCA()* function within the DESeq2 package, and the PCA plot was visualised with the top 500 genes, selected by highest row variance.

4.2.5 Pathway analysis of DEGs

Over-representation pathway analysis was conducted using the R package clusterProfiler (v4.6.2) to interpret the biological functions of DEGs. There were 249 upregulated DEGs and 354 downregulated DEGs identified in Section 4.2.4. Three databases and ontologies were used for the analysis: Gene Ontology (GO), Kyoto Encyclopedia of Genes and Genomes (KEGG) and Reactome. The background gene list was the annotation for human genome and loaded using the package org.Hs.eg.db (v3.16.0). *P*-values were adjusted using the Benjamini-Hochberg method and adjusted *P*-values less than 0.05 were significant. The top pathways are visualised in dot plots using the package ggplot2 (v4.0.0).

4.2.6 Construction and analysis of PPI network

DEGs were loaded to the STRING database. The protein-protein interaction (PPI) network was constructed and visualised with the medium confidence (0.400) as minimum threshold for the required interaction score. The network was then exported to Cytoscape v3.10.3 and analysed using the Cytoscape plugin cytoHubba v0.1 to identify important hub nodes. The top ten ranked

nodes from the PPI network were depicted using four different algorithms: Maximal Clique centrality (MCC), Betweenness, Closeness and Degree.

4.2.7 PGA2 stimulation

PGA2 stimulated in human ACFs was performed with optimisation. Stock PGA2 solution (#ab120879, Abcam, UK) at 10 mg/mL was diluted in FBM-3 antibiotic-free medium with 0.5% FBS to a range of concentrations for optimisation: 0, 0.1, 1, 5, 10 and 20 μM. PGA2 was added to the cells and incubated at 37℃ for 24 or 48 hours. Cell viability was checked after treatment before proceeding with downstream experiments.

4.2.8 ELISA for IL-6 and IL-1β

Cell secretomes for enzyme-linked immunosorbent assay (ELISA) were collected from PGA2 stimulation experiments (as described in Section 4.2.7). To assess how PGA2 regulates inflammatory response, key inflammatory cytokines including IL-6 and IL-1β levels in secretomes were detected using Human IL-6 DuoSet ELISA (#DY206) and Human IL-1β/IL-1F2 DuoSet ELISA (#DY201), respectively (both from R&D Systems, US) following the same protocol. A 96-well plate was coated with 100 μL of diluted Capture Antibody in 1X PBS per well, sealed and incubated at room temperature for overnight. Solutions were aspirated using the Tecan Hydroflex Automated Microplate Washer (Tecan, Switzerland). Plate was washed three times with 400 μL of Wash Buffer per well. 300 μL of Block Buffer (1% BSA in 1X PBS) was loaded to each well and incubated at room temperature for 1 hour. For IL-6 ELISA only, secretome samples were diluted 1:10 in antibiotic-free medium with 0.5% FBS before loading to the plate. After repeating the washing step, 100 μL of standard or diluted sample in Reagent Diluent (1% BSA in 1X PBS) was added to each well and incubated at room temperature for

20 min in dark. Washing step was then repeated, followed by adding 100 µL of diluted Detection Antibody in Reagent Diluent and incubated at room temperature for 2 hours. Plate was washed and incubated with 100 µL of Streptavidin-HRP B working solution at room temperature for 20 min in dark. After the final washing step, the wells were incubated with 100 µL of TMB Substrate Solution at room temperature for 20 min in dark. Reaction was stopped by 100 µL of Sulfuric Acid Stop Solution. Absorbance was measured at 450 nm using a microplate reader (BMG LABTECH, Germany) and wavelength correction was applied at 540 nm.

4.2.9 IL-6 neutralisation assay

IL-6 neutralisation assay was performed according to previous study with modifications[213]. In brief, human ACFs were plated at 10,500 cells/cm^2 in 6-well plates and once attached, the cells were replaced with FBM-3 antibiotic-free medium with 0.5% FBS for 2 hours for serum starvation. 50 ng/mL of Human IL-6 Recombinant Protein (#200-06, Gibco, US) was pre-incubated with NeutraKine (neutralising IL-6, #69001-1-Ig) or NeutraControl (neutralising control, #69501-1-Ig) antibody (Proteintech, US) at 37℃ for 1 hour prior to treating the cells. IL-6 neutralising solutions were diluted in the serum-starved medium with 100 µM of L-ascorbic acid (#A92902, Sigma-Aldrich, US) to stimulate collagen synthesis and secretion[214]. Cells were treated with 1 mL of IL-6 neutralising solution at 37℃ for 24 hours. After treatment, the culture medium in each well was collected and centrifuged at 500 g at 4℃ for 5 min to remove debris and particulates. The clear supernatant (secretome) was transferred to a new tube and stored at -20℃ until running the total collagen detection assay.

4.2.10 Total collagen detection assay

Collagen was measured in the cell secretome collected from IL-6 neutralisation assay (as described in Section 4.2.9). Quantification of total secreted collagen was performed using the Sirius Red Total Collagen Detection Assay Kit (#9062, Chondrex, US) in accordance with the manufacturer's protocol. 1 mL of cell culture supernatant was mixed with 250 µL of Concentrating Solution, vortexed and incubated at 4°C for overnight. The solution was centrifuged at 10,000 rpm for 3 min. After discarding the supernatant, pellet was dissolved in 100 µL of 0.05 M acetic acid. Standard solutions were prepared by serial dilutions in 0.05 M acetic acid. Sirius Red Solution (500 µL) was added to 100 µL of standard or sample, vortexed and incubated at room temperature for 20 min. Tubes were then centrifuged at 10,000 rpm for 3 min and supernatant was removed carefully. The pellet was resuspended in 500 µL of Washing Solution, centrifuged at 10,000 rpm for 3 min and then the pellet was dissolved completely in 250 µL of Extraction Buffer. Finally, 200 µL of the standard or sample extracted solution was loaded a 96-well plate. Absorbance was measured at 510 and 550 nm using a microplate reader (BMG LABTECH, Germany).

4.3 Results

4.3.1 NR4A1 deficiency alters the transcriptional profiles of human ACFs

To assess biological pathways and potential target genes downstream of NR4A1 in mediating fibrotic responses in human ACFs, ACFs from sinus rhythm donors were transfected with NR4A1-siRNA or negative control-siRNA and analysed by bulk RNA-seq. A total number of 13166 genes were detected. PCA analysis revealed clustering of individual donors, indicating a strong donor-specific effect (Figure 4.3.1a). Hence, I performed paired analysis for the differential analysis to identify DEGs between the conditions (NR4A1 knockdown vs. negative control). NR4A1 knockdown significantly regulated 603 genes, including 249 upregulated DEGs and 354 downregulated DEGs (Figure 4.3.1b). RNA-seq confirmed reduction of *NR4A1* in knockdown condition (Figure 4.3.1c), and consistent downregulation of fibrotic markers *ACTA2* and *POSTN* (Figure 4.3.1d-e), as reported in the *in vitro* findings in Chapter 3. The top 100 DEGs from differential analysis are provided in Supplementary Table 1.

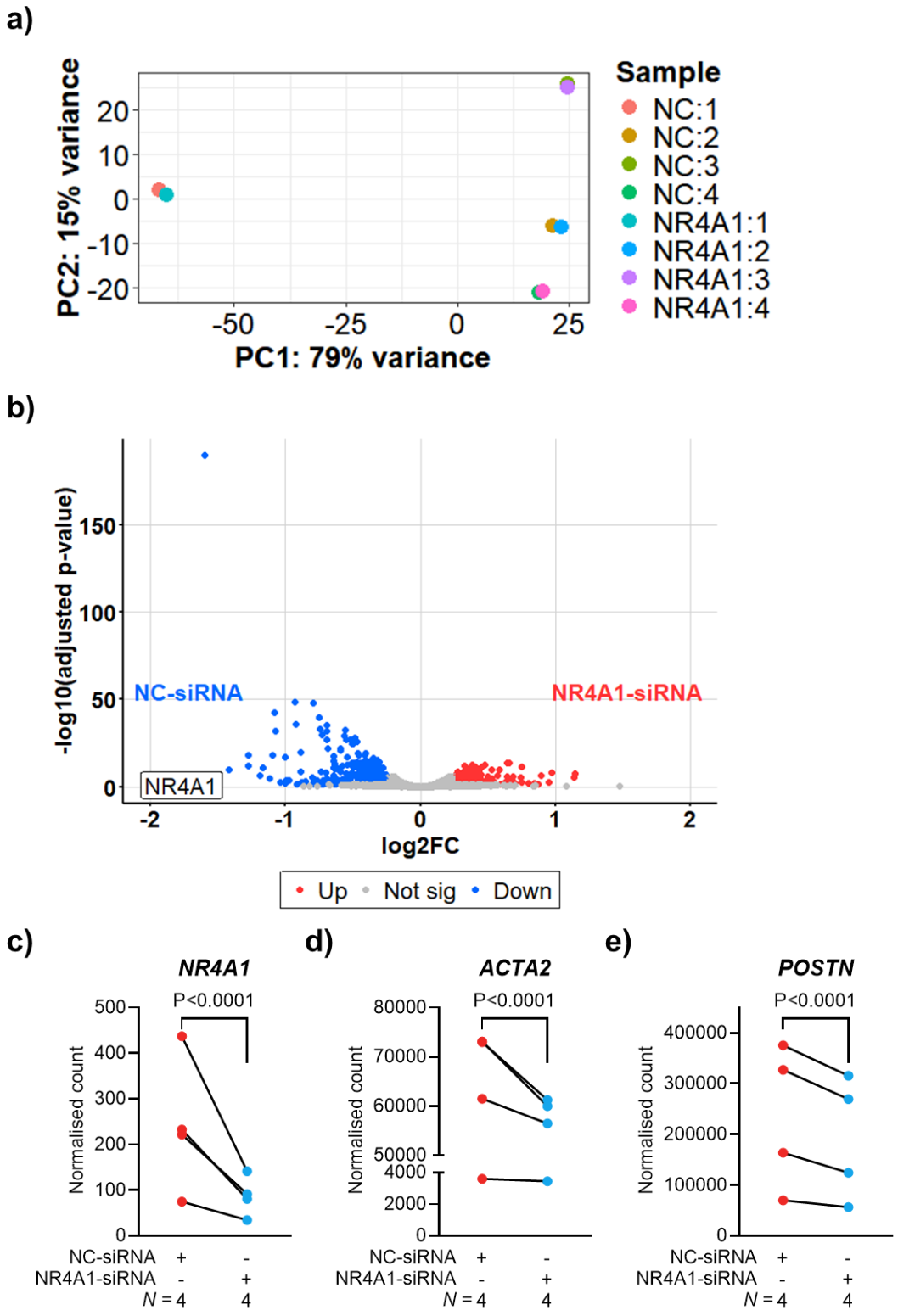

Figure 4.3.1 Transcriptional changes in human ACFs with NR4A1 knockdown. (**a**) PCA plot showing the overall effect of variances for the top 500 genes between NR4A1 siRNA-

mediated knockdown condition compared with negative control in human ACFs. (**b**) Volcano plot showing the distribution of gene expression changes comparing NR4A1 knockdown compared with negative control. Red dots represent significantly upregulated genes (adjusted *P*-value < 0.05, log2FC > 0.25) while blue dots represent significantly downregulated genes (adjusted *P*-value < 0.05, log2FC < -0.25). (**c-e**) Dot plots showing *NR4A1*, *ACTA2* and *POSTN* normalised counts in NR4A1 knockdown compared with negative control. Normalised count is explained in Section 4.2.4. Experiments performed using sinus rhythm donor-derived human ACFs. Data are paired lines (**c-e**); each paired line represents an independent biological replicate (*N*). *P*-values are determined from differential expression analysis in DESeq2 using Wald test.

4.3.2 Transcriptomic analysis identifies distinct biological pathways regulated by NR4A1 in human ACFs

To elucidate the biological significance of the transcriptomic alterations induced by NR4A1 knockdown, pathway analysis was performed separately for upregulated and downregulated DEGs. Three independent databases – GO Biological Process (BP), KEGG and Reactome – were applied to ensure a comprehensive characterisation of the enriched pathways.

Enriched pathways from the upregulated DEGs revealed a coordinated shift in the transcriptional landscape, primarily centred on metabolic adaptation and stress-responsive signalling. There was a significant enrichment of genes involved in the response to oxygen deprivation from GO BP (Figure 4.3.2a). This was further supported by KEGG analysis, which identified the hypoxia-inducible factor-1 (HIF-1) signalling pathway as the top pathway (Figure 4.3.2b). Linked to this hypoxic signature was a profound shift in cellular energetics. A significant upregulation of the glycolytic process, pyruvate metabolic process, and ADP/ATP metabolic signalling was observed. Beyond metabolism, GO and KEGG analyses identified enrichment in multiple signalling cascades. Notably, the regulation of RUNX1 expression and activity was enriched in Reactome (Figure 4.3.2c).

Analysis of the downregulated DEGs following NR4A1 knockdown revealed a significant impairment in pathways governing structural integrity, cell-matrix interactions and leukocyte coordination (Figure 4.3.2d-f). In GO and Reactome analysis, a major consequence of NR4A1 deficiency was the downregulation of genes essential for ECM organisation, elastic fibre formation and syndecan interactions. This structural organisation was mirrored in the KEGG analysis, highlighted by significant pathways in focal adhesion and ECM-receptor interaction. Interestingly, the loss of NR4A1 in ACFs resulted in the downregulation of key inflammatory

recruitment pathways, marked by terms related to leukocyte migration and cell chemotaxis. This was corroborated by the KEGG enrichment of cytokine-cytokine receptor interaction and interleukin-10 signalling in Reactome. Additionally, the downregulated DEGs were attributed to terms such as “Rheumatoid arthritis” and “Dilated cardiomyopathy” in the KEGG analysis, suggesting the clinical relevance of these downregulated genes in chronic inflammatory and remodelling disorders.

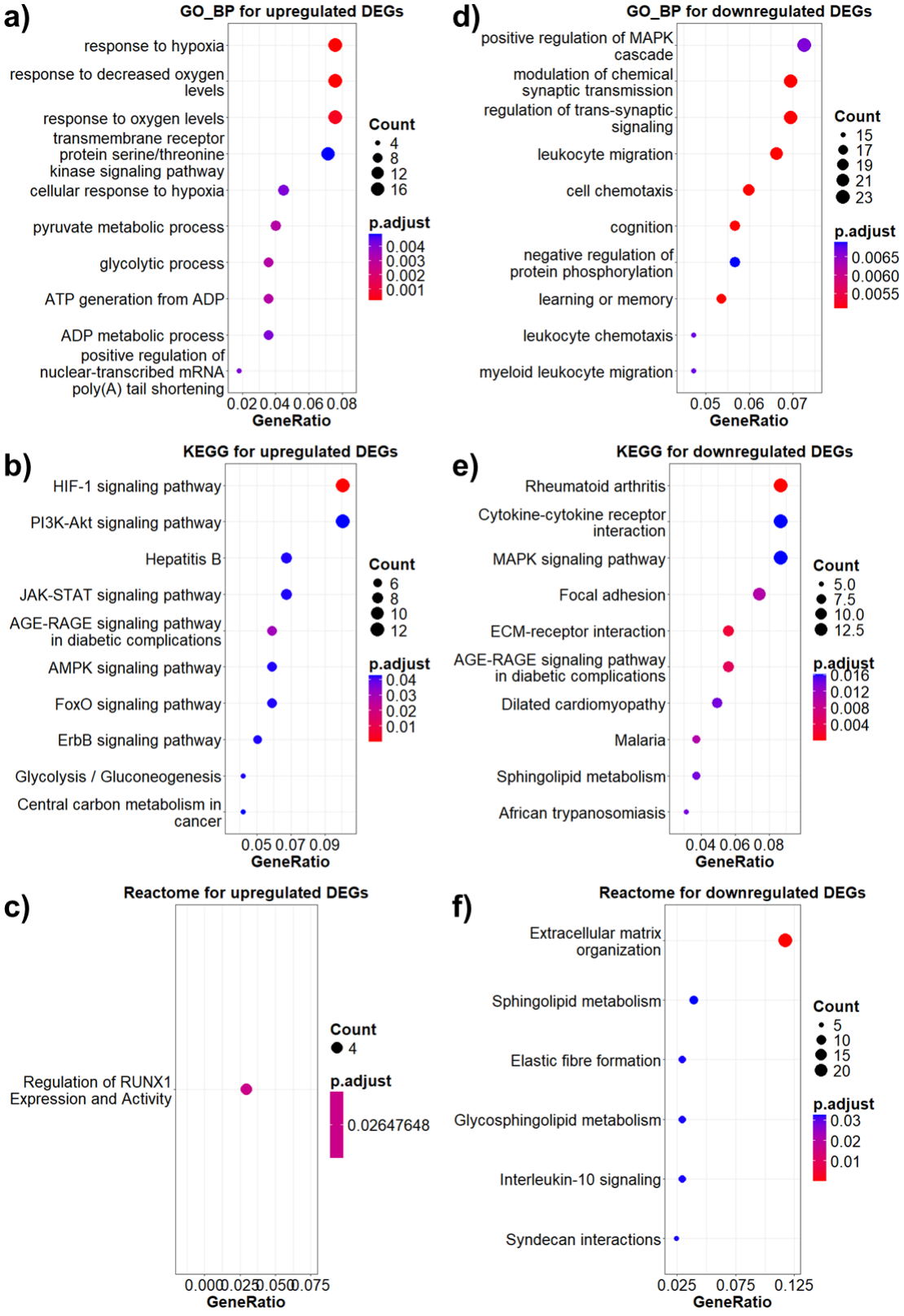
a)
GO_BP for upregulated DEGs
response to hypoxia
response to decreased oxygen levels
response to oxygen levels
transmembrane receptor protein serine/threonine kinase signaling pathway
cellular response to hypoxia
pyruvate metabolic process
glycolytic process
ATP generation from ADP
ADP metabolic process
positive regulation of nuclear-transcribed mRNA poly(A) tail shortening
0.02 0.04 0.06 0.08
GeneRatio
Count
4
8
12
16
p.adjust
0.004
0.003
0.002
0.001
d)
GO_BP for downregulated DEGs
positive regulation of MAPK cascade
modulation of chemical synaptic transmission
regulation of trans-synaptic signaling
leukocyte migration
cell chemotaxis
cognition
negative regulation of protein phosphorylation
learning or memory
leukocyte chemotaxis
myeloid leukocyte migration
0.05 0.06 0.07
GeneRatio
Count
15
17
19
21
23
p.adjust
0.0065
0.0060
0.0055
b)
KEGG for upregulated DEGs
HIF-1 signaling pathway
PI3K-Akt signaling pathway
Hepatitis B
JAK-STAT signaling pathway
AGE-RAGE signaling pathway in diabetic complications
AMPK signaling pathway
FoxO signaling pathway
ErbB signaling pathway
Glycolysis / Gluconeogenesis
Central carbon metabolism in cancer
0.05 0.07 0.09
GeneRatio
Count
6
8
10
12
p.adjust
0.04
0.03
0.02
0.01
e)
KEGG for downregulated DEGs
Rheumatoid arthritis
Cytokine-cytokine receptor interaction
MAPK signaling pathway
Focal adhesion
ECM-receptor interaction
AGE-RAGE signaling pathway in diabetic complications
Dilated cardiomyopathy
Malaria
Sphingolipid metabolism
African trypanosomiasis
0.04 0.06 0.08
GeneRatio
Count
5.0
7.5
10.0
12.5
p.adjust
0.016
0.012
0.008
0.004
c)
Reactome for upregulated DEGs
Regulation of RUNX1 Expression and Activity
0.000 0.025 0.050 0.075
GeneRatio
Count
4
p.adjust
0.02647648
f)
Reactome for downregulated DEGs
Extracellular matrix organization
Sphingolipid metabolism
Elastic fibre formation
Glycosphingolipid metabolism
Interleukin-10 signaling
Syndecan interactions
0.025 0.075 0.125
GeneRatio
Count
5
10
15
20
p.adjust
0.03
0.02
0.01

Figure 4.3.2 Pathway over-representation analysis of DEGs in human ACFs with NR4A1 knockdown. (**a-c**) Dot plots showing the top ten enriched pathways from GO biological processes, KEGG and Reactome for the upregulated DEGs comparing the NR4A1-siRNA knockdown group to negative control-siRNA group. (**d-f**) Dot plots showing the top ten enriched pathways from GO biological processes, KEGG and Reactome for the downregulated DEGs comparing the NR4A1-siRNA knockdown group to negative control-siRNA group. X-axis is gene ratio (proportion of genes from the input list within a biological pathway). Y-axis is the annotation of the enriched biological pathways. Number of DEG counts present in each pathway is visualised as the dot size. Adjusted *P*-values are visualised as colour gradient and calculated using the Benjamini-Hochberg method.

4.3.3 Therapeutic compounds re-establish gene signature induced by NR4A1 knockdown in human ACFs

To predict therapeutic compounds that would induce similar transcriptional changes regulated by NR4A1 knockdown in human ACFs, I performed the Connectivity Map (CMap) analysis. The CMap approach compares user-defined gene expression signatures with a large reference database of transcriptional profiles generated by chemical or drug perturbations obtained in human cell lines[215]. It enables the potential identification of compounds with shared or opposing mechanisms of action as NR4A1. The Query CMap tool has a technical limit of 150 genes for each upregulated and downregulated list. Hence, DEGs from my NR4A1 knockdown RNA-seq dataset with adjusted p-value < 0.05 and log2FC > 0.5 or < -0.5 were selected to run CMap analysis. The analysis is summarised in Table 4.3.3. Seven compounds have high positive connectivity scores (> 90), indicating functional similarity and recapitulating the transcriptional effects of NR4A1 knockdown. Within the seven compounds, five are classified as a glucocorticoid receptor agonist (fluorometholone, fluocinonide, hydrocortisone, fludroxycortide and fluticasone), while the other two are inositol monophosphatase (IMPase) inhibitor (L-690330 and L-690488).

Table 4.3.3 Top-ranked compounds identified by CMap analysis of the NR4A1 knockdown RNA-seq gene signature

Score	Type	ID	Name	Description
96.29	compound	BRD-A13133631	fluorometholone	Glucocorticoid receptor agonist
95.94	compound	BRD-A15297126	fluocinonide	Glucocorticoid receptor agonist
94.81	compound	BRD-A07000685	hydrocortisone	Glucocorticoid receptor agonist
94.59	compound	BRD-A49765801	fludroxycortide	Glucocorticoid receptor agonist
92.09	compound	BRD-K28470988	L-690330	Inositol monophosphatase inhibitor
91.47	compound	BRD-K14791739	fluticasone	Glucocorticoid receptor agonist
90.35	compound	BRD-K69328504	L-690488	Inositol monophosphatase inhibitor

4.3.4 Transketolase and integrin β1 are top downregulated genes in NR4A1 knockdown in human ACFs

To identify potential downstream targets of NR4A1, the DEGs from RNA-seq data were selected. The downregulated DEGs were specifically focused on as they followed the same regulatory direction as NR4A1 regulation by knockdown. Among the top five most significantly downregulated genes by log2FC (*TKT*, *NR4A1*, *ITGB1P1*, *CBX6* and *ITGB1*), *TKT* and *ITGB1* were selected for further investigation.

TKT (transketolase) was prioritised as it was the most significantly downregulated gene, exhibiting an exceptionally high statistical significance (log2FC = -1.596, adjusted *P*-value = 8.4695×10^{-191}). Additionally, *ITGB1* (integrin β1) was selected for further investigation because both the functional gene and its associated pseudogene (*ITGB1P1*) appeared within the top five downregulated DEGs. Integrins like *ITGB1* are well-established mediators of fibrotic responses in cardiac fibroblasts[216], making it a highly relevant candidate in the context of atrial fibrosis.

Raw transcript counts showed a consistent reduction of *TKT* and *ITGB1* expression in human ACFs from all four sinus rhythm donors following NR4A1 knockdown (Figure 4.3.4a-b). To validate these transcriptomic findings, the gene and protein expression of both targets were assessed by qPCR and western blot, respectively. NR4A1-deficient cells demonstrated significant downregulation of TKT at the mRNA level (Figure 4.3.4c) and protein level (Figure 4.3.4d). Similarly, NR4A1 knockdown reduced *ITGB1* at the mRNA level (Figure 4.3.4e). ITGB1 protein levels showed a similar reducing trend in NR4A1-deficient cells (Figure 4.3.4f).

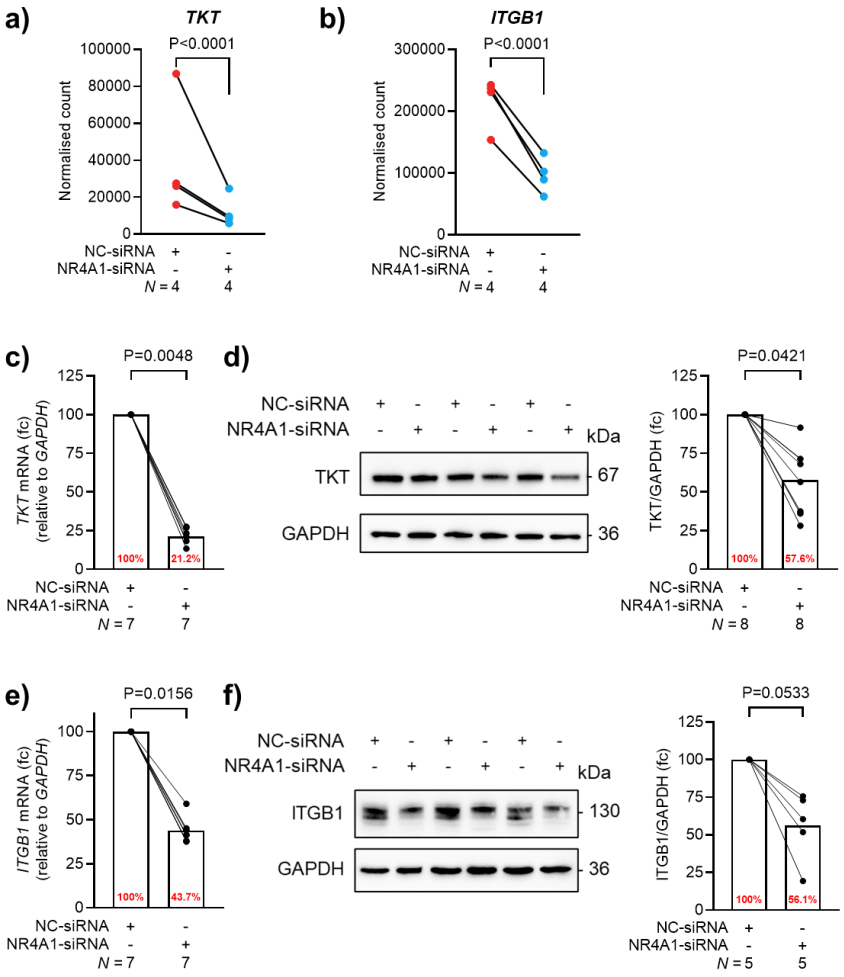

Figure 4.3.4 Validation of top downregulated genes in human ACFs with NR4A1 knockdown. (**a**-**b**) Dot plots showing normalised counts of *TKT* and *ITGB1* in ACFs with NR4A1 knockdown compared with negative control (NC-siRNA). (**c**-**d**) TKT gene and protein expression in NR4A1-deficient human ACFs compared with NC-siRNA. (**e**-**f**) ITGB1 gene and total protein (all bands) expression in NR4A1-deficient human ACFs compared with NC-siRNA. Experiments performed using sinus rhythm donor-derived human ACFs. Data are paired lines (**a**-**b**) or mean with paired lines (**c**-**f**); each paired line represents an independent biological replicate (*N*). Data are expressed as a percentage of the negative control group (NC-siRNA) (**c**-**f**). *P*-values are determined from differential expression analysis in DESeq2 using Wald test (**a**-**b**) or raw values and reported as two-sided using paired t-test (**c**-**d**), Wilcoxon test (**e**) and ratio paired t-test (**f**).

4.3.5 NR4A1-mediated fibrotic regulation is not dependent on transketolase or integrin β1 signalling

To assess the effects of TKT and ITGB1 regulation on fibrotic responses in human ACFs, siRNA-knockdown of each target was performed. For TKT knockdown, successful knockdown was confirmed by the reduction of *TKT* mRNA in Lonza human ACFs (Figure 4.3.5a). TKT deficiency in ACFs did not regulate the mRNA levels of *ACTA2* (Figure 4.3.5b), *COL1A1* (Figure 4.3.5c) and *POSTN* (Figure 4.3.5d). For ITGB1 knockdown, successful knockdown was confirmed by the reduction of *ITGB1* mRNA in human ACFs derived from sinus rhythm donors (Figure 4.3.5e). ITGB1 deficiency significantly upregulated *ACTA2* mRNA ($P = 0.0153$; Figure 4.3.5f). However, the effects on *COL1A1* and *POSTN* gene expression were not significant (Figure 4.3.5g-h).

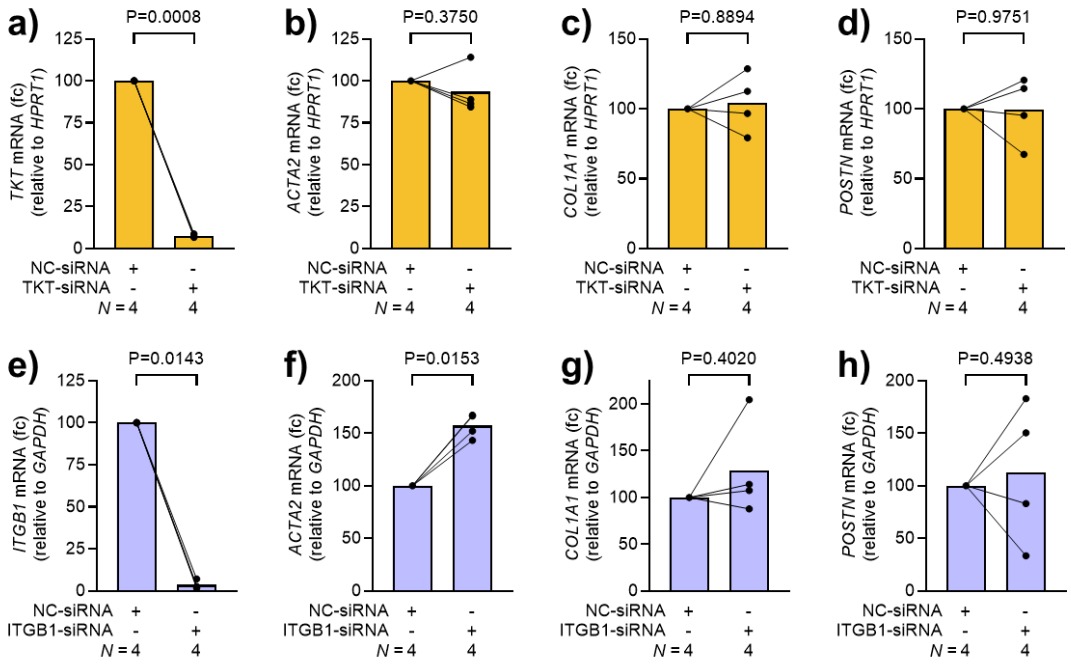

Figure 4.3.5 Effect of transketolase or integrin β1 deficiency on gene expression of selected fibrotic markers. (**a**) Successful knockdown of TKT in human ACFs. (**b-d**) *ACTA2*, *COL1A1* and *POSTN* mRNA levels in TKT-deficient human ACFs (coloured in yellow). (**e**) Successful knockdown of ITGB1 in human ACFs. (**f-h**) *ACTA2*, *COL1A1* and *POSTN* mRNA levels in

ITGB1-deficient human ACFs (coloured in purple). Experiments performed using Lonza human ACFs (**a-d**) and sinus rhythm donor-derived human ACFs (**e-h**). Data are mean with paired lines; each paired line represents an independent biological replicate (*N*). Data are expressed as a percentage of the negative control group (NC-siRNA). *P*-values are determined from raw values and reported as two-sided using paired t-test (**a**, **c**-**h**) and Wilcoxon test (**b**).

4.3.6 Topological analysis identifies IL-6 as a key downstream effector of NR4A1

To further investigate the functional hierarchy of the DEGs from the RNA-seq data, a PPI network was constructed to visualise the systematic coordination of ACFs in response to NR4A1 knockdown. The initial network was generated using the STRING database, followed by employing the cytoHubba plugin in Cytoscape to pinpoint the most biologically significant proteins within this network. To ensure the robustness of the selection of core hub proteins and minimise algorithmic bias, four distinct topological ranking methods were utilised, and the complete results are provided in Table 4.3.6. A representative illustration of the core hub network using the MCC algorithm is demonstrated (Figure 4.3.6a), highlighting the top ten ranked core hub targets. The integration of the top-ranked targets across all four algorithms consistently identified IL-6 as a primary core hub. IL-6 achieved the highest cumulative rank (Figure 4.3.6b), suggesting it serves as a critical signalling node within the NR4A1-regulated transcriptomic landscape. Given the significant downregulation of *IL6* following NR4A1 knockdown from RNA-seq data (Figure 4.3.6c) and *in vitro* validation in ACFs from sinus rhythm donors (Figure 4.3.6d), these results indicate that IL-6 is a key downstream effector likely mediating the fibrotic responses in ACFs.

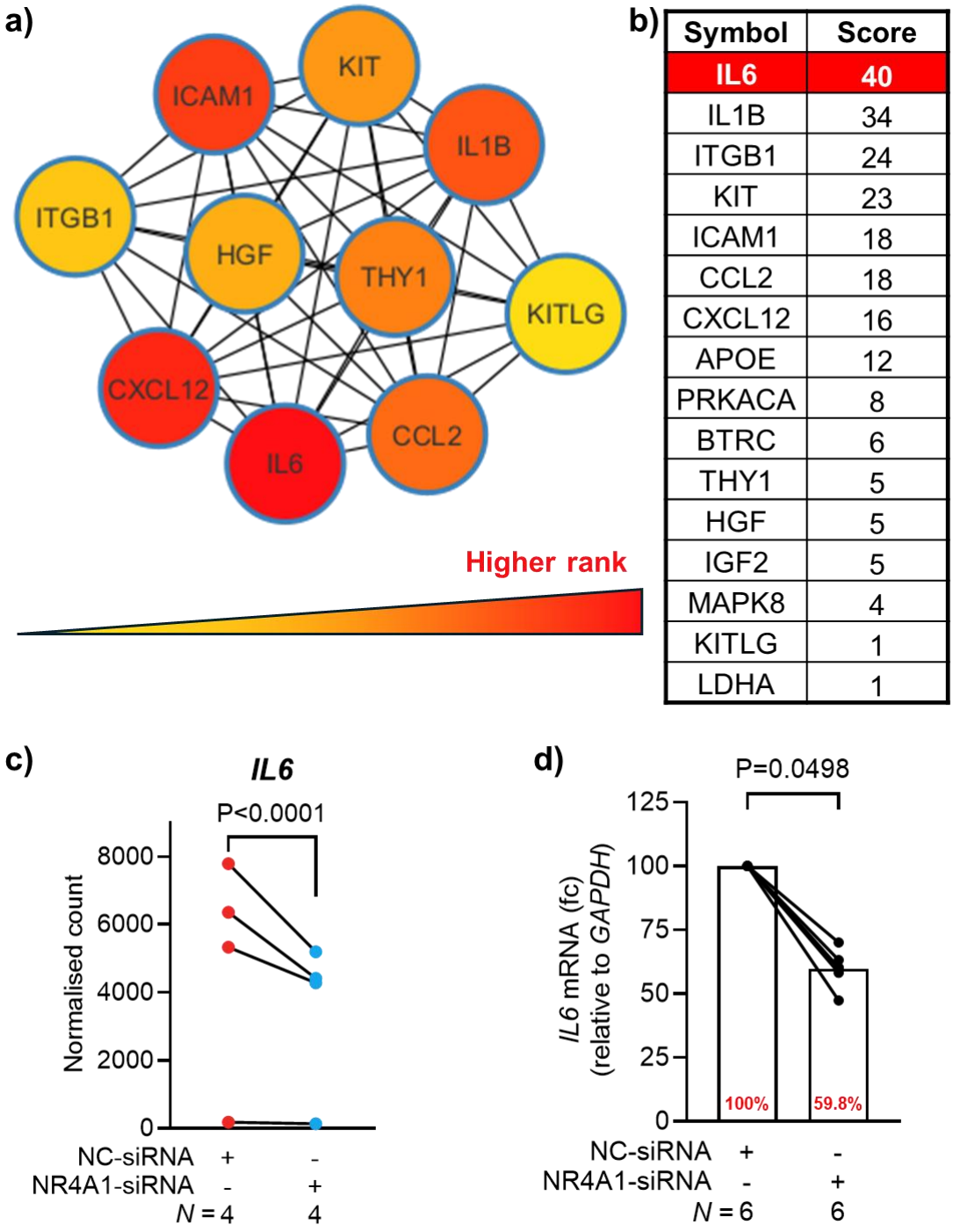

Figure 4.3.6 Identification of key downstream effector of NR4A1 in PPI network analysis.

PPI network of DEGs was constructed using the STRING database and exported to Cytoscape. The top ten hub genes were ranked using the CytoHubba plugin based on four algorithms. (**a**) Representative core hub network based on the MCC algorithm showing the top ten ranked hub

genes. Nodes represent targets and darker colour intensity corresponds to higher ranking in the network. (**b**) A score is assigned to the targets in each core hub network, top rank (1^{st}) corresponds to a score of 10, and 10^{th} rank corresponds to a score of 1. The sum of scores from all four algorithm-based networks are presented in the table and ordered from highest to lowest total score. (**c**) Dot plot showing normalised counts of *IL6* in ACFs with NR4A1 knockdown compared with negative control. (**d**) Bar graph showing *IL6* mRNA levels in NR4A1-deficient human ACFs compared with negative control (NC-siRNA). Experiments performed using sinus rhythm donor-derived human ACFs (**c-d**). Data are expressed as a percentage of NC-siRNA (**d**). *P*-values are determined from differential expression analysis in DESeq2 using Wald test (**c**) or raw values and reported as two-sided using paired t-test (**d**).

Table 4.3.6 Identification of core hub genes in topological analysis using cytoHubba

cytoHubba algorithm 1: MCC		
Rank	**Symbol**	**MCC score**
1	IL6	986678
2	CXCL12	913002
3	ICAM1	852149
4	IL1B	824190
5	CCL2	752361
6	THY1	742858
7	KIT	719740
8	HGF	608338
9	ITGB1	472270
10	KITLG	446638
cytoHubba algorithm 2: Degree		
Rank	**Symbol**	**Degree score**
1	IL6	70
2	IL1B	67
3	ITGB1	43
4	KIT	43
5	CCL2	42
6	ICAM1	40
7	CXCL12	39
8	APOE	35
9	HGF	32
10	IGF2	29

cytoHubba algorithm 3: Closeness		
Rank	**Symbol**	**Closeness score**
1	IL6	209.5333
2	IL1B	206.4
3	KIT	187.9095
4	ITGB1	186.1595
5	CCL2	185.6429
6	ICAM1	182.7595
7	APOE	182.0667
8	CXCL12	180.3095
9	IGF2	176.2095
10	MAPK8	175.5929
cytoHubba algorithm 4: Betweenness		
Rank	**Symbol**	**Betweenness score**
1	IL6	21487.25
2	IL1B	20265.33
3	PRKACA	12431.81
4	ITGB1	11978.22
5	BTRC	11424.35
6	APOE	11168.23
7	KIT	10806.99
8	MAPK8	8676.623
9	IGF2	8375.493
10	LDHA	7802.146

4.3.7 Putative NR4A1 binding sites are identified within the IL6 gene

To determine whether *IL6* could be a direct transcriptional target of NR4A1, I performed an *in-silico* transcription factor binding site analysis using the JASPAR database[217]. My analysis identified seven putative NR4A1 binding sites within the upstream regulatory region of the human *IL6* gene with a relative score above 0.8 (Table 4.3.7).

Subsequently, I used the UCSC Genome Browser to analyse the putative NR4A1 binding sites[218]. Out of the seven predicted motifs, there were four located within the promoter region upstream of the *IL6* transcription start site, a region typically enriched for functional transcription factor binding sites that regulate gene transcription[219]. Out of those, one predicted motif (AAAGTGCA) was close to the transcription start site (-202 bp upstream of transcription start site) and moderately conserved over species, indicated by the phastCons100way score = 0.4970 and the phyloP100way score = 0.6126. This predicted motif also overlaps with DNase I hypersensitivity peak clusters derived from assays by the ENCODE project (cluster score = 1000 out of 1000) and overlaps with binding regions of twenty-three transcription factors derived from chromatin immunoprecipitation-sequencing (ChIP-seq) data by the ENCODE project. Together with the RNA-seq data demonstrating *IL6* downregulation associated with NR4A1 knockdown, my *in-silico* predictions support that NR4A1 may transcriptionally regulate *IL6* through direct binding to its promoter.

Table 4.3.7 Prediction of NR4A1 binding sites within the human *IL6* gene promoter region

JASPAR							Distance to TSS	Evolutionary conservation		Chromatin accessibility		
Name	Score	Relative score	Start	End	Strand	Predicted sequence	bp	phastCons100way	phyloP100way	Cluster score	Overlap with ChIP-seq peaks?	Overlap with CREs?
MA1112.3. NR4A1	9.441154	0.8953813	620	627	+	AGAGGTCA	-1381	0	0.173634	719	Yes (29)	Promoter
MA1112.3. NR4A1	8.532392	0.8777464	580	587	+	AAATGTTA	-1421	0.634843	0.894919	719	Yes (29)	Promoter
MA1112.3. NR4A1	7.953786	0.8665183	269	276	-	AAATTTCA	-1732	0.550197	0.740937	NA	Yes (5)	Proximal enhancer
MA1112.3. NR4A1	6.735245	0.8242872	1799	1806	-	AAAGTGCA	-202	0.497047	0.612626	1000	Yes (23)	Promoter
MA1112.3. NR4A1	6.170368	0.8319105	1268	1275	+	AGAGGGCA	-733	0.089567	0.418362	1000	Yes (36)	Proximal enhancer
MA1112.3. NR4A1	5.158574	0.8122762	46	53	-	AAAGGTTT	-1955	0	-0.134803	467	Yes (1)	NA
MA1112.3. NR4A1	4.829051	0.8058817	549	556	-	TGAGGTCA	-1452	0.984252	1.25151	719	Yes (27)	Promoter

4.3.8 IL-6 increases collagen secretion in human ACFs

To establish an *in vitro* model of IL-6 stimulation, human ACFs from sinus rhythm donors were incubated for 24 hours with 50 ng/mL of human IL-6 recombinant protein. Gene expression of fibrotic markers was profiled in IL-6-stimulated cells to assess any pro-fibrotic effects on the transcriptional level. Apart from *COL1A1* showing a trend of increased mRNA levels (P = 0.0857), IL-6 stimulation did not change expression of *ACTA2*, *COL3A1*, *POSTN* and *FN1* (Figure 4.3.8a). Previous studies found increased collagen production in IL-6-treated adult rat ventricular fibroblasts[220,221]. Therefore, I tested whether the same applies to human ACFs from sinus rhythm donors and found that total collagen content was significantly increased by IL-6 stimulation in human ACF secretomes (P = 0.0225; Figure 4.3.8b). This elevation was reversed by the IL-6 neutralising antibody (P = 0.0049; Figure 4.3.8b), confirming the specificity of IL-6-mediated effects.

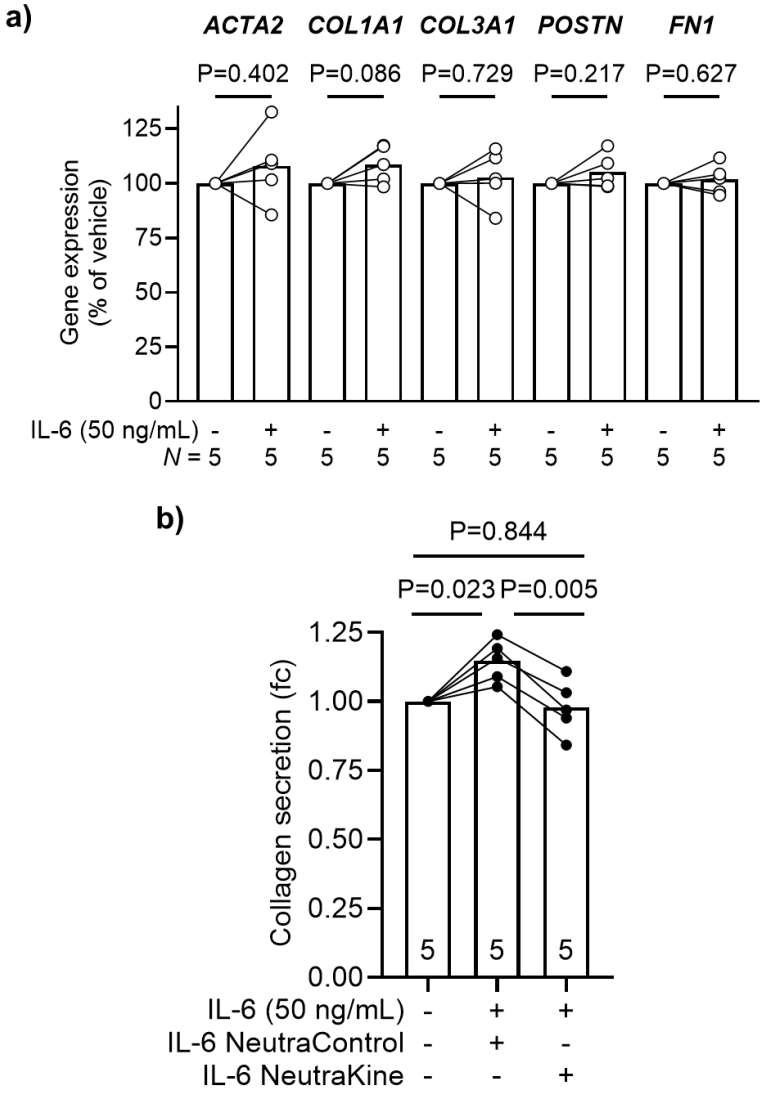

Figure 4.3.8 Effect of IL-6 stimulation on fibrotic responses in human ACFs. (**a**) mRNA levels of selected fibrotic markers under 50 ng/mL IL-6 stimulation in human ACFs. (**b**) Total collagen content in secretome of IL-6-stimulated human ACFs co-treated with IL-6 neutralising (NeutraKine) or neutralising control (NeutraControl) antibodies. Experiments performed using sinus rhythm donor-derived human ACFs. Data are mean with paired lines; each paired line represents an independent biological replicate (*N*). Data are expressed as a percentage of the vehicle control group (**a**) or fold change of the negative control group (vehicle) (**b**). *P*-values are determined from raw values and reported as two-sided using ratio paired t-test (**a**) and lognormal repeated-measures one-way ANOVA with post-hoc Tukey's test (**b**).

4.3.9 PGA2 stimulates the upregulation of pro-inflammatory cytokines in human ACFs

In addition to confirming IL-6 as a downstream target of NR4A1 in human ACFs, this study also evaluated how the endogenous NR4A1 ligand, PGA2, regulates pro-inflammatory cytokines such as IL-6 and IL-1β. Dose optimisation of PGA2 stimulation was carried out with a range of concentrations (0-20 μM) in human ACFs from sinus rhythm donors. Cytotoxic effects of PGA2 were observed in ACFs when treated at 20 μM and excluded for analysis. *IL6* mRNA was increased in a dose-response manner by 24 hours treatment of PGA2, and the upregulation was significant at 10 μM of PGA2 (Figure 4.3.9a). The extent of *IL6* upregulation was consistent and sustained even at 48 hours treatment of PGA2 (Figure 4.3.9b). *IL1B* mRNA was similarly increased in a dose-response manner by 24 hours treatment of PGA2, and the upregulation was significant at both 5 and 10 μM of PGA2 (Figure 4.3.9c). For 48 hours treatment, although *IL1B* expression was gradually elevated as PGA2 concentration increased, the extent of upregulation was much lower compared to 24 hours PGA2 treatment (Figure 4.3.9d). Therefore, the final conditions of PGA2 stimulation were established at 10 μM for 24 hours in the following experiments.

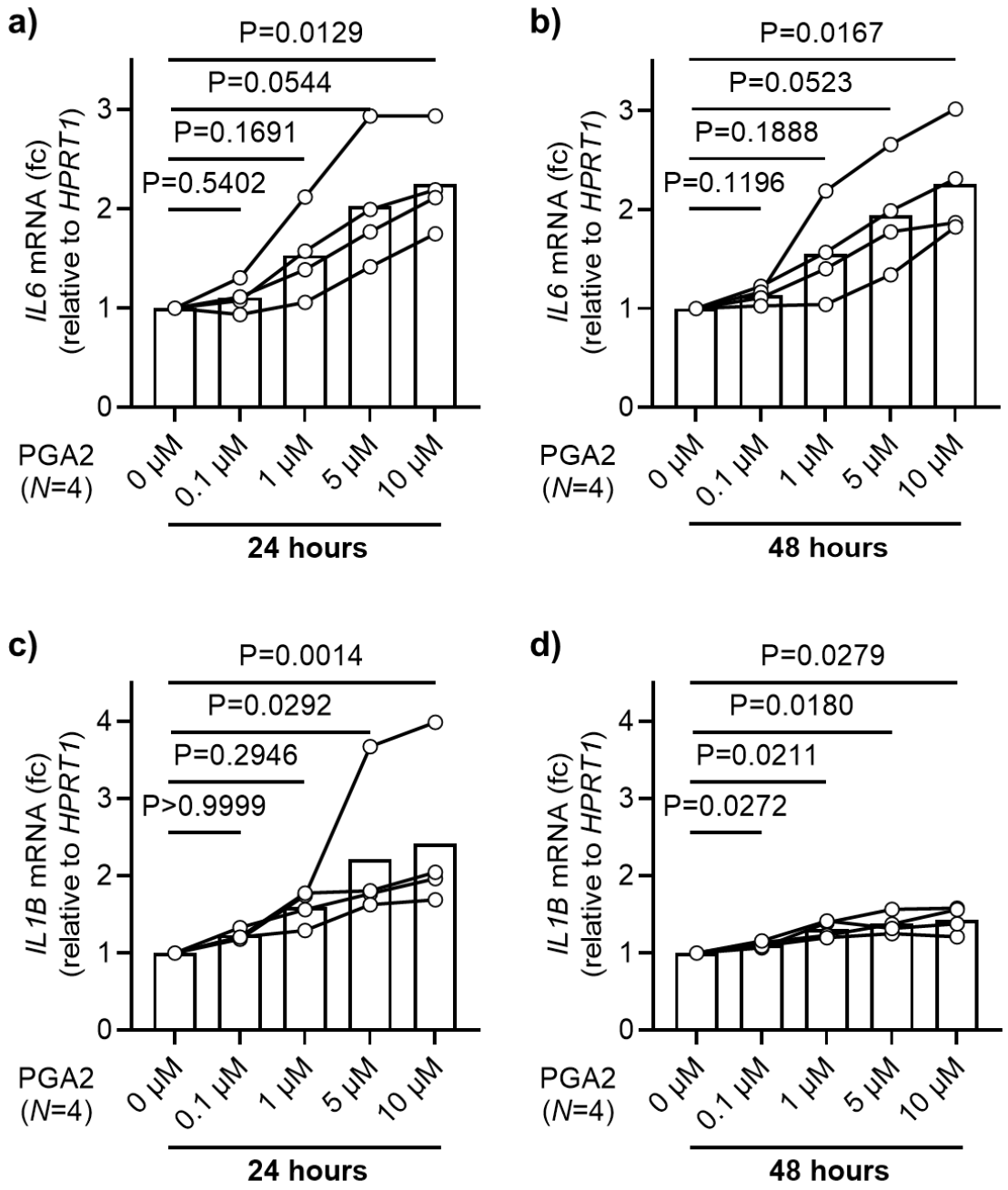

Figure 4.3.9 Effect of PGA2 stimulation on gene expression of pro-inflammatory cytokines *IL6* and *IL1B* in human ACFs. (**a**-**b**) Gene expression of *IL6* in human ACFs at 24- or 48-hour PGA2 stimulation with 0, 0.1, 1, 5 and 10 μM concentrations. (**c**-**d**) Gene expression of *IL1B* in human ACFs with 24- or 48-hour PGA2 stimulation with 0, 0.1, 1, 5 and 10 μM concentrations. Experiments performed using sinus rhythm donor-derived human ACFs. Data

are mean with paired lines; each paired line represents an independent biological replicate (*N*). Data are expressed as a percentage of the vehicle control group (0 μM). *P*-values are determined from raw values and reported as two-sided using lognormal repeated-measures one-way ANOVA with post-hoc Dunnett's test (**a**-**b**, **d**) and Friedman test with post-hoc Dunn's test (**c**).

4.3.10 NR4A1 deficiency suppresses the PGA2-induced upregulation of IL-6

When Lonza human ACFs were stimulated by PGA2 alone, *IL6* mRNA (Figure 4.3.10a) and IL-6 secreted protein levels (Figure 4.3.10b) were increased compared with non-stimulated control. However, the elevated levels of IL-6 by PGA2 stimulation were attenuated and suppressed in NR4A1-deficient cells. These regulatory effects were similarly detected in *IL1B* gene expression (Figure 4.3.10c). Although IL-1β protein levels were evaluated within the same ACF secretome samples, they remained below the ELISA detection limit, suggesting minimal expression in human ACFs.

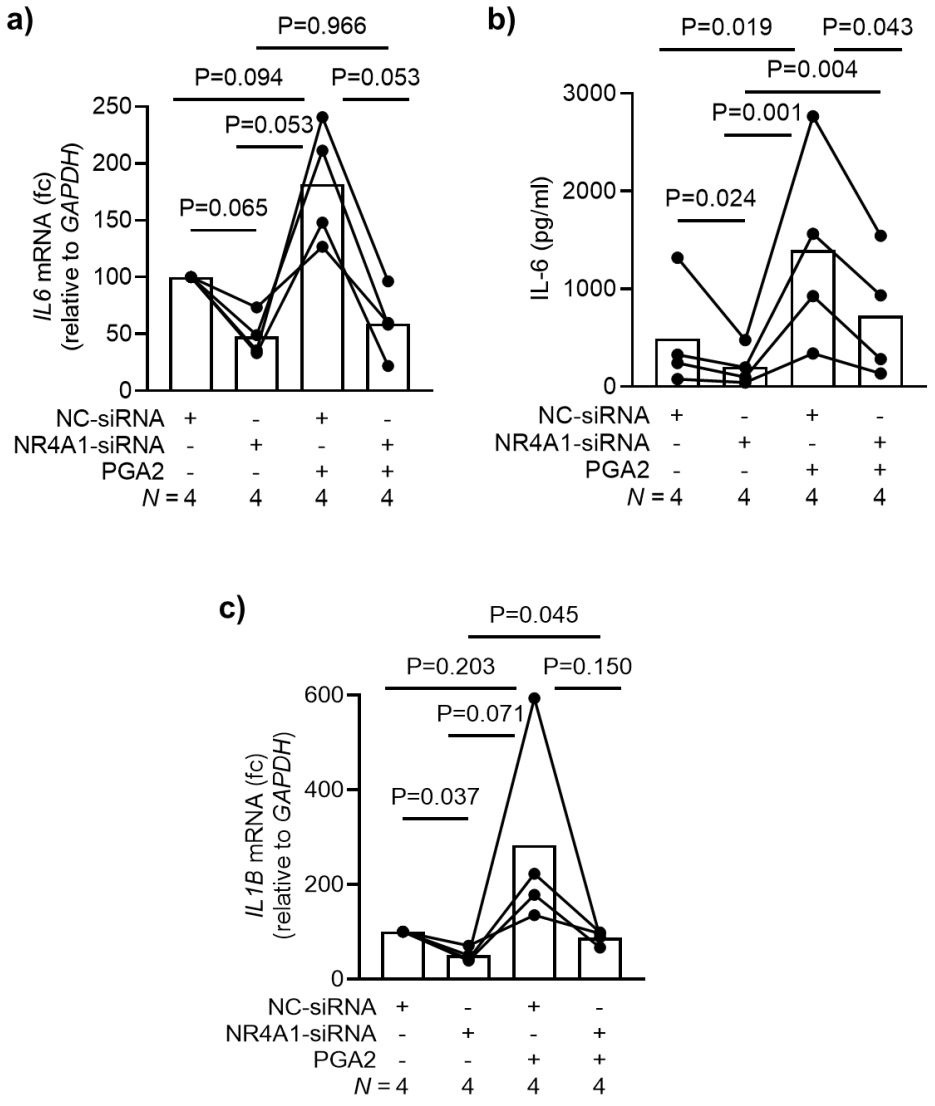

Figure 4.3.10 Effect of NR4A1 deficiency on PGA2-stimulated upregulation of IL-6 in human ACFs. (**a**) *IL6* mRNA levels in PGA2-stimulated human ACFs with NR4A1 knockdown. (**b**) IL-6 levels in secretome of PGA2-stimulated human ACFs with NR4A1 knockdown. (**c**) *IL1B* mRNA levels in PGA2-stimulated human ACFs with NR4A1 knockdown. Experiments performed using Lonza human ACFs. Data are mean with paired lines; each paired line represents an independent biological replicate (*N*). Data are expressed as a percentage of the negative control group (NC-siRNA without PGA2 stimulation) (**a**, **c**) or absolute values (**b**). *P*-values are determined from raw values and reported as two-sided using lognormal repeated-measures one-way ANOVA with post-hoc Tukey's test.

4.4 Discussion

This chapter aimed to explore the transcriptional changes downstream of NR4A1 knockdown in human ACFs. The RNA-seq data substantiates the *in vitro* functional findings from my previous chapter, confirming NR4A1 as a pro-fibrotic regulator in human ACFs. Beyond the downregulation of *ACTA2* and *POSTN* validated by qPCR, NR4A1-deficient ACFs exhibited suppression of broader fibroblast activation markers, including *ITGA5*, *TNC*[222]. Interestingly, canonical myofibroblast markers such as *COL1A1*, *FAP*, *FN1* and *TGFB1* were not altered at the transcript level. This dissociation suggests that NR4A1 may govern distinct aspects of the fibrotic phenotype – specifically ECM organisation and cell-matrix interaction – rather than the global ECM synthesis. This aligns with studies demonstrating that activated fibroblasts and differentiated myofibroblasts represent heterogeneous states, where morphology, contractility and secretory functions can be dissimilar[223,224].

Pathway analysis of upregulated DEGs initially indicates that NR4A1 knockdown drives ACFs toward a state of "pseudohypoxia" and metabolic reprogramming. However, the unexpected enrichment of HIF-1 pathway genes under normoxic conditions must be interpreted cautiously. HIF-1 is a classic transcription factor whose active subunit is tightly regulated at the post-translational level by the von Hippel-Lindau ubiquitylation complex, which targets it for rapid degradation and inactivation of transcriptional activity in the presence of normal oxygen levels[225]. Because this acute oxygen-sensing mechanism operates independently of the gene expression machinery, elevated RNA levels of HIF-1 pathway targets do not necessarily equate to functional protein activity or pathway execution. Indeed, examination of my NR4A1 knockdown RNA-seq dataset reveals that canonical downstream targets of HIF-1, such as *VEGF* and *FGF*, are not significantly regulated. This suggests that despite the transcriptomic

enrichment of hypoxia-associated genes, the actual functional downstream effects of the HIF-1 pathway are absent.

Consequently, the accompanying enrichment of glycolytic pathways may represent an incomplete transcriptomic stress response rather than a functional metabolic shift. This glycolytic reprogramming typically points to a Warburg-like metabolic shift that is often observed in highly proliferative cancer cells[226]. Existing literature on NR4A1 and glycolysis is contradictory; while it acts as a suppressor in hepatocellular carcinoma[227], it has been shown to promote glycolysis in hypoxic pulmonary artery smooth muscle cells[228]. However, a critical paradox emerges in this dataset. While the Warburg-like effect typically fuels the high energetic demands of myofibroblast differentiation and collagen secretion[229], NR4A1-deficient ACFs exhibit this metabolic transcriptomic signature alongside a suppressed fibrotic phenotype. Rather than a state of true metabolic uncoupling, it is probable that these NR4A1-deficient cells experience early transcriptional glycolytic stress but lack the functional HIF-1 protein activity and downstream machinery to translate this into a pro-fibrotic response. Ultimately, metabolic flux analysis and functional measurements of cellular energy levels are required to validate the true metabolic state of these cells and confirm this speculation.

Conversely, the downregulated DEG reveal that NR4A1 is essential for structural remodelling and immunomodulation. The suppression of focal adhesion and ECM-receptor interaction pathways implies that NR4A1 may contribute to the physical integrity of the ACF-ECM interface. Since the ECM serves as both a scaffold and a reservoir for signalling molecules[230], its disruption may impact intercellular communication required to orchestrate cardiac remodelling and fibrosis following injury.

Furthermore, the downregulation of leukocyte migration and cytokine-cytokine receptor interactions highlights an immune-regulatory role. of NR4A1. Indeed, previous studies showed that NR4A1 deletion prevents LPS-induced pro-inflammatory response by switching macrophages to an anti-inflammatory phenotype[160]. Additionally, the association of NR4A1 with immunomodulatory response is consistent with the NF-κB-linked pathway that was enriched in the specific *NR4A1+* fibroblast subtype[132]. Atrial fibrosis is driven by a vicious cycle of inflammation and fibrotic remodelling, which triggers and perpetuates AF[231]. Inflammatory cells release pro-inflammatory cytokines like TNF-α, IL-1β and IL-6 to stimulate upregulation of pro-fibrotic mediators like TGF-β, driving activation and differentiation of cardiac fibroblasts. On the contrary, myofibroblasts produce excessive amount of ECM proteins and chemokines, further activating and recruiting more immune cells to enhance this cardiac inflammatory-fibrotic response. Therefore, these data suggest NR4A1 may act as a master regulator integrating inflammatory signalling with fibrotic remodelling in human ACFs.

To further translate these transcriptomic changes into potential pharmacological insights, the NR4A1 knockdown gene expression signature was utilised to query the CMap database. The analysis yielded seven top-ranking compounds with a high positive connectivity score (> 90), indicating these drugs strongly mimic the NR4A1-deficient cellular phenotype. Remarkably, five of these seven compounds are glucocorticoid receptor agonists. Glucocorticoid receptor activation is a canonical pharmacological mechanism for immunosuppressive and anti-inflammatory effects[232]. It acts primarily through the transrepression of NF-κB and the subsequent dampening of pro-inflammatory cytokines, including IL-6[233]. Additionally, glucocorticoid receptor agonists modulate inflammatory response by promoting the transactivation of anti-inflammatory genes[234]. Clinical studies show contradictory effects of glucocorticoids in patients with AF. While a meta-analysis has demonstrated that the administration of glucocorticoids lowers postoperative AF incidence especially at low dose[235],

another study indicate glucocorticoid use increases the risk of developing AF or flutter by nearly 2-fold[236]. Nevertheless, this pharmacological insight aligns with my pathway analysis, reinforcing the findings that NR4A1 depletion in human ACFs resulted in downregulation of pro-inflammatory gene signatures. Furthermore, the remaining two compounds from CMap analysis were IMPase inhibitors. IMPase is a key enzyme that plays critical role in the myo-inositol metabolism, which regulates calcium homeostasis, signal transduction and metabolism[237]. The observation that IMPase inhibitors mimic NR4A1 knockdown transcriptional changes suggests that NR4A1 may regulate intracellular second messenger pathways for ACF activation, alongside promoting inflammation.

To dissect the molecular axis downstream of NR4A1, I initially investigated top downregulated targets. *TKT*, a key enzyme in the pentose phosphate pathway[238], was downregulated; however, TKT knockdown was unable to replicate the anti-fibrotic effects of NR4A1 deficiency. While transketolase promotes fibrosis in the liver[239], its lack of effect in human ACFs suggests tissue-specific regulatory mechanisms, ruling it out as the primary NR4A1 downstream mediator in this context.

Similarly, knockdown of ITGB1 yielded unexpected results, upregulating *ACTA2* levels. This is likely a compensatory response: the loss of a major mechano-transducer like integrin β1 may trigger a feedback loop, driving ACFs to upregulate other contractile elements (such as αSMA) to preserve tension and structural integrity. Furthermore, ITGB1 knockdown did not alter *COL1A1* or *POSTN* expression, indicating that targeting a single integrin subunit is insufficient to disrupt the broader fibrotic remodelling due to redundancy and complex regulation in ECM-receptor signalling in human ACFs. Consequently, the approach focusing on top individual DEGs proved limited biological interpretation.

To identify the master regulators orchestrating this complex response, a PPI network approach was adopted, taking protein functions into consideration beyond the transcriptional level from pathway analysis. The PPI network analysis of all DEGs identified IL-6 as the top core hub, positioning the cytokine a s a central node connecting the altered transcriptomic landscape by NR4A1 knockdown. This finding bridges the gap between the observed anti-fibrotic phenotype and the downregulated inflammatory signatures upon NR4A1 deficiency, reinforcing the hypothesis that NR4A1 orchestrates atrial fibrosis through an immunomodulatory mechanism.

The identification of IL-6 as a downstream effector of NR4A1 is highly consistent with the pathophysiology of AF. Elevated circulating levels and trans-signalling levels of IL-6 are well established biomarkers for AF incidence[240–242]. In postoperative AF, an upregulated IL-6 signalling was identified, which was attributed to the atrial macrophages as the main cell type[243]. While IL-6 as a pro-inflammatory mediator is mainly released by macrophages in cardiovascular disease, the current data confirms that human ACFs are not merely passive responders but active sources of IL-6. I demonstrated that treatment with exogenous recombinant IL-6 directly stimulates collagen secretion in human ACFs, and this pro-fibrotic response was abolished by IL-6 neutralisation. This suggests an autocrine loop in ACFs where NR4A1-driven IL-6 secretion promotes accumulation of key ECM components, providing a mechanistic explanation for the anti-fibrotic phenotype observed in NR4A1-deficient cells. Further studies are required to determine if NR4A1 directly binds the *IL6* promoter response elements or functions as a coactivator for other transcription within the nucleus.

To delineate the upstream regulation of this NR4A1/IL-6 signalling, I investigated PGA2, an endogenous cyclopentenone prostaglandin identified as an endogenous agonist for NR4A1. The results revealed a pro-inflammatory effect where PGA2 treatment significantly upregulated IL-

1β and IL-6 expression in human ACFs. Importantly, this response was partially dependent on NR4A1 availability in the cells. NR4A1 knockdown effectively suppressed the PGA2-induced elevation of these pro-inflammatory cytokines. This supports NR4A1 as a mediator of PGA2-induced pro-inflammatory signalling and pro-fibrotic output (IL-6).

This observation adds a novel layer of complexity to the biological role of NR4A1. In macrophages, NR4A1 is characterised as a repressor of inflammation by inactivating and limiting NF-κB transcriptional activity[244]. In contrast, my data in human ACFs indicates that NR4A1 acts as an activator of inflammatory signalling. This dichotomy suggests that NR4A1 function is highly cell-type specific and context-dependent. In the distinct microenvironment of the atrium, the PGA2-NR4A1-IL6 axis appears to drive a maladaptive response, potentially contributing to the vicious cycle of inflammation and fibrosis the atrial myocardium.

Collectively, this chapter elucidates a novel immuno-fibrotic mechanism driving atrial fibrosis. NR4A1 functions as a critical transducer that integrates upstream lipid signalling – specifically the endogenous ligand PGA2 – to orchestrate a pro-inflammatory program centred on IL-6. This suggests a regulatory PGA2-NR4A1-IL6 axis, where NR4A1-dependent cytokine secretion may contribute to the AF-associated ECM remodelling in atrial myocardium. These findings highlight the active role of fibroblasts in immune signalling and differentiating a distinct activated fibroblast subtype from the myofibroblasts. It also suggests that targeting the NR4A1-IL6 axis could offer a therapeutic benefit by simultaneously dampening atrial inflammation and fibrosis.

CHAPTER 5: PROFILING OF NR4A1 AND ASSOCIATED SIGNALLING COMPONENTS IN AF

5.1 Introduction

In the preceding chapter, I provided evidence for a potential mechanistic signalling pathway, PGA2-NR4A1-IL6, mediating fibrotic responses in human ACFs. Specifically, my findings demonstrated that NR4A1 acts as a master regulator of intrinsic inflammation, driving a pro-fibrotic phenotype through the upregulation of IL-6. My results indicate that this could be potentially triggered by the endogenous ligand PGA2. Crucially, this mechanism was identified in fibroblasts isolated directly from human atrial tissue, distinguishing these findings from prior studies reliant on rodent ventricular models[160,161]. Given that AF pathology is dominated by atrial-specific remodelling, a process distinct from ventricular fibrosis in embryological origin and response to pro-fibrotic stimuli[44,245], these findings hold significant translational promise. However, demonstrating a molecular mechanism *in vitro* is only the initial step. To validate the clinical relevance of this axis, it is essential to profile how these specific signalling components are regulated in the complex, physiological environment of the arrhythmic atrium, specifically in patients with persistent AF.

Atrial fibrosis is the hallmark of structural remodelling in long-standing AF, creating substrates that perpetuates the arrhythmia and renders electrical cardioversion ineffective[246]. ACFs are the main drivers of this structural remodelling process[247]. Despite its central role in disease progression, atrial fibrosis remains a significant unmet clinical need in AF. Current pharmacological strategies for AF primarily control rate or rhythm to restore sinus rhythm[20], but there are no FDA-approved therapies that specifically suppress or reverse atrial fibrosis in AF.

This therapeutic gap highlights the importance of understanding the mechanisms driving atrial remodelling in AF, such as the inflammatory-fibrotic axis. Systematic and local inflammation are major drivers of AF pathogenesis[83]. Clinical data consistently shows that pro-inflammatory cytokines, particularly IL-6, are elevated in AF patients and correlated strongly with left atrial size and AF duration[242,248]. However, given NR4A1's pleiotropic roles in different organs affecting complex biological functions[249], targeting NR4A1 globally or inflammation broadly is fraught with risk and side effects. Therefore, validating the specific NR4A1-IL6 axis in human AF ACFs could offer a more precise approach by targeting the downstream pathogenic effector (IL-6) or the upstream atrial-specific trigger (PGA2), rather than the nuclear receptor itself.

Despite the clear *in vitro* evidence for NR4A1's pro-fibrotic role in human ACFs (chapters 3 and 4), the existing findings regarding NR4A1 expression in AF are often contradictory. Understanding the precise regulation of NR4A1 in atrial tissues from patients is critical to reconciling these disparities. Transcriptional profiling of human left atrial appendage tissues has yielded inconsistent results. For instance, GSE69890 bulk RNA-seq dataset reveals a significant downregulation of *NR4A1* in persistent AF tissues compared to sinus rhythm[250]. In contrast, another large-scale bulk RNA-seq data in the CTSN cohort reports unchanged *NR4A1* left atrial expression in persistent AF[132].

This transcriptional complexity extends to animal models and single-cell resolution. In a transcriptomic study of horse AF models (both naturally occurring persistent AF and tachypacing-induced AF), *NR4A1* was significantly downregulated in both left and right atria[251]. However, a proteomic comparison in these models reveals a discordance. While the transcript was downregulated in AF, the protein levels of NR4A1 remained unchanged[251,252].

This suggests that post-transcriptional regulation of NR4A1 levels in AF may play a role in AF. Additionally, high-resolution scRNA-seq of freshly isolated human fibroblasts from right atrial appendages also indicates a downregulation of *NR4A1*, alongside *IL6*, in patients with persistent AF[78]. These contradictions – where NR4A1 appears downregulated in transcriptomic datasets yet drives atrial fibrotic responses in *in vitro* functional assays – post a critical question: is NR4A1 association with AF defined not solely by its transcriptional regulation, but also by its protein abundance or PTMs?

Recent evidence has clarified NR4A1's functional role in AF, supporting the pro-fibrotic hypothesis[189]. A novel study by Wei et al. identified NR4A1 as a direct downstream binding target of the long non-coding RNA (lncRNA) Dleu2. Dleu2 is upregulated in the atria of persistent AF patients and positively associates with left atrial fibrosis. Mechanistically, Dleu2 upregulation increases atrial remodelling and AF susceptibility *in vivo*, and this could be reversed by NR4A1 silencing by injecting adenovirus vector containing the NR4A1-targeting short hairpin RNA. While this study provides crucial *in vivo* validation that the NR4A1 pathway promotes AF incidence and atrial remodelling, it focused largely on tissue-level and cardiomyocyte phenotypes, and lncRNA interactions. It did not dissect the cellular signalling within the ACF itself, nor did it investigate the involvement of endogenous ligands. Furthermore, the potential for PTMs of NR4A1 remains completely unexplored in human ACFs. Investigating these regulatory layers is essential to understand how NR4A1 switches from a normal homeostatic factor to a disease driver in AF.

5.1.1 Hypothesis and aims

Hypothesis: persistent AF is associated with altered NR4A1 regulation at post-transcriptional and subcellular levels. The aims of this chapter are as follows:

1. Quantify and compare NR4A1 mRNA and protein expression in human ACFs isolated from patients with persistent AF versus controls in sinus rhythm
2. Profile the expression of upstream and downstream pathway components, specifically PGA2 and IL-6, in human ACFs to determine if they are dysregulated in persistent AF
3. Assess post-transcriptional changes and localisation of NR4A1 in human ACFs between persistent AF and sinus rhythm

5.2 Materials and Methods

The following methods described in this section were used specifically in this chapter.

5.2.1 Proteasome inhibition

Proteasome inhibition was achieved by treatment with MG132 (#HY-13259, MedChemExpress, US). MG132 was dissolved in DMSO to a stock concentration of 10 mM and further diluted in FBM-3 antibiotic-free medium with 0.5% FBS to reach a final concentration for treatment in human ACFs. After starvation, MG132 was added to the cells and incubated at 37°C for 6 hours. Cell viability was checked after treatment before proceeding with downstream experiments.

5.2.2 Collection of cell secretome

Human ACFs were plated at 10,500 cells/cm^2 in one well of a 6-well plate and cultured at 37°C for overnight. Growth medium was removed next day and replaced with 1 mL FBM-3 antibiotic-free medium with 0.5% FBS for serum starvation at 37°C for 2 hours. After starvation, cells were cultured with 1 mL FBM-3 antibiotic-free medium with 0.5% FBS per well at 37°C for 24 hours. Medium was collected and centrifuged at 500 g at 4°C for 5 min to remove debris and particulates. The clear supernatant (secretome) was transferred to a new tube and stored at -20°C until use.

5.2.3 Measurement of IL-6 levels using ELISA

The IL-6 levels in cell secretome were detected using the Human IL-6 DuoSet ELISA (#DY206, R&D Systems, US). A 96-well plate was coated with 100 µL of diluted Capture Antibody in

1X PBS per well, sealed and incubated at room temperature for overnight. Solutions were aspirated using the Tecan Hydroflex Automated Microplate Washer (Tecan, Switzerland). Plate was washed three times with 400 µL of Wash Buffer per well. 300 µL of Block Buffer (1% BSA in 1X PBS) was loaded to each well and incubated at room temperature for 1 hour. Secretome samples were diluted 1:10 in antibiotic-free medium with 0.5% FBS before loading to the plate. After repeating the washing step, 100 µL of standard or diluted sample in Reagent Diluent (1% BSA in 1X PBS) was added to each well and incubated at room temperature for 20 min in dark. Washing step was then repeated, followed by adding 100 µL of diluted Detection Antibody in Reagent Diluent and incubated at room temperature for 2 hours. Plate was washed and incubated with 100 µL of Streptavidin-HRP B working solution at room temperature for 20 min in dark. After the final washing step, the wells were incubated with 100 µL of TMB Substrate Solution at room temperature for 20 min in dark. Reaction was stopped by 100 µL of Sulfuric Acid Stop Solution. Absorbance was measured at 450 nm using a microplate reader (BMG LABTECH, Germany) and wavelength correction was applied at 540 nm.

5.2.4 Measurement of PGA2 levels using ELISA

PGA2 levels in cell secretome were detected using the Prostaglandin A2 ELISA Kit (#A326820, Antibodies.com, UK). In brief, the pre-coated 96-well plate was washed with 350 µL of Wash Buffer two times, each time for 1-2 min. Solutions were aspirated using the Tecan Hydroflex Automated Microplate Washer (Tecan, Switzerland). 50 µL of standard or sample was loaded to the wells, followed by immediate addition of 50 µL of Biotinylated Detection Antibody working solution. Plate was sealed and incubated at 37°C for 45 min. Wash Buffer was added to wash the plate three times, each time for 1-2 min. After aspiration, 100 µL of HRP-Streptavidin Conjugate (SABC) working solution was added to each well. The sealed plate was

incubated at 37°C for 30 min. Solution was aspirated and plate was washed with Wash buffer for five times, each time for 1-2 min. 90 µL of TMB Substrate was loaded to each well, and then the sealed plate was incubated at 37°C. Reaction was stopped after 20 min by adding 50 µL of Stop Solution to each well, and absorbance was measured at 450 nm using a microplate reader (BMG LABTECH, Germany).

5.2.5 Subcellular fractionation

Human ACFs were cultured in a T75 flask to 80-90% confluency and then proceeded with fractionation. Subcellular protein fractionation was performed using the ProteoExtract Subcellular Proteome Extraction Kit (#539790, Millipore, US) according to manufacturer's protocol with minor modifications. Specifically, after trypsinisation, the cell suspension was centrifuged at 300 g at 4°C for 10 min. Cell pellet was washed twice with 1 mL of cold Wash Buffer, incubated with gentle agitation at 4°C for 5 min and centrifuged at 300 g at 4°C for 10 min. Supernatant was removed and the remaining pellet was immediately mixed with 1 mL of cold Extraction Buffer I with 5 µL of Protease Inhibitor Cocktail. The suspension was incubated with gentle agitation at 4°C for 10 min, followed by centrifugation at 1,000 g at 4°C for 10 min. The supernatant was collected to a new tube and labelled as fraction 1. The pellet was immediately resuspended with 1 mL of cold Extraction Buffer II with 5 µL of Protease Inhibitor Cocktail. The suspension was incubated with gentle agitation at 4°C for 30 min, and then centrifuged at 6,000 g at 4°C for 10 min. The supernatant was collected to a new tube and labelled as fraction 2. The pellet was resuspended in 500 µL of Extraction Buffer III with 5 µL of Inhibitor Cocktail and 1.5 µL of Benzonase nuclease. The suspension was incubated with gently agitation at 4°C for 10 min, followed by centrifugation at 6,800 g at 4°C for 10 min. Finally, the supernatant was transferred to a new tube and labelled as fraction 3. The remaining pellet was resuspended with 500 µL of Extraction Buffer IV with 5 µL of Protease Inhibitor

Cocktail and this solution was labelled as fraction 4. All fraction lysates were stored at -20°C until use. Protein expression in subcellular fractions was detected using western blot as described in Section 2.5. All four fractions from the same donor were loaded on the same gel. After quantification, protein was expressed as a ratio of cytoplasmic to nuclear fraction for each donor.

5.2.6 Phosphorylation of NR4A1

Protein lysates of human ACFs were prepared as described in Section 2.5.1. Phosphorylated and unphosphorylated forms of NR4A1 were assessed by gel electrophoresis using the SuperSep Phos-tag (50 μmol/L) 12.5% 17 well pre-cast gel (#195-17991, FUJIFILM Wako, Japan), followed by western blot (minor modifications from Section 2.5.2).

Each sample (12 μL) was mixed with 3 μL of 4X NuPAGE LDS Sample buffer and 1.2 μL of 1 M dithiothreitol, followed by heating at 95°C for 5 min. The Precision Plus Protein Unstained Standards were used as molecular weight marker (#1610363, Bio-Rad, US). Molecular weight marker (10 μL) or protein lysate (5 μg in 10 μL) was loaded to each well and separated using the Phos-tag gel with 1X NuPAGE MOPS SDS Running Buffer (#NP0001, Invitrogen, US) at constant 70 V for 10 min and continued at 130 V for 1.5 hours. After electrophoresis, the gel was washed with gentle rocking in Running Buffer with 1 mM EDTA to remove zinc from the gel for optimal transfer efficiency at room temperature for 10 min. The gel was washed again with gentle rocking in fresh Running Buffer at room temperature for 10 min. The wet transfer approach was applied, and current was applied at 300 mA at 4°C for 1 hour. After transfer, the blocking and antibody incubation steps are described in Section 2.5.2, except blocking conditions were changed to 4°C for overnight to remove background, and 1X PBS-T was replaced by 1X Tris-buffered saline with 0.1% Tween 20 (1X TBS-T).

To identify the protein band corresponding to unphosphorylated NR4A1, a control sample was prepared by treating the protein lysate with Calf Intestinal Alkaline Phosphatase (CIP). 1 µg of protein was dephosphorylated by incubating with 0.25 U Quick CIP (#M0525, New England Biolabs, US) at 30°C for 30 min. After quantifying the protein bands, the individual phosphorylated forms of NR4A1 are expressed as the percentages of total NR4A1 phosphorylated signals for each sample.

5.3 Results

5.3.1 Clinical and demographic characteristics of patients

In this chapter, atrial biopsies were collected from a total of 46 patients for ACF isolation for comparison of persistent AF and sinus rhythm groups. Clinical and demographic characteristics are summarised in Table 5.3.1. Age, sex and body mass index were not significantly different between the groups. Sinus rhythm controls more frequently underwent CABG and had a higher prevalence of ischaemic heart disease. AF patients were more frequently prescribed β-blockers, anticoagulants and diuretics at baseline compared to sinus rhythm controls. All remaining characteristics were comparable between groups.

Table 5.3.1 Clinical and demographic characteristics of patients for ACF isolation

Mann-Whitney test (age), unpaired t-test (body mass index), and Fisher's exact test (categorical characteristics) were used for statistical comparison.

Characteristics	Total (*N*=46)	Sinus rhythm (*N*=24)	Persistent AF (*N*=22)	*P*-value
Age, years (SD)	67.9 (8.2)	66.9 (6.6)	68.9 (9.7)	0.2959
Sex, male (%)	34 (74)	16 (67)	18 (82)	0.3214
Body mass index, kg/m^2 (SD)	27.6 (3.9)	27.7 (3.9)	27.5 (4.0)	0.8708
CABG (%)	16 (35)	12 (50)	4 (18)	0.0324
Hypertension (%)	25 (54)	14 (58)	11 (50)	0.7675
Ischaemic heart disease (%)	11 (24)	10 (42)	1 (5)	0.0046
Stroke/transient ischaemic attack (%)	4 (9)	1 (4)	3 (14)	0.3364
Myocardial infarction (%)	9 (20)	6 (25)	3 (14)	0.4638
Peripheral arterial disease (%)	4 (9)	3 (13)	1 (5)	0.6093
Diabetes mellitus (%)	6 (13)	5 (21)	1 (5)	0.1896
Chronic kidney disease (%)	1 (2)	0 (0)	1 (5)	0.4783
Heart failure with reduced ejection fraction (%)	8 (17)	4 (17)	4 (18)	> 0.9999
β-blockers (%)	27 (59)	9 (38)	18 (82)	0.0031
Amiodarone/flecainide	0 (0)	0 (0)	0 (0)	> 0.9999
Aspirin/clopidogrel (%)	15 (33)	11 (46)	4 (18)	0.0625
Anticoagulants (%)	24 (52)	4 (17)	20 (91)	< 0.0001
Calcium channel blockers (%)	11 (24)	7 (29)	4 (18)	0.4966
Digoxin (%)	3 (7)	0 (0)	3 (14)	0.1014
Nitrates (%)	5 (11)	3 (13)	2 (9)	> 0.9999
Diuretics (%)	19 (41)	6 (25)	13 (59)	0.0349
Statins (%)	25 (54)	12 (50)	13 (59)	0.5683
Angiotensin-converting enzyme inhibitors and angiotensin receptor blockers (%)	34 (74)	17 (71)	17 (77)	0.7419

5.3.2 Characterisation of human ACFs from sinus rhythm donors and persistent AF patients

The human ACFs isolated from sinus rhythm donors and persistent AF patients were characterised by measuring the expression of selected markers, TGF-β1 and collagen 1. *TGFB1* mRNA levels were significantly elevated in AF ACFs (P = 0.0159; Figure 5.3.2a). *COL1A1* mRNA levels were not significantly different between the conditions (P = 0.2494; Figure 5.3.2b). Protein levels of mature collagen 1 were also measured, which demonstrated an increasing trend in AF ACFs relative to sinus rhythm (Figure 5.3.2c).

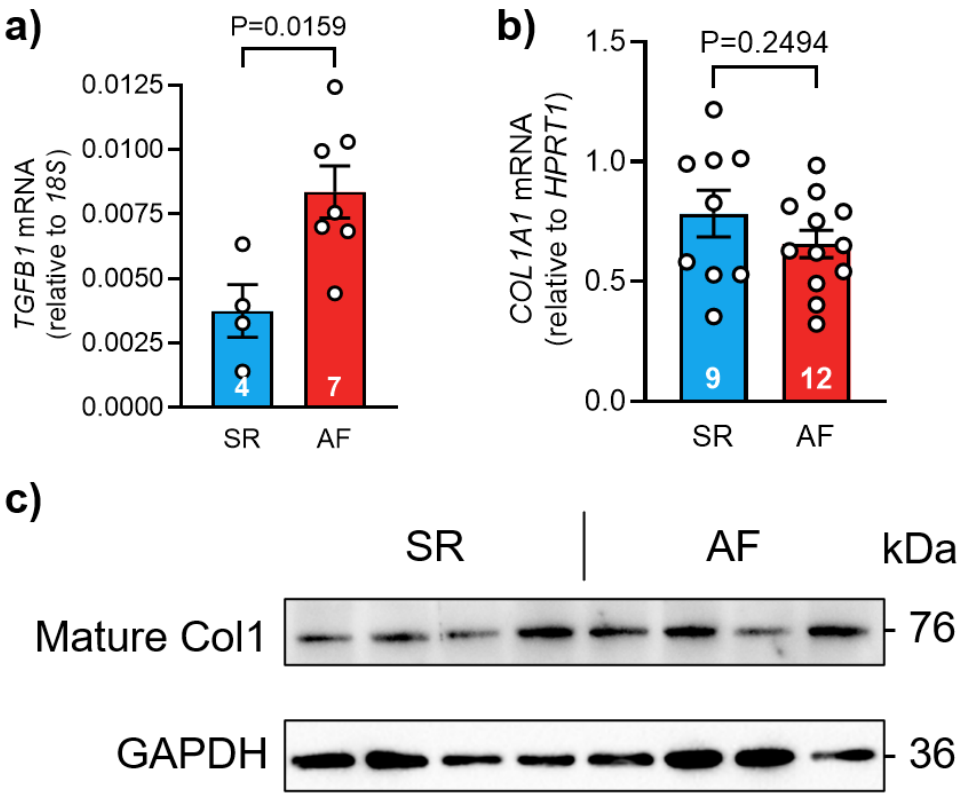

Figure 5.3.2 Characterisation of ACFs from sinus rhythm donors and persistent AF patients. (**a**) *TGFB1* mRNA levels in ACFs from patients with persistent AF and sinus rhythm (SR) controls. (**b**) *COL1A1* mRNA levels in ACFs in SR and AF ACFs. (**c**) Mature collagen 1 protein levels in SR and AF ACFs. Data are mean ± SEM; each dot represents an independent biological replicate (N) (**a**, **b**). P-values are determined from raw values and reported as two-sided using unpaired t-test (**a**, **b**).

5.3.3 Expression profiling of NR4A1 in human ACFs from patients with persistent AF

The expression of NR4A1 in human ACFs was compared between sinus rhythm and persistent AF. For gene, *NR4A1* mRNA levels were not significantly different between groups (P = 0.4456; Figure 5.3.3a). However, NR4A1 protein levels were upregulated in AF by 1.82-fold increase (P = 0.0302; Figure 5.3.3b-c). To determine whether the elevated protein levels in AF were due to reduced proteasomal degradation, I treated control ACFs with the proteasome inhibitor MG132, a widely used 26S proteasome inhibitor that blocks the ubiquitin-dependent protein degradation[253]. Cells were treated with MG132 for 6 hours and did not result in an increase in the abundance of NR4A1 protein compared with vehicle control (Figure 5.3.3d).

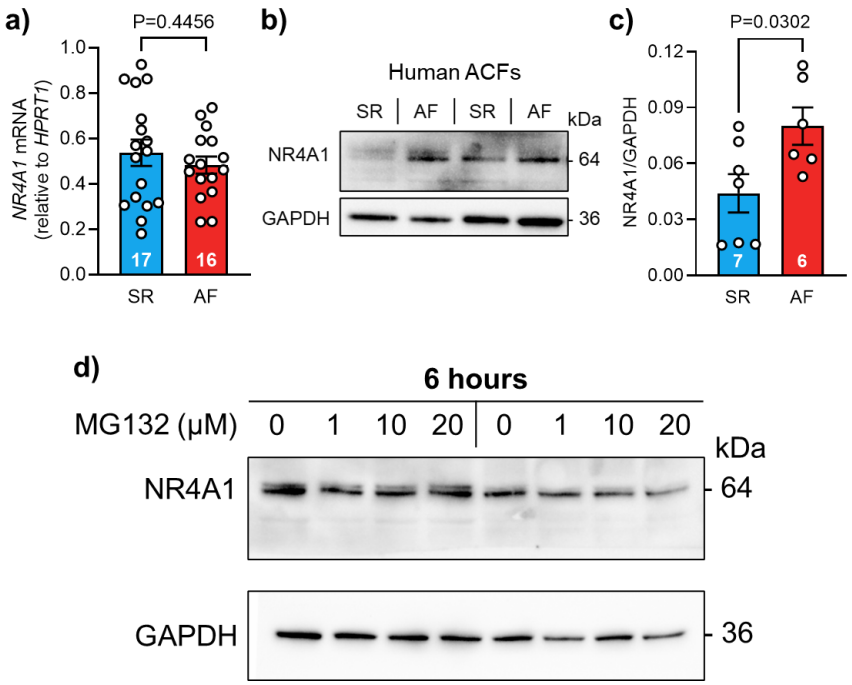

Figure 5.3.3 Gene and protein expression of NR4A1 in ACFs from persistent AF patients. (**a**) *NR4A1* mRNA levels in ACFs from patients with persistent AF and sinus rhythm (SR) controls. (**b-c**) NR4A1 protein levels in SR and AF ACFs. (**d**) NR4A1 protein levels in SR ACFs at 6-hour MG132 treatment with 0, 1, 10 and 20 μM concentrations. Data are mean ± SEM; each dot represents an independent biological replicate (N) (**a**, **c**). P-values are determined from raw values and reported as two-sided using unpaired t-test (**a**, **c**).

5.3.4 Secretion of IL-6 and PGA2 in human ACFs is elevated in patients with persistent AF

I have identified PGA2 and IL-6 as the signalling components associated with the NR4A1 regulation in atrial fibrotic responses. Building on the findings from my previous chapter, the expression of these targets was examined in AF compared with control human ACFs. While the mRNA levels of *IL6* were not different between AF and sinus rhythm fibroblasts ($P = 0.6667$; Figure 5.3.4a), the secreted levels of IL-6 were significantly elevated in the secretome collected from persistent AF than control ACFs ($P = 0.0464$; Figure 5.3.4b). In addition to IL-6, I also measured PGA2 in fibroblast secretomes, and the findings revealed higher levels of PGA2 production by AF fibroblasts ($P = 0.0373$; Figure 5.3.4c).

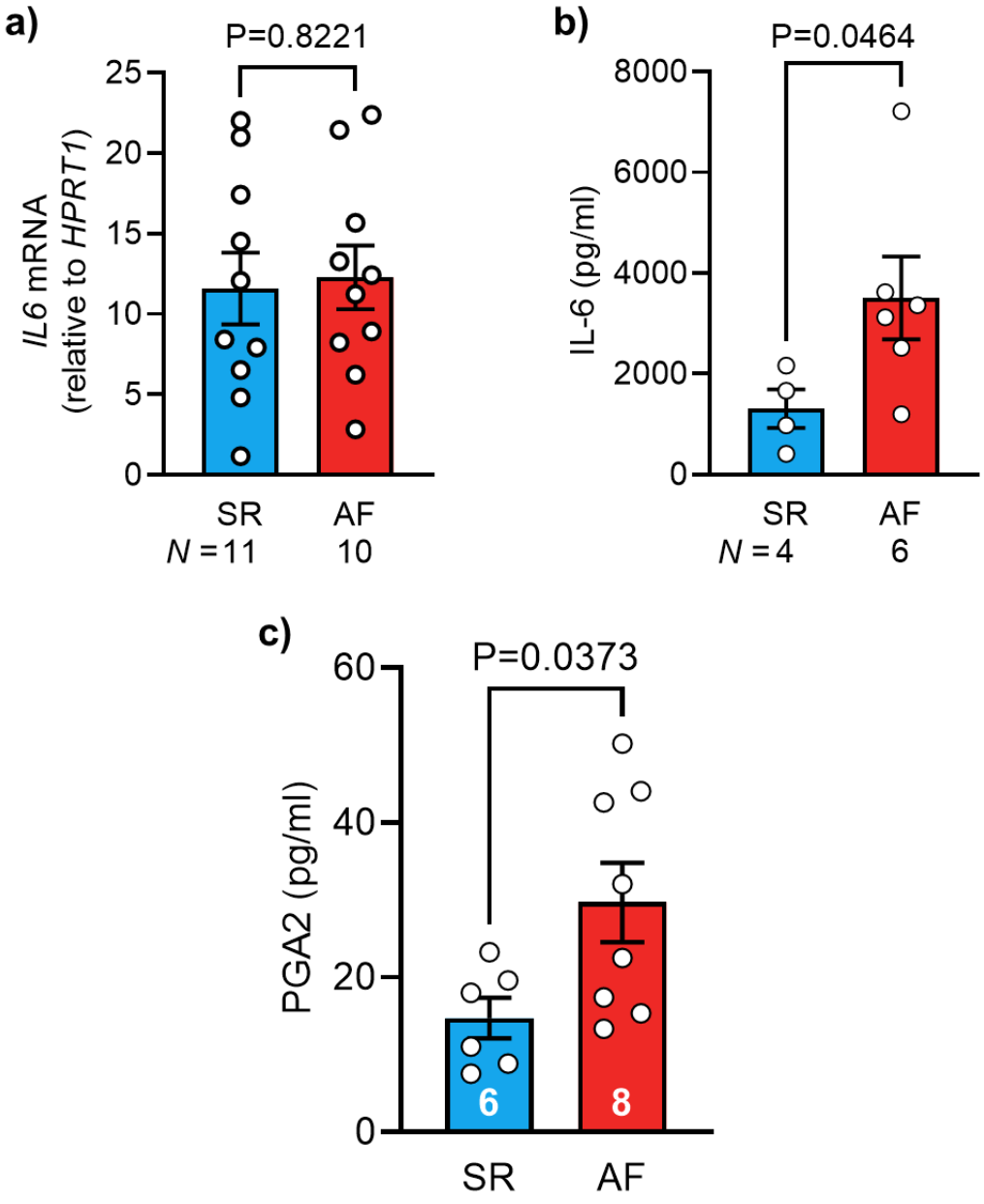

Figure 5.3.4 Secreted levels of NR4A1-associated signalling components in ACFs from AF patients. (**a**) *IL6* mRNA levels in ACFs from patients with persistent AF or sinus rhythm (SR) controls. (**b-c**) IL-6 and PGA2 protein levels in ACF secretome collected from patients with persistent AF or SR controls. Data are mean ± SEM; each dot represents an independent biological replicate (*N*). *P*-values are determined from raw values and reported as two-sided using unpaired t-test (**a**, **c**) and Welch's t-test (**b**).

5.3.5 Non-nuclear NR4A1 is enriched in ACFs from patients with persistent AF

In order to confirm subcellular localisation of NR4A1, I stained ACFs from persistent AF and control patients with specific anti-NR4A1 antibody (Figure 5.3.5a). In control (sinus rhythm) cells (biological donors $N = 8$), NR4A1 was mainly expressed in the nucleus, corresponding to its primary subcellular localisation where it acts as a transcription factor. In contrast, NR4A1 in AF cells (biological donors $N = 8$) was present not only in the nucleus but also localised outside - intracellularly. For each biological donor, at least three images and a minimum of ten cells in total were analysed. The immunostaining images were quantified for the percentage of non-nuclear NR4A1 for each cell, and the averaged percentage from all cells were calculated for each biological donor. I demonstrated a significant increase of non-nuclear NR4A1 in AF ACFs compared with sinus rhythm ($P = 0.0321$; Figure 5.3.5b).

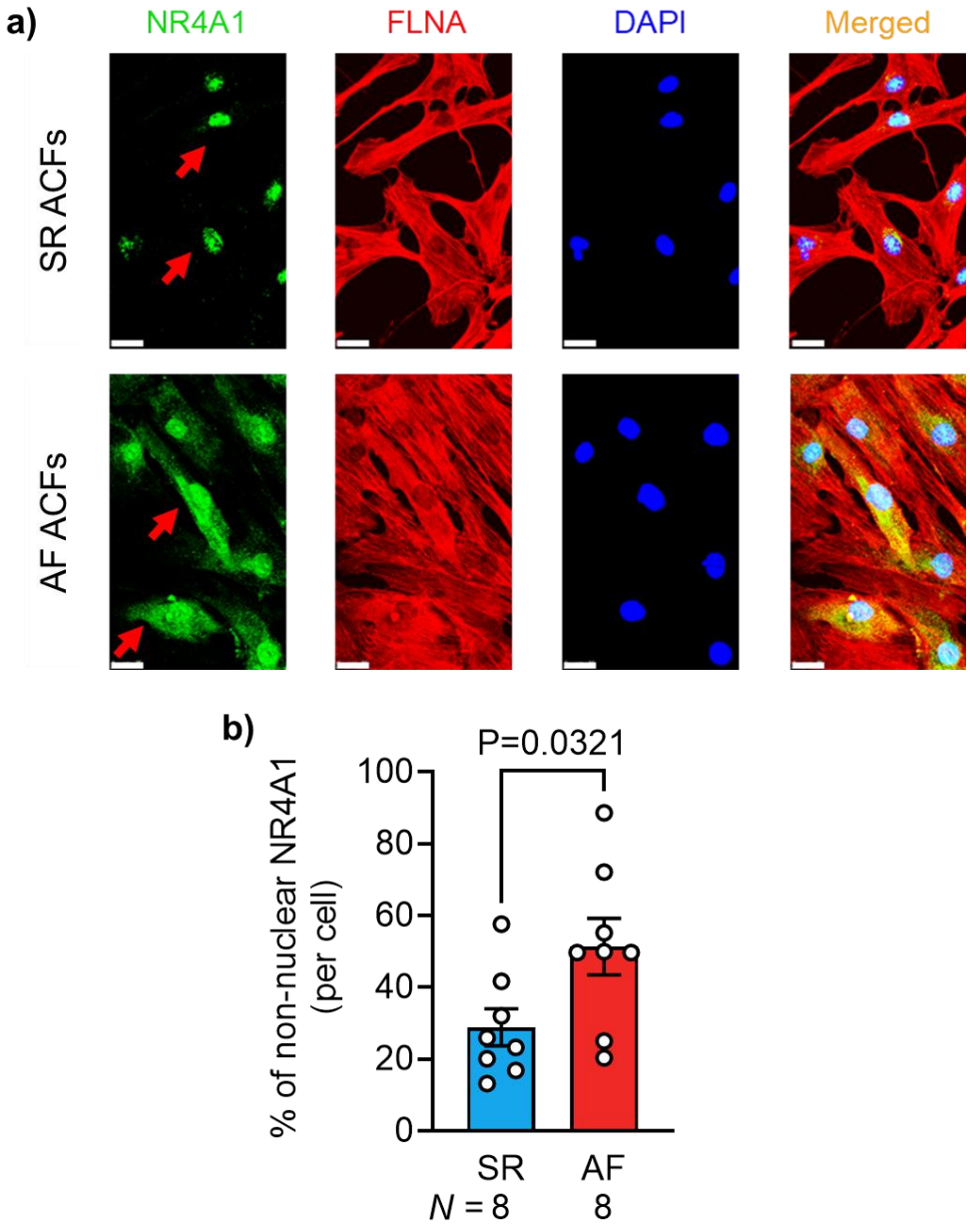

Figure 5.3.5 Protein localisation of NR4A1 in ACFs from persistent AF patients. (**a**) Immunofluorescence images visualising NR4A1 localisation in ACFs from patients with persistent AF or sinus rhythm (SR) controls. Red arrows show representative cells. Scale bar = 25 µm. (**b**) Quantification of non-nuclear NR4A1 in AF and control cells. Data are mean ± SEM; each dot represents an independent biological replicate (*N*). Data are quantified from at least three images and a minimum of ten cells for each *N*. Data are expressed as the percentage of non-nuclear NR4A1 per cell. *P*-values are reported as two-sided using unpaired t-test.

5.3.6 Expression of cytoplasmic NR4A1 is increased in AF ACFs

To validate the changes in subcellular distribution of NR4A1 in AF ACFs as demonstrated in immunostaining, I performed subcellular fractionation followed by western blotting to examine the NR4A1 compartment-specific expression in control and AF fibroblasts. Cellular proteins were separated into four fractions: cytoplasmic (F1), membrane (F2), nuclear (F3) and cytoskeletal (F4). Fraction purity was confirmed by enrichment of calpain 1 in the cytoplasmic fraction, N-cadherin in the membrane fraction, histone H3 and lamin A/C in the nuclear fraction, and vimentin and lamin A/C in the cytoskeletal fraction (Figure 5.3.6a). In sinus rhythm cells, NR4A1 protein was detected in nuclear fraction mainly and partially in the membrane fraction (Figure 5.3.6b). However, in AF ACFs, nuclear abundance of NR4A1 was associated with a significant increase in cytoplasmic fraction of NR4A1 (Figure 5.3.6b). The cytoplasmic to nuclear ratio of NR4A1 was quantified and indicated a significant increase in AF fibroblasts relative to control ($P = 0.0481$; Figure 5.3.6c).

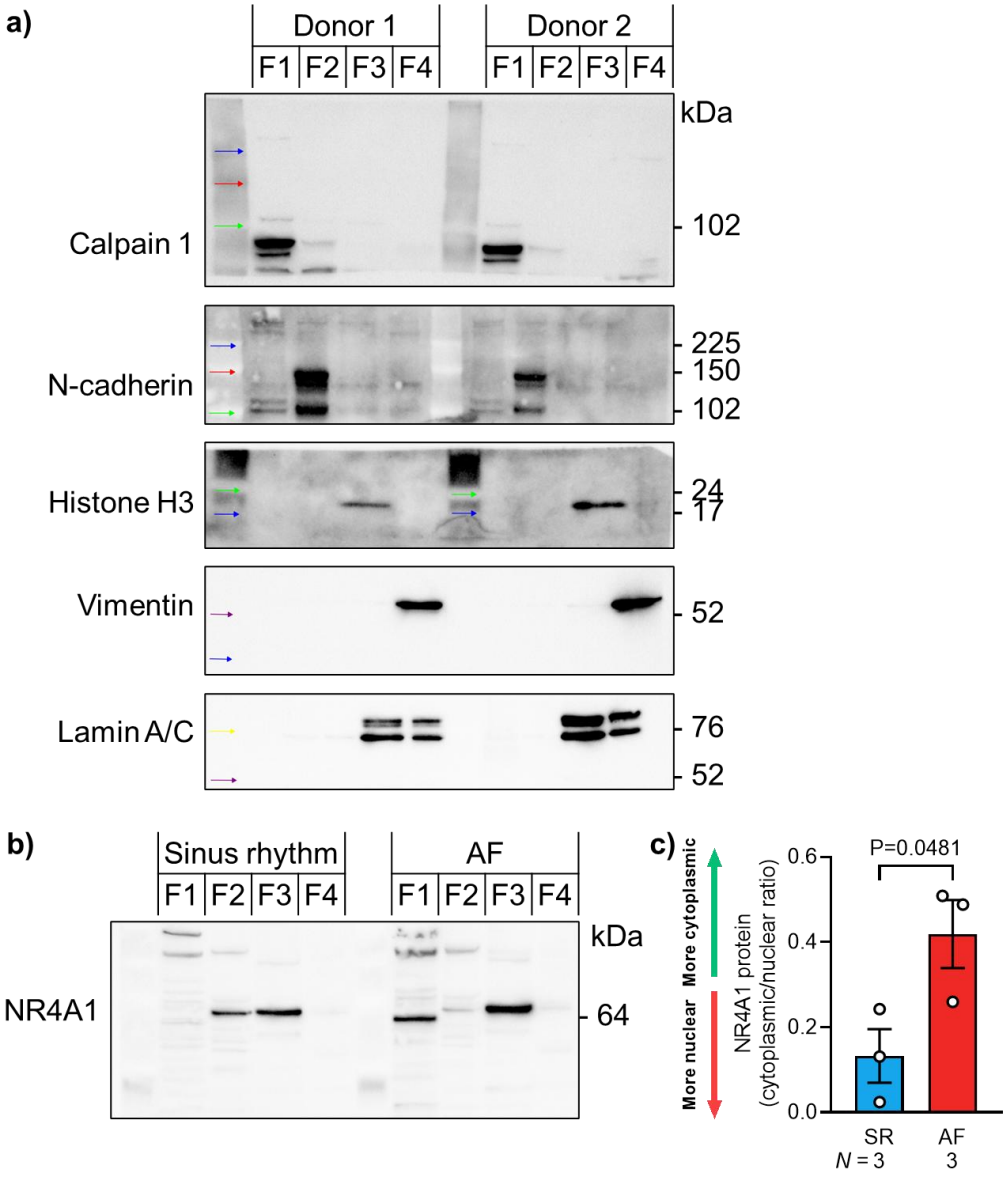

Figure 5.3.6 Compartment-specific expression of NR4A1 in ACFs from persistent AF patients. (**a**) Protein expression of fractionation control markers to confirm fraction purity in ACFs. F1, cytoplasmic; F2, membrane; F3, nuclear; F4, cytoskeletal. (**b**) Representative blot showing NR4A1 protein expression in different subcellular fractions of ACFs from patients with AF or sinus rhythm (SR) controls. (**c**) Quantification of cytoplasmic to nuclear ratio of NR4A1 expression in persistent AF or SR ACFs. The ratio is calculated within each biological donor. Data are mean ± SEM; each dot represents an independent biological replicate (*N*). *P*-values are determined from raw values and reported as two-sided using unpaired t-test.

5.3.7 NR4A1 phosphorylation is not altered in AF ACFs

In addition to its expression, the biological functions of NR4A1 are regulated by post-translational modifications, such as phosphorylation and SUMOylation[145]. Ser351 has been reported as the main phosphorylation site of NR4A1. NR4A1 phosphorylation level at Ser351 was measured in AF and control ACFs, but no differences were observed between the conditions (P = 0.8322; Figure 5.3.7a). To account for the complete profile of NR4A1 phosphorylation, I utilised Phos-tag gel (in combination with western blot) to separate different phosphorylated species. The separation of bands was visualised on the membranae (Figure 5.3.7b), revealing three degrees of NR4A1 phosphorylated isoforms and the non-phosphorylated form. The second degree of NR4A1 phosphorylation (P2) was mostly expressed in ACFs compared with other isoforms (Figure 5.3.7c). The expression of NR4A1 non-phosphorylated and phosphorylated isoforms in ACFs were quantified, but none of the isoforms were significantly regulated in AF compared with sinus rhythm (Figure 5.3.7d).

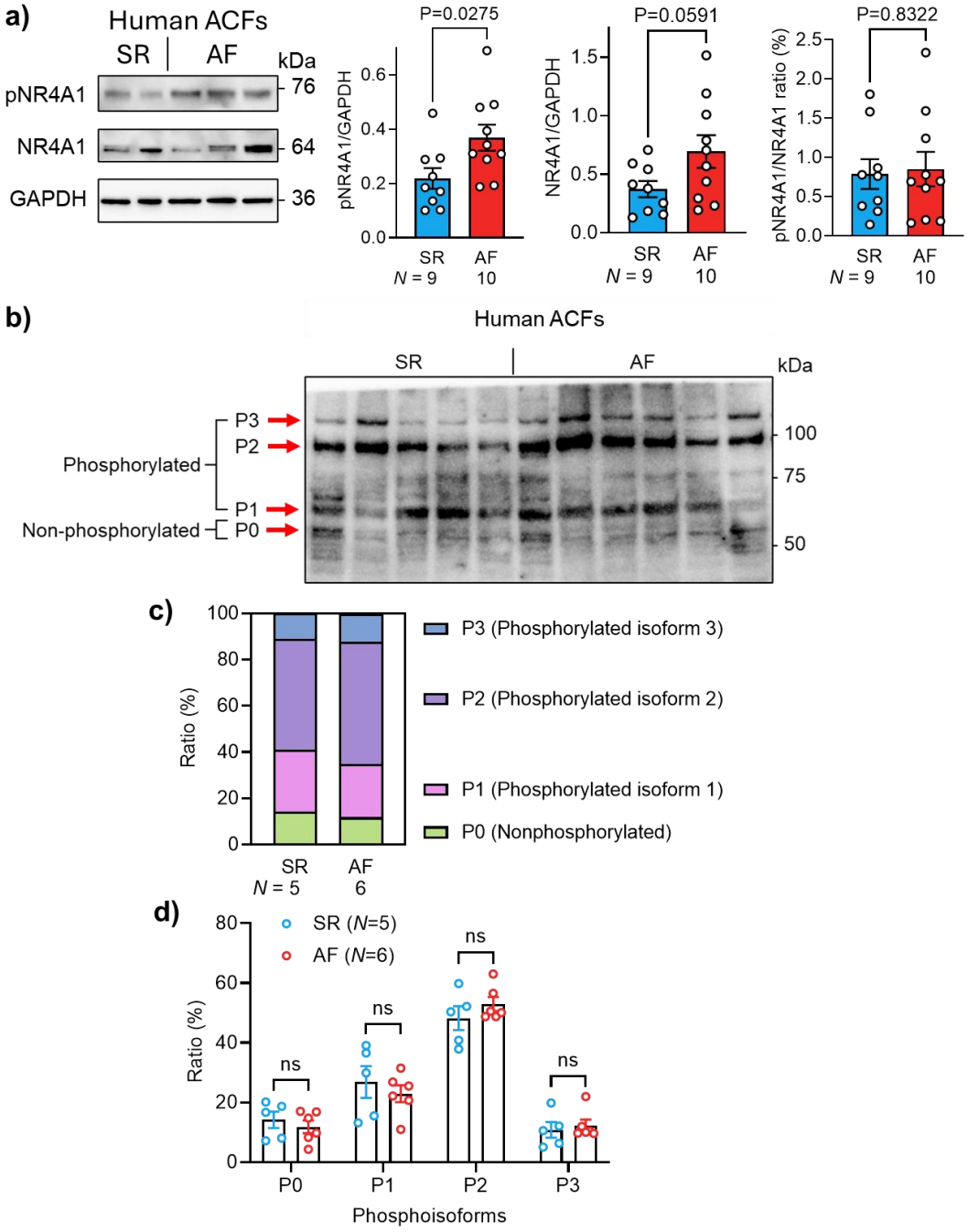

Figure 5.3.7 Phosphorylation level of NR4A1 in ACFs from persistent AF patients. (**a**) Representative blots and quantification showing phosphorylated NR4A1 (Ser351) levels in persistent AF or sinus rhythm (SR) control ACFs. (**b**) Proteins separated by Phos-tag gel and immunoblotted for phosphorylated isoforms of NR4A1. Higher extent of phosphorylation appears as slower-migrating bands. (**c-d**) Quantified ratios of phosphorylated NR4A1 isoforms

in AF or SR cells. The ratios of different phosphorylated isoforms were calculated within each donor, and the mean ratio was presented (**c**). Data are mean ± SEM (**a**, **d**); each dot represents an independent biological replicate (*N*). *P*-values are determined from raw values and reported as two-sided using unpaired t-test (**a**) and two-way ANOVA with Bonferroni correction (**d**).

5.4 Discussion

This chapter expands my *in vitro* findings of NR4A1-mediated fibrotic responses in human ACFs within a clinical cohort of patients with persistent AF. The significantly higher utilisation of β-blocker, anticoagulants, and diuretics in the persistent AF group was expected and aligns with current clinical guidelines for rate control, stroke prevention and fluid management[180]. Conversely, the higher frequency of CABG in the sinus rhythm group reflects a higher baseline prevalence of ischaemic heart disease, for which CABG is a primary revascularisation strategy[254]. Selection an appropriate control group for atrial tissue sampling is inherently challenging, as tissue is only accessible during cardiac surgery. CABG patients are more frequent in control group because they typically present a lower prevalence of AF compared to those undergoing valvular heart disease surgery[255], which formed the mainstay of our cohort. While these clinical characteristics provide a representative context for evaluating NR4A1 in AF-associated remodelling, the differences between groups reflect the practical constraints of surgical sample availability and the inherent comorbidities of the patient population.

The basal phenotype of cultured ACFs from sinus rhythm donors and AF patients was evaluated to determine whether disease-associated characteristics were retained following isolation and *in vitro* culture. AF ACFs exhibited significantly higher *TGFB1* mRNA expression than sinus rhythm ACFs. This finding is consistent with a previous study demonstrating increased TGF-β1 expression in left atrial tissues from persistent AF patients[256], supporting the preservation of a key pro-fibrotic molecular signature in the cultured AF ACFs. Furthermore, previous transcriptomic characterisation of isolated human ACFs by our group demonstrated significantly reduced expression of the transcription factor *FOXF1* in AF ACFs compared with control ACFs[78]. As *FOXF1* is recognised as an anti-fibrotic regulator that suppresses collagen production and myofibroblast invasion in pulmonary fibrosis[257], its downregulation provides

additional evidence that AF ACFs retain a disease-associated pro-fibrotic phenotype following isolation. In contrast, collagen 1 expression was not significantly different between the two groups and should therefore be interpreted with caution. It is possible that routine *in vitro* culture conditions, which are known to promote fibroblast activation[258], may attenuate AF-specific differences in ECM protein expression, thereby reducing the distinction between sinus rhythm and AF ACFs. Nevertheless, the combined evidence from increased *TGFB1* expression and the previously reported reduction in *FOXF1* supports that AF ACFs retain key disease-associated phenotypic characteristics following isolation, supporting their suitability as an *in vitro* model for investigating the molecular mechanisms underlying atrial fibrosis in AF.

Previous bulk RNA-seq datasets indicated downregulated *NR4A1* gene expression in the left atrial appendages of AF patients[250]. This could be attributed to the cellular composition, as the atrial myocardium is composed of more cardiomyocytes (30.1%) than fibroblasts (24.3%)[101,184]. Since NR4A1 plays a distinct anti-fibrotic role in cardiomyocytes, as opposed to a pro-fibrotic role in cardiac fibroblasts[161], bulk tissue analysis is likely to mask fibroblast-specific changes. My qPCR analysis of ACFs from thirty-three patients showed no significant difference in *NR4A1* mRNA levels between sinus rhythm and AF.

While gene regulation is crucial, protein abundance ultimately dictates biological function[259]. Western blot analysis revealed a significant increase in NR4A1 protein expression in AF ACFs. This discordance between mRNA and protein levels is a well-documented biological phenomenon, often attributed to variations in protein half-life, translation efficiency, post-translational stability or modifications[202]. Since proteasome inhibition with MG132 did not increase NR4A1 protein levels, reduced proteasomal degradation is unlikely to explain this discrepancy. Instead, the elevated NR4A1 protein abundance may reflect alternative regulatory

mechanisms such as enhanced translation efficiency, microRNA-mediated regulation, and post-translational modifications. NR4A1 degradation has been reported to be regulated by SUMOylation and ubiquitination in HEK293T cells[260].

Notably, unlike transcriptomics, NR4A1 protein expression is often below the detection threshold in cardiac mass spectrometry-based proteomics[252,261]. This is due to low expression of transcription factors like NR4A1 relative to structural proteins that are highly abundant in the cardiac tissues[262]. Therefore, the specific detection of elevated NR4A1 protein in isolated AF ACFs is a critical finding, aligning with its established pro-fibrotic role in human ACFs.

The elevation of NR4A1 protein in AF ACFs coincided with a pro-inflammatory secretory profile, characterised by an elevated release of IL-6. This finding at the cellular level mirrors the increased circulating IL-6 seen in AF patients[242]. These results underscore the translational potential of IL-6 targeting. Selective blockade of IL-6 trans-signalling using olamkicept has been shown to alleviate cardiac inflammation and AF inducibility in heart failure mice models[241]. Furthermore, direct ligand neutralisation with ziltivekimab, a human monoclonal antibody, has demonstrated efficacy in lowering cardiovascular event rates and residual inflammatory risk[263,264]. Ziltivekimab is currently being evaluated in multiple Phase 3 clinical trials[265], representing a promising strategy for mitigating inflammation-associated structural remodelling in the heart.

Additionally, this is the first time that increased secretion of PGA2 by human ACFs in AF has been identified. This contrasts with a systemic (serum) metabolomics study showing lower circulating PGA2 levels in AF patients compared with healthy controls[266]. This discrepancy

suggests that atrial-specific metabolic reprogramming may differ from systemic metabolic profiles. The increased local production of PGA2 may indicate a dysregulated PGE2 metabolism in AF ACFs, potentially acting as an autocrine signal to modulate NR4A1 activity.

The disconnection between NR4A1 mRNA and protein levels suggests an additional layer of complexity involving upstream regulators like small RNAs (lncRNA, miRNA). It was recently demonstrated that NR4A1 can be regulated by lncRNA Dleu2 to promote AF and atrial remodelling[189]. Non-coding RNAs are known to tightly regulate electrical and structural remodelling in AF through diverse mechanistic pathways[267]. Specifically, dysregulation of miRNAs such as miRNA-4443, miRNA-1202 and miRNA-21 regulate TGF-β1 signalling to promote pro-fibrotic effects in human ACFs and arrhythmogenesis in AF[268–270]. Although these studies did not directly examine NR4A1 regulation, they highlight the importance of non-coding RNA-mediated remodelling in AF pathology. Therefore, specific non-coding RNAs may act as critical post-transcriptional regulators of NR4A1 in AF ACFs – a promising avenue for future investigation.

Beyond total protein abundance, immunostaining and fractionation confirmed a significant non-nuclear (cytoplasmic) enrichment of NR4A1 in AF ACFs. Interestingly, fractionation revealed distinct molecular weights for cytoplasmic and nuclear NR4A1 by a few kilodaltons (kDa). This may correspond to the canonical 64 kDa isoform (cytoplasmic) and the 66 kDa N-terminal variant (nuclear)[271]. According to the biochemical structure of NR4A1 as visualised in AlphaFold[272], the C-terminus is highly structured, whereas the N-terminus is intrinsically disordered and highly flexible (Figure 5.4). This suggests that the transition from the 66 kDa to 64 kDa isoform may be attributed to a specific cleavage site within the N-terminal domain. While the functional distinction between these isoforms remains understudied, the net result is

an accumulation of NR4A1 in the cytoplasm in addition to its nuclear expression. Alternatively, the minor shift in the migration of NR4A1 bands could be an artifact of differences in the buffer compositions used during protein extraction for each fraction.

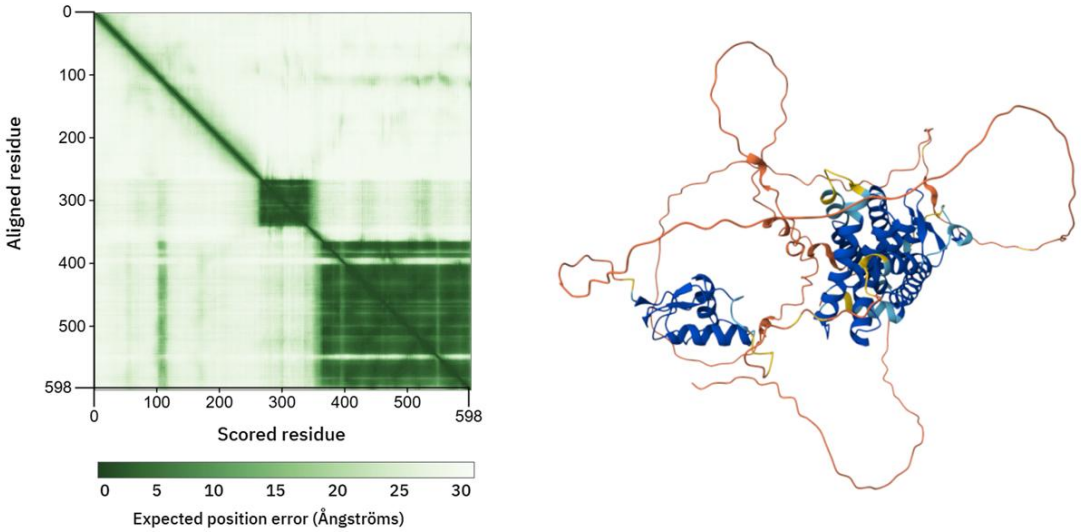

Figure 5.4 Predicted structural architecture of the NR4A1 protein. Representative protein structure of the NR4A1 (UniProt ID: P22736-1) generated via AlphaFold. (**Left**) Predicted Aligned Error plot illustrating the inter-residue confidence scores. Low-error cluster corresponding to the structured C-terminus (dark green tile), while the high error-regions indicate the intrinsically disordered nature of the N-terminal domain (light green tile). (**Right**) Three-dimensional biochemical structure of NR4A1 as predicted by AlphaFold.

Under physiological conditions, NR4A1 localised in the nucleus. However, cellular stress signals can induce NR4A1 nucleocytoplasmic translocation, switching its function from a transcription factor to a modulator of non-genomic effects such as apoptosis and autophagy[134,147]. While translocation of NR4A1 is often driven by phosphorylation (by kinases like AKT, JNK, or MAPK1)[134], my results showed no significant difference in NR4A1 phosphorylation levels between SR and AF. This suggests that the cytoplasmic retention of

NR4A1 in AF ACFs is possibly driven by alternative mechanisms, such as interaction with nuclear exportins and nucleoporins or other PTMs, which warrants further investigation.

Collectively, I characterise a distinct NR4A1 profile in AF ACFs in this chapter; stable mRNA but elevated protein, accompanied by cytoplasmic translocation and a pro-inflammatory secretory phenotype. The decoupling of NR4A1 levels from its phosphorylation status implies a novel regulatory mechanism driving its export in AF. My findings suggest that targeting the subcellular distribution of NR4A1, or its downstream effectors like IL-6, may offer new therapeutic avenues for atrial fibrosis in AF.

CHAPTER 6: CHARACTERISATION OF NR4A1 INTERACTOME IN HUMAN ACFs

6.1 Introduction

In the preceding chapter, my investigation into the regulation of NR4A1 in human ACFs yielded a critical finding: NR4A1 protein exhibits a distinct subcellular localisation in persistent AF. Specifically, I observed significantly enriched cytoplasmic expression of NR4A1 in ACFs isolated from patients with AF compared to those in sinus rhythm.

Classically, NR4A1 is characterised as a nuclear receptor that resides in the nucleus, where it functions as a transcription factor to regulate gene expression. However, evidence suggests that its subcellular localisation is dynamic and stress-responsive[147]. Under specific pathological stimuli, such as oxidative stress or apoptotic signalling, NR4A1 is known to translocate from the nucleus to cytoplasm or mitochondria. This translocation is not merely a deactivation mechanism; instead, it often signifies a functional switch. Once exported to the cytoplasm, NR4A1 engages in non-genomic interactions with distinct binding partners, altering cellular phenotype and fate[147]. Consequently, identifying the specific protein partners of NR4A1 within AF ACFs is essential to understanding the pathophysiology of persistent AF.

The enrichment of cytoplasmic NR4A1 in AF ACFs implies an active dysregulation of nucleocytoplasmic transport. The cellular homeostasis of protein nuclear export is a tightly regulated process orchestrated through the nuclear pore complex (NPC)[273]. The primary mediator of this nuclear export is exportin 1 (XPO1)[274]. Mechanistically, proteins destined for nuclear export possess a leucine-rich NES. XPO1 binds to this NES domain and recruits Guanosine Triphosphate Ran (RanGTP) to form a trimeric export complex, which then navigates through the NPC. Upon reaching the cytoplasm, GTP hydrolysis induces dissociation of the complex, releasing the cargo protein. Importantly, previous findings in human vascular

cells have demonstrated that NR4A1 nuclear export is dependent on the XPO1 machinery[275]. In that study, the interferon alpha-inducible protein 27 was identified as a critical docking site of NR4A1 at the nuclear envelope, facilitating the NR4A1-XPO1 interaction and nuclear export. This precedent raises a new research direction for AF: the cytoplasmic shift of NR4A1 in AF ACFs may be driven by the recruitment of specific, AF-associated proteins that facilitate its interaction with the nuclear export machinery.

To identify other functional binding partners of NR4A1, a targeted hypothesis-driven approach is insufficient. Instead, an unbiased evaluation of the NR4A1 interactome is required. Co-immunoprecipitation (co-IP) coupled with mass spectrometry (MS) represents an available approach for such discovery[276]. Unlike yeast two-hybrid systems or proximity labelling approaches that often require the fusion of exogenous tags, co-IP allows for the isolation of endogenous complexes in their native state[277]. By capturing NR4A1 and its stable binding partners directly from patient-derived ACFs, this method offers a snapshot of the functional protein interactions in AF. While technically demanding, this workflow provides the unique opportunity to uncover novel interactors that may regulate NR4A1 nuclear export or downstream pro-fibrotic signalling in the context of AF.

6.1.1 Rationale and aims

The cytoplasmic enrichment of NR4A1 in AF ACFs may be driven by differential interactions with nuclear export machinery or cytoplasmic retention factors, facilitating a non-genomic pro-fibrotic signalling. Given the exploratory nature of interactome profiling, I adopt a hypothesis-free discovery rationale in this chapter with the following aims:

1. Profile the global NR4A1 interactome in human ACFs isolated from patients with persistent AF versus controls in sinus rhythm to identify AF-specific binding partners
2. Examine the dataset for NR4A1-interacting protein(s) associated with the NPC or nucleocytoplasmic transport that may facilitate NR4A1 translocation in AF ACFs
3. Determine if NR4A1 interactors in AF ACFs mapped to distinct biological pathways distinct from its nuclear transcriptional role

6.2 Materials and Methods

The following methods described in this section were used specifically in this chapter. Schematic representation of the interactome experimental workflow (Sections 6.2.1-6.2.3) is visualised in Figure 6.2.

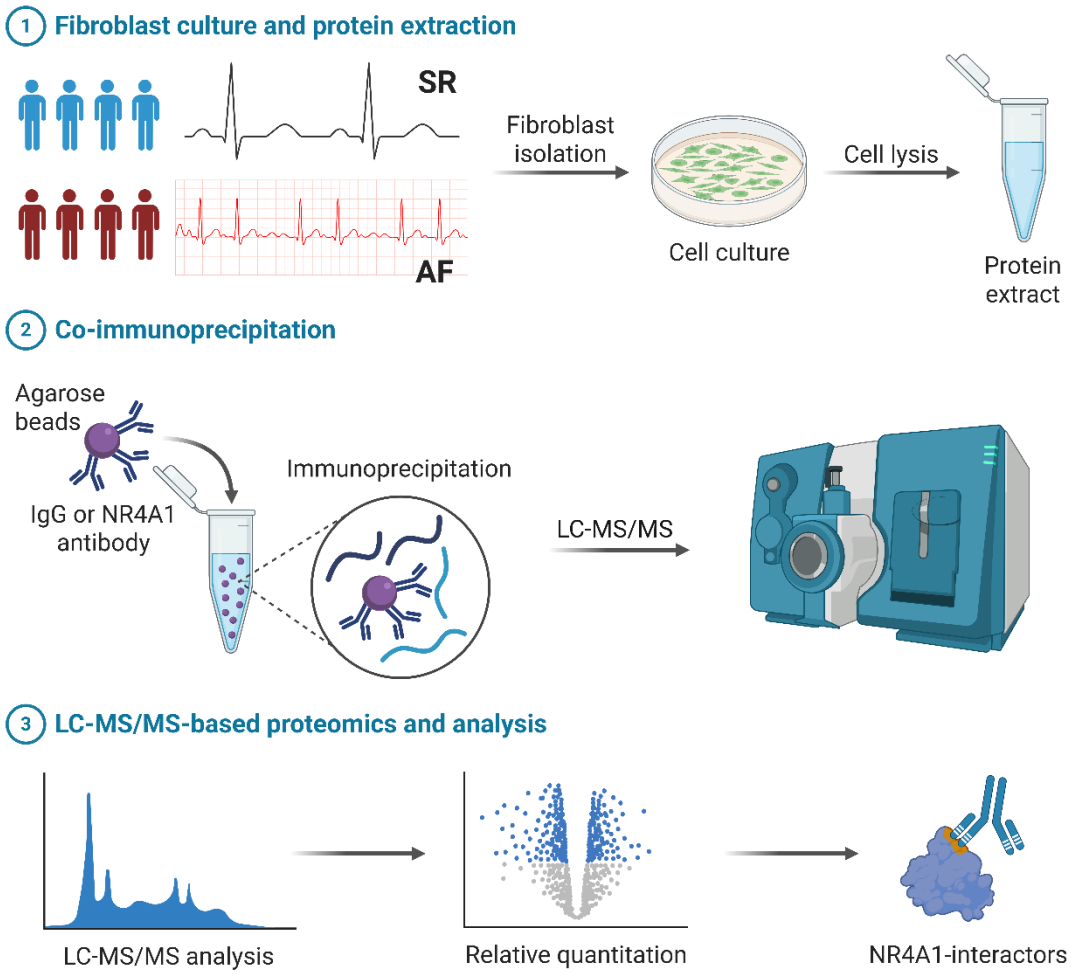

Figure 6.2 Schematic illustration of the NR4A1 interactome experimental workflow. Proteins are extracted from ACFs from patients with persistent AF or those in sinus rhythm (SR), followed by immunoprecipitation with anti-NR4A1 or IgG isotype control antibody. Samples are processed for MS to quantify protein abundance. Proteins enriched in NR4A1-immunoprecipitated samples are identified as NR4A1 interactors.

6.2.1 Co-IP

Human ACFs were cultured in a T75 flask to 80-90% confluency and then proceeded to protein extraction. Cells were lysed in 400 µL of lysis buffer for each T75 flask and stored at -20°C, as described in Section 2.5.1. Lysates were pre-cleared by adding 20 µL of Protein A/G PLUS-Agarose beads (#sc-2003, Santa Cruz Biotechnology, US) to 400 µL of lysate and incubated at 4°C for 1 hour with gentle agitation. Samples were centrifuged at 900 g at 4°C for 2 min. Supernatants were transferred to new tubes and kept on ice for immunoprecipitation.

A pre-cleared lysate (100 µL) was mixed with either 10 µL of anti-NR4A1 rabbit antibody (#25851-1-AP, Proteintech, US) or 5 µL of rabbit immunoglobulin G (IgG) isotype control antibody (#3900S, Cell Signaling Technology, US). The mixtures were incubated at 4°C for overnight with gentle agitation. Next day, samples were incubated with 50 µL of Agarose beads at 4°C for 4 hours with rotary agitation. After incubation, the tubes were centrifuged at 900 g for 2 min, and the beads were washed three times with 1 mL of cold 1X PBS. For each washing step, tubes were incubated at 4°C for 15 min with rotary agitation, followed by centrifugation at 900 g for 2 min. After the final wash and removal of supernatant, beads were immediately stored at -80°C and sent to service provider (Biogenity, Denmark) for MS or proceeded to western blot.

For downstream western blot, 40 µL of 1X NuPAGE LDS Sample Buffer was added to the washed beads and incubated at 95°C for 10 min. After centrifuging samples at 900 g for 2 min, supernatants were collected to new tubes at stored at -20°C. Before running the gel, 1X NuPAGE Sample Reducing Agent was added to the samples. Gel electrophoresis and western blot were performed as described in Section 2.5.2.

6.2.2 Sample preparation and analysis for MS

Sample preparation and MS analysis were performed by Biogenity (Denmark) according to their standard operating protocols. Briefly, beads were transported on dry ice and lysed in a buffer containing 6M guanidine hydrochloride, 10 mM TCEP, 40 mM chloroacetamide, 50 mM HEPES pH 8.5. Samples underwent sonication in a Bioruptor Pico sonication water bath, followed by sequential proteolytic digestion: first with lysyl endopeptidase (37°C, 3 hours) and subsequently with trypsin (37°C, 16 hours). Reactions were stopped with 1% trifluoroacetic acid (TFA). Resulting peptides were desalted using SOLAμ HRP Solid Phase Extraction plates, vacuum-concentrated, and reconstituted in A* buffer (2% acetonitrile, 1% TFA) containing iRT peptides.

MS analysis was conducted using the EASY-nLC 1200 System coupled to the Orbitrap Exploris mass spectrometer equipped with a FAIMS Pro Interface (CV -45 V). Peptides were separated on a C18 analytical column over a 70-minute gradient (10-60% Buffer B) at 250 nL/min. Data was acquired in data-independent acquisition mode across three narrow m/z windows (400-1,000 m/z range). Full MS and MS2 spectra were collected at resolutions of 120,000 and 60,000, respectively, using high-energy collisional dissociation collision energy (32%). System consistency was maintained via complex cell lysate quality control standards.

6.2.3 Data processing and analysis

Raw data analysis was performed by Biogenity. Raw MS files were analysed using Spectronaut (v19.0, Biognosys, Switzerland). The spectra were matched against the Homo sapiens UniProt database. Following the BGS workflow, the data was searched with oxidation (M) and acetylation on protein N-termini as dynamic modifications. Cysteine carbamidomethylation

was set as a static modification. Data was analysed with proteotypicity filter turned on, MS quantity level set to MS1 and local normalisation turned on. Data were then filtered, only retaining proteins with two unique peptides for downstream analysis and if they meet either criterion: (1) proteins with at least 60% valid values across all samples or (2) proteins with at least 75% valid values within an experimental group. After filtering, missing values in the remaining data were imputed using a hybrid imputation method in the R package imputeLCMD. The maximum likelihood estimate method was selected for Missing at Random values, and the quantile regression imputation of left-censored data method was selected for Missing Not at Random values. PCA was performed using the *prcomp()* function, and k-means clustering was performed using the *kmeans()* function in R. Graphs were visualised using the package ggplot2 (v4.0.0). Differential analysis and statistical significance between groups were assessed using limma for normally distributed proteins[278] or Wilcoxon signed-rank test for non-normally distributed proteins in R.

To classify function and subcellular localisation of all proteins from the proteomics dataset, I used the *groupGO()* function in the R package clusterProfiler (v4.6.2) and set for level 3 annotation. Classification of proteins was performed for all three GO ontologies: BP, Cellular Component (CC) and Molecular Function (MF). The background gene list was the annotation for human genome and loaded using the package org.Hs.eg.db (v3.16.0).

6.2.4 siRNA knockdown and immunostaining

For siRNA-mediated knockdown of nucleoporin 214 (NUP214), it was performed as described in Section 2.3 with minor modifications. Human ACFs were plated at 5,000 cells in each well of a sterilised microscope glass slide with removable 8-well chamber (#80841, ibidi, Germany). Once cells reached 60-80% confluency, cells were directly transfected with the lipofectamine-

siRNA complex in Opti-MEM medium with 10% FBS. As opposed to standard transfection protocol, 10% FBS was used in this specific setting because stress induced by low serum-induced stress promotes nuclear localisation of NR4A1[279]. After 6 hours of transfection, cells were replaced with growth medium with 10% FBS and incubated at 37°C for 48 hours. Immunostaining was performed on the ACFs as described in Section 2.6.

6.3 Results

6.3.1 NR4A1 protein is successfully enriched by co-IP

Prior to using MS to evaluate the NR4A1 interactome, I collected human ACF lysates from sinus rhythm donors, followed by immunoprecipitating NR4A1 in these samples using NR4A1-specific antibodies to validate the efficiency and specificity of pulldown. As shown in immunoblotting (Figure 6.3.1a), there was minimal signal in the beads only condition. In the IgG isotype control, a strong signal was detected at approximately 52 kDa, which corresponds to the molecular weight of IgG heavy chain[280]. In contrast, enrichment of NR4A1 was observed in the pulldowns obtained with two alternative NR4A1 antibodies (IP1: #25851-1-AP, Proteintech; IP2: #MA5-32647, Invitrogen). Antibodies used in IP1 and IP2 recognise overlapping regions of NR4A1, targeting amino acids 1-269 and 10-49, respectively. Although NR4A1 was not observed in the input lysate, it could be lowly expressed and underexposed. Hence, I exposed the input lane individually using a more sensitive ECL substrate and increasing the exposure time (Figure 6.3.1b). This improves the NR4A1 detection. Based on the greater NR4A1 enrichment achieved in lane 1, the NR4A1 antibody used in IP1 was selected for subsequent MS-based proteomic profiling, with the IgG isotype control included to account for non-specific binding and background.

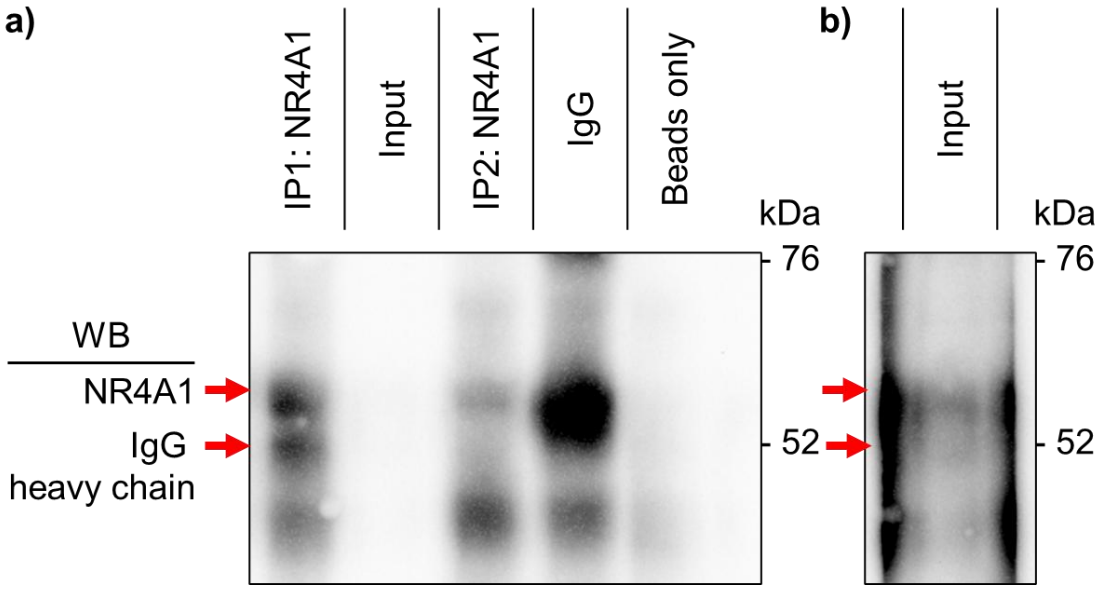

Figure 6.3.1 Validation of NR4A1 IP in human ACFs. (a) Representative blot showing the IP of NR4A1 in human ACF lysates. Lane 1 IP using NR4A1 antibody (#25851-1-AP). Lane 2 corresponds to input. Lane 3 IP using NR4A1 antibody (#MA5-32647). Lane 4 IP using rabbit IgG isotype control antibody. Lane 5 corresponds to agarose beads only. (**b**) Enhanced NR4A1 signal in input (lane 2) by using ECL substrate with higher sensitivity and longer exposure. Same membrane used in (**a**). Experiments performed using sinus rhythm donor-derived human ACFs.

6.3.2 Proteomics show distinct NR4A1 interactome profiles in human ACFs between sinus rhythm and persistent AF

To characterise the interactome of NR4A1 in ACFs under sinus rhythm and persistent AF conditions, co-IP coupled with MS was performed using a NR4A1-specific antibody (NR4A1_IP) and an IgG control (IgG_IP). Each condition included four biological replicates derived from independent donors. After the initial data was processed with filtering and imputation, PCA was performed to assess global proteomic variation across samples. PC1 accounted for 18% and PC2 accounted for 11% of the total variance (Figure 6.3.2a). Separation along PC1 distinguished NR4A1_IP samples from IgG_IP controls (with the exception of one sample from the AF IgG_IP group), indicating the protein enrichment by NR4A1-specific antibody represents a major source of variance. K-means clustering yielded consistent results, segregating IgG_IP controls into cluster 1 and NR4A1_IP samples into cluster 2 (Figure 6.3.2b). Therefore, it confirms that the NR4A1-specific pulldown primarily drives the proteomic changes of the interactome dataset.

To identify proteins specifically associated with NR4A1 in human ACFs, I performed the differential protein analysis between NR4A1_IP and IgG_IP, in sinus rhythm and AF separately. Due to the limited statistical power associated with small sample size (N = 4 per group), multiple testing correction using the Benjamini-Hochberg procedure did not yield statistically significant proteins at a FDR < 0.05. Given the exploratory nature of investigating NR4A1 interactome and the restricted protein set analysed, I defined NR4A1-interacting proteins as those with a non-adjusted P-value < 0.01 and showed positive enrichment relative to IgG_IP controls (log2FC > 0). Using these criteria, I identified twenty NR4A1-interacting proteins in sinus rhythm including NR4A1 as the top protein with smallest P-value ($P = 3.2 \times 10^{-5}$) (Figure 6.3.2c), supporting the specificity of the pulldown. In AF cells, I identified thirty-seven NR4A1-

interacting proteins including NR4A1 as the top protein with smallest *P*-value ($P = 1.6 \times 10^{-4}$) (Figure 6.3.2d), once again supporting the specificity of the pulldown. Interactors (non-adjusted P-value < 0.05) from the differential analysis for sinus rhythm and AF are provided in Supplementary Table 2 and Supplementary Table 3, respectively.

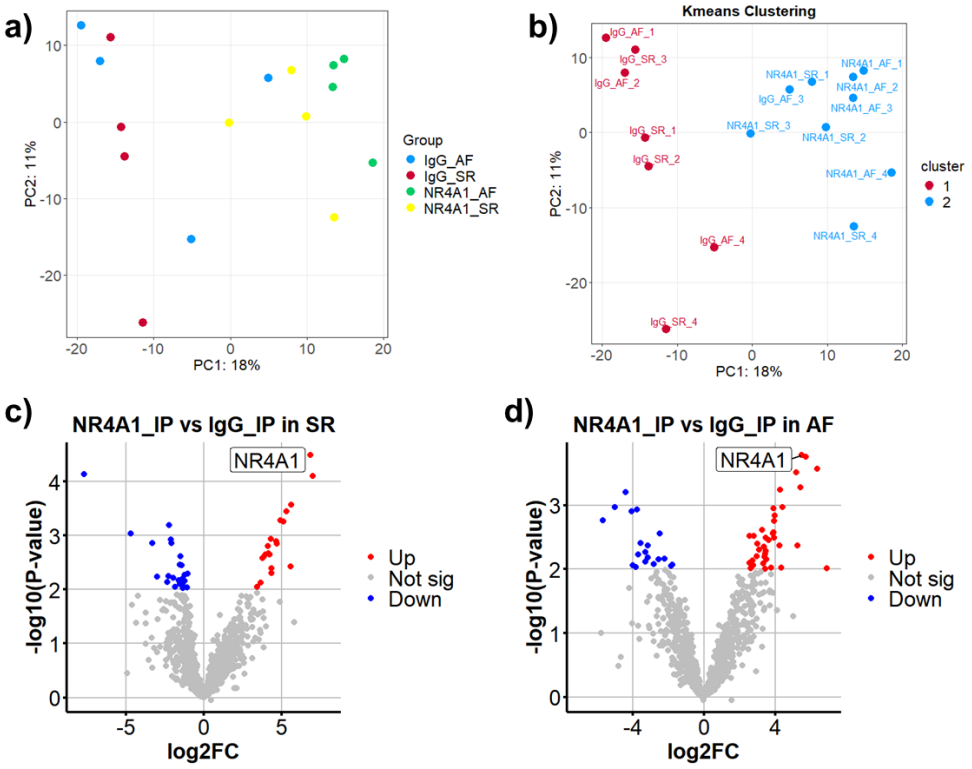

Figure 6.3.2 Proteomic profiles of NR4A1 interactome in sinus rhythm and persistent AF ACFs. (**a**) PCA plot showing the overall effect of variances between the NR4A1_IP and IgG_IP conditions in sinus rhythm (SR) and persistent AF ACFs. (**b**) K-means clusters segregating IgG_IP into cluster 1 and NR4A1_IP into cluster 2. (**c**) Volcano plot showing the distribution of protein level changes in NR4A1_IP relative to IgG_IP in SR cells. (**d**) Volcano plot showing the distribution of protein changes in NR4A1_IP relative to IgG_IP in AF cells. Red dots represent significantly enriched proteins in NR4A1_IP (non-adjusted *P*-value < 0.01, log2FC > 0) while blue dots represent significantly enriched proteins in IgG_IP (non-adjusted *P*-value < 0.01, log2FC < 0).

6.3.3 NR4A1-interacting proteins play different biological functions between sinus rhythm and AF ACFs

The NR4A1-interacting proteins in human ACFs were summarised in Table 6.3.3 and categorised by their main subcellular location. Nine proteins were found to be enriched in NR4A1 interactome from both sinus rhythm and AF ACFs: C1QC, C4A, HRG, MFAP4, NR4A1, PAPSS1, PON1, TFG and VAC14. This set of proteins highlights innate immune and ECM-related factors. Notably, C1QC and C4A are complement components of the classical pathway[281], and MFAP4 is an ECM glycoprotein with roles in elastic fibre assembly and immune responses[282–284]. Other NR4A1 interactors reflect secretory and metabolic functions. Hence, NR4A1 is a nexus between ACFs and immunomodulation/ECM remodelling pathways in general.

Eleven NR4A1-interacting proteins were uniquely identified in sinus rhythm ACFs: AKAP8L, ARPC1B, C1R, CSDE1, DDX17, ECHS1, EEF1G, HEXB, IARS1, RPS27 and SLIRP. These proteins primarily modulate cellular housekeeping, act as structural proteins and possess metabolic functions. Twenty-eight AF-specific NR4A1 interactors show upregulation of stress and activation pathways. The proteins are associated with inflammatory kinases (STAT2, MAP4K4), ECM modifiers (PLOD1), vesicle trafficking or cytoskeleton, metabolism and translational machinery. Therefore, NR4A1 interactors in AF ACFs point to a network linking immune signalling, cytokine responsiveness and ECM production. Given the observation of elevated cytoplasmic NR4A1 expression in AF ACFs from previous chapter, non-nuclear NR4A1 could thus directly interact with the AF-specific proteins that localised outside of the nucleus.

Table 6.3.3 NR4A1-interacting proteins in sinus rhythm and AF ACFs

Main subcellular location	NR4A1_IP: SR and AF (9)	NR4A1_IP: SR only (11)	NR4A1_IP: AF only (28)
Nuclear	NR4A1 PAPSS1	AKAP8L DDX17	ASCC3 CSNK2B DDX46 DKC1 MPHOSPH10 SNRNP200
Cytoplasmic		ARPC1B CSDE1 EEF1G IARS1 RPS27	CTNNA1 DCTN4 DYNC1LI1 ECHDC1 KANK2 MAP4K4 RPL22 RPS12 RPS26 SCYL1 STAT2 TARS1
Endoplasmic reticulum	TFG		PDIA5 PLOD1 STT3B
Endosomal	VAC14		REP15

Lysosomal		HEXB	
Mitochondrial		ECHS1 SLIRP	ATAD3A LETM1 MRPL11
Vesicle			AP3B1
Membrane			LRRFIP2 NT5E
Secreted/Extracellular	C1QC C4A HRG MFAP4 PON1	C1R	

6.3.4 NR4A1 interaction with NUP214 is enriched only in AF ACFs

To understand mechanisms driving the enriched cytoplasmic expression of NR4A1 specifically in AF ACFs, I extracted proteins from the NR4A1 interactome full dataset that is annotated with the GO term "nucleocytoplasmic carrier activity". It includes six proteins: calreticulin (CALR), importin α-1 (KPNA2), importin β-1 (KPNB1), nucleoporin 214 (NUP214), GTP-binding nuclear protein Ran (RAN) and XPO1. The protein abundance of these six proteins in the NR4A1 interactome is visualised (Figure 6.3.4).

Instead of assessing the data through statistical comparisons between groups (*P*-values), I implemented an alternative reproducibility-based strategy to identify potential interactors. A protein was defined as a unique interactor if it met the following criteria: (1) detected in at least three out of four biological replicates in the NR4A1_IP group, and (2) detected in one or none of the four biological replicates in the IgG_IP control group. These criteria ensure that the interactors are consistently associated with NR4A1 across donors and largely absent from the non-specific IgG pulldown controls, representing specific and reproducible interactions.

XPO1, an important protein responsible for nuclear export[285], was detected in 3/4 NR4A1_IP samples in sinus rhythm, present in all NR4A1_IP samples in AF, and was completely absent in IgG_IP controls (Figure 6.3.4a). It suggests that NR4A1 interacts with XPO1 in human ACFs in general and not specific to AF. KPNA2 and KPNB1 involve in the nuclear import machinery[286]. KPNA2 fulfilled the criteria for unique interaction in sinus rhythm but not in AF cells (Figure 6.3.4b), whereas KPNB1 was detected across both sinus rhythm and AF samples but did not fulfil the criteria as a unique interactor of NR4A1 in either condition (Figure 6.3.4c). NUP214 emerged as a robust interactor in AF, appearing in all NR4A1_IP samples while being largely absent in IgG_IP controls (Figure 6.3.4d). This unique interaction of NUP214 was not

observed in sinus rhythm cells. CALR and RAN were not classified as unique interactors of NR4A1 in either condition based on the pre-defined criteria (Figure 6.3.4e-f). The analysis is summarised in Figure 6.3.4g.

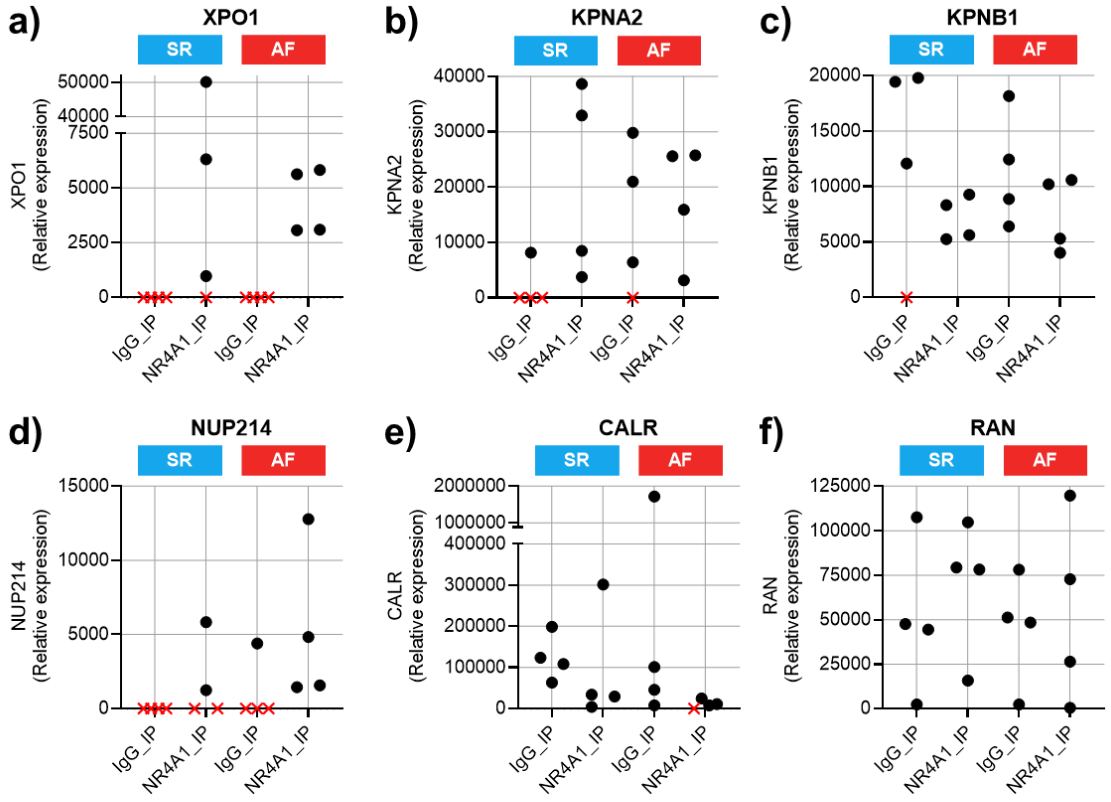

g)

Proteins	XPO1	KPNA2	KPNB1	NUP214	CALR	RAN
SR	✓	✓	X	X	X	X
AF	✓	X	X	✓	X	X

Unique interactor of NR4A1: ✓ = Yes, X = No

Figure 6.3.4 Proteins associated with nucleocytoplasmic transport in NR4A1 interactome. (**a-f**) Dot plots showing relative abundance of six proteins in NR4A1 interactome that are associated with nucleocytoplasmic carrier activity: XPO1, KPNA2, KPNB1, NUP214, CALR and RAN. Black dots represent detected protein level while red cross symbols represent protein not detected or below detection threshold. (**g**) Table summarising the classification of the six selected proteins as a unique interactor of NR4A1 or not.

6.3.5 Expression profiling of NUP214 in human ACFs from patients with persistent AF

Since NUP214 was identified to be a unique interactor of NR4A1 in AF, I profiled its expression in AF ACFs. There is a trend towards higher *NUP214* mRNA level in AF than sinus rhythm cells, but statistical significance was not reached ($P = 0.0686$; Figure 6.3.5a). I also measured *NR4A1* gene expression in the same samples and showed a positive correlation between *NUP214* and *NR4A1* mRNA levels ($R = 0.5623$, $P = 0.0052$; Figure 6.3.5b). In addition to gene expression, protein levels of NUP214 were measured, which demonstrated an increasing trend in AF ACFs relative to sinus rhythm ($P = 0.1759$; Figure 6.3.5c-d).

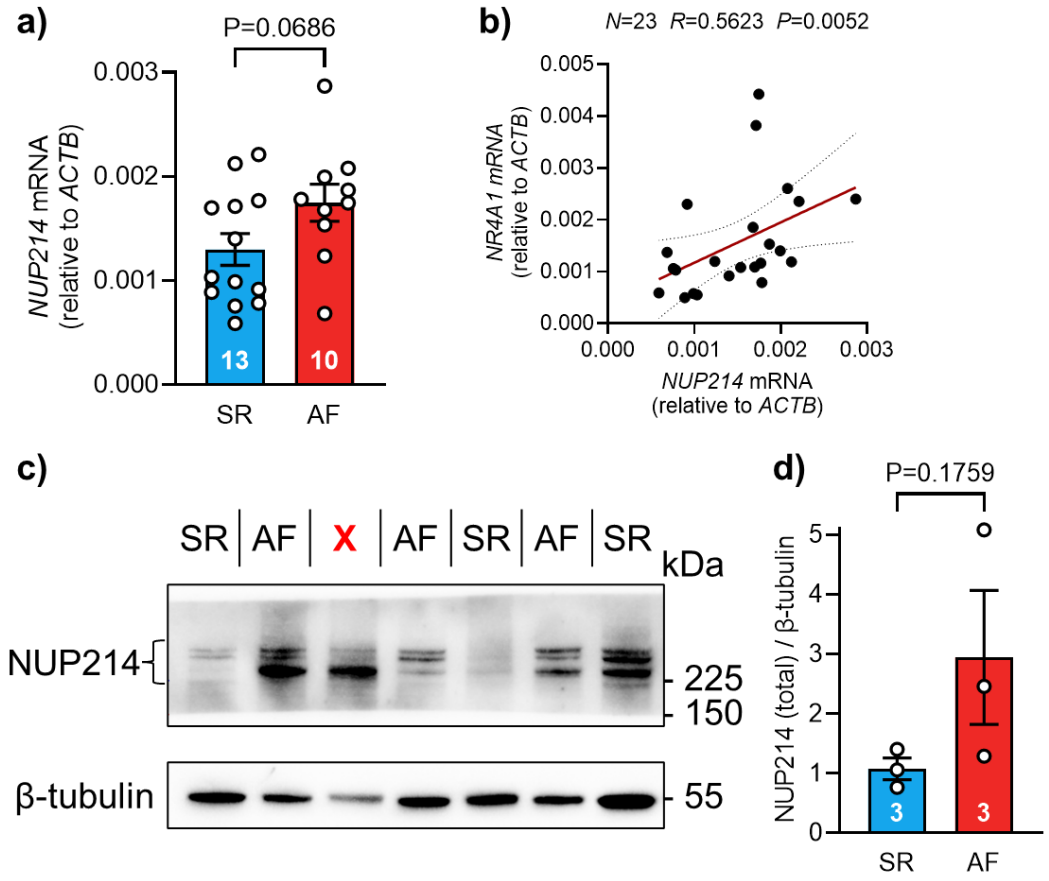

Figure 6.3.5 Gene and protein expression of NR4A1 in ACFs from persistent AF patients. (**a**) *NUP214* mRNA levels in ACFs from patients with persistent AF or sinus rhythm (SR) controls. (**b**) Correlation between *NUP214* and *NR4A1* mRNA levels in ACFs (SR and AF). (**c-d**) Total protein levels of NUP214 in ACFs from patients with persistent AF or SR controls. Lane 3 (red cross) is excluded from quantification as indicated by the outlier test and underloading of housekeeping protein (β-tubulin) compared to other lanes. Data are mean ± SEM; each dot represents an independent biological replicate (*N*). *P*-values are determined from raw values and reported as two-sided using unpaired t-test (**a**, **d**) and Spearman's correlation test (**b**).

6.3.6 NUP214 deficiency restores nuclear localisation of NR4A1 in AF ACFs

I further investigated the potential role of NUP214 in driving NR4A1 cytoplasmic translocation in AF using siRNA-mediated knockdown. Successful knockdown of NUP214 was confirmed by the reduction of NUP214 protein levels (Figure 6.3.5a). The NUP214-deficient AF ACF showed NR4A1 expression predominantly in the nucleus, comparing to the nuclear and cytoplasmic localisation in the negative control condition (Figure 6.3.5b). Quantification has also confirmed predominantly nuclear localisation of NR4A1 in NUP214 knockdown cells, indicated by the reduced percentage of non-nuclear NR4A1 per cell ($P < 0.0001$; Figure 6.3.6c).

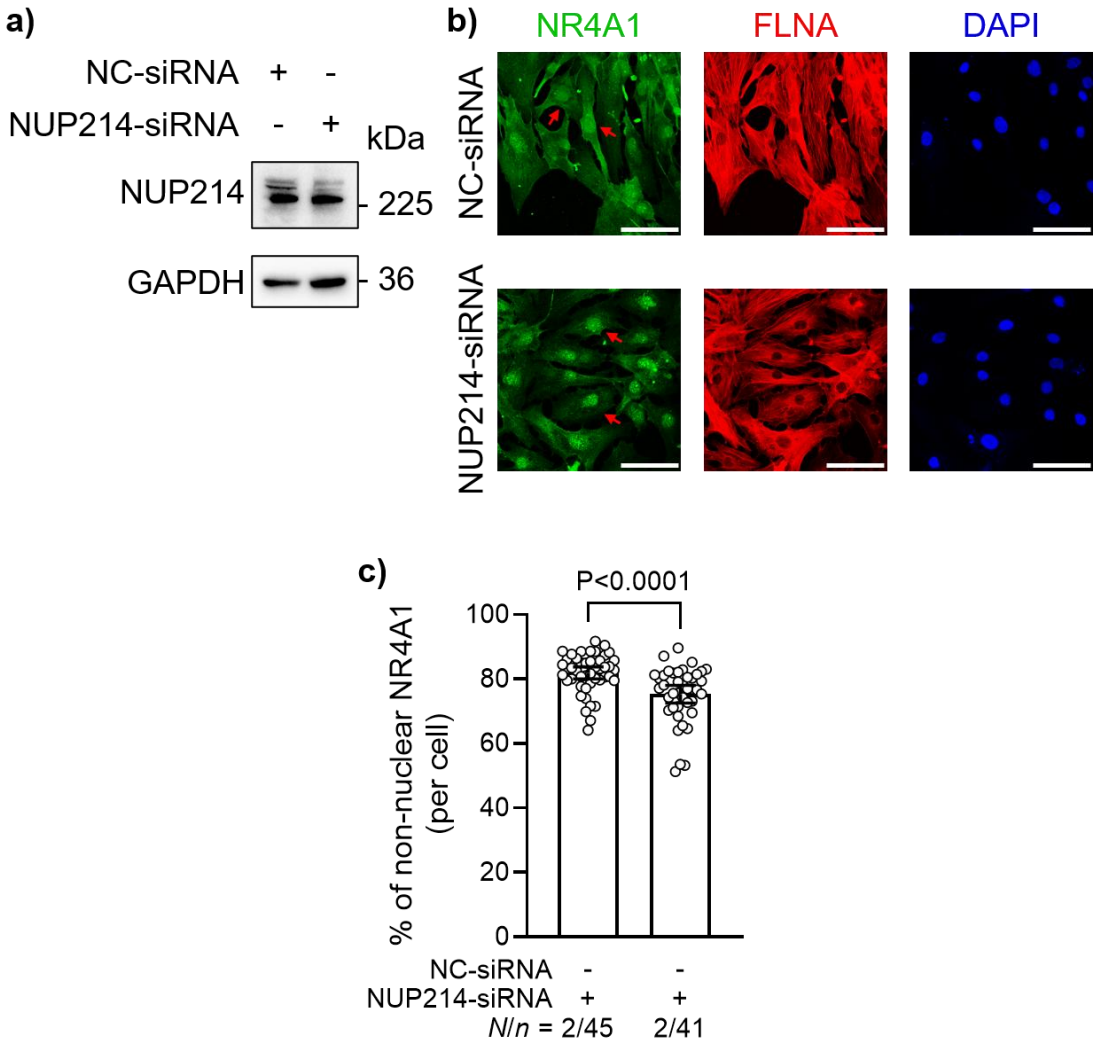

Figure 6.3.6 Protein localisation of NR4A1 in AF-ACFs with NUP214 knockdown. (**a**) Total protein levels of NUP214 in AF ACFs with NUP214 siRNA-mediated knockdown condition compared with negative control (NC-siRNA) (**b**) Immunofluorescence images visualising NR4A1 localisation in NUP214-deficient ACFs from persistent AF patients. Red arrows indicate representative cells. Scale bar = 75 µm. (**c**) Quantification of non-nuclear NR4A1 in AF ACFs with NUP214- or NC-siRNA. Data are mean ± SEM; each dot represents an individual cell (*n*) from two biological donors (*N* = 2). Data are expressed as the percentage of non-nuclear NR4A1 per cell. *P*-values are reported as two-sided using Mann-Whitney test.

6.4 Discussion

In this chapter, I profiled the NR4A1interactome in ACFs from sinus rhythm and AF patients, identifying protein partners that are differentially regulated in the context of persistent AF. Given the primary role of NR4A1 as a transcription factor, previous studies have focused on this aspect through running chromatin immunoprecipitation sequencing (ChIP-seq) analysis. To my knowledge, this work represents the first study of the NR4A1 interactome in human cardiac fibroblasts. This is a critical dataset, as it points toward the potential non-genomic functions of NR4A1 beyond the direct transcriptional regulation of its target genes.

Unlike RNA-seq, which typically yields thousands of DEGs for robust pathway analysis, interactome proteomics inherently produces a more restricted dataset and presents statistical challenges. To overcome this limitation to understand the biological functions of NR4A1 interactors, I applied a filtering threshold using non-adjusted p-values < 0.01 to narrow down a few potential protein candidates. It allows the examination of NR4A1 interactors in human ACFs generally, specific to sinus rhythm only, or specific to AF only.

NR4A1 is a nuclear protein, but its subcellular localisation is highly dynamic. In response to stress signals, NR4A1 translocates to the cytoplasm or other intracellular compartments such as mitochondria[134]. In a HEK293 cell model assessing autophagic cell death, cytoplasmic NR4A1 was observed alongside nuclear NR4A1 in 14% of the cells, yet NR4A1 was mainly localised in the nucleus and remained transcriptionally competent[287]. This underscores that NR4A1 can function simultaneously as a transcriptional regulator and a cytoplasmic protein interactor. When comparing the NR4A1 interactors detected in sinus rhythm and AF ACFs, it is surprising that relatively few proteins are shared between both conditions (9 proteins), as

opposed to 11 sinus rhythm-specific interactors and 28 AF-specific interactors. The limited interactome overlap between sinus rhythm and AF suggest that NR4A1 adopts distinct protein interactions mediating biological functions and pathways in AF.

The NR4A1 interactors exclusive to AF ACFs provide critical insights into the consequences of the cytoplasmic translocation observed in the previous chapter. Notably, STAT2 and MAP4K4, which regulate TNF-α and IFN signalling[288,289], as well as LRRFIP2, a regulator of the NLRP3 inflammasome, were identified as AF-specific interactors of NR4A1. This suggests that non-nuclear NR4A1 may engage with immunomodulators to drive inflammatory pathways in AF. STAT2 has been previously linked to inflammatory cardiac dysfunction in AF[290]. Although LRRFIP2 has not been directly linked to AF, it regulates the NLRP3 inflammasome that plays a causal role in AF pathogenesis[89]. Moreover, the interaction with PLOD1 is of particular relevance. PLOD1 is an enzyme (lysyl hydroxylase) essential for crosslinking fibrillar collagen and stabilising the fibrotic ECM[291]. Together, these interactions imply that in AF ACFs, cytoplasmic NR4A1 may act as a signalling scaffold, engaging with inflammatory and ECM modulators to actively drive activation and phenotypic change in the cells. To validate these interactions, reciprocal pulldown of the AF-specific interactors should be performed to confirm their association with NR4A1.

To overcome the limitations of proteomic datasets and statistical challenges, I adopted another approach – the reproducibility-based strategy – rather than a conventional statistical framework to study NR4A1 unique interactors. Evaluating NR4A1 interactors in a small clinical cohort (*N* = 4 per group) reduces statistical power, as inter-individual variability can mask biologically meaningful but variably expressed protein interactions. Furthermore, conventional statistical testing in proteomics often requires the imputation of missing values for lowly-expressed

proteins, which can artificially influence the variance estimates and reduce statistical power[292,293]. In contrast, my reproducibility-based strategy evaluates protein abundance prior to imputation, which allows for a direct and transparent assessment of a protein's presence or absence. By utilising IgG_IP controls to filter out non-specific binding and background noise, this analysis provides additional insights into enriched proteins specifically associated with NR4A1.

The cytoplasmic retention of NR4A1 in AF ACFs could be driven by altered dynamics with nucleocytoplasmic transport proteins including exportins, importins and nucleoporins[294]. My interactome data revealed a shift in transport machinery binding in AF. NUP214, one of six proteins annotated with nucleocytoplasmic carrier activity in GO, was uniquely enriched in the AF interactome. NUP214 is located on the cytoplasmic side of the NPC and acts as a molecular clamp that stabilises the XPO1 export complex during the terminal steps of nuclear export[295]. NUP214 binds to XPO1 with high affinity at its C-terminal FG repeat region compared to other nucleoporins[295]. Conversely, KPNA2 was identified as a unique NR4A1 interactor in sinus rhythm cells but was absent in AF. Therefore, the gain of NUP214 binding and the loss of KPNA2 binding provide a potential dual mechanism for the cytoplasmic accumulation of NR4A1 in AF: stabilised nuclear export coupled with reduced nuclear import.

In parallel with the increased NR4A1 protein and cytoplasmic translocation in ACFs from patients with persistent AF, I observed a trend toward higher NUP214 expression in AF cells. Interestingly, *NUP214* mRNA level positively correlated with *NR4A1* mRNA expression, suggesting a potential co-regulatory mechanism. The increased availability of NUP214 in AF ACFs may facilitate enhanced NR4A1-NUP214 binding, ultimately improving the efficiency and stability of XPO1-mediated nuclear export through the NPC.

To functionally explore the NR4A1-NUP214 relationship, I targeted NUP214 in AF ACFs. Previous study has shown that siRNA-mediated depletion of NUP214 in HeLa cells leads to a significant nuclear accumulation of transcription factor NFAT through a XPO1-dependent export mechanism[296]. Adopting a similar approach, my preliminary findings demonstrated that NUP214 knockdown in AF ACFs successfully rescued the phenotype, significantly reducing the percentage of non-nuclear NR4A1 and restoring its nuclear localisation. This positions the NR4A1-NUP214 interaction as a promising, functional therapeutic target to suppress the maladaptive non-genomic functions of NR4A1 in AF and worth to be followed up in future studies.

While interactome proteomics infers the physical proximity of protein pairs, this is only the initial step in delineating biological function of the proteins. First, physical binding does not confirm functional activation, nor does it establish the directionality of the modification. Second, functional signalling interactions are often transient and stimulus-dependent, which can be difficult to fully capture using standard co-IP coupled with MS approaches. Finally, interactions identified in cell lysates may not reflect the active conformations of proteins within living cells. Therefore, while my NUP214 knockdown data supports a functional interaction, follow-up structural biology examinations and functional assays are necessary to fully elucidate the biological activation of these complexes.

CHAPTER 7: DISCUSSION

7.1 Discussion

7.1.1 Overview and rationale

AF is the most prevalent sustained cardiac arrhythmia worldwide[5]. Its disease burden escalates with progression to more advanced stages, including persistent and long-standing AF[297]. In these chronic phenotypes, structural remodelling of the atria constitutes a major therapeutic challenge, as it both perpetuates the arrhythmia and limits the efficacy of rhythm control interventions such as catheter ablation[298]. Structural remodelling is characterised by fibrosis, myocyte loss, and electrical uncoupling[299]. Cardiac fibroblasts are the primary cellular mediators of atrial fibrosis, driving the deposition and remodelling of the ECM through their activation and differentiation into contractile myofibroblasts[105]. Despite the established importance of fibroblast activation in AF-associated structural remodelling, the underlying molecular mechanisms that govern this process in the atrial context remain incompletely understood.

The collaboration between the Reilly and Lettre groups revealed fibroblast heterogeneity within the human left atrial appendage beyond the classical activated and quiescent phenotypes, identifying a discrete NR4A1-enriched fibroblast subpopulation, designated aFB3[132]. NR4A1 is an orphan nuclear receptor and transcription factor with established roles in regulating fibrotic responses across multiple organ systems, including the heart[133]. However, the precise role and mechanistic basis of NR4A1 driving atrial fibrotic responses, and its relevance to the pathophysiology of persistent AF, had not been previously characterised. Therefore, my work presented in this thesis is designed to address three objectives: (1) to determine the functional consequences of NR4A1 regulation on fibrotic responses in human ACFs, (2) to define the transcriptional changes downstream of NR4A1 and identify associated signalling components in human ACFs, and (3) to profile NR4A1 expression, subcellular localisation, and protein interactions in ACFs isolated from patients with persistent AF relative to sinus rhythm controls.

7.1.2 Chapter 3 findings: NR4A1 as a pro-fibrotic regulator in human ACFs

In this chapter, my loss and gain of function experiments established that NR4A1 promotes fibrotic responses in human ACFs. siRNA-mediated knockdown of NR4A1 resulted in reduced expression of established fibrotic markers (αSMA, periostin), and suppressed cell proliferation, whilst pharmacological activation using Csn-B upregulated fibrotic marker expression in both unstimulated and TGF-β1-stimulated ACFs. Importantly, the attenuation of TGF-β1-induced fibrotic responses following NR4A1 depletion suggests that NR4A1 partially acts downstream of canonical TGF-β1 signalling, in addition to modulating basal fibroblast tone. The pro-fibrotic function of NR4A1 identified in human ACFs therefore reflects a cell-type-specific regulatory role, underscores the importance of contextualising NR4A1 biology within the persistent AF disease setting. Whilst the functional consequences of NR4A1 regulation were demonstrated, the precise molecular mechanism remained undefined at this stage, motivating the transcriptomic investigation undertaken in chapter 4.

7.1.3 Chapter 4 findings: NR4A1-IL-6 signalling axis in human ACFs

Building on the functional findings on the previous chapter, in this chapter, I applied bulk RNA-seq to comprehensively profile the transcriptional landscape of human ACFs following NR4A1 knockdown. Transcriptomic analysis confirmed the downregulation of fibrotic markers (*ACTA2*, *POSTN*) in NR4A1-deficient cells, consistent with the observations in chapter 3. Pathway analysis revealed a broader phenotypic shift characterised by coordinate downregulation of gene signatures associated with ECM remodelling and immunomodulation, indicating that NR4A1 orchestrates a transcriptional programme involving fibrotic and inflammatory responses.

To nominate a primary signalling target mediating NR4A1-driven responses, a PPI network was constructed from the DEGs, which identified IL-6 as the primary hub target. *In silico* analysis of the human *IL6* gene promoter region using JASPAR predicted a high-confidence putative NR4A1

binding site, providing preliminary evidence for direct transcriptional regulation of *IL6* by NR4A1. Functional validation confirmed that IL-6 stimulation increased total collagen secretion in human ACFs, and the effect was abrogated by IL-6 neutralisation, establishing IL-6 as a pro-fibrotic effector in this cellular context. Furthermore, stimulation with PGA2 upregulated IL-6 secretion in human ACFs, and this effect was significantly attenuated by NR4A1 knockdown.

Notably, the gene expression signatures induced by NR4A1 knockdown exhibited resemblance to transcriptional patterns associated with glucocorticoid treatment in human cells, as identified through CMap analysis, suggesting a potential overlap between NR4A1-dependent and glucocorticoid-regulated anti-inflammatory pathways. This convergence may reflect shared downstream suppression of target genes and warrants further investigation as a mechanistic link.

The identification of a positive NR4A1-IL6 regulatory relationship in ACFs is of particular mechanistic interest when considered alongside the established literature in immune cells. In myeloid-derived cells, NR4A1 has been shown to negatively regulate IL-6 at the transcriptional level through inactivating the NF-κB signalling, thereby exerting an anti-inflammatory effect[244]. The present findings reveal a strikingly divergent regulatory pattern in ACFs, where NR4A1 activity is instead associated with IL-6 upregulation and a pro-inflammatory, pro-fibrotic phenotype. The mechanistic basis for this divergence in ACFs – whether attributable to differential co-activator recruitment, distinct chromatin accessibility at the *IL6* promoter, or alternative NR4A1 PTMs – represents an important direction for future investigation. My findings collectively delineated a NR4A1-IL-6 signalling axis through which NR4A1 may coordinate both inflammatory and fibrotic pathways in human ACFs (Figure 7.1.3), and its pathological relevance was subsequently examined in the context of persistent AF in chapter 5.

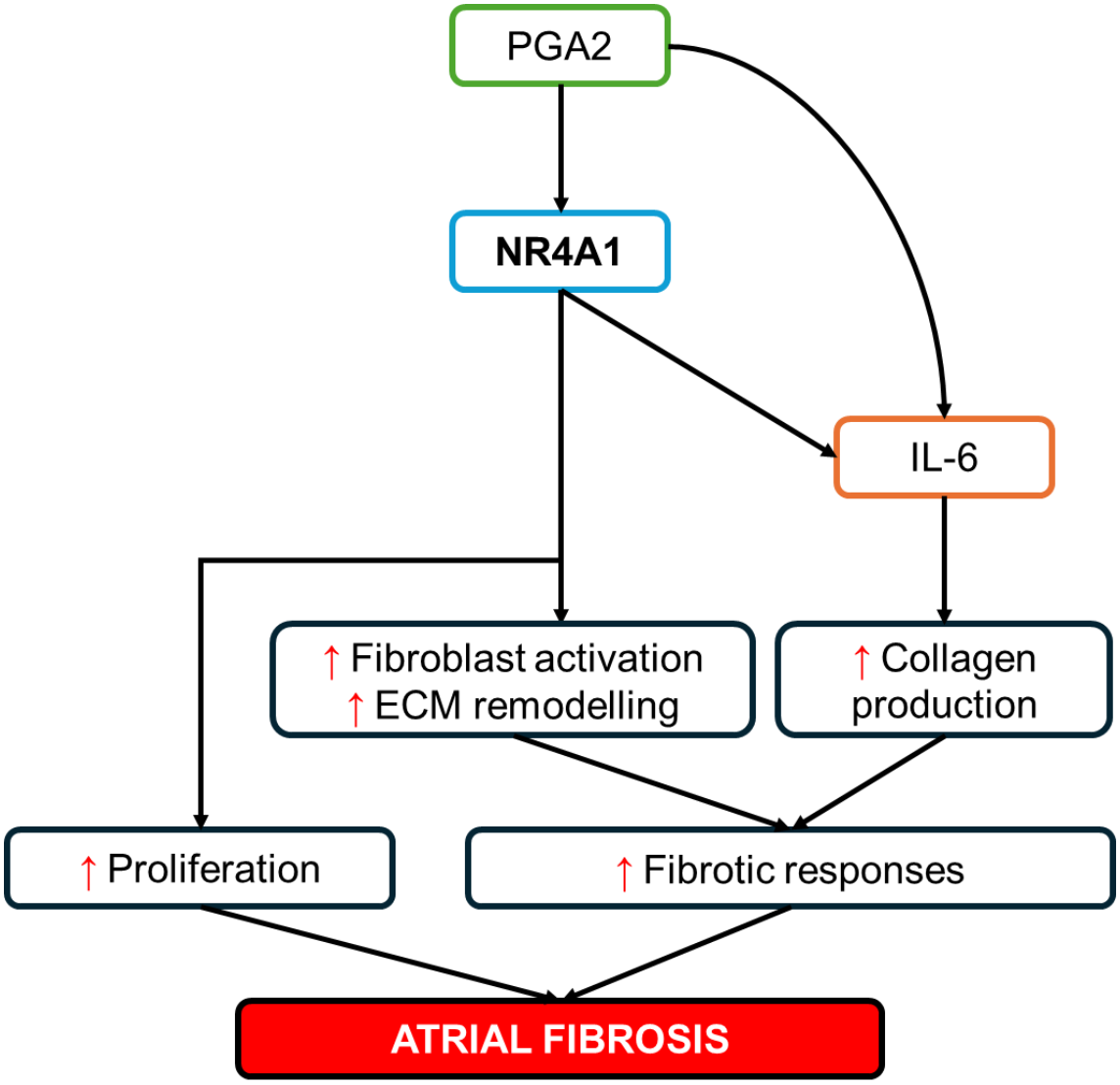

Figure 7.1.3 Schematic illustration of the proposed NR4A1-IL-6 signalling mechanism mediating fibrotic responses in human ACFs.

7.1.4 Chapter 5 findings: cytoplasmic redistribution of NR4A1 in persistent AF ACFs

In this chapter, I translated the mechanistic findings of the preceding chapters into the clinical context of persistent AF. NR4A1 protein abundance was significantly elevated in AF ACFs in relative to sinus rhythm controls, accompanied by increased secretion of both IL-6 and PGA2 in cell culture supernatants. The coordinate upregulation of NR4A1, its endogenous ligand PGA2,

and its downstream effector IL-6 in AF ACFs potentially form a self-reinforcing pro-fibrotic signalling loop that may contribute to the perpetuation of atrial structural remodelling in persistent AF.

Beyond changes in total protein abundance, immunostaining revealed a redistribution in NR4A1 subcellular localisation in AF ACFs, with a significantly increased non-nuclear (cytoplasmic) fraction compared to sinus rhythm controls. This finding needs to be carefully considered, as a direct observation might suggest that cytoplasmic sequestration of NR4A1 attenuates its pro-fibrotic nuclear transcriptional activity, implying a compensatory response to persistent AF. However, this interpretation is complicated by the observation that nuclear NR4A1 expression remains present in AF ACFs, indicating that the nuclear transcriptional pool of NR4A1 is not diminished. Instead, the cytoplasmic accumulation represents an additive compartmentalisation, rather than a redistribution at the expense of nuclear activity.

This raises the possibility that cytoplasmic NR4A1 may serve distinct, non-genomic functions in AF ACFs. NR4A1 has been reported to interact with cytoplasmic signalling proteins in other cellular contexts, influencing processes such as apoptosis, inflammation, autophagy independent of direct DNA binding[134,147]. It remains an open and clinically important question whether non-genomic functions of NR4A1 operate in human ACFs, and whether they are pro- or anti-fibrotic. The possibility therefore exists that cytoplasmic NR4A1 in AF ACFs is not merely a sequestered, inactive pool, but an active signalling species contributing to the disease phenotype.

Given that NR4A1 phosphorylation status and proteasomal degradation level did not differ significantly between sinus rhythm and AF ACFs, the accumulated cytoplasmic localisation of NR4A1 in AF could not be explained by these PTM mechanism. This observation pointed towards

an alternative post-translational layer of NR4A1 regulation in AF ACFs, such as SUMOylation, which has been reported to promote cytoplasmic retention of NR4A1 in HEK293 cells[145]. It also suggests a dysregulation of the nucleocytoplasmic transport machinery as a potential mechanism. The nature of this transport dysregulation was therefore investigated through interactome profiling in chapter 6.

7.1.5 Chapter 6 findings: NUP214 as a potential mediator of NR4A1 nuclear export in persistent AF ACFs

In this chapter, I studied NR4A1 protein interactome to investigate the NR4A1 protein function and its interactors, contributing to molecular machinery involved in biological process, including the molecular basis of NR4A1 cytoplasmic accumulation in AF ACFs. Co-IP of NR4A1 coupled with MS analysis enabled the comparative interactome profiling in ACF lysates between sinus rhythm and persistent AF groups. The results revealed that sinus rhythm and AF ACFs display distinct NR4A1 interactome profiles, indicating that the altered subcellular distribution of NR4A1 in AF is accompanied by fundamental changes in its protein interaction network. The interactome composition reflects the broader phenotypic reprogramming of ACFs in persistent AF and suggests that NR4A1 is integrated into distinct protein complexes.

To identify candidate drivers of the AF-specific cytoplasmic redistribution of NR4A1, proteins with known nucleocytoplasmic transport functions were extracted from the interactome dataset. This analysis identified NUP214, a component of the cytoplasmic face of NPC with an established role in facilitating XPO1-dependent nuclear export[295], as a unique NR4A1-interacting protein in AF ACFs that was absent from the sinus rhythm interactome. The specificity of this interaction to the AF condition suggests that NUP214 engagement with NR4A1 may not be a constitutive feature in ACFs, but rather an aberrant interaction enriched in the disease state. This represents

the first reported interaction between NR4A1 and NUP214, identifying a novel nuclear export mechanism for this receptor in cardiac fibroblast context (Figure 7.1.5).

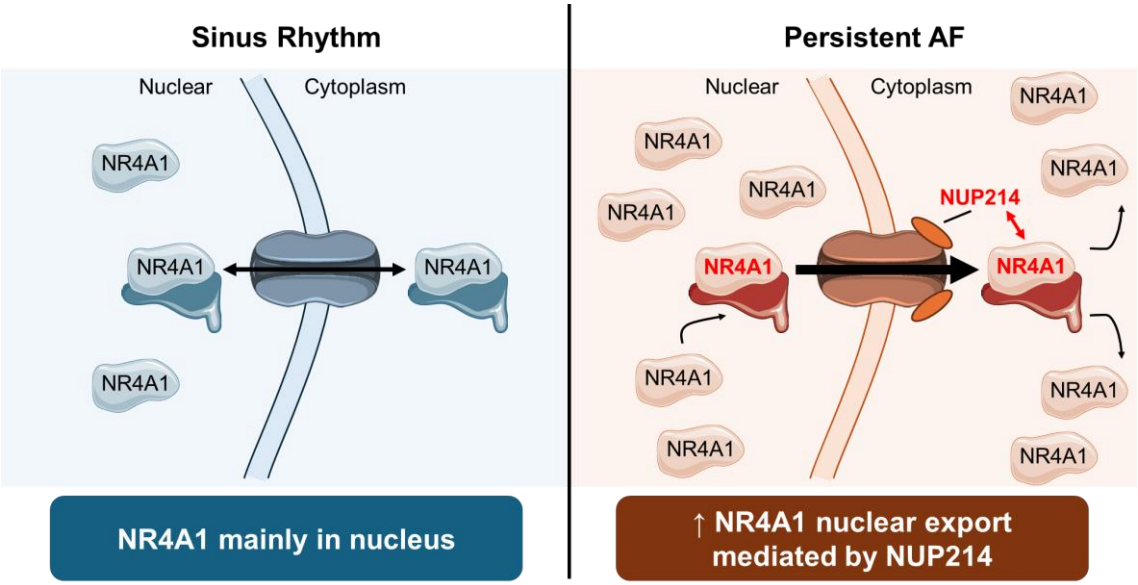

Figure 7.1.5 Schematic illustration of the proposed NR4A1-NUP214 interaction-mediated nuclear export mechanism in AF ACFs. Images and icons provided by Servier Medical Art.

Preliminary data further indicated a trend towards elevated NUP214 levels in AF ACFs, and siRNA-mediated knockdown of NUP214 in AF ACFs was associated with partial restoration of nuclear NR4A1 localisation. The partial, rather than complete, rescue of nuclear NR4A1 following NUP214 depletion is consistent with a multifactorial model of nucleocytoplasmic transport dysregulation in AF ACFs, in which NUP214 is a significant but not exclusive contributor. Additional mechanisms, such as altered importin-mediated nuclear import, may act in together with NUP214 upregulation to drive the observed NR4A1 redistribution in AF ACFs.

7.2 Impact of findings

The findings presented in my thesis contribute to the field of AF research at several levels: (1) contextualising a newly described ACF subpopulation, (2) consolidating and extending the emerging literature on NR4A1 in cardiac fibroblast biology, and (3) establishing two novel mechanistic insights specific to the ACF context in persistent AF.

7.2.1 Contextualising the NR4A1-enriched ACF subpopulation

The relative abundance of the NR4A1-enriched ACF subpopulation was not significantly different between sinus rhythm controls and patients with persistent AF[132], indicating that the pathological significance of these cells in AF is unlikely to be explained by changes in cell number alone. Instead, this observation emphasises the importance of understanding the functional biology of the aFB3 subpopulation; specifically, what NR4A1-driven transcriptional and phenotypic responses are activated or dysregulated within these cells.

The RNA-seq and functional *in vitro* data generated in my thesis provide a mechanistic basis for understanding what the NR4A1-enriched ACF subpopulation may do in the context of atrial remodelling. The changes observed in downregulated inflammatory signalling and ECM remodelling pathways upon NR4A1 knockdown in human ACFs suggest that NR4A1 actively drives an activated, inflamed, ECM-remodelling phenotype in these cells. Notably, the transcriptional and functional profile associated with NR4A1 activity in human ACFs points to a phenotype that is distinct from the classical myofibroblast subtype, which is primarily defined by contractile and ECM-secretory activity[300]. This distinction aligns with a growing body of evidence demonstrating cardiac fibroblast heterogeneity in cardiovascular diseases[107,301], in which molecular, secretory, and functional profiles differ substantially between myofibroblasts and other

fibroblast subtypes, including inflammatory and senescent fibroblasts characterised by elevated secretion of mediators such as IL-6, IL-1β and MCP-1. Therefore, the findings provide functional depth to the single-cell classification of NR4A1-enriched ACFs, suggesting that this subpopulation may represent an immunomodulatory fibroblast state with pathological relevance to AF-associated inflammation and fibrotic remodelling.

In contrast, the changes observed in upregulated HIF-1 and metabolic signalling imply an incomplete stress response, but the absence of significant regulation in HIF-1 downstream targets suggests that the metabolic reprogramming phenotype in the cells may be restricted to the transcriptional or transcriptomic level. Metabolic regulation and the downstream functional outcomes associated with NR4A1-deficient cells need to be further explored.

7.2.2 Novel mechanistic insights into the ACF phenotype in persistent AF

This work presents the first fibroblast-specific mechanistic characterisation of NR4A1 regulation in persistent AF, and advances two distinct but complementary mechanistic insights that contribute together to a more integrated understanding of how the AF-specific ACF phenotype is established and maintained.

The first mechanistic contribution consolidates and refines the understanding of NR4A1 as a pro-fibrotic regulator in human ACFs, coordinating both inflammatory signalling and ECM remodelling, pathways that are directly relevant to the atrial structural remodelling in persistent AF[39]. Whilst prior work in cardiac fibroblasts has shown that NR4A1 exerts pro-fibrotic effects through modulation of TGF-β signalling[160,161], my RNA-seq data presented in this thesis reveal that NR4A1 knockdown induces a phenotypic shift towards downregulated inflammatory and

ECM remodelling gene programmes in the absence of exogenous TGF-β1 stimulation. This demonstrates that NR4A1 regulates fibrotic and inflammatory responses in human ACFs under basal conditions, independently of TGF-β1, indicating that the pro-fibrotic activity of NR4A1 is not contingent on a single upstream pathway. It further highlights the mechanistic diversity and complexity of NR4A1-mediated fibrotic signalling in cardiac fibroblasts. NR4A1 appears to function as a broader transcriptional coordinator of the activated fibroblast state rather than acting solely as a downstream effector of TGF-β. Moreover, by demonstrating NR4A1-driven inflammatory regulation in the context of ACFs, my work translates a regulatory function previously described in cancer and immune cell biology into a cardiac-specific framework[302], with direct relevance to the chronic atrial inflammatory environment observed in persistent AF[303].

The second mechanistic contribution is the identification of aberrant non-nuclear accumulation of NR4A1 in ACFs from patients with persistent AF, which has not been reported previously. Whilst NR4A1 is canonically characterised as a nuclear transcription factor[134], the cytoplasmic redistribution of NR4A1 observed in AF ACFs suggests that the AF-associated microenvironment is associated with a non-canonical localisation of the protein. Interactome proteomics implicate increased interaction between NR4A1 and the NPC component NUP214 as a potential driver of this translocation, directing towards a dysregulated nuclear export mechanism as a molecular event. This finding extends the functional repertoire of NR4A1 in ACFs beyond transcriptional regulation, raising the possibility that cytoplasmic NR4A1 engages distinct protein interactions or signalling cascades in the AF context. Whether cytoplasmic NR4A1 in ACFs exerts additional functions that amplify the inflammatory and fibrotic phenotype remains an open question that warrants dedicated investigation.

7.2.3 Validation and extension of the NR4A1 literature in the cardiac and AF contexts

The pro-fibrotic role of NR4A1 in cardiac fibroblasts has previously been demonstrated in rodent-based experimental models[160,161], and the findings of my thesis consistently replicate and reinforce these observations in an independent cellular system. The present work crucially extends this evidence in two important respects. First, the ACF model employed here is the first in which NR4A1-mediated pro-fibrotic regulation has been validated in human cardiac fibroblasts, conferring substantially greater physiological and translational relevance than rodent systems. Species-specific differences in cardiac fibroblast biology, transcriptional regulation, and inflammatory signalling are well documented[304]. Second, the cells used in this work were isolated from the atria rather than from the ventricles, which has been the predominant source in prior NR4A1 cardiac fibroblast studies[160,161]. The atrium is the primary anatomical site of AF-associated structural remodelling[34]. This atrial origin is a critical contextual distinction, given the substantial differences in fibroblast expression profiles, electrophysiological coupling, and remodelling responses between atrial and ventricular chambers[73,74].

The identification of IL-6 as a promising target within the NR4A1-regulated pathway in human ACFs carries translational significance. IL-6 is one of the most extensively studied circulating biomarkers in AF[305]. Elevated plasma IL-6 levels have been reproducibly associated with incident AF, greater arrhythmia burden, increased risk of recurrence following catheter ablation, and worse long-term cardiovascular outcomes[305]. My findings introduce a new mechanistic dimension to this established clinical association by situating IL-6 within a fibroblast-specific, NR4A1-driven regulatory axis in the atria. This reframes our understanding of IL-6 in AF beyond its established role as a systemic inflammatory mediator or a secreted product of circulating immune cells[306]. While cardiac fibroblasts are known to produce and secrete IL-6[307], the positive regulation of IL-6 by upstream NR4A1 in ACFs has not been previously described. This may contribute to both local structural remodelling and the systemic inflammatory state observed clinically in AF. This

mechanistic linkage between NR4A1, ACF-derived IL-6, and the persistent AF phenotype therefore strengthens NR4A1 as a therapeutically relevant target. It encourages further investigation into whether circulating IL-6 levels in AF patients reflect, at least in part, NR4A1 transcriptional activity within the ACFs, or whether NR4A1-dependent IL-6 production by ACFs may primarily contribute to the autocrine or paracrine signalling environment.

7.3 Limitations and future directions

7.3.1 Cohort heterogeneity and clinical confounders

The patient cohort in this work comprised individuals admitted for elective cardiac surgery, which afforded a unique opportunity to obtain left atrial biopsies for subsequent fibroblast isolation. Although patients were stratified into sinus rhythm and persistent AF groups with the aim of investigating an AF-specific NR4A1 profile, clinical heterogeneity across the cohort is an inherent limitation of human clinical studies and must be carefully considered when interpreting the findings. While the persistent AF group is defined by continuous AF episodes lasting more than 7 days[8], patients have different duration of AF and longer duration allows the accumulation of pro-arrhythmic and fibrotic substrates. This variability should be taken into consideration given the practical limitations of biopsy availability from AF patients for ACF isolation and experiments.

Some patients presented with comorbidities associated with adverse cardiovascular remodelling, including hypertension, ischaemic heart disease, and prior myocardial infarction. These may independently influence fibroblast phenotype, fibrosis, and inflammatory signalling[105]. Furthermore, concomitant medications are known to modulate both fibrotic and inflammatory signalling pathways, including anti-arrhythmic agents, renin-angiotensin-aldosterone system inhibitors, and statins[308]. Therefore, they may confound intergroup comparisons of NR4A1-associated biological effects.

The sinus rhythm patients served as a matched control rather than a healthy control population, and the clinical background of each participant was therefore carefully reviewed. Where feasible, I prioritised patients with relatively uncomplicated medical histories for sinus rhythm versus AF

comparisons to minimise confounding. Whilst covariate adjustment through multivariable statistical modelling can partially address discrepancies in clinical characteristics between groups, this approach necessitates sufficiently large sample sizes and is not readily applicable to small-scale *in vitro* experiments with limited biological replicates. Further studies should therefore aim to validate *in vitro* findings in larger cohorts and implement multivariable adjustment to improve group comparability. Moreover, sex as a biological variable warrants explicit consideration in future work, given emerging evidence that AF-associated fibrotic remodelling and fibroblast biology exhibit sex-dependent differences[309,310]. Female has been associated with greater atrial fibrosis burden (quantified from LGE-MRI images)[310,311] and upregulated expression of TGF-β signalling targets in AF[312], which may influence the generalisability of the NR4A1 findings reported in my work. Previous studies have demonstrated that variations in endogenous levels of testosterone and oestrogens modulate NR4A1 expression in males and females, respectively[313]. Oestrogen signalling supresses cardiac fibroblast proliferation and MMP activation[314]. Therefore, accounting for sex as a covariate in patient selection and data analysis should be considered in future cohort design.

7.3.2 Threshold selection of differential expression analysis

A limitation of this study is the use of a less stringent threshold of $|\log2FC| > 0.25$ for defining DEGs in the DESeq2 bulk RNA-seq analysis, rather than the more commonly adopted cutoff of $|\log2FC| > 1$. I selected the lower threshold to improve sensitivity for detecting more subtle transcriptional changes that may still contribute to NR4A1-mediated signalling pathways. This approach increases the likelihood of including genes with modest effect sizes whose biological significance may be limited, thereby increasing the risk of false-positive prioritisation. Therefore, the DEGs identified in this study were interpreted cautiously and validated using gene-level (qPCR) and protein-level (western blot and ELISA) analyses.

7.3.3 Pharmacological modulation of NR4A1 and compound screening

In the present human ACF *in vitro* model, siRNA-mediated knockdown was employed as the primary approach to assess NR4A1 loss of function. Whilst effective, siRNA knockdown has limitations including transient duration of action[315], and pharmacological approaches should be pursued in parallel to strengthen the translational relevance of these findings. Bis-indole derived compounds, including C-DIM8 and C-DIM14, have been developed as selective NR4A1 antagonists and represent well-characterised pharmacological reagents to inhibit NR4A1 activity[316]. Notably, C-DIM8 treatment in breast cancer cells was reported to closely recapitulate the phenotypic effects observed following siRNA-mediated NR4A1 knockdown[317–319], supporting the pharmacological validity of this approach as a complementary strategy in cardiac fibroblasts.

In addition to direct NR4A1 antagonism, the CMap analysis conducted in my thesis identified glucocorticoids as compounds whose transcriptomic signatures resemble those of NR4A1 knockdown in human ACFs. Treating human ACFs with compounds like fluorometholone, fluocinonide and hydrocortisone, and evaluating downstream fibrotic and inflammatory responses would provide an independent line of evidence for the translational potential of NR4A1 modulation, whilst simultaneously informing whether glucocorticoid-mediated effects in the atrial cells are partly NR4A1-dependent. Beyond these candidates, high-throughput pharmacological screening approaches, including phenotypic cell-based assays or target-based screening using NR4A1 luciferase reporter systems, could be employed to identify novel NR4A1 modulators with improved selectivity and pharmacokinetic properties suitable for cardiac applications[320]. This screening strategy would substantially expand the pipeline of candidate therapeutics for NR4A1-targeted intervention in AF.

7.3.4 Validating direct binding of NR4A1 to the IL6 promoter

RNA-seq analysis identified downregulation of *IL6* expression in human ACFs following NR4A1 knockdown, implicating *IL6* as a putative downstream transcriptional target of NR4A1. However, whilst NR4A1 functions primarily as a transcription factor, transcriptomic association alone is insufficient to establish NR4A1 direct regulatory control over *IL6*. The JASPAR *in silico* analysis performed in my thesis predicted NR4A1 binding sites within the promoter region of the human *IL6* gene, providing a mechanistic hypothesis that requires experimental validation. Chromatin immunoprecipitation followed by qPCR would confirm NR4A1 occupancy at the predicted binding site in human ACFs, whilst ChIP-seq would further provide a genome-wide, unbiased assessment of NR4A1 chromatin binding and compare the occupancy across different bindings sites within the *IL6* gene.

Directed physical interaction between the NR4A1 protein and the *IL6* promoter DNA sequence can be confirmed using electrophoretic mobility shift assay, which would demonstrate specific protein-DNA binding *in vitro*. Functional significance of this interaction could subsequently be established through a luciferase reporter assay, utilising both wild-type and site-directed mutant versions of the predicted NR4A1 binding motif. Loss of NR4A1-induced luciferase activity upon mutation of the binding site would provide definitive evidence of binding-dependent transcriptional regulation. Collectively, these experimental approaches would establish *IL6* as a direct transcriptional target of NR4A1 in human ACFs and would substantially strengthen the mechanistic framework presented in my thesis. It would also be informative to assess whether NR4A1 regulates *IL6* transcription through direct DNA binding, indirect co-factor interactions, or chromatin remodelling as these mechanisms carry distinct implications for therapeutic targeting.

7.3.5 Validating direct activation of NR4A1 by PGA2 in human ACFs

The findings of my thesis demonstrate that NR4A1 knockdown significantly attenuates PGA2-induced pro-inflammatory responses in human ACFs, providing indirect evidence for a PGA2-NR4A1 activation axis in ACFs. However, direct biochemical evidence that PGA2 physically binds and activates NR4A1 in this cellular model is currently lacking. Although PGA2 has been reported as an endogenous ligand of NR4A1 in other biological contexts[209], analogous validation experiments can be conducted specifically in human ACFs to establish the relevance of this interaction in the atrial fibrotic response. Relevant experimental approaches include NurRE-binding assays and NR4A1 transactivation assays using luciferase reporters, which would demonstrate the functional receptor activation by PGA2 in ACFs. Structural biochemical techniques could further characterise the binding affinity and kinetics of PGA2-NR4A1 interaction with quantitative precision. Complementary molecular docking and molecular dynamics simulations would provide *in silico* support for the proposed binding model within the NR4A1 ligand-binding domain. Competitive binding assays using known NR4A1 ligands would further validate PGA2 as a direct activator rather than an indirect modulator in ACFs. Establishing this direct ligand-receptor engagement between PGA2 and NR4A1 in human ACFs would substantially reinforce the upstream regulatory axis identified in this work and provide a more complete mechanistic model of NR4A1 activation in AF-associated atrial fibrotic responses.

7.3.6 Characterising the NR4A1-NUP214 interaction and consequences of NR4A1 nuclear export in AF

The cytoplasmic translocation of NR4A1 observed in AF ACFs represents a novel cellular mechanism that extends the functional repertoire of NR4A1 beyond its canonical role as a nuclear transcription factor. Nucleocytoplasmic shuttling of transcription factors is recognised as a critical post-translational regulatory layer that governs protein activity, co-factor interactions and

downstream signalling outputs[321]. Despite the clear importance of nuclear transport in disease biology, this process remains poorly characterised in AF relative to other disease contexts, including cancer, neurodegeneration and autoimmunity, in which aberrant transcription factor localisation has been more extensively studied[321]. Enhanced nuclear translocation and activation of the transcription factor STAT3 has been demonstrated in left atrial tissue of an AF-induced adult porcine model[322], suggesting that dysregulated nuclear transport may be a broader pathological feature of atrial remodelling in AF.

My interactome proteomics analysis conducted in this work identified the nuclear pore complex protein NUP214 as a candidate interactor potentially mediating NR4A1 nuclear export in AF ACFs. This interaction warrants experimental validation such as co-IP and proximity ligation assay, which could confirm physical association between NR4A1 and NUP214 in human ACFs under persistent AF. Structural prediction using AlphaFold 3 could delineate the binding interface between the two proteins[323], informing the rational design of inhibitory peptides or small-molecular disruptors targeting this specific protein-protein interaction. Functional rescue experiments, using pharmacological or peptide-mediated blockade of the NR4A1-NUP214 interaction could assess the reversal of NR4A1 cytoplasmic translocation and attenuation of the fibrotic and inflammatory phenotypes in AF ACFs. This would provide compelling therapeutic proof-of-concept for targeting NR4A1 nuclear export as a novel mechanism in AF. In parallel, live-cell imaging using fluorescently tagged NR4A1 and photoactivatable probes would allow real-time visualisation of NR4A1 subcellular dynamics and localisation. Such experiments would inform the kinetics and reversibility of NR4A1 nuclear export and establish whether translocation is a transient adaptive response or a stable pathological state in AF ACFs.

7.3.7 Limitations of the in vitro model and translation to in vivo models

My current findings are established exclusively from an *in vitro* human ACF model, which possesses inherent limitations that constrain the interpretation and generalisability of the results. Firstly, the current sources of human ACF *in vitro* represent a bulk model including all types of fibroblasts. The lack of segregation in different ACF subpopulations suggests that my current findings are not restricted to the NR4A1-enriched ACF subpopulation as identified in our recent work[132]. In my ACF *in vitro* model, the NR4A1 siRNA knockdown experiments will affect the NR4A1+ subpopulation more than the other two subpopulations (quiescent and activated phenotypes), where NR4A1 is minimally expressed. Therefore, future work requires different approaches to investigate the specific NR4A1+ subpopulation for siRNA studies, for example enrichment of NR4A1+ ACF subpopulation using fluorescence-activated cell sorting for siRNA experiments, and expression profiling of the specific NR4A1+ ACF subpopulation in sinus rhythm and AF samples using spatial transcriptomics or proteomics.

Standard two-dimensional cell culture on rigid plastic surfaces has been shown to induce constitutive activation of cardiac fibroblasts to a myofibroblast-like state, independent of disease-specific stimulation[258]. This baseline activation state may confound comparisons between sinus rhythm and AF ACFs, reduce the dynamic range of experimental responses, and limit how the *in vitro* model reflects the ACF phenotype in human heart. To more accurately recapitulate the physiological complexity of the atrial microenvironment, future studies could adopt more physiologically relevant culture systems.

AF-associated fibrotic and inflammatory remodelling involves dynamic crosstalk among multiple cell types, including cardiac fibroblasts, cardiomyocytes, macrophages and other immune cells, and endothelial cells[324]. Co-culture models incorporating these cell types would better reflect the

multicellular remodelling dynamics relevant to NR4A1 regulation in the heart. Cardiac organoids represent a promising alternative platform, where emerging protocols have successfully integrated multiple cardiac cell types into three-dimensional structures that recapitulate human cardiac expression profiles and functional properties[325,326]. Applying NR4A1 loss or gain of function approaches within these organoid systems would further support the understanding of how NR4A1 regulates fibrotic remodelling in a three-dimensional, multicellular context.

Translation to *in vivo* models is a critical and necessary next step to validate the biological significance of my NR4A1 findings presented in this thesis. Cardiac fibroblast-specific or left atrial-specific conditional knockout of NR4A1 would allow interrogation of NR4A1 function in a cardiac fibroblast-specific context *in vivo*. This can be achieved through Cre-loxP systems driven by fibroblast-selective promoters such as Periostin-Cre or Tcf21-Cre[327], or delivery of NR4A1-targeting short hairpin RNA via adeno-associated viral vectors within the left atrial atrium. The specificity of NR4A1 modulation for ACFs and the potential to leverage atrial-targeted drug delivery strategies may mitigate systemic off-target effects, an important consideration given that NR4A1 performs regulatory roles in diverse tissues including the brain, lung, kidney, intestinal tract, and immune system[249]. These approaches should be implemented in established murine models of AF, such as rapid atrial pacing or atrial-specific liver kinase B1 knockdown models[328], as well as in larger animal persistent AF models[329], to assess the impact of NR4A1 regulation on AF inducibility, duration and atrial remodelling.

Cardiac tissues harvested from these *in vivo* models can be evaluated for atrial fibrosis by Masson's Trichrome and Picrosirius Red staining, immune cell infiltration by immunohistochemistry, and the expression of key fibrosis and inflammation markers by qPCR and western blot. Beyond the atria, assessment of ventricular fibrosis and cardiomyocyte

hypertrophy would provide insights into the cardiac complications of NR4A1 modulation in AF. In parallel, blood collected from these models can be assessed for circulating levels of NR4A1-associated signalling components characterised in this thesis, including PGA2 and IL-6. This provides a systemic readout of NR4A1-mediated effects on cardiac remodelling in AF. If NR4A1 antagonism or inhibition demonstrates favourable anti-fibrotic and anti-inflammatory efficacy in these *in vivo* models, further pre-clinical studies, ensuring toxicological profiling, pharmacokinetic and pharmacodynamic characterisation, and assessment of long-term safety, would be essential prerequisites before progressing NR4A1-targeting molecules towards early-phase clinical trials.

7.4 Clinical translation of NR4A1 findings in persistent AF

The findings of this thesis collectively position NR4A1 as a molecular candidate for clinical translation in persistent AF, with potential utility both as a disease-modifying therapeutic target and as a marker of atrial remodelling severity.

7.4.1 NR4A1 as a therapeutic target in persistent AF

Current pharmacological and interventional strategies for rhythm control in AF include anti-arrhythmic drugs and catheter ablation[330]. They primarily target the electrophysiological drivers of arrhythmia but do not specifically address the underlying structural substrate, particularly atrial fibrosis, that perpetuates AF and drives recurrence[331].The pro-fibrotic and pro-inflammatory NR4A1-mediated signalling pathways characterised in this work suggest that NR4A1 antagonism could represent a complementary, disease-modifying approach that specifically targets the structural remodelling substrate rather than solely addressing the adverse electrophysiological phenotype. In the context of persistent AF, NR4A1-targeted therapy could be envisioned as an adjunct to catheter ablation, with the goal of reducing atrial fibrotic burden prior to or following the procedure, thereby improving ablation outcomes and reducing arrhythmia recurrence. Alternatively, anti-fibrotic NR4A1 antagonism could be integrated into the rhythm management strategy in patients with persistent AF at early stages, aiming to halt or slow the progression of structural remodelling before the arrhythmia becomes self-sustaining.

7.4.2 NR4A1 and its signalling components as biomarkers

Beyond therapeutic targeting, NR4A1 and the downstream effectors characterised in this work hold promise as circulating or tissue-based biomarkers of AF-associated atrial remodelling. The NR4A1-IL-6 regulatory pathway provides mechanistic underpinning for the association with AF

and raises the possibility that NR4A1 contributes to the systemic inflammatory state observed in AF patients. Creating combined or multivariate NR4A1-linked signatures (IL-6, PGA2 or other NR4A1-regulated transcriptomic signatures) in peripheral blood could allow stratification of AF patients according to their underlying fibrotic and inflammatory burden, thereby informing treatment selection. This may (in combination with other existing clinical biomarkers of AF or structural remodelling) facilitate the identification of individuals who are most likely to benefit from ablation, anti-fibrotic pharmacotherapy, or both.

By assessing biopsies obtained at the time of cardiac surgery, NR4A1 protein expression and subcellular localisation in ACFs could serve as intraoperative biomarkers of remodelling severity with prognostic value for post-operative AF recurrence and atrial functional recovery. When NR4A1 expression is measured in cardiac samples from clinical cohorts with larger sample size, association and correlation with clinical characteristics will offer additional insights into the atrial remodelling in AF. Future studies employing digital pathology approaches, such as whole-slide image analysis and artificial intelligence-assisted quantification of NR4A1 expression and localisation in atrial tissue sections[332], could facilitate the clinical-scale implementation of NR4A1 as a tissue biomarker.

7.4.3 Expanding to right atrium and ventricular remodelling

The present work focused on fibroblasts isolated from the left atrium, reflecting the established role of the left atrium as the predominant anatomical site of AF initiation and maintenance. However, the pathophysiology of AF extends to the right atrium and the ventricles[333,334], and these chambers represent important sites of disease-relevant remodelling. Right and left atrial fibrosis are strongly correlated in AF patients[335]. Whether NR4A1 expression, subcellular localisation, and transcriptional activity are similarly dysregulated in fibroblasts from right atria remains

unknown. Comparative analysis of NR4A1 regulation profiles between left and right ACFs from AF patients would establish whether the NR4A1-mediated mechanism is chamber-specific or represents a generalised fibroblast response to AF-associated stimuli in the atrium.

AF-associated ventricular remodelling represents a further clinically significant dimension of AF-related cardiac injury[336]. It incorporates ventricular remodelling, hypertrophy, and dysfunction resulting from prolonged rapid irregular ventricular rate[337,338]. Given the established pro-fibrotic role of NR4A1 signalling and the phenotypic differences between atrial and ventricular fibroblast biology[74], the role of NR4A1 in ventricular fibroblasts isolated from AF patients warrants further investigation. This would determine whether the pro-fibrotic mechanisms identified in ACFs translate to the ventricular compartment and may ultimately provide mechanistic insights into AF-induced cardiomyopathy.

A major methodological challenge in expanding the current findings beyond the isolated atrial cellular model lies in the need to preserve spatial context to understand how NR4A1 expression and regulatory activity vary across chambers of the heart, between fibrotic and non-fibrotic regions, and in relation to surrounding cell types. Application of spatial transcriptomics or proteomics approaches would provide a multi-modal molecular portrait of the NR4A1 regulatory network within the structural and cellular context of the human heart in AF. Cell-cell interaction analysis from spatially resolved data would allow systematic investigation of how NR4A1 activity in subpopulations of cardiac fibroblasts is influenced by the signalling landscape from adjacent cardiomyocytes, macrophages and endothelial cells within the remodelling heart. It also enables an understanding of how NR4A1 coordinates fibrotic remodelling across atrial and ventricular compartments in AF. This spatial omics approach would represent a powerful and transformative extension of the current work, providing both mechanistic depth and the spatial resolution

necessary to translate findings from isolated cell models to the structural complexity of the human heart.

7.5 Conclusions of the project

The work presented in this thesis identifies NR4A1 as a novel pro-fibrotic and pro-inflammatory regulator in human ACFs and characterises a signalling mechanism centred on NR4A1 that is specifically dysregulated in persistent AF. siRNA-mediated NR4A1 knockdown attenuated both fibrotic and inflammatory phenotypes in human ACFs, including suppression of PGA2-stimulated pro-inflammatory responses. NR4A1 protein abundance was significantly enriched in ACFs from patients with persistent AF relative to sinus rhythm controls, accompanied by elevated secretion of PGA2 and IL-6. This implicates NR4A1 as a central coordinator of the activated fibroblast phenotype in AF. Transcriptomic profiling and interactome proteomics further revealed novel NR4A1-regulated targets and protein interactions that extend the known cardiovascular biology of this nuclear receptor. A particularly novel observation was the aberrant cytoplasmic accumulation of NR4A1 in AF ACFs, implicating dysregulated nucleocytoplasmic transport as an additional mechanism underpinning NR4A1 dysfunction in AF. It is potentially mediated through increased interaction with the nuclear pore protein NUP214. Collectively, these findings position NR4A1 and its associated signalling components as potential candidates for therapeutic targeting and disease stratification in persistent AF. Pharmacological NR4A1 antagonism could offer a fibroblast-targeted approach to suppress the structural remodelling that underlies AF perpetuation. NR4A1, in combination with IL-6 and PGA2, may be utilised as a biomarker framework for stratifying patients by fibrotic burden. *In vivo* validation in persistent AF models will be essential to confirm the physiological relevance of these findings. Overall, this work makes a substantial and original contribution to the understanding of ACF biology in AF, identifying NR4A1 as a previously unrecognised molecular node linking inflammatory and fibrotic remodelling in human ACFs. By establishing a mechanistic framework, the findings of this study may ultimately inform the development of atrial-targeted therapies for persistent AF.

References

1. Chugh, S. S. *et al.* Worldwide epidemiology of atrial fibrillation: A global burden of disease 2010 study. *Circulation* **129**, 837–847 (2014).

2. Linz, D. *et al.* Atrial fibrillation: epidemiology, screening and digital health. *The Lancet Regional Health - Europe* **37**, 100786 (2024).

3. Staerk, L., Sherer, J. A., Ko, D., Benjamin, E. J. & Helm, R. H. Atrial Fibrillation: Epidemiology, Pathophysiology, Clinical Outcomes. *Circ. Res.* **120**, 1501–1517 (2017).

4. Rago, A. *et al.* Gender Differences in Atrial Fibrillation: From the Thromboembolic Risk to the Anticoagulant Treatment Response. *Medicina 2023, Vol. 59, Page 254* **59**, 254 (2023).

5. Kornej, J., Börschel, C. S., Benjamin, E. J. & Schnabel, R. B. Epidemiology of Atrial Fibrillation in the 21st Century: Novel Methods and New Insights. *Circ. Res.* **127**, 4–20 (2020).

6. Antoun, I. *et al.* Hypertension and Atrial Fibrillation: Bridging the Gap Between Mechanisms, Risk, and Therapy. *Medicina 2025, Vol. 61, Page 362* **61**, 362 (2025).

7. Shantsila, E., Choi, E. K., Lane, D. A., Joung, B. & Lip, G. Y. H. Atrial fibrillation: comorbidities, lifestyle, and patient factors. *The Lancet Regional Health - Europe* **37**, 100784 (2024).

8. Joglar, J. A. *et al.* 2023 ACC/AHA/ACCP/HRS Guideline for the Diagnosis and Management of Atrial Fibrillation: A Report of the American College of Cardiology/American Heart Association Joint Committee on Clinical Practice Guidelines. *Circulation* **149**, E1–E156 (2024).

9. Liu, Y. *et al.* Atrial fibrillation: from pathogenesis to novel treatment options. *Molecular Biomedicine 2025 6:1* **6**, 144- (2025).

10. Vitolo, M., Proietti, M., Shantsila, A., Boriani, G. & Lip, G. Y. H. Clinical Phenotype Classification of Atrial Fibrillation Patients Using Cluster Analysis and Associations with Trial-Adjudicated Outcomes. *Biomedicines 2021, Vol. 9, Page 843* **9**, 843 (2021).

11. Chen, L. Y. *et al.* Atrial Fibrillation Burden: Moving Beyond Atrial Fibrillation as a Binary Entity: A Scientific Statement From the American Heart Association. *Circulation* **137**, e623–e644 (2018).

12. Becher, N., Metzner, A., Toennis, T., Kirchhof, P. & Schnabel, R. B. Atrial fibrillation burden: a new outcome predictor and therapeutic target. *Eur. Heart J.* **45**, 2824–2838 (2024).

13. Escolar Conesa, A. *et al.* Evaluation of the Presence of Native Valvular Disease in Patients With Atrial Fibrillation Using the EHRA (Evaluated Heartvalves, Rheumatic, or Artificial) Classification. *Clin. Cardiol.* **48**, e70172 (2025).

14. Volgman, A. S. *et al.* Management of Atrial Fibrillation in Patients 75 Years and Older: JACC State-of-the-Art Review. *J. Am. Coll. Cardiol.* **79**, 166–179 (2022).

15. Mistrulli, R. *et al.* Atrial Fibrillation in Patients with Hypertrophic Cardiomyopathy and Cardiac Amyloidosis: From Clinical Management to Catheter Ablation Indication. *Journal of Clinical Medicine 2024, Vol. 13, Page 501* **13**, 501 (2024).

16. Lip, G. Y. H. The ABC pathway: an integrated approach to improve AF management. *Nature Reviews Cardiology 2017 14:11* **14**, 627–628 (2017).

17. Machado, A. M., Leite, F. & Pereira, M. G. Integrated Care in Atrial Fibrillation: A Multidisciplinary Approach to Improve Clinical Outcomes and Quality of Life. *Healthcare 2025, Vol. 13, Page 325* **13**, 325 (2025).

18. Pham, H. N. *et al.* Advances in Atrial Fibrillation Management: A Guide for General Internists. *Journal of Clinical Medicine 2024, Vol. 13, Page 7846* **13**, 7846 (2024).

19. Nesapiragasan, V. *et al.* Catheter Ablation Approaches for the Treatment of Arrhythmia Recurrence in Patients with a Durable Pulmonary Vein Isolation. *Balkan Med. J.* **40**, 386–394 (2023).

20. Hindricks, G. *et al.* 2020 ESC Guidelines for the diagnosis and management of atrial fibrillation developed in collaboration with the European Association for Cardio-Thoracic Surgery (EACTS): The Task Force for the diagnosis and management of atrial fibrillation of the Europe…. *Eur. Heart J.* **42**, 373–498 (2021).

21. Carlisle, M. A., Fudim, M., DeVore, A. D. & Piccini, J. P. Heart Failure and Atrial Fibrillation, Like Fire and Fury. *JACC Heart Fail.* **7**, 447–456 (2019).

22. Brandes, A. *et al.* Cardioversion of atrial fibrillation and atrial flutter revisited: current evidence and practical guidance for a common procedure. *EP Europace* **22**, 1149–1161 (2020).

23. Alobaida, M. & Alrumayh, A. Rate control strategies for atrial fibrillation. *Ann. Med.* **53**, 682–692 (2021).

24. Gehr, T. W. B. & Sica, D. A. Antiarrhythmic Medications. *Semin. Dial.* **3**, 33–38 (2024).

25. Investigators, T. A. F. F. I. of R. M. (AFFIRM). A Comparison of Rate Control and Rhythm Control in Patients with Atrial Fibrillation. *New England Journal of Medicine* **347**, 1825–1833 (2002).

26. Kirchhof, P. *et al.* Early Rhythm-Control Therapy in Patients with Atrial Fibrillation. *New England Journal of Medicine* **383**, 1305–1316 (2020).

27. Srivastava, M. *et al.* Direct oral anticoagulants for stroke prevention in patients with atrial fibrillation: A network meta-analysis of randomized trials. *Indian Heart J.* https://doi.org/10.1016/J.IHJ.2025.12.002 (2025) doi:10.1016/J.IHJ.2025.12.002.

28. Cosín-Sales, J. *et al.* Safety and Effectiveness of Oral Anticoagulants in Atrial Fibrillation: Real-World Insights Using Natural Language Processing and Machine Learning. *J. Clin. Med.* **13**, 6226 (2024).

29. Akin, I. & Nienaber, C. A. Left atrial appendage occlusion: A better alternative to anticoagulation? *World J. Cardiol.* **9**, 139–146 (2017).

30. Chung, M. K. *et al.* Lifestyle and Risk Factor Modification for Reduction of Atrial Fibrillation: A Scientific Statement From the American Heart Association. *Circulation* **141**, E750–E772 (2020).

31. Grigoriou, K. *et al.* Lifestyle modification in atrial fibrillation: Mechanisms, phenotypes and ablation outcomes. *Exp. Physiol.* https://doi.org/10.1113/EP093386;REQUESTEDJOURNAL:JOURNAL:1469445X;WGROUP:STRING:PUBLICATION (2026) doi:10.1113/EP093386;REQUESTEDJOURNAL:JOURNAL:1469445X;WGROUP:STRING:PUBLICATION.

32. Wijffels, M. C. E. F., Kirchhof, C. J. H. J., Dorland, R. & Allessie, M. A. Atrial fibrillation begets atrial fibrillation: A study in awake chronically instrumented goats. *Circulation* **92**, 1954–1968 (1995).

33. Lu, Z. *et al.* Atrial fibrillation begets atrial fibrillation: autonomic mechanism for atrial electrical remodeling induced by short-term rapid atrial pacing. *Circ. Arrhythm. Electrophysiol.* **1**, 184–192 (2008).

34. Nattel, S., Burstein, B. & Dobrev, D. Atrial remodeling and atrial fibrillation: mechanisms and implications. *Circ. Arrhythm. Electrophysiol.* **1**, 62–73 (2008).

35. Lee, H. C. Electrical remodeling in human atrial fibrillation. *Chin. Med. J. (Engl).* **126**, 2380–2383 (2013).

36. Mariani, M. V. *et al.* Incidence and Determinants of Spontaneous Cardioversion of Early Onset Symptomatic Atrial Fibrillation. *Medicina 2022, Vol. 58, Page 1513* **58**, 1513 (2022).

37. Heijman, J., Voigt, N., Wehrens, X. H. T. & Dobrev, D. Calcium dysregulation in atrial fibrillation: The role of CaMKII. *Front. Pharmacol.* **5 MAR**, 82089 (2014).

38. Chaldoupi, S. M., Loh, P., Hauer, R. N. W., De Bakker, J. M. T. & Van Rijen, H. V. M. The role of connexin40 in atrial fibrillation. *Cardiovasc. Res.* **84**, 15–23 (2009).

39. Jalife, J. & Kaur, K. Atrial remodeling, fibrosis, and atrial fibrillation. *Trends Cardiovasc. Med.* **25**, 475–484 (2015).

40. Krogh-Madsen, T., Abbott, G. W. & Christini, D. J. Effects of Electrical and Structural Remodeling on Atrial Fibrillation Maintenance: A Simulation Study. *PLoS Comput. Biol.* **8**, e1002390 (2012).

41. Al Ghamdi, B. & Hassan, W. Atrial Remodeling And Atrial Fibrillation: Mechanistic Interactions And Clinical Implications. *J. Atr. Fibrillation* **2**, 395–416 (2009).

42. Karakasis, P. *et al.* Atrial Fibrosis in Atrial Fibrillation: Mechanistic Insights, Diagnostic Challenges, and Emerging Therapeutic Targets. *International Journal of Molecular Sciences 2025, Vol. 26, Page 209* **26**, 209 (2024).

43. Maesen, B. *et al.* Endomysial fibrosis, rather than overall connective tissue content, is the main determinant of conduction disturbances in human atrial fibrillation. *EP Europace* **24**, 1015–1024 (2022).

44. LI, C. Y., ZHANG, J. R., HU, W. N. & LI, S. N. Atrial fibrosis underlying atrial fibrillation (Review). *Int. J. Mol. Med.* **47**, 1–1 (2021).

45. Dzeshka, M. S., Lip, G. Y. H., Snezhitskiy, V. & Shantsila, E. Cardiac Fibrosis in Patients With Atrial Fibrillation: Mechanisms and Clinical Implications. *J. Am. Coll. Cardiol.* **66**, 943–959 (2015).

46. Kwan, E. *et al.* Functional and Structural Remodeling as Atrial Fibrillation Progresses in a Persistent Atrial Fibrillation Canine Model. *JACC Clin. Electrophysiol.* **11**, 720–734 (2025).

47. Akoum, N. *et al.* Atrial Fibrosis Quantified Using Late Gadolinium Enhancement MRI is Associated With Sinus Node Dysfunction Requiring Pacemaker Implant. *J. Cardiovasc. Electrophysiol.* **23**, 44–50 (2012).

48. Sonaglioni, A., Nicolosi, G. L., Sonaglioni, A. & Nicolosi, G. L. Left Atrial Reservoir Strain in Cardiovascular and Systemic Disease: Advances and Clinical Applications From Physiology to Practice. *Reviews in Cardiovascular Medicine 2025 26 (12)* **26**, 46198 (2025).

49. Lee, K. N. *et al.* Therapeutic implications of galectin-3 in patients with atrial fibrillation. *Scientific Reports 2022 12:1* **12**, 784- (2022).

50. Takemoto, Y. *et al.* Galectin-3 Regulates Atrial Fibrillation Remodeling and Predicts Catheter Ablation Outcomes. *JACC Basic Transl. Sci.* **1**, 143–154 (2016).

51. Begg, G. A. *et al.* Intra-cardiac and peripheral levels of biochemical markers of fibrosis in patients undergoing catheter ablation for atrial fibrillation. *EP Europace* **19**, 1944–1950 (2017).

52. Rossi, V. A. *et al.* Predictors of left atrial fibrosis in patients with atrial fibrillation referred for catheter ablation. *Cardiol. J.* **29**, 413–422 (2022).

53. Ruan, Z. B., Peng, Q., Sun, X. J., Wang, F. & Zhu, L. Serum miR-15a-5p may predict recurrence of atrial fibrillation after catheter ablation: a single center retrospective study. *PeerJ* **13**, 1–15 (2025).

54. Abed, H. S. *et al.* Obesity results in progressive atrial structural and electrical remodeling: Implications for atrial fibrillation. *Heart Rhythm* **10**, 90–100 (2013).

55. Schoonderwoerd, B. A., Smit, M. D., Pen, L. & Van Gelder, I. C. New risk factors for atrial fibrillation: causes of 'not-so-lone atrial fibrillation'. *EP Europace* **10**, 668–673 (2008).

56. Li, S. *et al.* Left ventricular fibrosis by extracellular volume fraction and the risk of atrial fibrillation recurrence after catheter ablation. *Cardiovasc. Diagn. Ther.* **9**, 57885–57585 (2019).

57. Chen, L. *et al.* Association Between Extracellular Volume Assessed by Cardiac MRI and New-Onset Atrial Fibrillation in Patients With ST-Segment Elevation Myocardial Infarction. *Korean J. Radiol.* **26**, 546–556 (2025).

58. Sasaki, N. *et al.* Transthoracic echocardiographic backscatter-based assessment of left atrial remodeling involving left atrial and ventricular fibrosis in patients with atrial fibrillation. *Int. J. Cardiol.* **176**, 1064–1066 (2014).

59. Ling, L. H. *et al.* Diffuse ventricular fibrosis in atrial fibrillation: Noninvasive evaluation and relationships with aging and systolic dysfunction. *J. Am. Coll. Cardiol.* **60**, 2402–2408 (2012).

60. Cha, Y. M., Redfield, M. M., Shen, W. K. & Gersh, B. J. Atrial fibrillation and ventricular dysfunction: A vicious electromechanical cycle. *Circulation* **109**, 2839–2843 (2004).

61. Schach, C. *et al.* Time to Recovery from Systolic Dysfunction Correlates with Left Ventricular Fibrosis in Arrhythmia-Induced Cardiomyopathy. *Life 2024, Vol. 14, Page 330* **14**, 330 (2024).

62. Fashanu, O. E. *et al.* Galectin-3 and incidence of atrial fibrillation: The Atherosclerosis Risk in Communities (ARIC) study. *Am. Heart J.* **192**, 19–25 (2017).

63. Ho, J. E. *et al.* Galectin 3 and incident atrial fibrillation in the community. *Am. Heart J.* **167**, 729-734.e1 (2014).

64. Rosenberg, M. A. *et al.* Circulating fibrosis biomarkers and risk of atrial fibrillation: The Cardiovascular Health Study (CHS). *Am. Heart J.* **167**, 723-728.e2 (2014).

65. Kubota, T. *et al.* Left atrial pathological degeneration assessed by integrated backscatter transesophageal echocardiography as a predictor of progression to persistent atrial fibrillation: Results from a prospective study of three-years follow-up. *Cardiovascular Ultrasound 2012 10:1* **10**, 28- (2012).

66. Neilan, T. G. *et al.* Myocardial Extracellular Volume Expansion and the Risk of Recurrent Atrial Fibrillation After Pulmonary Vein Isolation. *JACC Cardiovasc. Imaging* **7**, 1–11 (2014).

67. McLellan, A. J. A. *et al.* Diffuse ventricular fibrosis measured by T1 mapping on cardiac MRI predicts success of catheter ablation for atrial fibrillation. *Circ. Arrhythm. Electrophysiol.* **7**, 834–840 (2014).

68. Khan, R. & Sheppard, R. Fibrosis in heart disease: understanding the role of transforming growth factor-beta in cardiomyopathy, valvular disease and arrhythmia. *Immunology* **118**, 10–24 (2006).

69. Biernacka, A., Dobaczewski, M. & Frangogiannis, N. G. TGF-β signaling in fibrosis. *Growth Factors* **29**, 196–202 (2011).

70. Murphy-Ullrich, J. E. & Suto, M. J. Thrombospondin-1 regulation of latent TGF-β activation: A therapeutic target for fibrotic disease. *Matrix Biology* **68–69**, 28–43 (2018).

71. Humeres, C. *et al.* Fibroblast Smad7 Induction Protects the Remodeling Pressure-Overloaded Heart. *Circ. Res.* **135**, 453–469 (2024).

72. Saadat, S. *et al.* Pivotal Role of TGF-β/Smad Signaling in Cardiac Fibrosis: Non-coding RNAs as Effectual Players. *Front. Cardiovasc. Med.* **7**, 588347 (2021).

73. Rizvi, F. *et al.* Chamber-specific differences in human cardiac fibroblast proliferation and responsiveness toward simvastatin. *https://doi.org/10.1152/ajpcell.00056.2016* **311**, C330–C339 (2016).

74. Burstein, B., Libby, E., Calderone, A. & Nattel, S. Differential behaviors of atrial versus ventricular fibroblasts: A potential role for platelet-derived growth factor in atrial-ventricular remodeling differences. *Circulation* **117**, 1630–1641 (2008).

75. Kakkar, R. & Lee, R. T. Intramyocardial fibroblast myocyte communication. *Circ. Res.* **106**, 47–57 (2010).

76. Liu, Y. *et al.* Association of MMPs and TIMPs With the Occurrence of Atrial Fibrillation: A Systematic Review and Meta-analysis. *Canadian Journal of Cardiology* **32**, 803–813 (2016).

77. Lindsey, M. L. *et al.* A Novel Collagen Matricryptin Reduces Left Ventricular Dilation Post-Myocardial Infarction by Promoting Scar Formation and Angiogenesis. *J. Am. Coll. Cardiol.* **66**, 1364–1374 (2015).

78. Moreira, L. M. *et al.* Paracrine signalling by cardiac calcitonin controls atrial fibrogenesis and arrhythmia. *Nature 2020 587:7834* **587**, 460–465 (2020).

79. Reilly, S. N. *et al.* Up-regulation of MIR-31 in human atrial fibrillation begets the arrhythmia by depleting dystrophin and neuronal nitric oxide synthase. *Sci. Transl. Med.* **8**, (2016).

80. Zhang, D., Li, Z., Li, N. & Zhang, H. CACNB2 overexpression suppresses atrial fibroblast activation and atrial fibrosis to mitigate atrial fibrillation. *Cell. Signal.* **143**, 112448 (2026).

81. Zheng, E. *et al.* Exploring Anti-Inflammatory Treatment as Upstream Therapy in the Management of Atrial Fibrillation. *Journal of Clinical Medicine 2025, Vol. 14, Page 882* **14**, 882 (2025).

82. Ihara, K. & Sasano, T. Role of Inflammation in the Pathogenesis of Atrial Fibrillation. *Front. Physiol.* **13**, 862164 (2022).

83. Zhou, X. & Dudley, S. C. Evidence for Inflammation as a Driver of Atrial Fibrillation. *Front. Cardiovasc. Med.* **7**, 522644 (2020).

84. Poppenborg, T. *et al.* A short history of the atrial NLRP3 inflammasome and its distinct role in atrial fibrillation. *J. Mol. Cell. Cardiol.* **202**, 13–23 (2025).

85. Karakasis, P. *et al.* Inflammasome Signaling in Cardiac Arrhythmias: Linking Inflammation, Fibrosis, and Electrical Remodeling. *International Journal of Molecular Sciences 2025, Vol. 26, Page 5954* **26**, 5954 (2025).

86. Cong, X. *et al.* Interleukin-11 Is Elevated in Patients with Atrial Fibrillation, Correlates with Serum Fibrosis Markers, and Represents a Therapeutic Target for Atrial Fibrosis. *Cerebrovascular Diseases* **52**, 575–586 (2023).

87. Bai, W., Liu, Z. Q., He, P. Y. & Muhuyati. The role of IL-6, IL-10, TNF-α and PD-1 expression on CD4 T cells in atrial fibrillation. *Heliyon* **9**, e18818 (2023).

88. Merce, A.-G. *et al.* From Metabolic Syndrome to Atrial Fibrillation: Linking Inflammatory and Fibrotic Biomarkers with Atrial Remodeling and Imaging-Based Evaluation—A Narrative Review. *Metabolites 2026, Vol. 16, Page 59* **16**, 59 (2026).

89. Ajoolabady, A., Nattel, S., Lip, G. Y. H. & Ren, J. Inflammasome Signaling in Atrial Fibrillation: JACC State-of-the-Art Review. *J. Am. Coll. Cardiol.* **79**, 2349–2366 (2022).

90. Ren, H., Lai, H. & Chen, Z. Inflammatory and fibrotic signaling pathways mediated by cardiac macrophages in atrial fibrillation. *Front. Cardiovasc. Med.* **12**, 1692638 (2026).

91. Tan, Z. *et al.* Dapagliflozin attenuates atrial fibrosis via the HMGB1/RAGE pathway in atrial fibrillation rats. *Open Life Sci.* **20**, (2025).

92. Lee, K. W. *et al.* Pirfenidone prevents the development of a vulnerable substrate for atrial fibrillation in a canine model of heart failure. *Circulation* **114**, 1703–1712 (2006).

93. Zhang, H. Da *et al.* Semaglutide for the prevention of atrial fibrillation: A systematic review and meta-analysis. *Diabetes & Metabolic Syndrome: Clinical Research & Reviews* **18**, 103067 (2024).

94. Bohne, L. J. *et al.* Glucagon-Like Peptide-1 Protects Against Atrial Fibrillation and Atrial Remodeling in Type 2 Diabetic Mice. *Basic to Translational Science* **8**, 922–936 (2023).

95. Li, T. lun *et al.* Omentin-1 attenuates atrial fibrillation via Src/PI3K/Akt signaling-mediated anti-fibrotic effects in cardiac fibroblasts. *Eur. J. Pharmacol.* **996**, 177588 (2025).

96. Ji, Y. & Ning, Z. Paeoniflorin Inhibits Atrial Fibrosis and Atrial Fibrillation in Angiotensin II-Infused Mice Through the PI3K-Akt Pathway. *Dose-Response* **22**, (2024).

97. Song, Z. *et al.* BET Inhibitor JQ1 Attenuates Atrial Fibrillation Through Modulation of Fibrosis, Calcium Homeostasis, and Mitochondrial Function in a Murine Model. *International Journal of Molecular Sciences 2025, Vol. 26, Page 10363* **26**, 10363 (2025).

98. Hermanto, K. *et al.* Early rhythm control compared to rate control in atrial fibrillation – A systematic review, meta-analysis, and meta-regression. *Indian Pacing Electrophysiol. J.* **25**, 82–90 (2025).

99. Prabhu, S. *et al.* Regression of Diffuse Ventricular Fibrosis Following Restoration of Sinus Rhythm With Catheter Ablation in Patients With Atrial Fibrillation and Systolic Dysfunction: A Substudy of the CAMERA MRI Trial. *JACC Clin. Electrophysiol.* **4**, 999–1007 (2018).

100. Yang, H., Hu, Y., Kong, B., Shen, C. & Shuai, W. Low-intensity pulsed ultrasound attenuates atrial remodelling and atrial fibrillation after myocardial infarction: an experimental pre-clinical study. *EP Europace* **27**, 258 (2025).

101. Litviňuková, M. *et al.* Cells of the adult human heart. *Nature 2020 588:7838* **588**, 466–472 (2020).

102. Dostal, D., Glaser, S. & Baudino, T. A. Cardiac Fibroblast Physiology and Pathology. *Compr. Physiol.* **5**, 887–909 (2015).

103. Paraskevaidis, I., Tsougos, E. & Kourek, C. Cardio-Vascular Extracellular Matrix: The Unmet Enigma. *International Journal of Molecular Sciences 2026, Vol. 27, Page 544* **27**, 544 (2026).

104. Hall, C., Gehmlich, K., Denning, C. & Pavlovic, D. Complex relationship between cardiac fibroblasts and cardiomyocytes in health and disease. *J. Am. Heart Assoc.* **10**, 1–15 (2021).

105. Kurose, H. Cardiac Fibrosis and Fibroblasts. *Cells 2021, Vol. 10, Page 1716* **10**, 1716 (2021).

106. Krenning, G., Zeisberg, E. M. & Kalluri, R. The origin of fibroblasts and mechanism of cardiac fibrosis. *J. Cell. Physiol.* **225**, 631–637 (2010).

107. Chimenti, I. *et al.* The Role of Cardiac Fibroblast Heterogeneity in Myocardial Fibrosis and Its Novel Therapeutic Potential. *International Journal of Molecular Sciences 2025, Vol. 26, Page 5882* **26**, 5882 (2025).

108. Ali, S. R. *et al.* Developmental heterogeneity of cardiac fibroblasts does not predict pathological proliferation and activation. *Circ. Res.* **115**, 625–635 (2014).

109. Cartledge, J. E. *et al.* Functional crosstalk between cardiac fibroblasts and adult cardiomyocytes by soluble mediators. *Cardiovasc. Res.* **105**, 260–270 (2015).

110. Tsoporis, J. N., Izhar, S., Proteau, G., Slaughter, G. & Parker, T. G. S100B-RAGE dependent VEGF secretion by cardiac myocytes induces myofibroblast proliferation. *J. Mol. Cell. Cardiol.* **52**, 464–473 (2012).

111. Flores-Vergara, R. *et al.* Communication Between Cardiomyocytes and Fibroblasts During Cardiac Ischemia/Reperfusion and Remodeling: Roles of TGF-β, CTGF, the Renin Angiotensin Axis, and Non-coding RNA Molecules. *Front. Physiol.* **12**, 716721 (2021).

112. Dolmatova, E. *et al.* Cardiomyocyte ATP release through pannexin 1 aids in early fibroblast activation. *https://doi.org/10.1152/ajpheart.00251.2012* **303**, 1208–1218 (2012).

113. Tsai, C. T. *et al.* Tachycardia of atrial myocytes induces collagen expression in atrial fibroblasts through transforming growth factor β1. *Cardiovasc. Res.* **89**, 805–815 (2011).

114. Thompson, S. A., Copeland, C. R., Reich, D. H. & Tung, L. Mechanical coupling between myofibroblasts and cardiomyocytes slows electric conduction in fibrotic cell monolayers. *Circulation* **123**, 2083–2093 (2011).

115. Cadosch, N., Gil-Cruz, C., Perez-Shibayama, C. & Ludewig, B. Cardiac Fibroblastic Niches in Homeostasis and Inflammation. *Circ. Res.* **134**, 1703–1717 (2024).

116. Zhang, W. *et al.* Necrotic Myocardial Cells Release Damage-Associated Molecular Patterns That Provoke Fibroblast Activation In Vitro and Trigger Myocardial Inflammation and Fibrosis In Vivo. *J. Am. Heart Assoc.* **4**, (2015).

117. Cowling, R. T., Kupsky, D., Kahn, A. M., Daniels, L. B. & Greenberg, B. H. Mechanisms of cardiac collagen deposition in experimental models and human disease. *Translational Research* **209**, 138–155 (2019).

118. Su, X. *et al.* SNAP25-dependent membrane trafficking of the Kv1.5 channel regulates the onset of atrial fibrillation. *Nature Communications 2025 16:1* **16**, 3730- (2025).

119. Poulet, C. *et al.* Altered physiological functions and ion currents in atrial fibroblasts from patients with chronic atrial fibrillation. *Physiol. Rep.* **4**, e12681 (2016).

120. Jakob, D. *et al.* Heterogeneity and Remodeling of Ion Currents in Cultured Right Atrial Fibroblasts From Patients With Sinus Rhythm or Atrial Fibrillation. *Front. Physiol.* **12**, 673891 (2021).

121. Pradhan, K. *et al.* MicroRNA-21 mediated cross-talk between cardiomyocytes and fibroblasts in patients with atrial fibrillation. *Front. Cardiovasc. Med.* **10**, 1056134 (2023).

122. Stapleton, P. A., Knuckles, T. L., Minarchick, V. C., Gautam, G. & Nurkiewicz, T. R. Cardiovascular System. *Encyclopedia of Toxicology: Third Edition* 730–747 (2014) doi:10.1016/B978-0-12-386454-3.00985-4.

123. Heywood, W. E. *et al.* A Proof of Principle 2D Spatial Proteome Mapping Analysis Reveals Distinct Regional Differences in the Cardiac Proteome. . **14**, 970 (2024).

124. Humeres, C. & Frangogiannis, N. G. Fibroblasts in the Infarcted, Remodeling, and Failing Heart. *JACC Basic Transl. Sci.* **4**, 449–467 (2019).

125. Fu, X. *et al.* Specialized fibroblast differentiated states underlie scar formation in the infarcted mouse heart. *J. Clin. Invest.* **128**, 2127–2143 (2018).

126. Kanisicak, O. *et al.* Genetic lineage tracing defines myofibroblast origin and function in the injured heart. *Nature Communications 2016 7:1* **7**, 12260- (2016).

127. Siamwala, J. H. *et al.* IL-1β-mediated adaptive reprogramming of endogenous human cardiac fibroblasts to cells with immune features during fibrotic remodeling. *Communications Biology 2023 6:1* **6**, 1200- (2023).

128. Muñoz-Espín, D. & Serrano, M. Cellular senescence: from physiology to pathology. *Nature Reviews Molecular Cell Biology 2014 15:7* **15**, 482–496 (2014).

129. Bowers, S. L. K., Meng, Q. & Molkentin, J. D. Fibroblasts orchestrate cellular crosstalk in the heart through the ECM. *Nature cardiovascular research* **1**, 312–321 (2022).

130. Talman, V. & Ruskoaho, H. Cardiac fibrosis in myocardial infarction-from repair and remodeling to regeneration. *Cell Tissue Res.* **365**, 563–581 (2016).

131. Simon-Chica, A. *et al.* Cardiac Macrophages and Fibroblasts Modulate Atrial Fibrillation Maintenance. *Circ. Res.* https://doi.org/10.1161/CIRCRESAHA.125.326291;SUBPAGE:STRING:FULL (2026) doi:10.1161/CIRCRESAHA.125.326291;SUBPAGE:STRING:FULL.

132. Leblanc, F. J. A. *et al.* Single-nucleus multi-omics implicates androgen receptor signaling in cardiomyocytes and NR4A1 regulation in fibroblasts during atrial fibrillation. *Nature Cardiovascular Research 2025 4:4* **4**, 433–444 (2025).

133. Gao, L. *et al.* The roles of orphan nuclear receptor 4 group A1 and A2 in fibrosis. *Int. Immunopharmacol.* **139**, 112705 (2024).

134. Kiriyama, Y., Nakatsuma, A., Tokumaru, H., Sadamoto, H. & Nochi, H. Functional Changes Associated With the Subcellular Localization of the Nuclear Receptor NR4A1. *Biochem. Res. Int.* **2025**, 4849733 (2025).

135. Safe, S., Shrestha, R. & Mohankumar, K. Orphan nuclear receptor 4A1 (NR4A1) and novel ligands. *Essays Biochem.* **65**, 877–886 (2021).

136. Lanig, H. *et al.* In Silico Adoption of an Orphan Nuclear Receptor NR4A1. *PLoS One* **10**, e0135246 (2015).

137. Kurakula, K., Van Der Wal, E., Geerts, D., Van Tiel, C. M. & De Vries, C. J. M. FHL2 Protein Is a Novel Co-repressor of Nuclear Receptor Nur77. *Journal of Biological Chemistry* **286**, 44336–44343 (2011).

138. Safe, S. Natural products and synthetic analogs as selective orphan nuclear receptor 4A (NR4A) modulators. *Histol. Histopathol.* **39**, 543–556 (2024).

139. Lee, M. *et al.* Flavone and Hydroxyflavones Are Ligands That Bind the Orphan Nuclear Receptor 4A1 (NR4A1). *Int. J. Mol. Sci.* **24**, 8152 (2023).

140. Zhang, L. *et al.* Resveratrol Binds Nuclear Receptor 4A1 (NR4A1) and Acts as an NR4A1 Antagonist in Lung Cancer Cells. *Mol. Pharmacol.* **102**, 80–91 (2022).

141. Han, Y. H. *et al.* Regulation of Nur77 nuclear export by c-Jun N-terminal kinase and Akt. *Oncogene* **25**, 2974–2986 (2006).

142. Pekarsky, Y. *et al.* Akt phosphorylates and regulates the orphan nuclear receptor Nur77. *Proc. Natl. Acad. Sci. U. S. A.* **98**, 3690–3694 (2001).

143. Li, X. xue *et al.* Nuclear Receptor Nur77 Facilitates Melanoma Cell Survival under Metabolic Stress by Protecting Fatty Acid Oxidation. *Mol. Cell* **69**, 480-492.e7 (2018).

144. Hu, H. *et al.* Bruceine A protects nuclear receptor 4A1 from ubiquitin-degradation to alleviate mesangial proliferative glomerulonephritis. *Signal Transduction and Targeted Therapy 2025 10:1* **10**, 397- (2025).

145. Zárraga-Granados, G. *et al.* The nuclear receptor NR4A1 is regulated by SUMO modification to induce autophagic cell death. *PLoS One* **15**, e0222072 (2020).

146. Dodat, F., Mader, S. & Lévesque, D. Minireview: What is Known about SUMOylation Among NR4A Family Members? *J. Mol. Biol.* **433**, 167212 (2021).

147. Pawlak, A., Strzadala, L. & Kalas, W. Non-genomic effects of the NR4A1/Nur77/TR3/NGFIB orphan nuclear receptor. *Steroids* **95**, 1–6 (2015).

148. Miao, L. *et al.* Glycerol kinase interacts with nuclear receptor NR4A1 and regulates glucose metabolism in the liver. *FASEB Journal* **33**, 6736–6747 (2019).

149. Safe, S. *et al.* Transcription factors specificity protein and nuclear receptor 4A1 in pancreatic cancer. *World J. Gastroenterol.* **27**, 6387–6398 (2021).

150. Palumbo-Zerr, K. *et al.* Orphan nuclear receptor NR4A1 regulates transforming growth factor-β signaling and fibrosis. *Nature Medicine 2014 21:2* **21**, 150–158 (2015).

151. Safe, S. & Karki, K. The paradoxical roles of orphan nuclear receptor 4A (NR4A) in cancer. *Molecular Cancer Research* **19**, 180–191 (2021).

152. Jiang, C. *et al.* NR4A1 suppresses breast cancer growth by repressing c-Fos-mediated lipid and redox dyshomeostasis. *Experimental & Molecular Medicine 2025 57:4* **57**, 804–819 (2025).

153. Wu, H. *et al.* Nuclear receptor NR4A1 is a tumor suppressor downregulated in triplenegative breast cancer. *Oncotarget* **8**, 54364–54377 (2017).

154. Zhang, L. *et al.* The Orphan Nuclear Receptor 4A1: A Potential New Therapeutic Target for Metabolic Diseases. *J. Diabetes Res.* **2018**, 9363461 (2018).

155. Kleberg, J. *et al.* Targeting Lineage-Specific Functions of NR4A1 for Cancer Immunotherapy. *International Journal of Molecular Sciences 2025, Vol. 26, Page 5266* **26**, 5266 (2025).

156. Kong, C. yan *et al.* Nuclear Receptor Subfamily 4 Group A Member 1 Exacerbates Cardiac Remodeling by Inhibiting Mitochondrial Function Through the Peroxisome Proliferator-Activated Receptor γ Coactivator-1α/Nuclear Respiratory Factor 1/Transcription Factor A Mitochondrial Ax…. *J. Am. Heart Assoc.* **14**, 42774 (2025).

157. Ye, H. *et al.* Nuclear receptor 4A1 Regulates Mitochondrial Homeostasis in Cardiac Post-Ischemic Injury by Controlling Mitochondrial Fission 1 Protein-Mediated Fragmentation and Parkin-Dependent Mitophagy. *Int. J. Biol. Sci.* **21**, 400–414 (2025).

158. Zhu, F. *et al.* The orphan receptor Nur77 binds cytoplasmic LPS to activate the non-canonical NLRP3 inflammasome. *Immunity* **56**, 753-767.e8 (2023).

159. Liu, P. *et al.* Noncanonical contribution of microglial transcription factor NR4A1 to post-stroke recovery through TNF mRNA destabilization. *PLoS Biol.* **21**, e3002199 (2023).

160. Widiapradja, A. *et al.* The orphan nuclear receptor Nr4a1 contributes to interstitial cardiac fibrosis via modulation of cardiac fibroblast and macrophage phenotype. *Cellular and Molecular Life Sciences 2024 81:1* **81**, 484- (2024).

161. Medzikovic, L. *et al.* Nuclear Receptor Nur77 Controls Cardiac Fibrosis through Distinct Actions on Fibroblasts and Cardiomyocytes. *International Journal of Molecular Sciences 2021, Vol. 22, Page 1600* **22**, 1600 (2021).

162. Yang, H. X. *et al.* Bellidifolin Ameliorates Isoprenaline-Induced Myocardial Fibrosis by Regulating TGF-β1/Smads and p38 Signaling and Preventing NR4A1 Cytoplasmic Localization. *Front. Pharmacol.* **12**, 644886 (2021).

163. Chen, Z. *et al.* Polypyrimidine Tract Binding Protein 1 Exacerbates Cardiac Fibrosis by Regulating Fatty Acid-Binding Protein 5. *ESC Heart Fail.* **10**, 1677–1688 (2023).

164. Ma, Y. L. *et al.* Semaglutide ameliorates cardiac remodeling in male mice by optimizing energy substrate utilization through the Creb5/NR4a1 axis. *Nature Communications 2024 15:1* **15**, 4757- (2024).

165. Ji, J. jing *et al.* Kallistatin/Serpina3c inhibits cardiac fibrosis after myocardial infarction by regulating glycolysis via Nr4a1 activation. *Biochimica et Biophysica Acta (BBA) - Molecular Basis of Disease* **1868**, 166441 (2022).

166. Chen, J. *et al.* Nur77 deficiency exacerbates cardiac fibrosis after myocardial infarction by promoting endothelial-to-mesenchymal transition. *J. Cell. Physiol.* **236**, 495–506 (2021).

167. Ma, G. *et al.* Nur77 ameliorates age-related renal tubulointerstitial fibrosis by suppressing the TGF-β/Smads signaling pathway. *FASEB J.* **36**, (2022).

168. Wang, H. *et al.* SPDEF ameliorates UUO-induced renal fibrosis by transcriptional activation of NR4A1. *Molecular Medicine 2024 30:1* **30**, 282- (2024).

169. Li, J.-M. *et al.* NR4A1 silencing alleviates high-glucose-stimulated HK-2 cells pyroptosis and fibrosis via hindering NLRP3 activation and PI3K/AKT pathway. *World J. Diabetes* **16**, 97544 (2025).

170. Tao, Y. *et al.* Nr4a1 promotes renal interstitial fibrosis by regulating the p38 MAPK phosphorylation. *Molecular Medicine 2023 29:1* **29**, 63- (2023).

171. Haub, J. *et al.* Intervention of Inflammatory Monocyte Activity Limits Dermal Fibrosis. *Journal of Investigative Dermatology* **139**, 2144–2153 (2019).

172. Servaas, N. H. *et al.* Nuclear Receptor Subfamily 4A Signaling as a Key Disease Pathway of CD1c+ Dendritic Cell Dysregulation in Systemic Sclerosis. *Arthritis Rheumatol.* **75**, 279–292 (2023).

173. Venu, V. K. P. *et al.* Nr4A1 modulates inflammation-associated intestinal fibrosis and dampens fibrogenic signaling in myofibroblasts. *https://doi.org/10.1152/ajpgi.00338.2019* **321**, G297–G297 (2021).

174. Yin, C., Evason, K. J., Asahina, K. & Stainier, D. Y. R. Hepatic stellate cells in liver development, regeneration, and cancer. *J. Clin. Invest.* **123**, 1902–1910 (2013).

175. Huang, Q. *et al.* NR4A1 inhibits the epithelial-mesenchymal transition of hepatic stellate cells: Involvement of TGF-β-Smad2/3/4-ZEB signaling. *Open Life Sci.* **17**, 447–454 (2022).

176. Fuchs, C. D. *et al.* GLP-2 Improves Hepatic Inflammation and Fibrosis in Mdr2-/- Mice Via Activation of NR4a1/Nur77 in Hepatic Stellate Cells and Intestinal FXR Signaling. *Cell. Mol. Gastroenterol. Hepatol.* **16**, 847–856 (2023).

177. Zeng, X. *et al.* NR4A1 is Involved in Fibrogenesis in Ovarian Endometriosis. *Cellular Physiology and Biochemistry* **46**, 1078–1090 (2018).

178. Hiwatashi, N., Bing, R., Kraja, I. & Branski, R. C. NR4A1 is an endogenous inhibitor of vocal fold fibrosis. *Laryngoscope* **127**, E317–E323 (2017).

179. Banno, A., Lakshmi, S. P., Reddy, A. T., Kim, S. C. & Reddy, R. C. Key Functions and Therapeutic Prospects of Nur77 in Inflammation Related Lung Diseases. *Am. J. Pathol.* **189**, 482–491 (2019).

180. Van Gelder, I. C. *et al.* 2024 ESC Guidelines for the management of atrial fibrillation developed in collaboration with the European Association for Cardio-Thoracic Surgery (EACTS). *Eur. Heart J.* **45**, 3314–3414 (2024).

181. Livak, K. J. & Schmittgen, T. D. Analysis of Relative Gene Expression Data Using Real-Time Quantitative PCR and the 2−ΔΔCT Method. *Methods* **25**, 402–408 (2001).

182. Nattel, S. Molecular and Cellular Mechanisms of Atrial Fibrosis in Atrial Fibrillation. *JACC Clin. Electrophysiol.* **3**, 425–435 (2017).

183. Burstein, B. & Nattel, S. Atrial Fibrosis: Mechanisms and Clinical Relevance in Atrial Fibrillation. *J. Am. Coll. Cardiol.* **51**, 802–809 (2008).

184. Tucker, N. R. *et al.* Transcriptional and Cellular Diversity of the Human Heart. *Circulation* **142**, 466–482 (2020).

185. An, N. *et al.* Single-cell RNA sequencing reveals the contribution of smooth muscle cells and endothelial cells to fibrosis in human atrial tissue with atrial fibrillation. *Molecular Medicine 2024 30:1* **30**, 247- (2024).

186. Schüttler, D. *et al.* Animal Models of Atrial Fibrillation. *Circ. Res.* **127**, 91–110 (2020).

187. Kaese, S. & Verheule, S. Cardiac electrophysiology in mice: A matter of size. *Front. Physiol.* **3 SEP**, 29023 (2012).

188. Wang, R. H. *et al.* The orphan receptor TR3 participates in angiotensin II-induced cardiac hypertrophy by controlling mTOR signalling. *EMBO Mol. Med.* **5**, 137–148 (2013).

189. Wei, F., Ma, Y., Xiang, H., Zhang, X. & Fan, J. LncRNA Dleu2 Serve as a Novel Biomarker for Ablation Recurrence and Promote Atrial Remodelling by Targeting Nr4a1 in Atrial Fibrillation. *J. Cell. Mol. Med.* **29**, e70618 (2025).

190. Zhan, Y. *et al.* Cytosporone B is an agonist for nuclear orphan receptor Nur77. *Nature Chemical Biology 2008 4:9* **4**, 548–556 (2008).

191. Reichart, D. *et al.* Pathogenic variants damage cell composition and single-cell transcription in cardiomyopathies. *Science (1979).* **377**, (2022).

192. Hilgendorf, I. *et al.* Ly-6 chigh monocytes depend on nr4a1 to balance both inflammatory and reparative phases in the infarcted myocardium. *Circ. Res.* **114**, 1611–1622 (2014).

193. Hu, H. *et al.* Knockdown of NR4A1 alleviates doxorubicin-induced cardiotoxicity through inhibiting the activation of the NLRP3 inflammasome. *Biochem. Biophys. Res. Commun.* **700**, 149582 (2024).

194. Yamaguchi, T. Atrial structural remodeling and atrial fibrillation substrate: A histopathological perspective. *J. Cardiol.* **85**, 47–55 (2025).

195. Nattel, S., Heijman, J., Zhou, L. & Dobrev, D. Molecular Basis of Atrial Fibrillation Pathophysiology and Therapy: A Translational Perspective. *Circ. Res.* **127**, 51–72 (2020).

196. Wang, H. *et al.* Nuclear receptor 4A1 ameliorates UUO-induced renal fibrosis by inhibiting the PI3K/AKT pathway. *Scientific Reports 2024 14:1* **14**, 24787- (2024).

197. Jiang, W., Xiong, Y., Li, X. & Yang, Y. Cardiac Fibrosis: Cellular Effectors, Molecular Pathways, and Exosomal Roles. *Front. Cardiovasc. Med.* **8**, 715258 (2021).

198. Garay, T. *et al.* Cell migration or cytokinesis and proliferation? – Revisiting the “go or grow” hypothesis in cancer cells in vitro. *Exp. Cell Res.* **319**, 3094–3103 (2013).

199. Wansa, K. D. S. A., Harris, J. M., Yan, G., Ordentlich, P. & Muscat, G. E. O. The AF-1 Domain of the Orphan Nuclear Receptor NOR-1 Mediates Trans-activation, Coactivator Recruitment, and Activation by the Purine Anti-metabolite 6-Mercaptopurine. *Journal of Biological Chemistry* **278**, 24776–24790 (2003).

200. Senali Abayratna Wansa, K. D., Harris, J. M. & Muscat, G. E. O. The Activation Function-1 Domain of Nur77/NR4A1 Mediates Trans-activation, Cell Specificity, and Coactivator Recruitment. *Journal of Biological Chemistry* **277**, 33001–33011 (2002).

201. Schwanhüusser, B. *et al.* Global quantification of mammalian gene expression control. *Nature 2011 473:7347* **473**, 337–342 (2011).

202. Vogel, C. & Marcotte, E. M. Insights into the regulation of protein abundance from proteomic and transcriptomic analyses. *Nature Reviews Genetics 2012 13:4* **13**, 227–232 (2012).

203. Lin, G. *et al.* Molecular mechanism of NR4A1/MDM2/P53 signaling pathway regulation inducing ferroptosis in renal tubular epithelial cells involved in the progression of renal ischemia-reperfusion injury. *Biochimica et Biophysica Acta (BBA) - Molecular Basis of Disease* **1870**, 166968 (2024).

204. Wu, L. *et al.* Atrial inflammation in different atrial fibrillation subtypes and its relation with clinical risk factors. *Clin. Res. Cardiol.* **109**, 1271–1281 (2020).

205. Deb, A. & Ubil, E. Cardiac fibroblast in development and wound healing. *J. Mol. Cell. Cardiol.* **70**, 47–55 (2014).

206. Flaig, R., Greschik, H., Peluso-Iltis, C. & Moras, D. Structural Basis for the Cell-specific Activities of the NGFI-B and the Nurr1 Ligand-binding Domain. *Journal of Biological Chemistry* **280**, 19250–19258 (2005).

207. Wang, Z. *et al.* Structure and function of Nurr1 identifies a class of ligand-independent nuclear receptors. *Nature 2003 423:6939* **423**, 555–560 (2003).

208. Hao, L. *et al.* Research on the in vitro anticancer activity and in vivo tissue distribution of Amoitone B nanocrystals. *Colloids Surf. B Biointerfaces* **117**, 258–266 (2014).

209. Lakshmi, S. P., Reddy, A. T., Banno, A. & Reddy, R. C. Molecular, chemical, and structural characterization of prostaglandin A2 as a novel agonist for Nur77. *Biochem. J.* **476**, 2757–2767 (2019).

210. Ohmura, T. *et al.* Regulation of lung endothelial permeability and inflammatory responses by prostaglandin A2: role of EP4 receptor. *https://doi.org/10.1091/mbc.e16-09-0639* **28**, 1622–1635 (2017).

211. Lee, S. Y. *et al.* Prostaglandin A2 activates intrinsic apoptotic pathway by direct interaction with mitochondria in HL-60 cells. *Prostaglandins Other Lipid Mediat.* **91**, 30–37 (2010).

212. Bryson, T. D., Ross, J., Peterson, E. & Harding, P. Prostaglandin E2 and an EP4 receptor agonist inhibit LPS-Induced monocyte chemotactic protein 5 production and secretion in mouse cardiac fibroblasts via Akt and NF-κB signaling. *Prostaglandins Other Lipid Mediat.* **144**, (2019).

213. Mir, S. A. *et al.* Inhibition of Signal Transducer and Activator of Transcription 3 (STAT3) Attenuates Interleukin-6 (IL-6)-induced Collagen Synthesis and Resultant Hypertrophy in Rat Heart. *Journal of Biological Chemistry* **287**, 2666–2677 (2012).

214. SR, P., S, M. & D, D. Induction of collagen synthesis by ascorbic acid. A possible mechanism. *Arch. Dermatol.* **123**, 1684–1686 (1987).

215. Subramanian, A. *et al.* A Next Generation Connectivity Map: L1000 Platform and the First 1,000,000 Profiles. *Cell* **171**, 1437-1452.e17 (2017).

216. Meagher, P. B. *et al.* Cardiac Fibrosis: Key Role of Integrins in Cardiac Homeostasis and Remodeling. *Cells 2021, Vol. 10, Page 770* **10**, 770 (2021).

217. Ovek Baydar, D. *et al.* JASPAR 2026: expansion of transcription factor binding profiles and integration of deep learning models. *Nucleic Acids Res.* **54**, D184–D193 (2026).

218. Casper, J. *et al.* The UCSC Genome Browser database: 2026 update. *Nucleic Acids Res.* **54**, D1331–D1335 (2026).

219. Faggioli, L., Costanzo, C., Donadelli, M. & Palmieri, M. Activation of the interleukin-6 promoter by a dominant negative mutant of c-Jun. *Biochimica et Biophysica Acta (BBA) - Molecular Cell Research* **1692**, 17–24 (2004).

220. Meléndez, G. C. *et al.* Interleukin 6 mediates myocardial fibrosis, concentric hypertrophy, and diastolic dysfunction in rats. *Hypertension* **56**, 225–231 (2010).

221. Mir, S. A. *et al.* Inhibition of Signal Transducer and Activator of Transcription 3 (STAT3) Attenuates Interleukin-6 (IL-6)-induced Collagen Synthesis and Resultant Hypertrophy in Rat Heart. *Journal of Biological Chemistry* **287**, 2666–2677 (2012).

222. Moita, M. R. *et al.* Transcriptome and proteome profiling of activated cardiac fibroblasts supports target prioritization in cardiac fibrosis. *Front. Cardiovasc. Med.* **9**, 1015473 (2022).

223. Tallquist, M. D. & Molkentin, J. D. Redefining the identity of cardiac fibroblasts. *Nat. Rev. Cardiol.* **14**, 484–491 (2017).

224. Gibb, A. A., Lazaropoulos, M. P. & Elrod, J. W. Myofibroblasts and Fibrosis. *Circ. Res.* **127**, 427–447 (2020).

225. Schofield, C. J. & Ratcliffe, P. J. Oxygen sensing by HIF hydroxylases. *Nat. Rev. Mol. Cell Biol.* **5**, 343–354 (2004).

226. Lu, H., Forbes, R. A. & Verma, A. Hypoxia-inducible Factor 1 Activation by Aerobic Glycolysis Implicates the Warburg Effect in Carcinogenesis. *Journal of Biological Chemistry* **277**, 23111–23115 (2002).

227. Bian, X. L. *et al.* Nur77 suppresses hepatocellular carcinoma via switching glucose metabolism toward gluconeogenesis through attenuating phosphoenolpyruvate carboxykinase sumoylation. *Nature Communications 2017 8:1* **8**, 14420- (2017).

228. Chen, C., Wen, J., Huang, W. & Li, J. NR4A1 enhances glycolysis in hypoxia-exposed pulmonary artery smooth muscle cells by upregulating HIF-1α expression. *BIOCELL* **47**, 2423–2433 (2023).

229. Pavlides, S. *et al.* Warburg meets autophagy: Cancer-Associated fibroblasts accelerate tumor growth and metastasis via oxidative stress, mitophagy, and aerobic glycolysis. *Antioxid. Redox Signal.* **16**, 1264–1284 (2012).

230. Valiente-Alandi, I., Schafer, A. E. & Blaxall, B. C. Extracellular matrix-mediated cellular communication in the heart. *J. Mol. Cell. Cardiol.* **91**, 228–237 (2016).

231. Pang, Z., Ren, Y. & Yao, Z. Interactions between atrial fibrosis and inflammation in atrial fibrillation. *Front. Cardiovasc. Med.* **12**, 1578148 (2025).

232. van der Laan, S. & Meijer, O. C. Pharmacology of glucocorticoids: Beyond receptors. *Eur. J. Pharmacol.* **585**, 483–491 (2008).

233. De Bosscher, K. *et al.* Glucocorticoid-mediated repression of nuclear factor-κB-dependent transcription involves direct interference with transactivation. *Proc. Natl. Acad. Sci. U. S. A.* **94**, 13504–13509 (1997).

234. Xavier, A. M., Anunciato, A. K. O., Rosenstock, T. R. & Glezer, I. Gene expression control by glucocorticoid receptors during innate immune responses. *Front. Endocrinol. (Lausanne).* **7**, 182794 (2016).

235. Zhou, Z., Long, Y., He, X. & Li, Y. Effects of different doses of glucocorticoids on postoperative atrial fibrillation: a meta-analysis. *BMC Cardiovascular Disorders 2023 23:1* **23**, 16- (2023).

236. Christiansen, C. F. *et al.* Glucocorticoid use and risk of atrial fibrillation or flutter: a population-based, case-control study. *Arch. Intern. Med.* **169**, 1677–1683 (2009).

237. Chen, Q., Shen, L. & Li, S. Emerging role of inositol monophosphatase in cancer. *Biomedicine & Pharmacotherapy* **161**, 114442 (2023).

238. Kochetov, G. A. & Solovjeva, O. N. Structure and functioning mechanism of transketolase. *Biochimica et Biophysica Acta (BBA) - Proteins and Proteomics* **1844**, 1608–1618 (2014).

239. Tong, L. *et al.* Transketolase promotes MAFLD by limiting inosine-induced mitochondrial activity. *Cell Metab.* **36**, 1013-1029.e5 (2024).

240. Shitole, S. G. *et al.* Assessment of Inflammatory Biomarkers and Incident Atrial Fibrillation in Older Adults. *Journal of the American Heart Association* **13**, (2024).

241. Li, X. *et al.* Selective blockade of interleukin 6 trans-signaling depresses atrial fibrillation. *Heart Rhythm* **20**, 1759–1770 (2023).

242. Marcus, G. M. *et al.* Interleukin-6 and atrial fibrillation in patients with coronary artery disease: Data from the Heart and Soul Study. *Am. Heart J.* **155**, 303–309 (2008).

243. Keefe, J. A. *et al.* Macrophage-mediated IL-6 signaling drives ryanodine receptor-2 calcium leak in postoperative atrial fibrillation. *J. Clin. Invest.* **135**, (2025).

244. Murphy, E. P. & Crean, D. Molecular Interactions between NR4A Orphan Nuclear Receptors and NF-κB Are Required for Appropriate Inflammatory Responses and Immune Cell Homeostasis. *Biomolecules 2015, Vol. 5, Pages 1302-1318* **5**, 1302–1318 (2015).

245. Avitall, B., Bi, J., Mykytsey, A. & Chicos, A. Atrial and ventricular fibrosis induced by atrial fibrillation: Evidence to support early rhythm control. *Heart Rhythm* **5**, 839–845 (2008).

246. Andrade, J., Khairy, P., Dobrev, D. & Nattel, S. The clinical profile and pathophysiology of atrial fibrillation: Relationships among clinical features, epidemiology, and mechanisms. *Circ. Res.* **114**, 1453–1468 (2014).

247. Jalife, J. & Kaur, K. Atrial remodeling, fibrosis, and atrial fibrillation. *Trends Cardiovasc. Med.* **25**, 475–484 (2015).

248. Psychari, S. N. *et al.* Relation of elevated C-reactive protein and interleukin-6 levels to left atrial size and duration of episodes in patients with atrial fibrillation. *Am. J. Cardiol.* **95**, 764–767 (2005).

249. Wang, Y., Li, N., Guan, W. & Wang, D. Controversy and multiple roles of the solitary nucleus receptor Nur77 in disease and physiology. *FASEB Journal* **39**, e70468 (2025).

250. Hsu, J. *et al.* Genetic Control of Left Atrial Gene Expression Yields Insights into the Genetic Susceptibility for Atrial Fibrillation. *Circ. Genom. Precis. Med.* **11**, e002107 (2018).

251. Haugaard, S. L. *et al.* The horse cardiac transcriptome: Moving towards a molecular understanding of atrial fibrillation. *Equine Vet. J.* https://doi.org/10.1111/EVJ.70115;PAGEGROUP:STRING:PUBLICATION (2025) doi:10.1111/EVJ.70115;PAGEGROUP:STRING:PUBLICATION.

252. Nissen, S. D. *et al.* Horse model of spontaneous atrial fibrillation share proteomic changes with humans. *Scientific Reports 2025 15:1* **15**, 31694- (2025).

253. Kisselev, A. F. & Goldberg, A. L. Proteasome inhibitors: from research tools to drug candidates. *Chem. Biol.* **8**, 739–758 (2001).

254. Kofoed, K. F. *et al.* Prolonged ischemic heart disease and coronary artery bypass — relation to contractile reserve. *European Journal of Cardio-Thoracic Surgery* **21**, 417–423 (2002).

255. Noubiap, J. J. *et al.* Meta-analysis of the incidence, prevalence, and correlates of atrial fibrillation in rheumatic heart disease. *Glob. Heart* **15**, (2020).

256. Kostin, S. *et al.* Atrial fibrillation in human patients is associated with increased collagen type V and TGFbeta1. *IJC Heart & Vasculature* **50**, 101327 (2024).

257. Black, M. *et al.* FOXF1 Inhibits Pulmonary Fibrosis by Preventing CDH2-CDH11 Cadherin Switch in Myofibroblasts. *Cell Rep.* **23**, 442–458 (2018).

258. Josvai, M. *et al.* hiPSC-derived cardiac fibroblasts dynamically enhance the mechanical function of hiPSC-derived cardiomyocytes on an engineered substrate. *Front. Bioeng. Biotechnol.* **13**, 1546483 (2025).

259. Monte, E., Rosa-Garrido, M., Vondriska, T. M. & Wang, J. Undiscovered Physiology of Transcript and Protein Networks. *Compr. Physiol.* **6**, 1851–1872 (2016).

260. Zhang, L., Xie, F., Zhang, J., Ten Dijke, P. & Zhou, F. SUMO-triggered ubiquitination of NR4A1 controls macrophage cell death. *Cell Death & Differentiation 2017 24:9* **24**, 1530–1539 (2017).

261. Zhao, S. *et al.* Atrial proteomic profiling reveals a switch towards profibrotic gene expression program in CREM-IbΔC-X mice with persistent atrial fibrillation. *J. Mol. Cell. Cardiol.* **190**, 1–12 (2024).

262. Simicevic, J. & Deplancke, B. Transcription factor proteomics—Tools, applications, and challenges. *Proteomics* **17**, 1600317 (2017).

263. Adamstein, N. H. *et al.* Association of Interleukin 6 Inhibition With Ziltivekimab and the Neutrophil-Lymphocyte Ratio: A Secondary Analysis of the RESCUE Clinical Trial. *JAMA Cardiol.* **8**, 177–181 (2023).

264. Ridker, P. M. *et al.* IL-6 inhibition with ziltivekimab in patients at high atherosclerotic risk (RESCUE): a double-blind, randomised, placebo-controlled, phase 2 trial. *The Lancet* **397**, 2060–2069 (2021).

265. May, M. Eleven clinical trials that will shape medicine in 2026. *Nature Medicine 2025 31:12* **31**, 3943–3947 (2025).

266. Li, L. *et al.* Integrated untargeted/targeted metabolomics identifies a putative oxylipin signature in patients with atrial fibrillation and coronary heart disease. *J. Transl. Int. Med.* **12**, 495–509 (2024).

267. Zeng, Y. *et al.* Non-coding RNA and arrhythmias: expression, function, and molecular mechanism. *Europace* **25**, 1296–1308 (2023).

268. Tao, H., Zhang, M., Yang, J. J. & Shi, K. H. MicroRNA-21 via Dysregulation of WW Domain-Containing Protein 1 Regulate Atrial Fibrosis in Atrial Fibrillation. *Heart Lung Circ.* **27**, 104–113 (2018).

269. Xiao, J. *et al.* MiRNA-1202 promotes the TGF-β1-induced proliferation, differentiation and collagen production of cardiac fibroblasts by targeting nNOS. *PLoS One* **16**, e0256066 (2021).

270. Xiao, J. *et al.* hsa-miR-4443 inhibits myocardial fibroblast proliferation by targeting THBS1 to regulate TGF-β1/α-SMA/collagen signaling in atrial fibrillation. *Brazilian Journal of Medical and Biological Research* **54**, e10692 (2021).

271. Ota, T. *et al.* Complete sequencing and characterization of 21,243 full-length human cDNAs. *Nature Genetics 2004 36:1* **36**, 40–45 (2003).

272. Jumper, J. *et al.* Highly accurate protein structure prediction with AlphaFold. *Nature 2021 596:7873* **596**, 583–589 (2021).

273. Jovanovic-Talisman, T. & Zilman, A. Protein Transport by the Nuclear Pore Complex: Simple Biophysics of a Complex Biomachine. *Biophys. J.* **113**, 6–14 (2017).

274. Azmi, A. S., Uddin, M. H. & Mohammad, R. M. The nuclear export protein XPO1 — from biology to targeted therapy. *Nature Reviews Clinical Oncology 2020 18:3* **18**, 152–169 (2020).

275. Papac-Milicevic, N. *et al.* The interferon stimulated gene 12 inactivates vasculoprotective functions of NR4A nuclear receptors. *Circ. Res.* **110**, (2012).

276. Maccarrone, G., Bonfiglio, J. J., Silberstein, S., Turck, C. W. & Martins-De-Souza, D. Characterization of a protein interactome by Co-Immunoprecipitation and shotgun mass spectrometry. *Methods in Molecular Biology* **1546**, 223–234 (2017).

277. Markham, K., Bai, Y. & Schmitt-Ulms, G. Co-immunoprecipitations revisited: an update on experimental concepts and their implementation for sensitive interactome investigations of endogenous proteins. *Analytical and Bioanalytical Chemistry 2007 389:2* **389**, 461–473 (2007).

278. Ritchie, M. E. *et al.* limma powers differential expression analyses for RNA-sequencing and microarray studies. *Nucleic Acids Res.* **43**, e47–e47 (2015).

279. Guo, H. *et al.* NR4A1 regulates expression of immediate early genes, suppressing replication stress in cancer. *Mol. Cell* **81**, 4041-4058.e15 (2021).

280. Charles A Janeway, J., Travers, P., Walport, M. & Shlomchik, M. J. The structure of a typical antibody molecule. https://www.ncbi.nlm.nih.gov/books/NBK27144/ (2001).

281. Charles A Janeway, J., Travers, P., Walport, M. & Shlomchik, M. J. The complement system and innate immunity. https://www.ncbi.nlm.nih.gov/books/NBK27100/ (2001).

282. Pedro Sousa Inês, L. *et al.* Microfibrillar-associated protein 4 interaction with inflammation and clinical characteristics in neuropsychiatric systemic lupus erythematosus. *Frontiers in Lupus* **2**, 1386256 (2024).

283. Pilecki, B. *et al.* Characterization of Microfibrillar-associated Protein 4 (MFAP4) as a Tropoelastin- and Fibrillin-binding Protein Involved in Elastic Fiber Formation. *Journal of Biological Chemistry* **291**, 1103–1114 (2016).

284. Niu, D. *et al.* Microfibrillar-associated protein 4 (MFAP4) genes in catfish play a novel role in innate immune responses. *Dev. Comp. Immunol.* **35**, 568–579 (2011).

285. Azizian, N. G., Azizian, N. G., Li, Y. & Li, Y. XPO1-dependent nuclear export as a target for cancer therapy. *Journal of Hematology & Oncology 2020 13:1* **13**, 61- (2020).

286. Chook, Y. M. & Süel, K. E. Nuclear import by karyopherin-βs: Recognition and inhibition. *Biochimica et Biophysica Acta (BBA) - Molecular Cell Research* **1813**, 1593–1606 (2011).

287. Bouzas-Rodríguez, J. *et al.* The Nuclear Receptor NR4A1 Induces a Form of Cell Death Dependent on Autophagy in Mammalian Cells. *PLoS One* **7**, e46422 (2012).

288. Duodu, P., Sosa, G., Canar, J., Chhugani, O. & Gamero, A. M. Exposing the Two Contrasting Faces of STAT2 in Inflammation. *Journal of Interferon and Cytokine Research* **42**, 467–481 (2022).

289. Singh, S. K. *et al.* Molecular Insights of MAP4K4 Signaling in Inflammatory and Malignant Diseases. *Cancers 2023, Vol. 15, Page 2272* **15**, 2272 (2023).

290. Li, C., Li, G., Tu, S., Bai, X. & Yuan, H. Integrative bioinformatics analysis reveals STAT2 as a novel biomarker of inflammation-related cardiac dysfunction in atrial fibrillation. *Open Medicine (Poland)* **18**, (2023).

291. Sadri, G. *et al.* Collagen type XIX regulates cardiac extracellular matrix structure and ventricular function. *Matrix Biology* **109**, 49–69 (2022).

292. Hamid, Z. *et al.* Assessment of label-free quantification and missing value imputation for proteomics in non-human primates. *BMC Genomics 2022 23:1* **23**, 496- (2022).

293. Schwämmle, V., Hagensen, C. E., Rogowska-Wrzesinska, A. & Jensen, O. N. PolySTest: Robust Statistical Testing of Proteomics Data with Missing Values Improves Detection of Biologically Relevant Features. *Molecular & Cellular Proteomics* **19**, 1396–1408 (2020).

294. Khan, A. U., Qu, R., Ouyang, J. & Dai, J. Role of Nucleoporins and Transport Receptors in Cell Differentiation. *Front. Physiol.* **11**, 515523 (2020).

295. Port, S. A. *et al.* Structural and Functional Characterization of CRM1-Nup214 Interactions Reveals Multiple FG-Binding Sites Involved in Nuclear Export. *Cell Rep.* **13**, 690–702 (2015).

296. Hutten, S. & Kehlenbach, R. H. Nup214 Is Required for CRM1-Dependent Nuclear Protein Export In Vivo. *Mol. Cell. Biol.* **26**, 6772–6785 (2006).

297. Vitolo, M. *et al.* Factors Associated with Progression of Atrial Fibrillation and Impact on All-Cause Mortality in a Cohort of European Patients. *J. Clin. Med.* **12**, 768 (2023).

298. Cheniti, G. *et al.* Atrial fibrillation mechanisms and implications for catheter ablation. *Front. Physiol.* **9**, 391650 (2018).

299. Takahashi, Y. *et al.* Histological validation of atrial structural remodelling in patients with atrial fibrillation. *Eur. Heart J.* **44**, 3339–3353 (2023).

300. Ma, Y. *et al.* Myofibroblasts and the extracellular matrix network in post-myocardial infarction cardiac remodeling. *Pflügers Archiv - European Journal of Physiology 2014 466:6* **466**, 1113–1127 (2014).

301. Abe, H. *et al.* NF-κB activation in cardiac fibroblasts results in the recruitment of inflammatory Ly6Chi monocytes in pressure-overloaded hearts. *Sci. Signal.* **14**, 4932 (2021).

302. Crean, D. & Murphy, E. P. Targeting NR4A Nuclear Receptors to Control Stromal Cell Inflammation, Metabolism, Angiogenesis, and Tumorigenesis. *Front. Cell Dev. Biol.* **9**, 589770 (2021).

303. Chung, M. K. *et al.* C-reactive protein elevation in patients with atrial arrhythmias: Inflammatory mechanisms and persistence of atrial fibrillation. *Circulation* **104**, 2886–2891 (2001).

304. Tallquist, M. D. Cardiac Fibroblast Diversity. *Annu. Rev. Physiol.* **82**, 63–78 (2020).

305. Harada, M., Van Wagoner, D. R. & Nattel, S. Role of Inflammation in Atrial Fibrillation Pathophysiology and Management. *Circulation Journal* **79**, 495–502 (2015).

306. Tanaka, T., Narazaki, M. & Kishimoto, T. IL-6 in Inflammation, Immunity, and Disease. *Cold Spring Harb. Perspect. Biol.* **6**, a016295 (2014).

307. Ancey, C. *et al.* SECRETION OF IL-6, IL-11 AND LIF BY HUMAN CARDIOMYOCYTES IN PRIMARY CULTURE. *Cytokine* **18**, 199–205 (2002).

308. Williams, E. A., Russo, V., Ceraso, S., Gupta, D. & Barrett-Jolley, R. Anti-arrhythmic properties of non-antiarrhythmic medications. *Pharmacol. Res.* **156**, 104762 (2020).

309. Pappritz, K. *et al.* Sex- and age-related differences in the inflammatory properties of cardiac fibroblasts: impact on the cardiosplenic axis and cardiac fibrosis. *Front. Cardiovasc. Med.* **10**, 1117419 (2023).

310. Volgman, A. S. *et al.* Women and atrial fibrillation. *J. Cardiovasc. Electrophysiol.* **32**, 2793–2807 (2021).

311. Akoum, N., Mahnkopf, C., Kholmovski, E. G., Brachmann, J. & Marrouche, N. F. Age and sex differences in atrial fibrosis among patients with atrial fibrillation. *EP Europace* **20**, 1086–1092 (2018).

312. Li, Z. *et al.* Gender differences in fibrosis remodeling in patients with long-standing persistent atrial fibrillation. *Oncotarget* **8**, 53714–53729 (2017).

313. Pérez-Sieira, S., López, M., Nogueiras, R. & Tovar, S. Regulation of NR4A by nutritional status, gender, postnatal development and hormonal deficiency. *Sci. Rep.* **4**, 4264- (2014).

314. McLarty, J. L., Li, J., Levick, S. P. & Janicki, J. S. Estrogen modulates the influence of cardiac inflammatory cells on function of cardiac fibroblasts. *J. Inflamm. Res.* **6**, 99–108 (2013).

315. Kato, Y. *et al.* Protocol for gene knockdown using siRNA in primary cultured neonatal murine microglia. *STAR Protoc.* **5**, 102867 (2024).

316. Hedrick, E. *et al.* Nuclear Receptor 4A1 (NR4A1) as a Drug Target for Renal Cell Adenocarcinoma. *PLoS One* **10**, e0128308 (2015).

317. Hedrick, E. *et al.* Potent inhibition of breast cancer by bis-indole-derived nuclear receptor 4A1 (NR4A1) antagonists. *Breast Cancer Research and Treatment 2019 177:1* **177**, 29–40 (2019).

318. Hedrick, E., Lee, S.-O., Doddapaneni, R., Singh, M. & Safe, S. NR4A1 Antagonists Inhibit β1-Integrin-Dependent Breast Cancer Cell Migration. *Mol. Cell. Biol.* **36**, 1383–1394 (2016).

319. Hedrick, E. *et al.* Nuclear receptor 4A1 as a drug target for breast cancer chemotherapy. *Endocr. Relat. Cancer* **22**, 831–840 (2015).

320. Roy, A. High-Throughput Screening (HTS) Technology. *Encyclopedia of Molecular Pharmacology* 1–13 (2021) doi:10.1007/978-3-030-21573-6_73-1.

321. Sigaeva, A., Hutchings, C., Cesnik, A., Lilley, K. S. & Lundberg, E. Subcellular localization as a driver of protein function. *Nature Reviews Molecular Cell Biology 2026* 1–18 (2026) doi:10.1038/s41580-026-00947-3.

322. Tsai, C. T., Lin, J. L., Lai, L. P., Lin, C. S. & Huang, S. K. S. Membrane translocation of small GTPase Rac1 and activation of STAT1 and STAT3 in pacing-induced sustained atrial fibrillation. *Heart Rhythm* **5**, 1285–1293 (2008).

323. Lee, C. Y. *et al.* Systematic discovery of protein interaction interfaces using AlphaFold and experimental validation. *Molecular Systems Biology 2024 20:2* **20**, 75–97 (2024).

324. Dong, Z., Coronel, R. & de Groot, J. R. Cellular and molecular cross-talk in atrial fibrillation: The role of non-cardiomyocytes in creating an arrhythmogenic substrate. *Journal of Physiology* **604**, 1629–1645 (2025).

325. Kim, H., Kamm, R. D., Vunjak-Novakovic, G. & Wu, J. C. Progress in multicellular human cardiac organoids for clinical applications. *Cell Stem Cell* **29**, 503–514 (2022).

326. Zhao, H.-Y., Jiang, J.-B., Wang, S.-N. & Miao, C.-Y. Technologies and applications of current human cardiac organoids. *Acta Pharm. Sin. B* **15**, 5734–5757 (2025).

327. Swonger, J. M., Liu, J. S., Ivey, M. J. & Tallquist, M. D. Genetic tools for identifying and manipulating fibroblasts in the mouse. *Differentiation* **92**, 66–83 (2016).

328. Hulsurkar, M. M. *et al.* Atrial-Specific LKB1 Knockdown Represents a Novel Mouse Model of Atrial Cardiomyopathy With Spontaneous Atrial Fibrillation. *Circulation* **144**, 909–912 (2021).

329. Ferreira, M. *et al.* Advancing Atrial Fibrillation Research: The Role of Animal Models, Emerging Technologies and Translational Challenges. *Biomedicines 2025, Vol. 13, Page 307* **13**, 307 (2025).

330. Gupta, D., Rienstra, M., van Gelder, I. C. & Fauchier, L. Atrial fibrillation: better symptom control with rate and rhythm management. *The Lancet Regional Health - Europe* **37**, 100801 (2024).

331. Woods, C. E. & Olgin, J. Atrial fibrillation therapy now and in the future: Drugs, biologicals, and ablation. *Circ. Res.* **114**, 1532–1546 (2014).

332. Zuraw, A. & Aeffner, F. Whole-slide imaging, tissue image analysis, and artificial intelligence in veterinary pathology: An updated introduction and review. *Vet. Pathol.* **59**, 6–25 (2022).

333. Zhao, J. *et al.* Chamber-specific wall thickness features in human atrial fibrillation. *Interface Focus* **13**, (2023).

334. Wijesurendra, R. S. & Casadei, B. Atrial fibrillation: effects beyond the atrium? *Cardiovasc. Res.* **105**, 238–247 (2015).

335. Hopman, L. H. G. A. *et al.* Right atrial function and fibrosis in relation to successful atrial fibrillation ablation. *Eur. Heart J. Cardiovasc. Imaging* **24**, 336–345 (2023).

336. Sossalla, S. & Vollmann, D. Arrhythmia-Induced Cardiomyopathy. *Dtsch. Arztebl. Int.* **115**, 335–341 (2018).

337. Fernández-Ruiz, I. Atrial fibrillation induces functional remodelling of the left ventricle. *Nat. Rev. Cardiol.* **19**, 285 (2022).

338. Mołek-Dziadosz, P. *et al.* Left ventricular remodeling in atrial fibrillation is associated with elevated NAP-2 and 3-nitrotyrosine. *Biomark. Med.* **19**, 157–164 (2025).

Appendix

Supplementary Table 1 Top 100 DEGs from NR4A1 knockdown RNA-seq dataset

Primary Gene name	baseMean	Log2 Fold change	p-value	Adj. p-value
TKT	25649.589	-1.596374318	6.43E-195	8.47E-191
MMGT1	2062.0254	-0.929057001	7.07E-53	4.65E-49
TMEM245	6757.2855	-0.791800193	1.48E-52	6.51E-49
PLPPR4	3311.1361	-1.080188184	1.57E-46	5.15E-43
ARSJ	3215.7808	-0.750141763	4.02E-44	1.06E-40
CTDSPL	2190.2027	-0.920829312	1.13E-39	2.49E-36
SCUBE3	12880.572	-0.692378963	5.07E-39	9.53E-36
TBC1D5	4119.6303	-0.740132667	5.07E-37	8.35E-34
SERINC3	14066.171	-0.559746826	1.33E-36	1.95E-33
ARMC1	1892.2308	-1.070715696	4.92E-36	6.48E-33
LHFPL2	4980.0471	-0.693936193	1.26E-35	1.50E-32
TGFB2	7067.35	-0.727777943	1.52E-33	1.67E-30
FUCA2	6598.6745	-0.564260449	1.06E-32	1.07E-29
RBMS1	7920.2654	-0.488047093	5.66E-32	5.32E-29
INSIG1	9340.6028	-0.691860004	1.63E-30	1.34E-27
KIF3B	5832.2406	-0.548791785	1.56E-30	1.34E-27
TXNIP	11143.413	-0.524442486	1.86E-30	1.44E-27
ALCAM	21505.497	-0.46899867	2.02E-29	1.48E-26
TNC	11465.804	-0.504333198	2.86E-28	1.98E-25
GDF15	5606.596	-0.502924752	5.13E-28	3.38E-25
EPDR1	4186.6192	-0.68381487	1.40E-25	8.80E-23
UBA7	3101.7369	-0.595230997	2.52E-25	1.51E-22
DENND10	3020.7815	-0.595086732	2.64E-24	1.51E-21
CHSY3	936.75799	-0.885962709	2.80E-23	1.54E-20
C5orf24	6988.9812	-0.462521114	9.27E-23	4.88E-20
TPM1	81814.988	-0.407355933	2.09E-22	1.06E-19
SRPRA	9177.6105	-0.453904861	1.24E-21	6.04E-19
CBX6	7372.5184	-1.272537288	1.37E-21	6.45E-19
HMGN2	8548.0025	-0.416202038	2.51E-21	1.14E-18
APBB1IP	815.86425	-1.098636453	2.63E-21	1.15E-18
UXS1	2688.4647	-0.641288374	6.94E-21	2.95E-18
DNAAF2	513.2636	-0.999988197	3.09E-20	1.27E-17
NGRN	2586.9017	-0.541382122	4.37E-20	1.74E-17
NEK7	20522.158	-0.352252497	8.11E-20	3.14E-17
USP22	16203.62	-0.346355037	7.01E-19	2.64E-16
SDC4	5777.9578	-0.404460263	7.73E-19	2.83E-16
TGOLN2	21021.063	-0.32354556	1.06E-18	3.76E-16
CCN3	1779.5105	-0.642950169	3.28E-18	1.14E-15
CTSL	20228.575	-0.312515471	6.11E-18	2.06E-15
LTBP1	23973.834	-0.41698134	6.35E-18	2.09E-15
SERINC1	19930.272	-0.331126467	8.74E-18	2.78E-15
ARF3	9086.237	-0.373183211	8.85E-18	2.78E-15
POSTN	212755.48	-0.308160954	2.04E-17	6.24E-15
RELN	13334.639	-0.46827464	2.59E-17	7.75E-15
CXCL1	14495.391	-0.486790695	4.48E-17	1.31E-14
LHFPL6	5242.8556	-0.451720349	6.18E-17	1.77E-14
NMD3	3348.9251	-0.50734443	8.57E-17	2.40E-14
JOSD1	4090.4329	-0.441738078	1.01E-16	2.77E-14
SLC4A4	2058.5005	0.644640487	1.56E-16	4.16E-14
ITGB8	3540.3417	0.655994743	1.58E-16	4.16E-14

CLIP4	5292.6489	-0.385068416	1.80E-16	4.65E-14
PODXL	1359.7764	-0.639421762	5.38E-16	1.36E-13
RND3	14666.088	-0.315585208	5.76E-16	1.43E-13
PEG10	9340.5042	0.383592475	9.57E-16	2.33E-13
STRADB	3587.6543	0.473268762	1.25E-15	2.98E-13
WDR37	1715.7309	-0.545036832	1.66E-15	3.90E-13
NA	230.80321	-1.277891881	2.56E-15	5.91E-13
SPATS2L	6395.9563	-0.432640694	2.72E-15	6.18E-13
USP7	5708.7804	-0.347445949	5.57E-15	1.24E-12
COL22A1	2674.4765	-0.577296978	8.12E-15	1.77E-12
SESN3	7752.338	0.326213752	8.18E-15	1.77E-12
TNFAIP2	4745.4071	-0.47448395	8.46E-15	1.80E-12
ITGA5	28310.5	-0.346061483	8.70E-15	1.82E-12
UNC45A	4318.9505	-0.40942048	1.12E-14	2.31E-12
PKP2	1865.6737	0.7504292	1.18E-14	2.39E-12
IL6	4207.5125	-0.475673921	1.36E-14	2.70E-12
HECA	2043.8505	-0.497614126	1.43E-14	2.80E-12
SYT11	4542.5775	-0.41908554	1.68E-14	3.25E-12
SYNE2	2618.1598	0.452420099	2.34E-14	4.47E-12
TNRC6B	3722.9189	0.401465106	2.85E-14	5.36E-12
LRRC17	18084.619	0.340221136	5.33E-14	9.88E-12
CXCL12	49621.388	-0.280642795	6.01E-14	1.10E-11
GM2A	2727.8698	-0.448696786	7.39E-14	1.33E-11
HIPK3	6582.4692	0.37658055	8.43E-14	1.50E-11
AKAP7	376.0332	-1.164774111	1.02E-13	1.79E-11
POGLUT3	5235.0779	-0.352892371	1.29E-13	2.24E-11
SPOCD1	1686.9302	-0.644869685	1.39E-13	2.37E-11
EEIG1	2658.4504	-0.442383056	1.53E-13	2.57E-11
RNF152	964.60507	-0.610961428	1.89E-13	3.15E-11
TNPO1	18309.432	-0.352386655	2.54E-13	4.19E-11
VLDLR	4012.1749	0.442406555	2.75E-13	4.47E-11
RBM24	916.49556	-0.632384067	5.02E-13	8.06E-11
NR4A1	164.36081	-1.418795238	6.26E-13	9.93E-11
SGPL1	3694.8009	0.363104212	6.53E-13	1.02E-10
ADAM12	27114.272	-0.345308108	7.08E-13	1.08E-10
PPM1F	3099.5548	-0.375750515	7.08E-13	1.08E-10
GPRC5A	3026.6396	0.52413727	7.32E-13	1.11E-10
CD47	7637.335	-0.30011362	9.67E-13	1.45E-10
CLPTM1L	5594.7176	-0.335695617	1.27E-12	1.87E-10
FRAS1	2294.489	0.581426271	1.36E-12	1.99E-10
ATP6V1C1	4120.4611	-0.408730075	1.53E-12	2.21E-10
CCL2	12959.109	-0.349616195	1.89E-12	2.70E-10
SUMF1	3682.0224	-0.396371927	3.14E-12	4.45E-10
ATP6V1G1	4120.9216	-0.340260203	3.92E-12	5.49E-10
MCAM	4123.2608	-0.448601002	4.41E-12	6.11E-10
P4HA2	14284.59	-0.314252745	4.63E-12	6.35E-10
SMS	4580.564	-0.446224754	7.52E-12	1.02E-09
TMEM109	3288.1606	-0.378217077	1.33E-11	1.78E-09
TNRC6A	8516.9539	0.276199008	1.37E-11	1.83E-09
KDM3A	3445.7318	0.368207908	1.43E-11	1.88E-09

Supplementary Table 2 NR4A1 interactors from interactome proteomics dataset (sinus rhythm)

Primary Gene name	UniprotID	Log2 Fold change	p-value	Adj. p-value
AP1M2	Q9Y6Q5	-7.682236847	7.26E-05	0.02656028
C1QC	P02747	6.983916922	7.91E-05	0.02656028
NR4A1	P22736	6.826471009	3.2E-05	0.02656028
EEF1G	P26641	5.612519697	0.000268	0.06750093
C4A	P0C0L4	5.310272777	0.000358	0.07212723
C1R	P00736	5.109854502	0.000545	0.0783443
PON1	P27169	4.913334812	0.000519	0.0783443
TXN	P10599	-2.227781209	0.000647	0.08147352
HRG	P04196	4.651062926	0.001276	0.09488978
JAK2	O60674	-3.311148285	0.001369	0.09488978
MFAP4	P55083	4.296352764	0.001165	0.09488978
PGRMC2	O15173	-2.092504941	0.001174	0.09488978
PHGDH	O43175	-2.086704222	0.001394	0.09488978
PPA1	Q15181	-4.685128787	0.000928	0.09488978
TFG	Q92734	4.698765981	0.001413	0.09488978
ARPC1B	O15143	4.112985957	0.001566	0.09854976
DDX17	Q92841	3.937368331	0.002242	0.11822828
ECHS1	P30084	4.161838746	0.002153	0.11822828
HEXB	P07686	3.745454488	0.002583	0.11822828
IARS1	P41252	4.239136884	0.002221	0.11822828
PAPSS1	O43252	3.845408696	0.002468	0.11822828
TBCE	Q15813	-1.512079851	0.002416	0.11822828
HSP90B1	P14625	-1.538523136	0.003467	0.15069185
LGALS1	P09382	-1.420699009	0.003591	0.15069185
RPS27	P42677	5.561347368	0.003771	0.15191473
AKAP8L	Q9ULX6	4.335234297	0.004016	0.15555438
VAC14	Q08AM6	4.337662745	0.00492	0.18348482
GAPDH	P04406	-1.05170262	0.005108	0.18371186
PPIB	P23284	-1.218978669	0.005315	0.1845584
ACTR10	Q9NZ32	-2.25401169	0.005624	0.1854143
PLCB2	Q00722	-2.988105756	0.005708	0.1854143
LDHB	P07195	-1.949831036	0.006063	0.19079095
HSP90AB1	P08238	-1.361025042	0.006304	0.19236178
HSPA5	P11021	-1.222920419	0.006868	0.19759324
TPM4	P67936	-1.601061819	0.006768	0.19759324
SH3GLB1	Q9Y371	-2.325384283	0.007292	0.20190202
SLIRP	Q9GZT3	3.654158701	0.007418	0.20190202
IGHG1	P01857	-1.554032523	0.00785	0.20269247
RAB18	Q9NP72	-1.346328441	0.007737	0.20269247
AKR1C1	Q04828	-1.854377385	0.009023	0.21363228
CSDE1	O75534	3.401427379	0.008998	0.21363228
HSPA8	P11142	-1.092136384	0.009211	0.21363228
HSPD1	P10809	-1.351613172	0.009334	0.21363228
PDIA6	Q15084	-1.330966813	0.008687	0.21363228
RPL36AL	Q969Q0	3.416101649	0.0115	0.25733637
ANXA2	P07355	-1.386687631	0.012846	0.26067507
CAP1	Q01518	-1.733651276	0.012523	0.26067507
CLUH	O75153	-4.207660614	0.012975	0.26067507
CSTB	P04080	-1.581611406	0.013043	0.26067507
DDX5	P17844	2.994261228	0.013885	0.26067507
LDHA	P00338	-1.283942506	0.013979	0.26067507
PRDX1	Q06830	-1.247026368	0.01316	0.26067507
RPL36	Q9Y3U8	2.735184872	0.01347	0.26067507
SNX9	Q9Y5X1	2.414305514	0.013253	0.26067507
DDOST	P39656	3.78058231	0.015173	0.26342886
GBF1	Q92538	2.871383885	0.014928	0.26342886
LAMP1	P11279	-1.435416248	0.014908	0.26342886
RAB7A	P51149	-1.096108182	0.014709	0.26342886
NUMB	P49757	-2.819048603	0.01547	0.26404237
CTSB	P07858	-2.070172025	0.017226	0.26801358
MAP1A	P78559	2.310205192	0.0173	0.26801358
OPTN	Q96CV9	4.886465057	0.017041	0.26801358
PAICS	P22234	-1.874344713	0.017187	0.26801358
PCBP3	P57721	-2.404577603	0.016304	0.26801358
RPS28	P62857	-1.2578763	0.017051	0.26801358
KRT9	P35527	-2.153463731	0.017626	0.26893171
SLC25A3	Q00325	2.785387508	0.018225	0.27392512
CDC42BPB	Q9Y5S2	2.886440642	0.018532	0.2744431

HDAC2	Q92769	-4.622165049	0.019094	0.27866124
EEF1D	P29692	-1.806822065	0.019757	0.28282256
IGLL5	B9A064	-1.130772583	0.020531	0.28282256
PKM	P14618	-0.93794772	0.020783	0.28282256
RPS11	P62280	2.848319659	0.020601	0.28282256
VIM	P08670	-0.870085403	0.020035	0.28282256
APMAP	Q9HDC9	-1.53284095	0.02164	0.28439553
GSTP1	P09211	-2.571645491	0.022784	0.28439553
HPX	P02790	2.179466353	0.023158	0.28439553
IGKC	P01834	-1.126756235	0.021779	0.28439553
ITGB1	P05556	-1.504614807	0.02288	0.28439553
NRDE2	Q9H7Z3	-1.583099511	0.021651	0.28439553
PLS3	P13797	-1.602547832	0.02212	0.28439553
SPECC1	Q5M775	-1.204278672	0.022368	0.28439553
CNOT1	A5YKK6	2.317306722	0.023958	0.28610435
G6PD	P11413	-2.646858255	0.02415	0.28610435
TPM3	P06753	3.178507117	0.023833	0.28610435
MRPL45	Q9BRJ2	-2.425786857	0.024877	0.29128803
CFL1	P23528	-1.003531766	0.02723	0.29173914
COLGALT1	Q8NBJ5	2.330323281	0.025631	0.29173914
DCTN4	Q9UJW0	3.577583183	0.027233	0.29173914
FSCN1	Q16658	3.228670103	0.026544	0.29173914
PITPNB	P48739	-3.734695451	0.026875	0.29173914
SCO1	O75880	3.796576545	0.025788	0.29173914
UGP2	Q16851	-1.040185169	0.026599	0.29173914
UNC80	Q8N2C7	-1.187803588	0.026153	0.29173914
EEF1A1	P68104	3.038805746	0.028411	0.3011544
ALDOA	P04075	-0.913458011	0.029055	0.30163223
CLPX	O76031	3.474535861	0.028798	0.30163223
RPL10A	P62906	1.054334577	0.0296	0.30415607
ARHGAP29	Q52LW3	3.82601279	0.033564	0.31295686
CCT6A	P40227	-1.086261878	0.033288	0.31295686
EEF2	P13639	-0.851193839	0.031602	0.31295686
HSPA9	P38646	-0.971249686	0.033232	0.31295686
KPNA2	P52292	2.334068885	0.032494	0.31295686
KRT1	P04264	-1.947176239	0.032494	0.31295686
PLIN3	O60664	-0.968959916	0.032879	0.31295686
RPP30	P78346	2.304750346	0.032286	0.31295686
TUBB	P07437	-1.13323305	0.031601	0.31295686
WDR1	O75083	-0.969974805	0.031627	0.31295686
ERLIN1	O75477	2.976895612	0.033982	0.31394362
CD59	P13987	-1.218156465	0.035951	0.3158246
LUC7L2	Q9Y383	1.963540354	0.035761	0.3158246
OGDH	Q02218	2.013869356	0.035817	0.3158246
S100A11	P31949	-2.946955419	0.035634	0.3158246
SPCS3	P61009	3.020807057	0.036067	0.3158246
UPRT	Q96BW1	3.132147543	0.035247	0.3158246
RCN2	Q14257	2.345125103	0.037399	0.32466187
FKBP10	Q96AY3	-1.252165324	0.040485	0.34636416
IGKV4-1	P06312	5.797808817	0.040587	0.34636416
C3	P01024	1.749840977	0.043763	0.34822849
DLST	P36957	2.429573739	0.04388	0.34822849
DYNC1H1	Q14204	1.877894385	0.043595	0.34822849
ERLIN2	O94905	1.807911706	0.04371	0.34822849
ESRRA	P11474	-1.574586392	0.042592	0.34822849
NSF	P46459	2.492810576	0.043918	0.34822849
PFN1	P07737	-3.735352642	0.042397	0.34822849
RPS29	P62273	-0.906632101	0.041726	0.34822849
ZNF670	Q9BS34	-4.323462319	0.04178	0.34822849
DAB2	P98082	1.681883545	0.048087	0.36076977
FAU	P62861	2.537271352	0.048365	0.36076977
H4C1; H4C2; H4C3; H4	P62805	-0.967142394	0.04651	0.36076977
MRPL11	Q9Y3B7	2.258666351	0.04807	0.36076977
PDLIM4	P50479	2.680628751	0.045909	0.36076977
PSMC2	P35998	2.319088787	0.047532	0.36076977
S100A6	P06703	2.199945779	0.048181	0.36076977
STRN4	Q9NRL3	2.690733841	0.047676	0.36076977
CLINT1	Q14677	3.980314304	0.048754	0.36099427
PRKDC	P78527	3.098152894	0.049377	0.36294026

Supplementary Table 3 NR4A1 interactors from interactome proteomics dataset (AF)

Primary Gene name	UniprotID	Log2 Fold change	p-value	Adj. p-value
NR4A1	P22736	5.479339426	0.000164	0.07741628
PON1	P27169	5.703323077	0.000177	0.07741628
TFG	Q92734	6.345030123	0.000273	0.07741628
C1QC	P02747	5.183066751	0.000307	0.07741628
SCYL1	Q96KG9	5.421974795	0.000531	0.09089539
STAT2	P52630	4.261826174	0.000571	0.09089539
JAK2	O60674	-4.404716186	0.00063	0.09089539
C4A	P0C0L4	4.401964421	0.001068	0.10475016
SKIC2	Q15477	-4.997931464	0.001087	0.10475016
LRRFIP2	Q9Y608	3.906977851	0.001126	0.10475016
LRPPRC	P42704	-3.748364584	0.001178	0.10475016
FKBP4	Q02790	-4.078817697	0.001245	0.10475016
ATAD3A	Q9NVI7	3.963289107	0.001463	0.11362823
PJA1	Q8NG27	-5.670092861	0.001712	0.11847597
PAPSS1	O43252	3.931228317	0.00176	0.11847597
MFAP4	P55083	3.259862233	0.002418	0.14148792
ECHDC1	Q9NTX5	3.902506658	0.002637	0.14148792
PARP6	Q2NL67	-2.480242834	0.002764	0.14148792
TARS1	P26639	3.857676567	0.002803	0.14148792
NT5E	P21589	2.565433127	0.003031	0.14148792
STT3B	Q8TCJ2	2.796425907	0.003035	0.14148792
ASCC3	Q8N3C0	3.446214729	0.003219	0.14148792
PLOD1	Q02809	3.941011564	0.003222	0.14148792
VAC14	Q08AM6	3.629322281	0.003549	0.14844262
PLCB2	Q00722	-3.558256332	0.003891	0.14844262
MAP4K4	O95819	2.991353928	0.004024	0.14844262
KANK2	Q63ZY3	4.22289591	0.004237	0.14844262
SH3GLB1	Q9Y371	-3.145065073	0.004247	0.14844262
DDX46	Q7L014	5.224560881	0.004262	0.14844262
MPHOSPH10	O00566	3.343856563	0.004456	0.1500094
AP3B1	O00203	3.082856685	0.004931	0.16066249
PDIA5	Q14554	3.451884421	0.005144	0.16235858
PA2G4	Q9UQ80	-3.280783353	0.005409	0.16554399
CTNNA1	P35221	3.440439708	0.005772	0.16917971
IGHG3	P01860	-3.706576516	0.005863	0.16917971
MRPL11	Q9Y3B7	2.962760007	0.006263	0.17341205
CSNK2B	P67870	3.377936792	0.006411	0.17341205
HDAC2	Q92769	-3.151351521	0.006524	0.17341205
GLS	O94925	-2.226455286	0.006954	0.17422873
CUL2	Q13617	-2.565105063	0.006975	0.17422873
LETM1	O95202	3.48151758	0.007073	0.17422873
SNRNP200	O75643	2.728854675	0.007342	0.1765636
YARS1	P54577	-3.286191346	0.0076	0.17817859
RPS26	P62854	2.552141165	0.008074	0.17817859
HRG	P04196	3.315126522	0.008166	0.17817859
RAB5A	P20339	-2.82529486	0.008352	0.17817859
EEF1B2	P24534	-1.772274002	0.008624	0.17817859
DYNC1LI1	Q9Y6G9	2.746199623	0.008755	0.17817859
MIF	P14174	-3.982736561	0.008768	0.17817859
COL8A1	P27658	-1.858604924	0.008821	0.17817859
LTF	P02788	-3.831110944	0.009307	0.17831
DCTN4	Q9UJW0	3.779494255	0.009435	0.17831
REP15	Q6BDI9	4.350179256	0.009489	0.17831
RPL22	P35268	6.89080613	0.009715	0.17831
RPS12	P25398	2.609523012	0.009776	0.17831
DKC1	O60832	3.441696652	0.009886	0.17831
TXN	P10599	-2.185198433	0.010449	0.18515303
SLC16A3	O15427	3.180734303	0.010974	0.18944385
IGLV1-51	P01701	-2.666563607	0.011067	0.18944385
GOLM1	Q8NBJ4	-1.981537686	0.011543	0.19193531
SNAP23	O00161	2.88460479	0.011592	0.19193531
GOLGA2	Q08379	3.022898936	0.011897	0.19206133
OGDHL	Q9ULD0	3.747916489	0.01198	0.19206133
LTN1	O94822	-2.713784584	0.012633	0.19542676
ARPC2	O15144	2.613316911	0.012693	0.19542676
PDIA6	Q15084	-1.865091152	0.01277	0.19542676
BNIP1	Q12981	1.92648715	0.013073	0.19707597
CUL5	Q93034	2.766631386	0.013365	0.19771788
IGKV3D-15	A0A087WS	-1.704528396	0.013507	0.19771788
YWHAB	P31946	-2.962388788	0.014162	0.20434459
EIF5	P55010	2.16012616	0.014511	0.20642937
HMOX2	P30519	-2.54157116	0.014749	0.2068953
AP2M1	Q96CW1	2.785117176	0.01563	0.21039459
RPS29	P62273	2.762511774	0.015653	0.21039459
MYO6	Q9UM54	3.46938203	0.016147	0.21039459
TPM2	P07951	-1.882723738	0.016345	0.21039459
FKBP8	Q14318	1.966593263	0.016475	0.21039459
NCOR2	Q9Y618	3.198857613	0.01651	0.21039459
PABPC1	P11940	-2.417629221	0.016563	0.21039459
RCN1	Q15293	-2.66379249	0.016665	0.21039459
SSR1	P43307	2.924980116	0.017053	0.21263437
EMC1	Q8N766	2.048837383	0.017349	0.21368347
STMN1	P16949	-2.277014062	0.017564	0.2137362
SEPTIN9	Q9UHD8	2.199955762	0.017804	0.21407241
LMCD1	Q9NZU5	2.746242861	0.018269	0.21707403
CMPK1	P30085	2.620074333	0.018637	0.21850142
HS2ST1	Q7LGA3	2.383271283	0.018866	0.21850142
PZP	P20742	2.648593463	0.019404	0.21850142

PRKCSH	P14314	-1.638696243	0.019639	0.21850142
ENG	P17813	-2.184189603	0.019669	0.21850142
TTN	Q8WZ42	-4.213748619	0.019687	0.21850142
HSP90B1	P14625	-1.691707514	0.020262	0.22243734
CSRP1	P21291	-2.046516374	0.02049	0.22252347
TAGLN2	P37802	-2.200740727	0.021538	0.22935749
DNAJA1	P31689	3.712002517	0.021573	0.22935749
PRKRA	O75569	2.154198323	0.022027	0.23057537
PDCD6	O75340	2.814931891	0.022144	0.23057537
PSMC6	P62333	2.747731763	0.023011	0.23430369
FSCN1	Q16658	3.696886316	0.02321	0.23430369
ATP6V1A	P38606	3.361241659	0.023279	0.23430369
YWHAH	Q04917	3.861674782	0.023445	0.23430369
FKBP15	Q5T1M5	1.846797508	0.023767	0.23430369
FAM120A	Q9NZB2	3.272252193	0.023923	0.23430369
HP	P00738	2.382317536	0.024296	0.23430369
HMGB1	P09429	-2.071835067	0.024558	0.23430369
PXDN	Q92626	1.921721786	0.02459	0.23430369
MCFD2	Q8NI22	3.09912228	0.025051	0.23623104
STRN4	Q9NRL3	2.49148497	0.025311	0.23623104
PFN1	P07737	-2.29450546	0.025612	0.23623104
S100A11	P31949	-1.876112752	0.025728	0.23623104
CD2AP	Q9Y5K6	2.346258851	0.026168	0.23681034
CCN2	P29279	-2.045373891	0.026391	0.23681034
HPX	P02790	1.602471575	0.026569	0.23681034
RPLP0	P05388	2.053313404	0.026744	0.23681034
ANKRD29	Q8N6D5	-3.057419159	0.026988	0.23681034
ENO1	P06733	-2.565871496	0.027198	0.23681034
CSTB	P04080	-1.948228778	0.028168	0.24123297
FKBP10	Q96AY3	-2.568823021	0.028307	0.24123297
GARS1	P41250	-1.84324294	0.028422	0.24123297
DARS1	P14868	2.450152314	0.028683	0.24141302
ECHS1	P30084	2.131681096	0.029104	0.24147784
GJA1	P17302	2.547431777	0.029643	0.24147784
LDHB	P07195	-1.931999171	0.029796	0.24147784
TKT	P29401	-2.362506459	0.029995	0.24147784
UBAP2L	Q14157	1.96285198	0.03027	0.24147784
PCBP2	Q15366	2.60274644	0.030428	0.24147784
RPS19	P39019	-1.075143053	0.030594	0.24147784
COL1A2	P08123	2.502329591	0.030603	0.24147784
ATP5MF	P56134	1.730684059	0.031258	0.24376088
UNC80	Q8N2C7	-2.333973607	0.031375	0.24376088
RPS14	P62263	2.657782052	0.032557	0.24830988
PPA1	Q15181	-3.202096323	0.032702	0.24830988
HSPB1	P04792	-1.375618836	0.032803	0.24830988
HSP90AB1	P08238	-1.345866207	0.033296	0.24830988
SLC25A3	Q00325	1.632982392	0.03374	0.24830988
ACTR2	P61160	1.8553123	0.033792	0.24830988
DPYSL3	Q14195	-1.352711716	0.033946	0.24830988
OSBPL8	Q9BZF1	3.166133629	0.034082	0.24830988
KRT73	Q86Y46	2.68097174	0.034173	0.24830988
EEF1A2	Q05639	-1.853202442	0.034821	0.25059455
IGKC	P01834	-1.738013991	0.035087	0.25059455
ANXA1	P04083	-2.228260468	0.035232	0.25059455
HNRNPUL2	Q1KMD3	2.518667411	0.036031	0.25350441
PCYOX1	Q9UHG3	-1.719520057	0.0367	0.25350441
TGM2	P21980	-1.449899756	0.036833	0.25350441
PDIA4	P13667	-1.909245327	0.037182	0.25350441
P4HB	P07237	-1.380962765	0.037282	0.25350441
AKAP8L	Q9ULX6	2.774318648	0.03731	0.25350441
DAB2	P98082	3.684326638	0.037398	0.25350441
SRP68	Q9UHB9	2.283981946	0.037729	0.25404152
AHNAK2	Q8IVF2	1.810723204	0.038667	0.25863064
PDLIM1	O00151	-1.42686487	0.030383	0.2645401
TUBA1C	Q9BQE3	3.391910143	0.040561	0.26952039
GAPDH	P04406	-0.963620265	0.040859	0.26972442
MBOAT7	Q96N66	2.0073044	0.041837	0.27159561
PDIA3	P30101	-1.389814774	0.042326	0.27159561
BAG3	O95817	2.645530997	0.042895	0.27159561
NAPG	Q99747	-2.050485147	0.04324	0.27159561
PPIA	P62937	-1.618063776	0.043625	0.27159561
EIF2S2	P20042	1.885193573	0.043784	0.27159561
KRT5	P13647	3.35613099	0.043845	0.27159561
SERBP1	Q8NC51	-2.570135747	0.043922	0.27159561
IGHG2	P01859	-1.938803605	0.044267	0.27159561
PRDX4	Q13162	4.097386217	0.044352	0.27159561
YWHAZ	P63104	-1.341897821	0.044432	0.27159561
TPM4	P67936	-1.309250019	0.044653	0.27159561
HSPD1	P10809	-1.459055237	0.044892	0.27159561
PYGB	P11216	-1.99885201	0.045106	0.27159561
RPL17	P18621	2.63361917	0.045176	0.27159561
ALG5	Q9Y673	1.523963199	0.045497	0.27190362
GOLIM4	O00461	2.183036115	0.046628	0.2744319
SLC25A5	P05141	2.653264915	0.046647	0.2744319
PSMD9	O00233	1.484517013	0.046735	0.2744319
TRIM25	Q14258	1.727398886	0.047151	0.27527334
RPL37A	P61513	2.718076466	0.04764	0.27653277
PPP6R3	Q5H9R7	-1.289804375	0.048666	0.28087501
ATP5ME	P56385	1.528024127	0.049748	0.2854872